TECHNISCHE UNIVERSITÄT MÜNCHEN

Fakultät für Medizin

Deciphering the role of Roquin RNA-binding proteins in late B cell development

Sabine Helmrath

Vollständiger Abdruck der von der Fakultät für Medizin der Technischen Universität München zur Erlangung eines
Doctor of Philosophy (Ph.D.)
genehmigten Dissertation.

Vorsitz: Prof. Dr. Allessandra Moretti

Betreuer*in: Prof. Dr. Marc Schmidt-Supprian

Prüfer*innen der Dissertation:

1. Prof. Dr. Andreas Pichlmair
2. Prof. Dr. Hassan Jumaa

Die Dissertation wurde am 23.11.2022 bei der Fakultät für Medizin der Technischen Universität München eingereicht und durch die Fakultät für Medizin am 16.01.2023 angenommen.

Abstract

Post-transcriptional gene regulation is facilitated by RNA binding proteins controlling all aspects of RNA life. They are the largest group of proteins in the cell and our investigations of their manifold functions in the context of immunological processes in health and disease has just begun[1]. Especial interest in the RNA binding proteins Roquin 1 and Roquin 2 arose by the discovery that mutations of Roquin 1 in mice and men are linked to a loss of peripheral tolerance and the development of autoimmune or inflammatory diseases, respectively[2,3]. While subsequent studies concentrated on the role of Roquins especially in T cells, their relevance in the B cell compartment is to date insufficiently addressed. Therefore, I generated mice with a B cell specific deletion of Roquin proteins. I thoroughly characterized late B cell developmental steps upon immunization evaluating the effect of Roquin protein gene dosage.

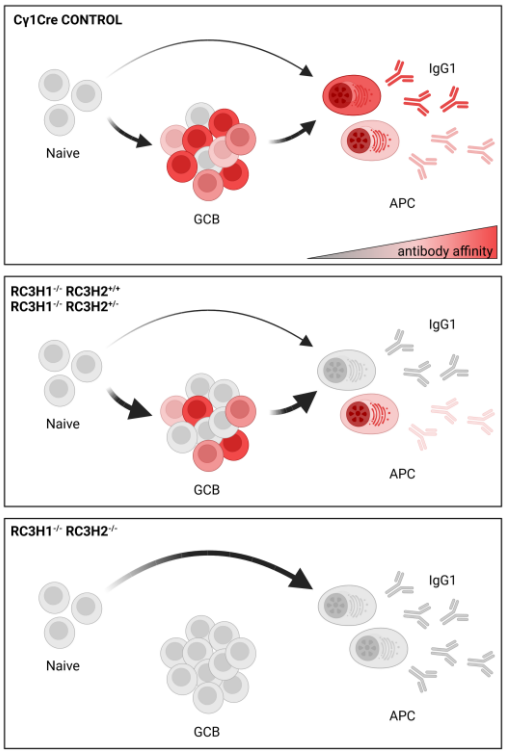

I was able to uncover that loss of both Roquin 1 and Roquin 2 leads to the absence of germinal center B cells (GCB) and a severe reduction in class-switched antibody-producing cells (APC) during a primary immune response. In striking contrast, Roquin 1 deficiency in the presence of one or two wildtype Roquin 2 alleles favors GCB generation upon immunization resulting in an overall enrichment of class-switched APCs compared to controls. In addition, I provided clear evidence that Roquin 1 is required for adequate somatic hypermutation and affinity maturation of GC-derived B cell receptors (BCR). Ablation of Roquin 1 causes a poor-quality antibody outcome with less antigen-specific B cells participating in the GC immune response. Mechanistically, *in vitro* analysis using the GC-like A20 cell line suggest that Roquin 1 and Roquin 2 ablated cells are incapable to enter the GC reaction due to enhanced cell apoptosis and an inability to metabolically adapt while APC formation promoting transcripts are upregulated. In conclusion, my PhD thesis demonstrates the substantial B cell intrinsic function of Roquin proteins during an immune reaction.

Zusammenfassung

RNA-Bindeproteine kontrollieren im Rahmen der post-transkriptionellen Genregulation alle Aspekte der mRNA-Reifung. Sie stellen die größte Gruppe von Proteinen in der Zelle dar und umfassende Untersuchungen ihrer vielfältigen Funktionen im Zusammenhang mit immunologischen Prozessen in gesunden oder erkrankten Organismen haben gerade erst begonnen. Besonderes Interesse an den RNA-Bindeproteinen Roquin 1 und Roquin 2 wurde durch die Entdeckung geweckt, dass Mutationen von Roquin 1 in Mäusen und in Menschen mit einem Verlust der peripheren Toleranz und der Entwicklung von Autoimmunerkrankungen bzw. chronischen Entzündungsreaktionen einhergehen. Während sich nachfolgende Studien vor allem auf die Rolle der Roquin Proteine in T Zellen konzentrierten, ist ihre Bedeutung für das B Zellkompartiment bisher nur unzureichend untersucht. Im Zuge dieses PhD Projektes, habe ich daher Mäuse mit einer B zellspezifischen Deletion von Roquin Proteinen erzeugt. Anschließend habe ich späte B Zellentwicklungsschritte nach Immunisierung umfassend und unter Berücksichtigung der Gendosierung der Roquin Proteine charakterisiert.

Dabei konnte ich zeigen, dass die Deletion von Roquin 1 und Roquin 2 zu einem vollständigen Verlust von Keimzentrums B Zellen und zu einer starken Verringerung der klassengewechselten, Antikörper produzierenden Zellen während einer primären Immunantwort führt. Im Gegensatz dazu wird die Bildung von Keimzentrums B Zellen nach einer Immunisierung begünstigt, wenn Roquin 1 zwar deletiert, aber ein oder zwei Allele von Roquin 2 noch funktional sind. Dies resultiert außerdem in einer Anreicherung von klassengewechselten, Antikörper produzierenden Zellen im Vergleich zu entsprechenden Kontrolltieren. Darüber hinaus konnte ich aufzeigen, dass Roquin 1 für die ausreichende somatische Hypermutation und Affinitätsreifung von B Zellrezeptoren der Keimzentrums B Zellen erforderlich ist. Der Verlust von Roquin 1 führt zu qualitativ mangelhaften Antikörpern und weniger antigenspezifische B Zellen nehmen an der Keimzentrumsimmunantwort teil. Auf molekularer Ebene deuten *in vitro* Analysen von Keimzentrums-ähnlichen A20 Zellen darauf hin, dass Roquin 1 und Roquin 2 defiziente Zellen nicht in der Lage sind an der Keimzentrumsreaktion teilzunehmen, da sie vermehrt in Apoptose gehen und/oder sich nicht metabolisch anpassen können, während plasmazellspezifische Transkripte verstärkt gebildet werden. Zusammenfassend zeigt meine Doktorarbeit, dass Roquin Proteine wichtige Funktionen in B Zellen im Rahmen der primären Immunantwort aufweisen.

Table of Contents

1 Introduction

1.1 Tolerance mechanisms of the immune system

The immune system is the body's defense against harmful pathogens such as viruses, bacteria, fungi and parasites. Defense mechanisms were classified into innate and adaptive immunity based on their speed of response and specificity against threat-causing microbes. While innate immunity reacts rapidly using a limited repertoire of receptors, adaptive immunity develops highly antigen-specific receptors more efficient to eliminate pathogens in the late phase of infection. Adaptive immunity further builds up an immunological memory potentially capable to life-long protect against re-infection[4,5].

B and T lymphocytes are cellular building blocks of the adaptive immune system with their surface B cell receptors (BCR) and T cell receptors (TCR) being able to recognize virtually any chemical structure. Outstanding receptor diversity is generated by the process of V(D)J recombination, in which gene segments are rearranged in a highly variable manner during cell differentiation. In the case of BCRs, variety is increased even further during late B cell maturation by single-nucleotide exchanges (somatic hypermutation). While the feature to produce exceptionally high antigen-specific receptors is desirable to elicit an immune response against foreign particles, it can be detrimental when targeted towards self-antigens. 50 % of all BCRs are estimated to be directed against host tissue generating the need for an effective control system to remove or silence self-reactive B lymphocytes[5,6].

Self-tolerance mechanisms which eliminate or silence autoreactive lymphocytes are active in primary lymphoid organs like the bone-marrow (BM) (central tolerance) as well as in peripheral organs such as spleen (SPL) and lymph nodes (LN) (peripheral tolerance). With respect to B cells, self-reactivity can lead to an arrest in B cell maturation and further receptor editing through ongoing V(D)J recombination. If BCR editing does not result in a less self-reactive BCR, chronic self-antigen exposure can induce cell death by upregulation of pro-apoptotic proteins such as BIM and competition for survival factors such as BAFF. Alternatively, cells can be rendered anergic by downregulation of BCR expression and

signaling. Autoreactive B cells that eventually still exit the bone marrow become a major threat to the immune system since they might enhance their self-antigen affinity during germinal center (GC) reaction and lead to the production of auto-antibodies by plasma cells (PC). To circumvent this, further B cell activation requires two signals: (I) antigen recognition via the BCR together with (II) T cell interaction or Toll-like receptor (TLR) signaling both providing additional proliferation stimuli. Especially the need for T-B cell interaction represents a powerful checkpoint since receptors from two cell types, T and B lymphocytes, need to simultaneously pass a series of self-tolerance barriers beforehand[5–8].

Despite these multifactorial self-tolerance processes able to act simultaneously and consecutively on a developing cell population, 3 – 5 % of the human population still suffer from autoimmune diseases, meaning the attack of the body by its own immune system. Autoimmunity can arise if single or accumulating, inherited or somatic mutations start to override self-tolerance checkpoints. The emergence of self-reactive cell clones then favors the evasion of even more checkpoints through an increased likelihood of positive clonal cooperation. Once all growth limiting checkpoints are breached, autoimmune symptoms manifest either organ-specifically like for example in type 1 diabetes or systemically including systemic lupus erythematosus (SLE) patients[7,9]. Especially loss of B cell tolerance and production of autoantibodies (ANAs) is a hallmark of autoimmunity and a rising prevalence of ANAs in the population within the last 40 years points toward an immediate need for new diagnostic and therapeutic interventions[9].

This thesis focuses on the functions of two proteins, namely Roquin 1 and Roquin 2, which both act in various cell types, including B cells, as essential modulators to restrain uncontrolled lymphocyte growth thereby prohibiting autoimmunity. Historically, Roquin proteins were discovered by a mouse model mimicking SLE in humans with following studies categorizing them as RNA-binding proteins. Research on Roquin proteins strengthened among others the current point of view that post-transcriptional gene regulation (PTGR) plays a major role in controlling proper immune function. However, our understanding of the Roquin proteins at present is primary based on their roles in T cells neglecting the importance of B cells, the potential source of ANA production, for immune surveillance. Therefore, this project aimed to decipher the role of Roquin proteins in B lymphocytes with special attention drawn to germinal center B cells (GCBs) and antibody producing cells (APCs).

The following chapters will give an overview of

- the steps of peripheral B cell development (chapter 1.2)
- our current (limited) knowledge about post-transcriptional regulators in GCB reactions (chapter 1.3),
- the discovery of Roquin proteins in mice (chapter 1.5.3),
- molecular characteristics of Roquin proteins including protein structure, intracellular localization and targets (chapter 1.5.1, 1.5.2 and 1.5.7),
- Roquin proteins involvement in adaptive immunity in mice (chapter 1.5.4, 1.5.6)
- Roquin 1 mutations found in human patients (chapter 1.5.5)

1.2 B cell biology

With regard to the main focus of this thesis on late B cell differentiation, this chapter gives a more detailed description of processes in the GC reaction upon T cell dependent immune responses. Nevertheless, for the reader to understand the origin of these GCBs, the maturation steps in the bone marrow preceding the GC reaction are presented next in an overview fashion.

1.2.1 Early B cell development

Early hematopoiesis begins when pluripotent, undifferentiated hematopoietic stem cells (pHSCs) colonize the liver, thymus and bone marrow of the fetus at day 10.5 of murine embryonic development (E10.5). Although B cell development starts in fetal liver, the bone marrow is being established as the life-long site of B cell generation starting from E17.5. pHSCs differentiate in a gradual process of lineage commitment into LIN^- $IL7R\alpha^+$ $SCA1^{lo}$ $cKIT^{lo}$ common lymphoid progenitors (CLPs) which are the source of T, NK and B lymphocytes. Further B lymphopoiesis steps into prepro and late pro B cells are dependent on the survival-promoting cytokine IL7 provided by stromal cells of the bone marrow niche. An important checkpoint of B cell maturation is the re-arrangement of the pre BCR heavy-chain initiated by joining the diversity (D) region to the joining (J) region in pro-B cells followed by attachment of the variable (V) gene segment. Successfully recombined VDJ heavy-chains (IgH) are expressed on the surface of pre B cells paired with the surrogate light chain (SLC) composed of the invariant proteins V_{preB} and λ5. Next, λ5-induced pre BCR aggregation enables pre BCR signaling even in the absence of ligand

which downregulates SLC transcription in a negative feedback loop, inhibits continuous re-arrangement of the second IgH allele (allelic exclusion) and induces a proliferation burst of 2 - 7 cell divisions via the PI3K-AKT kinase pathway[10–13]. Pre BCRs are evaluated for their auto-reactivity by the bone marrow microenvironment and their fitness determines whether and to which extent proliferation occurs. Concise and timed regulation of IL7R and pre BCR signaling is hereafter needed to attenuate cell cycling and initiate VJ light-chain re-arrangement in small pre B cells resulting in antigen-recognizing BCR presentation on immature B cells. In the following chapters, a BCR with a unique combination of VDJ of the heavy chain is named a “clone”. Immature B cells start to circulate into secondary lymphoid organs where they are screened for auto-reactivity and, if not eliminated, evolve through transitional stages T1 - T3 into mature B cells which are then ready for antigen exposure[10–13]. Immature B cells, characterized through the immaturity marker AA4.1^{+} which is still present on T1 and T2 cells as well, are capable to become one out of three mature B cell populations: B1 cells or marginal zone and follicular cells of the B2 cell lineage. The following chapters will discuss B2 related developmental processes only.

1.2.2 Marginal zone and follicular B cells

Mature marginal zone B cells (MZB, AA4.1^{-} IgM^{hi} IgD^{lo} CD21^{hi} CD1d^{hi} CD23^{-}) differ greatly in localization, life-span and function from follicular B cells (FOB, AA4.1^{-} IgM^{hi} IgD^{hi} CD21^{int} CD23^{+})[14,15].

MZB reside in the marginal zone of the spleen, a compartment in between of the highly vascularized red pulp and the follicle-containing white pulp[16]. In mice, once recruited, they are sessile for many years with a certain capacity of self-renewal without entering the circulation again. To establish and retain their unique microanatomical localization, MZB rely on migratory stimuli including binding of the DL1 ligand of red pulp endothelial cells to MZB Notch2 receptor, chemotaxis and actin cytoskeleton remodeling upon sensing of sphingosine-1-phosphate (SP1) by the MZB SP1 receptor and integrin-ligand interactions. Their migration is a requirement not only for their localization which is tightly linked to their function, but also for their lineage commitment. The latter is in addition driven by survival signals including BAFF which activate the canonical NFκB pathway and weak BCR signaling strength (e.g., because of low affinity for the antigen, little co-stimulation or activity of BCR inhibitory molecules such as CD22). This discriminates MZB from FOB

which reside, as their name already indicates, in the follicles of the white pulp of the spleen and can additionally be found in the blood or in lymph nodes. In FOB, the non-canonical NFκB pathway seems to play a more prominent role and they require high BCR signaling for their activation[14,15,17].

MZB are involved mainly, but not exclusively, in the T cell independent (TI) response (also called T2 response) to non-protein antigens which are transported to them via the blood stream[14,15]. Their lineage-determining markers CD1d and CD21 act as MHCI like molecules to present lipid antigens to invariant NKT cells (iNKT)[18] and BCR coreceptors to enhance B cell activation upon complement CD3 opsonized antigen recognition, respectively, thereby bridging adaptive to innate immunity[19,20]. MZBs execute their effector functions (antigen presentation and $CD4^+$ T cell activation, differentiation into short-term plasmablasts for low-affinity IgM antibody production to ultimately clear pathogens and apoptotic debris) rapidly within hours after antigen exposure in contrast to FOBs which need several days to undergo GC reaction and APC generation. This is also facilitated because their recognized antigens (lipopolysaccharides, glycolipids, nucleic acids e.g., from bacteria) are less complex containing repetitive motifs therefore enabling extensive BCR cross-linking. Their pre-activated state can also be perceived *in vitro* where they proliferate more upon LPS or αCD40 stimulation than their follicular counterparts[14,15,17,21]. In contrast, FOB mainly react to T cell dependent (TD) antigens (also called T1 responses) and require T cell help to produce GCBs which mature into high-affinity APCs or memory B cells.

1.2.3 Mechanistic conceptions of the germinal center reaction

GC formation is initiated through cognate B cell activation by BCR-mediated recognition of soluble antigen or antigen bound to the surface of follicular dendritic cells (FDCs) in secondary lymphoid organs. In order to get fully activated, B cells thereafter migrate to the T-B cell border where they eventually receive additional $CD4^+$ T cell help favoring their survival and differentiation[22]. Upregulation of the master transcription factor BCL6 is indispensable for subsequent B cell trafficking into the follicle and later maintenance of the GC response. BCL6 inhibits among others the transcription of the anti-apoptotic gene *Bcl2* allowing massive apoptosis to occur in the GC, *Myc* and *Prdm1* suppressing APC differentiation[23–25]. BCL6-deficient mice lose GCB cells and high-affinity antibodies, however BCL6 must be shut off for differentiation beyond the GC stage[25–27]. MYC is also

essential for GC induction enabling G0-G1 to S cell cycle transitions. MYC is only expressed in a portion of GCBs at day 4 after antigen encounter, however its loss causes a collapse of GC structures. It is assumed that MYC dependent proliferation based on CyclinD2 and CyclinD3 of GCBs precedes the proliferation control of BCL6 mediated by CyclinD3 only[24,28–30].

Once established, a GC is anatomically structured into a dense dark zone (DZ, $CXCR4^{hi}$ $CD83^{lo}$ $CD86^{lo}$) localized closer to the T cell zone and composed of proliferating centroblasts as well as DZ FDCs and a less compact light zone (LZ, $CXCR4^{lo}$ $CD83^{hi}$ $CD86^{hi}$) made from centrocytes, follicular helper T cells (T_{FH}) and LZ FDCs. DZ/LZ polarization is among others ensured by CXCL12 expression of LZ FDCs attracting $CXCR4^{hi}$ DZ cells. GCBs enter the DZ during late S-phase of their cell cycle and exit after mitosis either re-entering the LZ again or leaving the GC reaction as APC or memory B cell. Somatic hypermutation (SHM) leading to increased antibody affinities occurs in the DZ and thereby potentially improved BCRs are later selected in the LZ[24,29–31].

The selection process in the LZ is facilitated by various means: first, cognate T_{FH} cells recognize the enriched density of antigen-MHCII complexes on high-affinity B cells in contrast to a low density in low-affinity B cells. They stimulate B cells through ICOS-ICOSL, CD40-CD40L interactions and IL21, IL4, BAFF cytokine secretion. Duration and intensity of this T cell "entanglement" is thereby decisive for the number of cell cycle divisions the B cell will undergo later upon re-entry into the DZ. The more divisions the B cell is programmed to undergo, the more frequent and dominating its BCR clone becomes (from minimal 2 cell divisions up to a "clonal burst"). Second, BCR selection in the LZ is facilitated by long-term presentation of antigen on MHCI or Fc receptors of FDCs. Thereby, antigen amounts are limited which further drives BCR competition. In addition, FDCs are key players of the GC reaction through their capacity to secrete cytokines including IL15, IL1β promoting GCB proliferation, IL6 driving CSR and IL10 initiating APC differentiation[24,29,30,32]. Antibody secretion e.g., from GC-experienced plasma cells further limits antigen access inside the GC reaction and thus dynamically drives antibody affinity selection pressure[33].

It is yet unclear, whether positive selection leads to apoptosis and eradication of low-affinity clones (death-limited selection) or whether all B cell clones undergo apoptosis to a certain degree, but high-affinity clones bypassing complete eradication through their ample proliferation in the DZ (birth-limited selection)[29]. However, in the end only

10 – 30 % of centrocytes are selected by T_{FH} cells and FDCs and continue to migrate into the DZ again. During these cyclic rounds of DZ expansion and LZ selection, high-affinity B cell clones progressively outcompete low-affinity B cell clones. Affinity thereby must be understood relative to the competing clones of one GC, rather than absolute. Neighboring GCs might communicate with each other through soluble antibodies, but otherwise represent rather separate and isolated entities of BCRs targeting eventually the same antigen. Although affinity enhances over time within a given GC, a certain diversity is nevertheless maintained by the recurrent entry of newly activated B cells into the LZ of already established GCs together with parallel maturation of possibly more than 100 distinct clones within a single GC locus[24,29,30,33].

Although historically described as distinct microenvironmental sites based on their histological appearance, the expression changes from DZ to LZ B cells are subtle and CXCR4 knockout for example does not repress GC progression. Therefore DZ/LZ distinguishment can also be understood as timed, transient cellular states transitioning smoothly from one state to the next[24,29,30,34]. This concept is acknowledged by more recent studies which distinguish another zone (DZp, $CXCR4^+$ $CD83^+$) splitting the DZ into two entities ("new" DZp and "old" DZd). This DZp zone includes cells with high pathway activity of MYC and mTORC1 fostering cell division also visible by an enhanced proportion of cells in S-phase and reduced SHM activity[28,35]. Hence, new technologies are revising our classical view of two compartments inside the GC and the discovery of more GC regulators will lead as well to a more accurate GC understanding[36].

1.2.4 Timing of the germinal center reaction

In an experimental setting using TD hapten antigens (e.g., NP-CGG), mice start to develop PNA^+ GCBs at day 4 after challenge with the antigen located in follicular structures in the white pulp of the spleen and maintain until 3 - 4 weeks after immunization. GCs reach their maximum size at day 10 - 14, but are already fully established including DZ/LZ formation by day 7. Even beforehand, PNA^-, but already antigen-binding B cells can be detected in foci (named also "GC-less primary follicles") close to the T-cell containing periarteriolar lymphoid sheat (PALS) surrounding arteries of the spleen (T cell zone). These foci arise at day 2 after immunization, increase in size until day 8 and then vanish from day 10 until day 16. Between day 4 and day 8 class-switched IgGs are detectable both in foci and GC. SHM is occurring in GC at an estimated rate of 10^{-3} / bp / division

detectable from day 8 onwards. B cells of foci can either migrate into GC follicles (also called “secondary follicles”) or differentiate further into APCs and memory B cells, however there is no evidence that GCBs commute between GC reactions later. T cells, same as B cells, get activated through antigen outside the GC reaction. They initially provide T cell help at the T-B cell zone border before they enter the secondary follicle by day 3[30,37–40]. Overall, duration of GC responses greatly varies between antigens with viral antigens, for example, eliciting a prolonged GC response in comparison to NP-haptens[41].

1.2.5 Class-switch recombination and somatic hypermutation

Class-switch recombination (CSR) and SHM dictate antibody effector functions and affinity maturation. Both processes are achieved directly or indirectly by the activation induced deaminase (AID) which deaminates deoxycytidine (dC) to deoxyuridine (dU) thereby initiating certain DNA repair mechanisms. AID is encoded by the gene *Aicda* whose transcription is dependent on cell activation cues including CD40 or TLR engagement leading to e.g., NFκB or MYC activation. Nuclear import and phosphorylation precede AID activity which is restricted to the G1 cell cycle stage and largely to the Ig locus to prohibit cell toxic genome-wide mutagenesis[42–44].

During SHM, excision of the dU resulting in an abasic site is repaired by the non-canoncial mismatch repair mechanisms (NcMMR) involving the error-prone translesion DNA polymerase η which generates transitions and transversions at the original G:C site. During CSR, AID addresses the G-rich switch (S) regions upstream of the Ig constant loci (Cγ3, Cγ1, Cγ2b, Cγ2a, Cε or Cα). dU appearance activates the base excision repair (BER) resulting first in DNA single-strand breaks and if close enough to each other double-strand breaks (DSBs) which are primarily repaired by the nonhomologous end joining (NHEJ) mechanism resulting in deletions of DNA located between switch regions[42–44].

Pre-requisite for AID activity is chromatin accessibility (hyperacetylation), recruitment to the RNA polymerase II complex and thus ongoing, but slowed-down transcription. How the preferential targeting of the Ig locus is maintained is not yet fully resolved, but mutagenesis occurs favorably surrounding the V gene promotors, downstream enhancers or the S regions. In addition, a bias in the utilization of serine triplet codons from TCN in the BCR framework to AGC/AGT in the CDRs 1 - 3 gives rise to the accumulation of SHMs within the antigen-recognizing parts of the antibody [42–44].

AID transcription starts to increase already 2.5 days after immunizations coinciding with class-switched antibody emergence. Hence while SHM begins at day 7 in fully established DZ B cells, CSR can already be completed before secondary follicle formation. CSR drops upon SHM initiation and which isotype switch occurs is dependent on the receiving cytokines, which can be mimicked *in vitro*. CSR is a timely limited process also demonstrated by the fact that IgM^+ B cells can enter the GC reaction, too[45–47].

1.2.6 Marker genes of the germinal center reaction

Commonly used markers to identify GCBs are the loss of IgD surface expression or staining with the carbohydrate-recognizing lectin peanut agglutinin (PNA) protein which binds to GCBs 10 - 30 times more efficiently than to other B lymphocytes[48]. A monoclonal antibody called GL7 can be used to recognize IgD^- activated B cells. GL7 binds to N-acetylneuraminic acid (Neu5Ac), the precursor form of N-glycolylneuraminic acid (Neu5Gc) which is presented on the surface upon repression of the Neu5Ac → Neu5Gc modifying enzyme Cmah. Within the PNA positively stained B cells, $GL7^+$ and $GL7^-$ fractions can be seen[49,50]. Furthermore, the TNF family receptor FAS is selectively expressed on GCBs which by interaction with FASL on T_{FH} in the LZ of the GC reaction mediates apoptosis of weakly antigen-binding B cells[51,52]. Additionally, in mice GCBs and APCs downregulate the surface glycoprotein and enzyme CD38 which is known to mediate Ca^{2+} flux and thereby promotes lymphocyte growth[53].

1.2.7 Antibody-producing cells

APCs are the cellular factories of the humoral immune response preserving the serum antibody titers of the blood[54]. Their nomenclature is not stringent in literature, however antibody-secreting, still dividing plasmablasts are the precursors of fully differentiated, noncycling short-lived or long-lived plasma cells[55]. APCs emerge through either (I) TI reactions from MZB or B1 cells, (II) TD reactions from activated B cells in an extrafollicular response or (III) TD reactions from GCBs. The type of antigen is thereby decisive for the dominance and duration of the individual pathway. APCs are attracted to the B-T cell border of the red pulp in the spleen, the medullary cords of lymph nodes or bone marrow niches through CXCR4-CXCL12 interactions concomitant with a downregulation of CXCR5 inhibiting follicular entry or retention[56,57].

IgM$^+$ APCs are detectable first at day 2 - 3 after immunization with TD haptenated reagents in foci of the spleen while IgG1$^+$ APCs develop 3 days later. Extrafollicular APC generation peaks at day 6 - 8, but declines until day 14 again due to cell apoptosis if the antigen is capable to elicit an additional follicular response (short-lived plasma cells)[41,58]. In case of antigens only triggering the extrafollicular APC pathway including certain viruses and bacteria, the response can sustain for several weeks up to months[41]. Extrafollicular APCs serve as first line of antibody defense against rapidly spreading pathogens using mostly low affinity antibodies which might be class-switched. Even though their initial antigen affinity seems less decisive for their generation, increased affinity promotes proliferation and decreases apoptosis especially in IgG1$^+$ APCs suggesting a selection process also during the extrafollicular response[41,57]. All isotypes of IgM or IgG antibodies can be produced from extrafollicular APCs by day 5 with frequencies of ~35 % for IgG1, ~10 % for IgM and 10 - 30 % for IgG2b, IgG2c or IgG3 upon HEL^{2x}-SRBC treatments shown by Chan et al.[57]. However, CSR occurs prior to APC differentiation[59].

Follicular-derived APCs are selected for their high-affinity and preferentially exit the GC in late phases outnumbering early generated lower affinity APCs[60]. Their exit occurs before the completion of their differentiation program[61]. They are capable to survive long-term in the niches of the bone marrow where they start to appear at day 10 - 14 and peak between day 21 and day 35 after immunization as determined by monoclonal reagents[62]. They are capable to survive for more than 90 days without cell division through the help of stromal cells secreting the survival factors BAFF and APRIL as well as IL6 which induces XBP1 and BLIMP-1 both being necessary for cessation of their cell cycle [56,63–65]. Even 10 years after vaccination, long-lived plasma cells can still be found in human bone marrow niches[63].

In general, B cells and APCs can be distinguished by exclusive transcriptional programs. For example, APCs are widely characterized by the transcription factors BLIMP-, IRF4 and XBP1. BLIMP-1 represses B cell specific BCL6 as does IRF4, as well as PAX5 and MYC. IRF4 is needed for CSR, the formation, but not the maintenance of the GC reaction, the direct induction of BLIMP-1 expression and is highest expressed in APCs compared to all other B cell developmental stages[66]. XBP1 is involved in the unfolded protein response necessary to deal with the vast immunoglobulin production in the expanded rough endoplasmic reticulum of APCs[55,65]. Further APC characteristics include downregulation of B220 and CD19 expression levels (B220^{lo} CD19^{lo}), intermediate MHCII expression with

levels ranging between MHCII^{lo} naïve B cells and MHCII^{hi} GCBs, gain of surface CD138 expression (Syndecan-1) capable of binding extracellular matrix and growth factors, switch from BAFFR to TAC-I and BCMA and surface expression of CXCR4 necessary for their homing to the bone marrow[58,65,67]. Up to now, no protein markers could be found to distinguish the origin of APCs derived from either an extrafollicular or a follicular response[61].

1.3 RNA-binding proteins as central regulators of the immune system

It is essential that the body's immune response is tightly regulated to allow the detection and elimination of pathogens, thereby ensuring the health of the organism. This requires efficient and timely controlled intercellular cross-talks as well as intracellular adaptation of immune cells to collectively enable their coordinated recruitment, activation and differentiation. Post-transcriptional gene regulation (PTGR) is a major mechanism to enable these rapid intracellular modifications according to the current needs of the immune response. PTGR is mediated among others by RNA-binding proteins (RBPs) which can govern manifold steps during RNA processing – splicing, editing, nuclear export, cytoplasmic localization, decay and translation – and thereby actively shape the resulting proteome[68,69]. Our current understanding of RBPs in immunity, their function, their targets and recognition sites is still very limited. It is even more challenging to capture the cooperative or competing effects of multiple RBPs which might regulate a shared target through binding (I) at the same or (II) at distinct *cis*-sites or might (III) mediate target accessibility by changing secondary RNA structures[70].

More than 1500 RBPs accounting for ~10 – 20 % of the human proteome across tissues were identified so far with almost half of them binding to mRNA. Transcription factors are assumed to make up 3 % of the proteome, underlining the relevance of RBPs to the cell[71]. RBP dysfunction can be associated with cancer, autoimmunity, inflammatory and metabolic disorders, but so far only nine RBPs were studied extensively in the context of immune diseases (ZFP36, AUF1, KSRP, TIA-1, Roquin proteins, Zc3h12 (Regnase-1), HuR, PTBP1, Arid5a) and only two thereof (HuR and PTBP1) are linked to GCB function which is of particular interest to this project[69].

Nuclear RBPs assist the process of alternative splicing which enlarges the number of available transcripts in lymphocytes by three-fold. Alternative splicing is cell-type specific and more than 90 % of the multiple-exon containing genes in human B cells were shown to be alternatively spliced[72]. For example, alternative splicing plays a crucial role during immunoglobulin class switching from IgM to IgD, IgM secretion and IgE isoform production[73]. HuR (also called ELAVL1) and PTBP1, are both involved in alternative splicing processes. Further diversification of the transcriptome is facilitated through RNA

editing including methylations (e.g., N^6-methyladenosine) or adenine to inosine mRNA modifications which affect RNA structure as well as splicing. Lastly, nuclear RBPs assist the export of polyadenylated mRNA and prepare them for further processing in the cytoplasm[74].

Cytoplasmic RBPs organize the subcellular location of mRNAs and potentially transport them to cytoplasmic RNA granules including processing bodies (P-bodies) or stress granules (SG). Their localization determines further steps including translation, storage or decay. Thereby, three different mechanisms for mRNA clearance can be classified. First, RBPs of the UPF family carry out non-sense mediated decay of erroneous mRNA including RNA bound to the exon junction complex (EJC), RNA with an improper 5' CAP structure or premature stop codons. Second, RBPs can interact with microRNAs (miRNAs) by competing or synergizing to degrade shared target mRNAs[68]. For example, Roquin 1 was shown to interact with miR-146a to jointly degrade the target mRNA ICOS in cooperation with the endonuclease AGO2[75]. By contrast, cytoplasmic HuR competes with the miRNA loaded miRISC complex thereby inhibiting miRNA-dependent decay. Third, RBPs can recruit proteins to remove the 5' CAP structure or the poly(A)-tail which both protect mRNAs from exoribonuclease activity of XRN1 family proteins. This includes the decapping proteins DCP1 and DCP2 which are getting activated by further proteins of the decapping complex including EDC4 as well as the poly(A) ribonucleases CCR4-NOT, PARN or PAN2-PAN3. ZFP36, for example, promotes CCR4-NOT recruitment and Roquin proteins destabilize their targets by interaction with either CCR4-NOT or EDC4 (Fig. 1)[68,76].

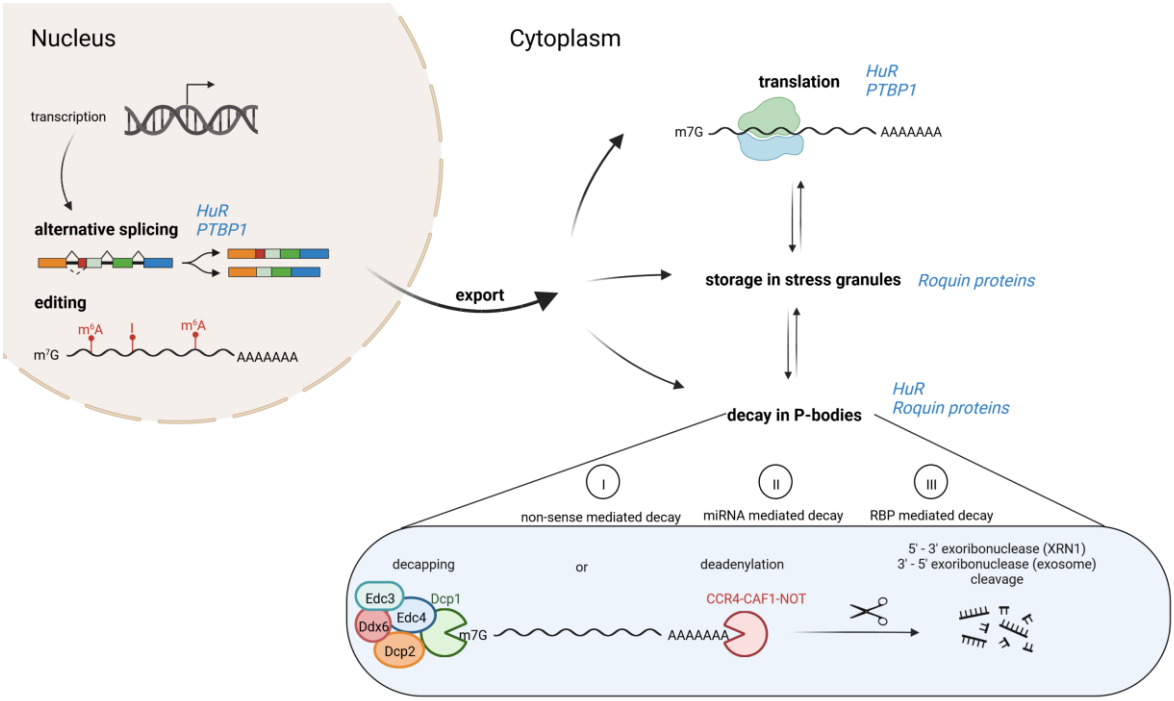

Figure 1: Overview of PTGR (adapted from Diaz-Munoz et al 2018)

The RBPs HuR and PTBP1 play an essential role for GCB biology and will thus be highlighted here in more depth.

Flow-cytometry analysis of HuR revealed elevated protein and mRNA expression levels in GCBs compared to non-GCB cells (~2-fold increase) and in *ex vivo* activated compared to non-activated B cells (~3-fold increase), respectively. B cell specific depletion mouse models (Mb1Cre $HuR^{F/F}$ mice) showed that B cells can mature normally in the absence of HuR, however GCB formation is drastically perturbed. This results in low immunoglobulin titers in these mice and diminished affinity maturation of antibodies upon immune challenge with T cell independent antigens. The observed reduction in GCB response (6-fold reduction at day 7 after immunization) might correlate with HuR interfering with cell metabolism upon B cell activation including promoting the expression of DLST (dihydrolipoamide S-succinyltransferase), an essential component of the TCA cycle. Thus, HuR deficient, but activated B cells fail to switch their metabolic program, as it is mandatory for proper GCB differentiation and proliferation, leading to increased reactive oxygen species (ROS) levels which ultimately cause B cell death[77,78].

Similarly, also PTBP1 mRNA and protein expression levels were shown to be increased in GCBs in comparison to non-GCBs (~1.5-fold increase) with B cell development not being impaired upon Mb1Cre mediated PTBP1 depletion. Homozygous ablation of the RBP resulted in diminution of GCBs and high-affinity antibodies as observed in Mb1Cre $HuR^{F/F}$ mice. PTBP1 is essential for proliferation especially for the transition of DZ GCBs through the S-phase of the cell cycle. Furthermore, its activity to regulate alternative splicing of c-MYC program related genes is important for LZ GCB positive selection[76,79].
RBPs including HuR and PTBP1 target hundreds of mRNAs. Hence, their dysregulation causes detrimental cellular defects and various disease outcomes. Especially HuR is well-studied in the context of inflammatory diseases including rheumatoid arthritis, facilitation of infectious diseases and promotion of tumorigenesis. HuR fosters cancer cell therapeutic resistance and is considered as a potential target for anti-tumor therapies[69,80].

Similarly, Roquin proteins were studied to affect GCB cell development with Roquin 1 mutations or CD19Cre ablation of Roquin 1 resulting in the expansion of GCBs[68,81]. The following chapters hence address Roquin proteins with a particular focus on B cell biology.

1.4 Roquin proteins

1.4.1 Protein structure

There are two Roquin paralogs termed Roquin 1 (Rc3h1) and Roquin 2 (Rc3h2 also known as membrane-associated nucleic acid binding protein Mnab), which are both ubiquitously expressed in mouse tissue with highest protein levels found in lymph nodes, thymus and elevated levels in spleen, lung and brain. In all tissue extracts as well as isolated lymphocyte cell populations, Roquin 1 was determined to be up to 5-times more abundant than Roquin 2 indicative for their deviating importance for cell functionality[82,83].

Roquin 1 and Roquin 2 emerged through a gene duplication event in vertebrates sharing a sequence similarity of > 80 % in N-terminal protein domains in mice and human as well as a high conservation between species (~75 % similarity compared to Roquin orthologues in *Caenorhabditis elegans* or *Drosophila melanogaster*). The two paralogues vary most in their C-terminus which contains several potential protein binding sites and thus might account for Roquin 1 and Roquin 2 diverging functions[84,85]. Two protein-coding transcripts

of Roquin 1 were detected which differ in their length of 5' and 3' untranslated regions (UTRs) and are translated into a full-length isoform of 1130 amino acids (AS) and a slightly shorter isoform of 1121 AS (~ 125 kDa). Similarly, three protein-coding transcripts of Roquin 2 with distinct 5' and 3' UTRs were identified resulting into 1125 AS or 1187 AS long protein isoforms (~ 131 kDa), respectively (Fig. 2). Although the functional roles of these varying protein isoforms were not investigated systematically so far, differential miRNA regulation in the UTR regions is expected[86].

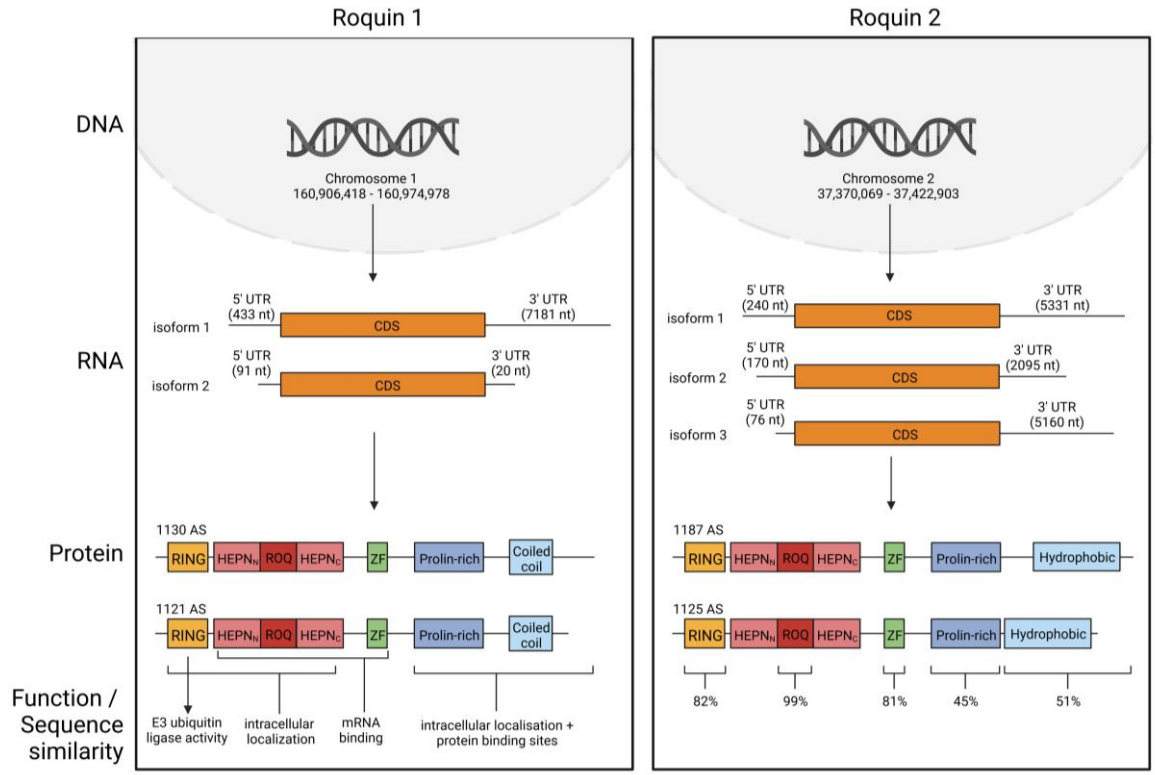

Figure 2: Roquin 1 and Roquin2 RNA transcript isoforms and protein domains (adapted from Pratama et al 2013 and Heissmeyer et al 2013)

Crystal structures of mouse and human Roquin 1 and Roquin 2 were resolved with a focus on the Roquin-determining ROQ domain which is necessary and sufficient for the property of the Roquin proteins to bind RNA. The ROQ domain can be further divided into three subdomains which all contribute to RNA binding, but distinguish between double-stranded RNA (dsRNA) or stem-loop RNA targets[87]. These three subdomains form two RNA binding sites which can bind RNA independently and simultaneously in Roquin 1 as well as in Roquin 2[88]. The N-terminal RNA binding region consists of a winged helix-turn-helix-like motif recognizing stem-loop structures while the helix-turn-helix motif of the C-terminal region interacts together with the adjacent HEPN (higher eukaryotes and prokaryotes nucleotide-binding) domains to enable dsRNA binding[89]. RNA

hairpin structures seem to be recognized rather by shape than sequence with triloops composed of a pyrimidine (Y)-purine (R)-pyrimidine motif being favored. These consensus decay elements (CDE) were identified in several well-known Roquin 1 targets and can now nicely be exploited experimentally (Fig. 3)[90,91]. Especially the tandem CDE stem-loop structure found in the 3' UTR of Nfκbid is very well recognized by Roquin 1 leading to a 475-fold enrichment of Nfκbid mRNA in Roquin immunoprecipitations[92]. Interestingly, Roquin proteins also regulate themselves through CDE elements in their respective 3' UTRs[92]. Although a complete inversion of the Y-R-Y motif to R-Y-R abolishes Roquin 1 interaction completely, minor mutations in the loop or the stem of the hairpin can be tolerated causing reduced ROQ binding affinities[90,91]. Transcriptome-wide studies identified ~3800 Roquin 1 mRNA targets in HEK293 cells containing > 16.000 potential binding sites. These binding sites were enriched, but not restricted to 3' UTR triloop hairpins with > 10 % occurrence in coding determining sequences (CDS) and a preference for U-rich binding sites also in hairpins containing 4 - 5 nucleotides within their loop structure[93]. Thus, ROQ binding is not limited to the consensus CDE and a versatile recognition of RNA structures might be crucial in the cell to enable fine-tuned mRNA regulation. mRNA binding is further stabilized through the minimal CCCH zinc finger motif which is not capable of specific Roquin mRNA binding on its own[84]. Finally, the ROQ domain facilitates concentration dependent Roquin 1 dimerization *in vitro* which might also play a role *in vivo* or during RNA duplex binding[91].

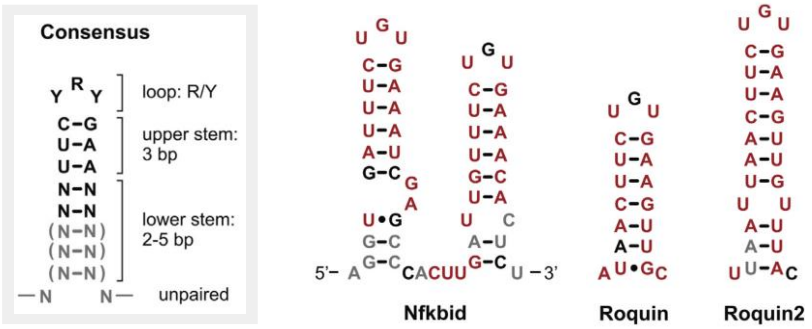

Figure 3: Roquin CDE consensus sequence and targets (adapted from Leppek et al. 2013)

The ROQ domain is connected up- and downstream by flexible linker regions to the $HEPN_N$ and $HEPN_C$ domains. The upstream RING (really interesting new gene) domain is essential for Roquin function since domain specific deletions in mice (*Rc3h1 ringless* 133 - 1130) cause phenotypes similar to complete protein knockout (KO) mice. This can be explained by defects in their intracellular localization upon ablation of the RING domain. Thereby, the RING domain acts in concert with the C-terminus as depletion of both RING

and C-terminal sequences (138 - 337 or 138 - 484) can rescue incorrect cytoplasmic localization. In addition, the RING domains marks Roquin proteins as potential E3 ubiquitin ligases. Although the biological consequences thereof are less understood, initial *in vitro* studies or research in worm point towards a capacity of Roquin proteins to interact with E2 enzymes driving polyubiquitination. Whether there is a cross-talk between Roquin proteins-caused protein degradation and mRNA decay activity remains to be clarified[86,88,94]. Studies on Rc3h1^{RINGLESS} have among others proven functional redundancies between Roquin 1 and Roquin 2 with Roquin 2 being able to partially compensate for Roquin 1 depletion. Conversely, defects in Roquin 1 are enhanced by simultaneous defects in Roquin 2[85].

1.4.2 Intracellular localization and protein interaction partners

Roquin proteins regulate mRNA stability and can induce mRNA degradation. This occurs in cytoplasmic processing bodies (P bodies) as well as stress granules (SG). Both are nonmembranous cytoplasmic foci formed dynamically out of messenger ribonucleoprotein particles (mRNPs) able to rapidly adjust cellular translation to promote cell survival under stress conditions including infection, hypoxia or mitochondrial stress. P bodies and SG are distinct from each other in composition and hence function, but close spatial proximity can allow for component exchange including the shuttling of Roquin proteins. Whereas P bodies are constitutively present in some cell types, both P bodies and SGs are induced upon cellular stress. P bodies contain mainly deadenylated RNA and proteins involved in mRNA decay or silencing. In contrast, SGs are composed of mRNAs disassembled from polysomes which are kept translationally silent to store them until cellular resources permit their further processing after a successful cellular stress response. The compartmentalization into SGs is therefore thought to favor translation of stress proteins including heat-shock proteins over others such as house-keeping genes to enhance cell survival. In addition to their function in mRNA metabolism, SGs separate RNA and signaling proteins from the rest of the cytoplasm enforcing altered signaling cascade outcomes[95–97].

Independent studies have shown colocalization of both Roquin proteins with the helicase RCK as a marker of P bodies and TIA-1 or eIF3 as markers of SGs in HEK293T or $CD4^+$ T cells. Roquin 1 overexpression itself can trigger SG formation in HEK293T cells

independent of additional chemical treatments and N-terminal protein domains including ROQ and RING are sufficient for SG localization[84]. Roquin proteins interact with components of the decapping pathway such as RCK and EDC4 in P-bodies[98]. Additionally, interaction with all components of the CCR4-NOT deadenylase complex and RNA-independent binding of Roquin 1 to CNOT1, CNOT8, NOT1 and CAF1a were validated by co-immunoprecipitation. Thereby, CAF1a and NOT1 binding are facilitated through the C-terminal domain[92]. Hence, Roquin proteins mediate target mRNA destabilization by recruitment of mRNA degrading protein complexes[93].

1.4.3 Roquin sanroque mice

Roquin 1 was first described in 2005 by Carola Vinuesa et al. during an ethylnitrosourea screen trying to identify autoimmunity-causing single-nucleotide polymorphisms (SNPs) in C57BL/6 mice. Mice carrying a homozygous T > G mutation leading to a Methionine 199 > Arginine (M199R) amino acid exchange in the ROQ domain of Roquin 1 presented with a phenotype resembling SLE in human. The mice were named "*sanroque*" referring to the patron saint of plagues (San Roque) who is told to have cured the victims of the bubonic plague that suffered from swollen lymph nodes as these mice do, too. Their enlarged lymph nodes are accompanied by hepatitis, glomerulonephritis with immune complex deposition and blood disorders including plasmacytosis, anemia and thrombocytopenia which are all also relevant to the human disease. Furthermore, sanroque mice display splenomegaly, hypergammaglobulinemia and antinuclear ANA production[3,99]. By contrast, heterozygous $Rc3h1^{san/+}$ mice do not develop full blown autoimmune characteristics[100]. These and subsequent studies showed that the lupus-like pathology of $Rc3h1^{san/san}$ mice is driven by T cells. Therefore, Roquin is a crucial mediator of peripheral T cell tolerance.

$Roquin^{san/san}$ mice display 3-fold elevated T_{FH} levels ($CD4^+$ $CXCR5^+$ $PD1^{hi}$ $BCL6^+$) even in unimmunized mice which triggers 2-fold increased IL21 cytokine secretion levels and an expansion of GCBs through augmented T cell help. Reduction of T_{FH} cells in numbers and efficacy by knockout of the intracellular adaptor molecule SAP, downstream of the TCR ($Rc3h1^{san/san}$ $SAP^{-/-}$ mice), abrogates some of the autoimmunity symptoms including ANA production and GC formation, albeit phenotypic changes as hypergammaglobulinemia and splenomegaly remain. On the contrary, knockout of IL21 ($Roquin^{san/san}$ $IL\text{-}21^{-/-}$ mice) has no rescue capability although IL21 plays a crucial role for T_{FH} generation[101,102]. Ablation of

GCB cells production through depletion of OBF1 (Rc3h1$^{san/san}$ OBF1$^{-/-}$ mice) likewise does not constrain autoimmunity, but instead causes even diminished survival rates. OBF1 (Oct-binding factor 1) is a transcription factor influencing the differentiation of naïve B cells into GCBs upon T-cell dependent antigen stimuli and therefore OBF1 deficient mice lack GCBs[103,104]. Rc3h1$^{san/san}$ OBF1$^{-/-}$ mice have equally enlarged spleens as Rc3h1$^{san/san}$ mice caused by non-B cells and show massive production of ANAs, especially anti-dsDNA IgM[105]. These IgM ANAs are likely to be derived from extrafollicular APCs or B1 cells[89].

On a molecular level, sanroque CD4^{+} T cells were shown to be enriched for the inducible T cell costimulatory protein (ICOS). ICOS is a CD28 paralogue whose surface expression is induced under wildtype (WT) conditions by T cell activation mediated from the TCR together with co-stimulatory molecules including CD28. ICOS binds its ligand ICOSL on antigen-presenting cells including B cells providing B cell help for further GC maturation. Aberrant T-B cell interaction via ICOS has been linked to lupus in mice[106] and human[107] promoting among others T_{FH} cell survival. Overt ICOS surface presentation also independent of strong T cell activation cues bypasses the natural hurdle of T_{FH} differentiation upon self-reactive antigen recognition[99]. Splenomegaly, lymphadenopathy, T_{FH} and GCB expansion in sanroque mice are attenuated upon additional hemizygous ICOS knockout (Rc3h1$^{san/san}$ ICOS$^{+/-}$ mice) and a direct interaction between the RBP Roquin 1 and ICOS mRNA could be validated[98,108]. Taken together, these results point towards a crucial role of Roquin 1 in prohibiting excessive T_{FH} accumulation through ICOS regulation. Nevertheless, neither heterozygous nor homozygous depletion of ICOS in sanroque mice can completely reverse the autoimmunity phenotype. Rc3h1$^{san/san}$ ICOS$^{-/-}$ on the contrary even present with increased splenomegaly compared to Rc3h1$^{san/san}$ and still produce ANAs which might be caused by deficiency of regulatory T cells (T_{reg})[109]. Therefore, other signaling pathways have been explored to contribute to the lupus development of sanroque mice.

Roquin 1 modulates IFNγ secretion in T_{FH} as well as T effector-like cells. IFNγ serum levels increase over time in Rc3h1$^{san/san}$ mice starting with disease onset at the age of 6 - 7 weeks and range above WT animals. Blockage of IFNγ signaling either by a full-body knockout of the IFNγ receptor (Rc3h1$^{san/san}$ IFNγR$^{-/-}$ mice), anti-IFNγ treatment or chimeric mouse reconstitution using IFNγR deficient T cells results in a reduction of T_{FH} and GCB cells to varying extents compared to sanroque control animals. Mechanistically, enhanced IFNγ signaling upon Roquin 1 mutation is thought to drive BCL6 expression and thereby

T_{FH} formation and maintenance which could be proven to be a solely T cell intrinsic and not B cell driven process[109]. Yet, heterozygous loss of BCL6 (Rc3h1$^{san/san}$ BCL6$^{+/-}$ mice) still leads to anti-dsDNA ANA formation albeit GCB formation decreases by 2-fold[101].

Beyond T_{FH}, Rc3h1$^{san/san}$ mice also contain enriched numbers of short-lived effector-like CD8^{+} T cells (SLECs; CD8^{+} KLRG1^{hi} CD62L^{lo} CD44^{hi})[110]. Their natural function is to liberate the body from virus-infected cells by secretion of cytotoxic perforin and granzymes and to initiate an innate immune response as well as to regulate their own expansion by IFNγ production. However, they also play a role in autoimmune tissue damage as occurring in diabetes patients[111]. Rc3h1$^{an/san}$ and hemizygous Rc3h1$^{san/san}$ IFNγ$^{+/-}$ revealed the potential of Roquin 1 to mediate CD8^{+} T cell homeostasis by restricting IFNγ mRNA levels which negatively affects SLEC accumulation and function and ultimately reduces the susceptibility to develop autoimmune diabetes[110].

The M199R mutation causes structural changes which do not prohibit RNA recognition or correct cytoplasmic localization[89]. Therefore, Roquin 1 targets including ICOS and IFNγ are still bound by M199R Roquin 1, however their degradation through Roquin 1-mediated recruitment of CCR4-NOT complex is impaired yet not completely abolished. In addition, direct interaction with the RBP Regnase-1 is abolished upon M199R mutation in Roquin 1 which impacts their cooperative regulation on shared mRNA targets such as ICOS[112]. Thus, the sanroque mutation leads to divergent biological outcomes compared to Roquin 1 knockout mouse models where Roquin 1 activity is fully abrogated but can partially be compensated again by Roquin 2[84,113]. Although current knockout mouse models do not recapitulate the autoimmunity phenotype of sanroque mice, still they are an ideal tool to study Roquin proteins tissue-specifically and serve to gain a better understanding of Roquin 1 and Roquin 2 interplay.

1.4.4 Roquin in T cells

Initial Roquin knockout studies performed by Bertossi et al. demonstrated that a full body knockout of Roquin 1 (Rc3h1$^{-/-}$ mice) is lethal in C56BL/6 background mice probably also due to a defective lung function immediately within 6 hours after birth[81]. Similarly, almost all Roquin 2 complete knockout C56BL/6 animals die within few days and present as well with impairment of proper lung function[83].

$CD4^+$ T cell specific knockout of Roquin (CD4Cre $Rc3h1^{F/F}$ mice) is unable to recapitulate the sanroque autoimmunity phenotype although elevated ICOS expression levels and elevated numbers of SLEC $CD8^+$ T cells could still be observed[81]. No immune defects were monitorable in CD4Cre $Rc3h2^{F/F}$ mice hinting towards the more prominent role of Roquin 1 compared to Roquin 2 correlating with their different expression intensities. However, combined knockout of both Roquin proteins (CD4Cre $Rc3h1^{F/F}$ $Rc3h2^{F/F}$ mice) adds an expansion of $CD4^+$ effector-like $CD44^{hi}$ $CD62L^{lo}$ T cells, T_{FH} cells and GCBs as well as splenomegaly and lymphadenopathy to the phenotypic characteristics seen in Roquin 1 single knockout animals. This underscores the relevance of Roquin 2 compensation despite its low expression level which is even unchanged upon Roquin 1 depletion in T cells[83].

In contrary to full body Roquin depletion mouse models, CD4Cre $Rc3h1^{F/F}$ $Rc3h2^{F/F}$ mice reach adulthood, however their lung physiology worsens over time with accumulating inflammatory processes, infiltration by APCs and thickening of artery walls resulting in a median survival of only 130 days. The precise underlying cause for their lung pathology is not yet identified, however serum levels revealed increased amounts of IL17A, IL6, TNF, IL10, but not IFNγ. Additionally, lung tissues of Roquin knockout mice were enriched for IL17A producing $CCR6^+$ cells and $CD4^+$ $ROR\gamma t^+$ cells pointing towards an accumulation of T_H17 cells[114]. Differentiation of T_H17 cells is induced by a cytokine milieu consisting of TGFβ, IL6, TNF and IL1β with TGFβ and IL6 being the key drivers of one of the lineage-determining transcription factors RORγt. T_H17 produce proinflammatory cytokines including IL21, IL17A, but also limit their own inflammatory effect by secretion of IL10[115]. CCR6 has been proposed to be relevant to T_H17 migration into inflamed tissue[116]. T_H17 cells dysregulation is found in many diseases including allergic asthma[115]. *Ex vivo* culturing of $CD4^+$ T cells under different stimuli revealed a 2-fold increased potential of Roquin 1 and Roquin 2 knockout cells to differentiate into IL17A producing T_H17 cells and reduced capability to produce $IL4^+$ T_H2 or $FoxP3^+$ T_{reg}. These data support that Roquin proteins are involved in T_H17 differentiation. Moreover, IL6, a mediator of T_H17 formation, was discovered to be post-transcriptionally regulated by Roquin 1[114].

Very recent findings connect Roquin 1 to $CD8^+$ T cell expansion and anti-tumor immunity. Cytotoxic $CD8^+$ T cells are being exploited during adoptive T cell transfer therapy against cancer raising interest to find optimized solutions to trigger their expansion *in vitro* and especially *in vivo*. Whole-genome CRISPR-Cas9 screens performed in activated OT-I cells revealed 2642 genes substantially regulating $CD8^+$ T cell survival and proliferation in mice. As a surprise to the authors, Roquin 1 ranked highest in their *in vivo* screen, even

higher than well-known tumor suppressors p53 and PTEN. Roquin 1 was shown also in subsequent experiments to efficiently limit $CD8^+$ T cell accumulation. Roquin 1 was reported to inhibit S-phase cell cycle progression since loss of Roquin 1 substantially increased the fraction of EdU^+ T cells *in vivo* and RNA sequencing GSEA analysis of Roquin 1 deficient $CD8^+$ T cells showed enrichment of cell cycle, G2M checkpoint and mitotic spindle gene sets. Besides this being a first study directly linking Roquin function to cell cycle, the authors further showed that Roquin 1 ablated OT-I cells possessed an enhanced ability to control EL4-OVA lymphoma tumor outgrowth[117]. Similarly, Roquin 1 mutants such as $Rc3h1^{san/san}$ expressed in OT-I $CD8^+$ T cells can attenuate tumor growth in a B16-OVA mouse model[112]. Roquin 1 connection to cell cycle progression and tumor suppressor function were confirmed in parallel studies specifically proposing a role of Roquin 1 in G1 to S transition through targeting of cell cycle promoting genes including CCNE1, CCND1, CDK6 and MCM2. Thereby, low Roquin 1 expression amounts were correlated with poor survival of breast cancer patients[118].

1.4.5 Roquin mutation in human

Beyond the murine immune system, a homozygous $R688^*$ mutation residing in the C-terminus of Roquin 1 leading to a truncated protein was described in a patient suffering from chronic inflammation resembling hemophagocytic lymphohistocytosis (HLH) without signs of autoimmunity. The mutation was shown to be hypomorphic with altered effects compared to the M199R sanroque mutation. Human $R688^*$ Roquin 1 or its murine counterpart $R687^*$ both fail to localize to P bodies, but can still be recruited to SGs. Their interaction with CCR4-NOT, but not Edc4 is abolished and target mRNAs including OX40 and ICOS are stabilized even more compared to M199R *in vitro*. The authors speculate that the R688* truncation reduces Roquin 1 functionality more drastically than the M199R mutation promoting inflammatory processes rather than autoimmune development as seen in this patient. This hypothesis is further based on the fact that the $R688^*$ heterozygous parents both suffer from autoimmune diseases. However, more research is needed to dissect the precise consequences of this graded Roquin 1 activity also in interplay with Roquin 2 in order to understand its contribution to the generation of either autoimmune, inflammatory or cancerous diseases[2].

Nevertheless, manifold analogies between this patient and Roquin mouse models could be detected. The patient was diagnosed with splenomegaly and lymphadenopathy. With

regard to adaptive immune cell populations, effector $CD4^+$, $CD8^+$ T cells and T_{reg} were expanded and naïve $CD4^+$ T cells were depleted. B cells containing a signature also found in SLE patients ($CD20^{hi}$ $CD11c^+$ $CD24^-$ $CD27^-$ $CD38^-$ $CXCR5^-$ IgD^+) were enriched and naïve B cells were overrepresented. This B cell maturation defect was further validated also in sanroque chimera. Corresponding to sanroque mice, increased cytokine release of IL6, IFNγ and TNF was detected. In addition, IL17A levels and T_H17 cells were elevated as seen before in CD4Cre $Rc3h1^{F/F}$ $Rc3h2^{F/F}$ mice. To summarize, the described Roquin mutation is very likely to be causal for the familial disease and, particularly interesting to this project, the authors provided a hint for the relevance of Roquin in human B cell development[2].

1.4.6 Roquin in B cells

Ablation of Roquin 1 in the hematopoietic system (VavCre $Rc3h1^{-/-}$ mice) gave first evidence for the role of Roquin 1 outside the T cell compartment. B cell specific homozygous Roquin 1 knockout (CD19Cre $Rc3h1^{F/F}$ mice), but not heterozygous ablation, results into a higher spleen cellularity caused by an increase of B cells, T_{reg}, $CD4^+$ and $CD8^+$ effector-like cells and eosinophils[81].

Unpublished work of Dr. David Riess in our laboratory shed light on the role of Roquin in early B cell development (CD19Cre mediated knockout of Roquin 1 and Roquin 2 in B cells). CD19Cre mouse lines exploit Cre recombinase expression under the control of the CD19 promotor which is activated at the pre B cell stage and results in a deletion frequency of 75 - 80 % in pre B cells and 90 - 95% in mature B cells[119]. Upon CD19Cre based Roquin 1 and Roquin 2 ablation (CD19Cre $Rc3h1^{F/F}$ $Rc3h2^{F/F}$ mice), B cell differentiation defects were detected first in splenic mature B cells while bone marrow B cell development was unperturbed. Later differentiation stages (transitional cells, FOB, MZB) were diminished in CD19Cre $Rc3h1^{F/F}$ $Rc3h2^{F/F}$ mice underlining the importance of Roquin paralogues for B cell maturation. CD19Cre-mediated depletion of Roquin proteins resulted in mild counterselection of mature knockout B cells. In line with previous publications, B cell extrinsic effects were monitored and an increase in effector-like T cells as well as T_{regs} was detected. Furthermore, *ex vivo* isolated splenic Roquin 1/2 protein knockout B cells appeared to be hyperactivated based on surface detection of CD25, CD69, CD80, CD86 and MHCII. However, they were unable to equally upregulate these activation markers further upon BCR-dependent stimuli (αIgM or αCD40) to match the

levels of control cells. The underlying reason for this hypoactivated status remains to be explored[82]. Gaining a more in-depth understanding of the influence of Roquin on B cell activation which is also essential for GCB formation and subsequent antibody production is therefore also part of this thesis. Connecting to the research done by David Riess, Roquin studies in CD19Cre mice were further expanded to CD19Cre Rc3h1$^{F/F}$ Rc3h2$^{F/+}$ and CD19Cre Rc3h1$^{F/F}$ mice in order to address the relevance of gene-dosage and Roquin 2 compensation for splenic B cell development.

1.4.7 Roquin mediated regulation of NFκB signaling

In vivo as well as *in vitro* studies confirmed the essential role of Roquin proteins in regulating NFκB signaling. NFκB signaling is classically divided into the canonical and non-canonical (or alternative) pathway with both pathways playing manifold roles in health and disease whereby their signaling outcome is very much cell type dependent. Conceptually, the NFκB pathways are composed of five transcription factors - p105/p50, RelA, c-Rel (canonical pathway) and p100/p52, RelB (non-canonical pathway) - which can form homo- or heterodimers. In unstimulated cells, these dimers are retained in the cytoplasm through binding to NFκB inhibitors (IκBα/ß/δ/ε/ζ, Bcl-3, IκBNS) which mask their nuclear localization signal (NLS). Stimulation of cells activates an internal signaling cascade resulting through different ways into activation of the trimeric IκB kinase (IKK) complex (IKKα, IKKß, IKKγ also called NEMO) which leads to phosphorylation and ubiquitylation of the NFκB inhibitors. Proteasomal degradation of the NFκB inhibitors subsequently releases the NFκB transcription factors which are then free to shuttle into the nucleus. Receptors involved in canonical NFκB activation are members of the tumor necrosis factor receptor (TNFR) family, TLR/IL-1R family or antigen receptors of T and B cells. The non-canonical NFκB pathway gets stimulated through TNF receptors, too. Activation patterns, complex formation, kinetics and negative feedback regulation distinguish the two pathways further[120–122].

Several NFκB pathway members were found to be regulated by Roquin proteins and loss of Roquin proteins results in distinct perturbances of the signaling cascade. Vogel et al. identified OX40 as Roquin 1 target and detected elevated RelB protein amounts and drastically increased nuclear levels of p52 upon CD4Cre mediated knockout of both Roquin 1 and 2[83]. OX40 (also called TNFRSF4 or CD134) is part of the TNFR family providing a costimulatory signal in addition to TCR activation which fosters T cell

proliferation, cytokine secretion and effector cell differentiation. In addition, OX40 promotes CXCR5 expression which is needed for T cell migration towards the B cell zone of the follicle and early T_{FH} cell differentiation. Both OX40 and ICOS are capable to activate PIP3K pathway signaling supporting IL21 expression[123–125]. Aberrant OX40L expression in myeloid antigen-presenting cells acting excessively on OX40 in T cells ultimately triggers an antibody response which was also connected to poor prognosis of autoimmune diseases including SLE[126].

The alternative NFκB pathway drives expression of the transcription factor IRF4 which could be demonstrated to be augmented on the transcript and protein level of Roquin 1/2 deficient T cells. As a positive feedforward loop, IRF4 is capable to affect ICOS by binding to its promotor regions[83,86,127]. The atypical NFκB proteins NfκBid (or IκBδ) or NfκBiz (or IκBζ) are widely recognized Roquin 1 targets together with IER3 which binds IκBα, IκBα itself and c-REL[92,93,114]. Moreover, Roquin 1 destabilizes the ubiquitin-editing enzyme A20 (or TNFAIP3) which interferes with NFκB signaling at multiple possible steps ultimately acting as a negative feedback regulator. Assays in TNFα treated HEK293 cells for example, showed elevated levels of A20 and reduced phosphorylation of IKK upon Roquin 1 siRNA knockdown[93]. However, the net outcome of the multifaceted regulation of the NFκB pathway by Roquin 1 cannot be generalized and always needs to be examined context dependently.

2 Aim of the Study

RNA-binding proteins are key regulators of all steps in RNA life and therefore control protein abundance and cell fate. Their malfunctioning is associated with severe hematopoietic malignancies, autoimmunity, inflammatory and tumorigenic diseases which leads to a growing interest in the field to better understand the multidimensional nature of their effector functions[1,69,128].

Roquin 1 and Roquin 2 are two RNA-binding proteins dictating mRNA decay and limiting T cell responses[3,7]. Although evidence suggests roles of Roquin proteins also in B cell differentiation, this branch remains so far under investigated[2,81].

Consequently, this project aimed to study the relevance of Roquin 1 and Roquin 2 in B lymphocytes focusing on late B cell differentiation. To achieve this goal, I wanted to perform an in-depth analysis of germinal center and antibody-producing B cells in suitable mouse models. In addition, I aimed to investigate the influence of Roquin proteins on hallmarks of the germinal center reaction including somatic hypermutation and class-switch recombination. Last, I planned to gain molecular insights by an *in vitro* RNA sequencing approach.

3 Materials and Methods

3.1 Instruments

Device	Utilisation	Brand
autoMACS Pro Separator	Automated cell separation	Miltenyi Biotec
BD Aria III	Flow cytometry sorter	Becton Dickinson
Countess II FL	Automated cell counter	Life technologies
Cytoflex S	Flow cytometry analyzer	Beckman Coulter
Cytoflex LX	Flow cytometry analyzer	Beckman Coulter
Nanodrop	DNA concentration measurements	Thermo Scientific
Neon Transfection System	Electroporator	invitrogen
MoFlo Astrios EQ	Flow cytometry sorter	Beckman Coulter
QuantStudio 1	Real-Time PCR System	Applied Biosystems
Qubit 2.0 Fluorometer	DNA/RNA quantification	Thermo Fisher
Spark	ELISA Reader	Tecan

Table 1: Instruments

3.2 Buffers and Media

Buffer	Ingredients
A20 cell culture medium	500 mL RPMI-1640 GlutaMax Supplement 10% heat-inactivated fetal calf serum (FCS, Sigma F0804, LOT BCCC4773) 1% Penicillin-Streptomycin (PenStrep) 2.5% HEPES 1% 200 mM L-Glutamine 0.5 mL 50 mM 2-Mercaptoethanol
Carbonate buffer 0.1 M, pH = 9.5	3.56 g $NaHCO_3$ 0.796 g Na_2CO_3 Fill up to 500 mL with dH_2O
CB buffer	500 mL 1x DPBS 2% heat-inactivated FCS 2 mM EDTA 1% PenStrep
FACS buffer	500 mL 1x DPBS 2.5 g BSA 0.01% NaN_3

Table 2: Buffers and media

Buffer	Ingredients
Geys‘ solution	14 mL dH_2O + 4 mL Solution A + 1 mL Solution B + 1 ml Solution C Solution A: 654 mM NH_4Cl 24.8 mM KCL 4,2 mM Na_2HPO_4 * 12 H_2O 8.8 µM KH_2PO_4 27.7 mM glucose 0.05 g phenol red fill up to 1 L with dH_2O Solution B: 20.7 mM $MgCl_2$ * 6 H_2O 5.68 mM $MgSO_4$ * 7 H_2O 30.6 mM $CaCl_2$ fill up to 100 mL with dH_2O Solution C: 268 mM $NaHCO_3$ fill up to 100 mL with dH_2O
Homemade genotyping buffer	100 µl 1 M Tris-HCL pH = 8,8 (final 100 mM) 500 µl 1 M KCL (final 500 mM) 150 µl 100 mM $MgCl_2$ (final 15 mM) 20 µl 100 mg/ml BSA (final 2 mg/ml) 10 µl 100% Triton X-100 (final 1%) Fill up to 1 ml with dH_2O Store at -20ºC
Mastermix genotyping buffer	20.95 µl dH_2O 3 µl homemade genotyping buffer 0.3 µl 100 mM $MgCl_2$ 0.5 µl 25 mM dNTPs
Running buffer	1920 mM Glycin 250 mM Tris 1% SDS fill up to 1 L with dH_2O
Stripping buffer	100 mL 100% methanol 100 mL 100% acetic acid fill up to 1 L with dH_2O
TBS 10x, pH = 7.5	500 mM Tris 1500 mM NaCl fill up to 1 L with dH2O
Transfer buffer	3.5 L dH2O 1 L methanol 0.5 L 10x running buffer

Table 2 (continued): Buffers and media

3.3 *In vivo* analyses

3.3.1 Housing of genetically modified mice

All mice described in this project were bred on a C57BL/6J genetic background. Mice were housed in specific pathogen-free animal facilities of the Center of Preclinical Research, TranslaTUM in Munich or facilities of Charles River Calco in Italy. All animal procedures were approved by the government of upper bavaria (licence no. 55.2-1-54-2532-234-2015). For experimental purposes, mice were sacrificed using isoflurane and cervical dislocation at an age of 8 weeks to maximum 17 weeks.

3.3.2 Alleles of genetically modified mice

For the scope of this PhD thesis, mouse alleles were combined in a new fashion, however all alleles have been published before individually.

Rc3h1 (Rc3h1tm1.1Mass)
An FRT-flanked neo cassette containing a 5' loxP site was inserted upstream of exon 4. An additional loxP site was inserted downstream of exon 6. Flp-mediated recombination removed the neo cassette and thus the sections of exon 4 to 6 are present floxed[81].

Rc3h2 (Rc3h2tm1c(KOMP)Wtsi)
The L1L2_Bact_P cassette was inserted at position 37411698 of chromosome 2, up-stream of the critical exon(s) (build GRCm38). The cassette consists of an FRT site followed by a lacZ sequence and a loxP site. The first loxP site is followed by a neomycin resistance gene under the control of the human beta-actin promoter, SV40 polyA, a second FRT site, and a second loxP site. A third loxP site is inserted downstream of the critical exon(s) at position 37410914. The critical exon(s) is thus flanked by loxP sites. A "conditional ready" (floxed) allele was generated by flp recombinase expression in mice carrying this allele[83].

CD19Cre (B6.129P2(C)-Cd19tm1(cre)Cgn/J; Jackson Stock No.: 006785)
A targeting vector containing Cre recombinase, the rabbit beta-globin intron/poly-A signal sequence, and an FRT-flanked neomycin resistance gene was used to disrupt exon 2 of the

CD19 gene and express Cre under endogenous promoter regulation. The herpes simplex virus thymidine kinase gene was placed 3' of the CD19 sequence to allow selection against random integration[129]. (Jackson Laboratories mouse strain 006785)

Cγ1Cre (B6.129P2(Cg)-Ighg1tm1(IRES-cre)Cgn/J; Jax Stock No.: 01611)

A targeting vector containing an IRES-cre was inserted into the 3' region of the Cγ1 locus between the last membrane-encoding exon and its poly-adenylation sites. This targeting design allows for the expression of a bicistronic mRNA consisting of the Cγ1 and Cre transcripts from the locus. An frt-flanked neo was removed via FLP recombinase expression[47].

CAR (Gt(ROSA)26Sortm1(CAG-CARΔ1(StopF))

A cDNA encoding human CARΔ1 4 (CARdelta1, aa 1-262) was inserted into the R26 locus under conditional control of a CAG promoter (conditional knock-in). CARΔ1 is expressed after recombination with a Cre recombinase of a loxP-flanked STOP cassette[130].

tdTomato (B6.Cg-Gt(ROSA)26Sortm9(CAG-tdTomato)Hze/J)

Knockin of a CAG-lox-Stop-lox-tdTomato allele between exon 1 and 2 of the Rosa26 locus. The expression of the fluorescent protein tdTomato (dTOM) is suppressed by a stop cassette, which can be removed by Cre-recombinase. Genes expressed from the Rosa26 locus have no known function[131,132].

Crossing of heterozygous CD19Cre ($CD19Cre^{I/+}$) or heterozygous Cγ1Cre ($Cγ1Cre^{I/+}$) expressing mice to loxP flanked Rc3h1 and Rc3h2 containing animals enabled B cell specific ablation of Roquin proteins in early or late B cell development, respectively. Thereby, Roquin 1 homozygous knockouts ($Rc3h1^{F/F}$) were combined with all three possible zygosities of Roquin 2 ($Rc3h2^{F/F}$, $Rc3h2^{F/+}$, $Rc3h2^{+/+}$) to study the effect of Roquin 1 deletion with or without additional Roquin 2 deficiencies. The fluorochrome tdTomato ($dTOM^{I/+}$) served as reporter in $Cγ1Cre^{I/+}$ expressing animals facilitating an indirect monitoring of Roquin knockout efficiencies. Equally, the presence of heterozygous CAR ($CAR^{I/+}$) in $CD19Cre^{I/+}$ mice allowed flow cytometry-based analysis of Roquin ablation in target B cell populations. Roquin knockout animals were analyzed in concert with age matched control animals which most of the time were determined as $CD19Cre^{I/+} \pm CAR^{I/+}$ or $Cγ1Cre^{I/+} \pm dTOM^{I/+}$ by genotyping. Only when urgently needed Roquin knockout animals ± reporter, but without Cre expression were used instead. This did not result in inconsistent biological readouts.

3.3.3 Genotyping of genetically modified mice

Genotyping polymerase-chain reactions (PCRs) could be standardized for all alleles except dTOM. Reaction setups are shown in table 3 and table 4, PCR programs in table 5 and 6. Genotyping primers as well as expected PCR product sizes in base pairs (bp) are listed in table 7. PCR products were loaded onto SYBR-safe (Thermo Scientific, Cat. No. S33102) stained 1.5 % agarose gels (Thermo Scientfic, Cat. No. 16500100).

Reagent	**Volume (µL)**
Mastermix genotyping buffer	25
10x Cresole	3
Primer A (stock 100 pmol / ul)	0.25
Primer B (stock 100 pmol / ul)	0.1
Primer C (stock 100 pmol / ul)	0.1
Homemade polymerase	0.5
DNA	1

Table 3: Genotyping PCR reaction setup for Rc3h1, Rc3h2, CD19Cre, Cγ1Cre, CAR

Reagent	**Volume (µL)**
2x GoTaq Mastermix (Promega, Cat. No. M7423)	15
H_2O	13.4
Primer A (stock 100 pmol / ul)	0.25
Primer B (stock 100 pmol / ul)	0.25
Primer C (stock 100 pmol / ul)	0.05
Primer D (stock 100 pmol / ul)	0.05
DNA	1

Table 4: Genotyping PCR reaction setup for dTOM

Cycle No.	**Temperature**	**Duration**	**Repetition of cycles**
1	94°C	3 min	
2	94°C	30 sec	Δ T = -0.5°C / cycle, 19 cycles
	65°C	30 sec	
	72°C	30 sec	
3	94°C	30 sec	
4	55°C	30 sec	
5	4°C	∞	

Table 5: PCR program for Rc3h1, Rc3h2, CD19Cre, Cγ1Cre, CAR

Cycle No.	**Temperature**	**Duration**	**Repetition of cycles**
1	95°C	3 min	
2	95°C	30 sec	35 cycles
	65°C	30 sec	
	72°C	2 min	
4	72°C	2 min	
5	4°C	∞	

Table 6: PCR program for dTOM

Allele	Primer Name	Primer sequence	PCR product size
Rc3h1	RoqflxRv RoqloxFw FlxFwN	AAAGCCCTCAAGATTCTTTGGGCA GTAAATGAGATTCAGTGTGTCCAG TACAAGGTAGAGACGTTTGGGAAG	WT: 144 bp Floxed: 190 bp Germline deleted: 293 bp
Rc3h2	MnabFw MnabFlxFw MnabRv2	TGCAGCCACCTCATATTAAC GCCCACGTCTTATTGGATG CCATGTTTTATTAGCAGGCAC	WT: 165 bp Floxed: 199 bp Germline deleted: 304 bp
CD19Cre	Cre8 CD19c CD19d	CCCAGAAATGCCAGATTA AACCAGTCAACACCCTTCC CCAGACTAGATACAGACCAG	WT: 452 bp Inserted: 500 bp
Cγ1Cre	Cγ1Cre A Cγ1Cre B Cγ1Cre C	TGTTGGGACAAACGAGCAATC GGTGGCTGGACCAATGTAAATA GTCATGGCAATGCCAAGGTCGCTAG	WT: 250 bp Inserted: 470 bp
CAR	R26- UP R26- LP R26CAG rev	AAAGTCGCTCTGAGTTGTTAT GCGAAGAGTTTGTCCTCAACC GGAGCGGGAGAAATGGATATG	WT: 600 bp Inserted: 310 bp
dTOM	Ai14fw Ai14rv WT1 fw WT rv	GGT TCG GCT TCT GGC GTG TGA CC AAG GCC GGC CGA ATT CGA TCT AGC GGC TCA GTT GGG CTG TTT TG ATA CTC CGA GGC GGA TCA CA	WT: 500 bp Inserted: 1162 bp Germline deleted: 291 bp

Table 7: Genotyping PCR primers and product sizes

3.3.4 Immunizations

Immunization with sheep red blood cells (SRBC)

Appropriate volumes (0.5 - 1.5 mL) of fresh SRBCs in alsevers solution (Thermo Scientific, Cat. No. 12977755) were diluted sterile under the hood in 50 mL cold 1x DPBS and centrifuged for 10 min at 2500 rpm, 4 °C. Supernatants were discarded and SRBCs were washed another three times using again 50 mL of cold 1x DPBS. Final pellets were resuspended in 1 mL of cold 1x DPBS. A pre-dilution of 1:2000 in 1x DPBS was prepared for subsequent manual cell counting using 1:1 trypanblue. SRBC concentration was adjusted to 10^9 cells / mL with 1x DPBS. 100 µL, meaning 10^8 of SRBCs, were immediately injected intra-peritoneally (i.p.) per mouse. Unimmunized control animals were injected with 100 µl sterile 1x DPBS instead. SRBC treated animals were sacrificed at day 4, day 7 or day 10 post-injection.

Immunization with NP-CGG (4-Hydroxy-3-nitrophenylacetyl-chicken gamma globulin), Ratio 30-39

NP-$CGG_{30\text{-}39}$ immunization reagent (Biosearch Technologies, N-5055D-5) was dissolved to 1 mg / mL in 1x DPBS and kept sterile as aliquots at -20 °C until further usage. Immediately before immunization NP-$CGG_{30\text{-}39}$ was mixed sterile 1:1 with Imject Alum Adjuvant (Thermo Scientific, Cat. No. PI77161) to boost immunization reactions. Mixtures were vortexed intensively and kept on a rotor for 1 h at RT to allow homogenous dissolving of NP-$CGG_{30\text{-}39}$ into the viscous alum reagent. 50 µg of NP-$CGG_{30\text{-}39}$ + alum was injected

i.p. in a total volume of 100 µl per mouse. Unimmunized control animals were injected with 100 µl of alum mixed 1:1 with sterile 1x DPBS. NP-CGG_{30-39} treated animals were bled from the vena facialis shortly before and after injection on a weekly basis. Mice were sacrificed at day 14 or day 35 post-immunization.

3.4 *Ex vivo* analysis

3.4.1 Mouse organ processing

Blood serum

After 2 min of isoflurane anesthesia, the body weight of mice was assessed and 0.5 – 1 mL of blood was taken from the heart. Blood samples were incubated in regular eppis at RT for at least 30 min to allow sufficient coagulation. Blood clot and blood cells were removed by centrifugation for 10 - 30 min, 11.000 g, 4 °C and serum supernatant was transferred into new tubes. Samples were stored until further usage at -80 °C. Serum preparation was done equivalent for blood taken from the vena facialis.

Spleen

Spleens were harvested, weighed and smashed on ice in 5 mL of cold CB buffer using the rough side of microscope glass slides. After centrifugation (5 min, 500 g, 4 °C), supernatants were carefully aspirated and remaining pellets were resuspended in 1 mL of FACS buffer. Erythrocytes were lysed though addition of 5 mL of Geys' solution and incubation for 5 min on ice. Lysis reaction was neutralized with 10 mL of FACS buffer. Cells were pelleted again, resuspended in 5 mL of FACS buffer and filtered through cotton filters of 5 mL serological pipets (Corning Costa, Cat. No. 4487). Living cell numbers were determined using 1:1 trypan blue dilution and Neubauer counting chambers.

Bone marrow

Femur and tibia of one or both legs were gathered. Bone marrow was flushed out on ice using 5 mL syringes and 20 G x 40 mm needles (Braun, Cat No. 3813353929). Cell processing was continued as described for spleen including red blood cell lysis.

Lymph nodes, mesenteric lymph nodes and peyer's patches

Six lymph nodes (2x inguinal, 2x brachial, 2x axillary) were collected and pooled into 5 mL of CB buffer. For the analysis of cytokine secretion of Roquin knockout follicular and marginal zone B cells, four superficial cervical lymph nodes were included in addition. Peyer's patches were dissociated from the intestine using one scalpel blade per animal. LN, mesenteric lymph nodes (mLN) as well as peyer's patches (PP) were processed as described before for spleen without the need of red blood cell lysis.

3.4.2 Flow cytometry

Antibodies

Antigen	Fluorochrome	Clone	Source	Dilution
7-AAD			Thermo Fisher	1:1000
Annexin V	APC	17-8007-74	invitrogen	1:20
B220	Brilliant Violet 510	RA3-6B2	BioLegend	1:100
B220	Brilliant Violet 650	RA3-6B2	eBioscience	1:100
B220	PerCP/Cy5.5	RA3-6B2	eBioscience	1:200
B220	Alexa Fluor 700	RA3-6B2	BD Bioscience	1:200
BAFFR	FITC	eBio7H22-E16	eBioscience	1:100
BCL-6	PE	K112-91	BD	1:400
BCL-6	PE/Cy7	K112-91	BD	1:400
BLIMP-1	Brilliant Violet 421	5E7	BD	1:200
CD119	Biotin	2E2	eBioscience	1:100
CD138	APC	281-2	BD	1:50
CD19	Biotin	eBio1D3	eBioscience	1:100
CD19	Alexa Fluor 700	1D3	eBioscience	1:200
CD19	APC-eFluor780	eBio1D3	eBioscience	1:300
CD1d	PerCP/Cy5.5	1B1	Biolegend	1:400
CD16/CD32		93	Thermo Fisher	1:200
CD21/35	FITC	7G6	BD	1:100
CD23 (FcεRII)	Alexa Fluor 700	B3B4	BioLegend	1:400
CD25	eFluor450	eBio3C7 (3C7)	eBioscience	1:300
CD38	PE/Cy7	90	Biolegend	1:500
CD38	APC-Cy7	90	BioLegend	1:400
CD3ε	eFluor450	eBio500A2	eBioscience	1:800
CD4	Alexa Fluor 700	RM4-5	BioLegend	1:200
CD44	APC-eFluor780	IM7	eBioscience	1:200
CD62L	Brilliant Violet 510	MEL-14	BioLegend	1:400
CD69	PE/Cy7	H1-2F3	eBioscience	1:100
CD80	Brilliant Violet 650	16-10A1	BioLegend	1:100
CD86	Brilliant Violet 605	GL1	BioLegend	1:200
CD86	Brilliant Violet 650	GL-1	BD	1:50
CD8α	BUV737	53-6.7	BD	1:200
CD93 (AA4.1)	APC	AA4.1	eBioscience	1:100
CD95	FITC	Jo2	BD	1:100
CD95	PE	Jo2	BD	1:200
CD95	PE/Cy7	Jo2	BD	1:200
CD95	Brilliant Violet 605	Jo2	BD	1:50
CXCR4	Biotin	2B11/CXCR4	BD	1:100
CXCR5	Biotin	L138D7	BioLegend	1:100
eF780 LD fixable dye	eF780		Thermo Fisher	1:1000
Foxp3	APC	FJK-16s	eBioscience	1:50
GL-7	eFluor450	GL7	eBioscience	1:200
IgD	FITC	11-26c/11-26	eBioscience	1:200

Table 8: Flow cytometry antibodies

Antigen	Fluorochrome	Clone	Source	Dilution
IgD	eFluor450	11-26c/11-26	eBioscience	1:200
IgE	Brilliant Violet 510	R35-72	BD	1:200
IgG2c	Brilliant Violet 605	R19-15	BD	1:100
IgG2b	BUV737	R12-3	BD	1:100
IgG3	Brilliant Violet 421	R40-82	BD	1:400
Igλ1	Biotin	R11-153	BD	1:100
IgM	PE/Cy7	II/41	eBioscience	1:800
Integrin αM (CD11b)	eFluor450	M1/70	eBioscience	1:800
Integrin αX	eFluor450	N418	eBioscience	1:200
IRF4	eFluor450	3E4	eBioscience	1:800
IRF4	PerCP/eFluor710	3E4	eBioscience	1:800
Near-IR LD dye	Near-IR		Invitrogen	1:1000
NP	PE		Biosearch Technologies	1:400
MHCII	PE	M5/114.15.2	eBioscience	1:200
PD-1	PE/Cy7	J43	eBioscience	1:500
PromoFluor-840			BioConnect	1:1000
Sca-1	FITC	D7	eBioscience	1:400
Streptavidin	BUV395	none	BD	1:200
Streptavidin	BUV737	none	BD	1:100
TCRß	Brilliant Violet 605	H57-597	BD	1:100

Table 8 (continued): Flow cytometry antibodies

Staining procedure

CFSE staining was performed in RPMI + 10% FCS medium containing final 2 µM of CFSE. After incubation with the CFSE mix for 8 min, RT in the dark, cells were washed twice with FCS containing RPMI medium to stop the CFSE labeling reaction. Afterwards cells were cultured at 37 °C, 5 % CO_2 for 2 or 3 days before cell harvesting.

Single cell suspensions were transferred into 96 V-bottom plates (Thermo Scientific, Cat. No. 249944) and kept on ice for all subsequent staining steps. Cells were washed three times in cold 1x DPBS (2 min, 950 g, 4 °C) to remove protein-containing media or FACS buffer. Afterwards, a live-dead dye diluted according to table 8 in 1x DPBS was added for 10 – 20 min simultaneously with anti-mouse CD16 / CD32 monoclonal antibodies, used to minimize unspecific binding of antibodies to Fc receptors. Live-dead stains as well as antibody staining was performed in a volume of 30 µL of staining solution per max. 1 Mio cells with one washing step in between of the individual staining reactions using 150 µL of FACS buffer. Extracellular antibodies were stained for 20 – 30 min in FACS buffer before fixation using the FoxP3 / Transcription Factor Staining Set (eBioscience, Cat. No. 00-5523-00) according to the manufacturers' instructions. To maintain eGFP, mNeptune or dTOM fluorochrome signals, relevant samples were instead fixated using 2 % formaldehyde (Carl Roth, Roti Histofix 4 % Cat. No. P087.4 diluted 1:1 with 1x DPBS). For intracellular blocking of Fc receptors, anti-mouse CD16 / CD32 was added in 1x Permeabilization buffer of the FoxP3 / Transcription Factor Staining Set for 30 min. Afterwards, intracellular antibodies were stained for 1 h in 1x Permeabilization buffer. In case of extra- or intracellular biotinylated antibodies, staining was carried out in two

consecutive steps. Manufacturers' instructions were followed for Annexin V Apoptosis Detection (eBioscience, Cat. No. 88-807-72). Stained cells were finally resuspended in 100 - 200 µL of FACS buffer and stored for maximum 4 days in the fridge. In case of DAPI cell cycle detection, DAPI (stock conc. 10 mg / mL, Sigma Aldrich, Cat. No. D8417) was added 1:6000 to final cell suspensions shortly before acquisition.

Sample acquisition

Samples were analyzed on the Cytoflex S or Cytoflex LX flow cytometer using the CytExpert Software or sorted on the BD Aria III or MoFlo Astrios EQ using the BD FACSDiva or CytExpert software, respectively. For sorting, cell suspensions were filtered directly before data acquisition through 35 µm nylon filters (Fisher Scientific, Cat. No. 08.771.23). Sorts at 4 °C using a 85 µm nozzle were preferred. Collection tubes were pre-filled with either 1 mL cold A20 cell culture medium, 10 % FCS or FACS buffer. Doublet exclusion was ensured via gating on singlets in forward scatter FSC-A vs FSC-H as well as sideward scatter SSC-A vs SSC-W. In case of DAPI stained samples, FSC-A vs FSC-H and additionally DAPI-A vs DAPI-W was employed instead. Spectral overlap of fluorochromes was compensated using unstained or live-dead stained splenocytes together with antibody-stained compensation beads (Thermo Fisher, Cat. No. 01-2222-42).

LEGENDplex

For analysis of cytokine secretion potential of follicular and marginal zone B cells in Roquin knockout mice, LEGENDplex mouse B cell panels (BioLegend, Cat. No. 740819) 13-plex) including the mouse targets IL4, IL6, IL12p70, IL17A, IL2, TNFα, Free Active TGFβ1, IL13, IFNγ, BAFF, BCMA, sCD40L, and IL10 were performed on *ex vivo* cell culture supernatants according to the manufacturers' instructions. A pilot experiment demonstrated that only IL6 an IL10 cytokine levels were detectable beyond background threshold levels. Thus, experiments thereafter were limited to those two targets using a customized kit from BioLegend.

SRBC-specific antibody detection

For analysis of SRBC-specific antibody content in blood sera of immmunized mice via flow cytometry, SRBCs were initially prepared as described before and were adjusted to a concentration of 10^8 cells / mL. Blood sera were prepared in a 7-step dilution series (1:50, 1:100, 1:200, 1:400, 1:800, 1:1600, 1:3200) in 1x DPBS and 50 µL thereof were transferred into 96 V-bottom plates (Thermo Scientific, Cat. No. 249570). Blood sera were incubated together with 2 Mio SRBCs / well for 20 min on ice. One well per sample of undiluted

serum (1 µL serum + 2 Mio SRBCs) was included as positive control and SRBCs without added serum served as negative control. After one wash with 150 µL FACS buffer (10 min, 950 g, 4 °C), SRBCs-IgG complexes were stained for 20 min in a total volume of 20 µL using IgG1-APC, IgM-PE-Cy7, Igκ-FITC or B220-eF450, respectively, including FMO controls. Lastly, samples were washed as before, taken up in 200 µL of FACS buffer and analyzed in duplicates via flow cytometry on the same day. FSC and SSC were tailored to distinguish small SRBCs from debris. The workflow is adapted from the method published by McAllister et al.[133].

3.4.3 Magnetic activated cell sorting (MACS)

Single-cell suspensions of spleen or lymph nodes were used to isolate and separate marginal zone and follicular B cells (Miltenyi Biotech Marginal Zone and Follicular B cell Isolation kit, Cat. No. 130-100-366). Alternatively, splenocytes were CD43-depleted before caspase staining using CD43 (Ly-48) MicroBeads (Miltenyi Biotech, Cat. No. 130-049-801). For B cell receptor amplicon sequencing, splenic GCBs of immunized mice were enriched using the Germinal center B cell (PNA) Micro Bead Kit (Miltenyi Biotech, Cat. No. 130-110-479) and PosselDS as program. All kits were used according to the manufacturers' instructions. Magnetic bead-based depletion or enrichment was conducted on the autoMACS Pro Separator. Purity of obtained eluate and flow-through fractions was checked for via flow cytometry.

3.4.4 Enzyme-linked immunosorbent assay (ELISA)

Detection of NP-specific immunoglobulins in blood sera of immunized mice by ELISA was conducted inspired by Heise et al. 2017[134]. In modification of the original protocol, Nunc-Immuno 96-well flat-bottom plates (Sigma-Aldrich, Cat. No. M5785) were coated with 0.5 µg / mL NP_2-BSA (rows B-H, columns 1-6), NP_{23}-BSA (rows B-H, columns 7-12) and anti-mouse IgG1 (Bethyl Cat No. A90-105A, stock 1 mg / mL) diluted 1:100 (row A, columns 1-12) in 0.1 M carbonate buffer, respectively. Blocking of unspecific binding sites was performed using 1 % BSA in 1x DPBS instead of 2 % FCS in PBS as written in the original publication. Blood sera were diluted 1:50, 1:100, 1:400, 1:1600, 1:6400, 1:256.000 in 1x DPBS + 1 % BSA and were loaded as single samples, not duplicates, due to limited amount of available starting material. NP_2- and NP_{23}-binding immunoglobulin detection

was performed as one mouse per plate to minimize plate specific batch effects. Serum was incubated on coated plates only for 1 h instead of 2 h. Mouse reference serum (Bethyl, Cat. No. RS10.101-6) was added to standard-coated wells as 1:3 dilution series with final concentrations of 10.000 µg / mL, 3333 µg / mL, 1111 µg / mL, 370 µg / mL, 123 µg / mL, 41 µg / mL, 14 µg / mL, 5 µg / mL, 1.5 µg / mL, 0.5 µg / mL, 0 µg / mL in 1 % BSA containing 1x DPBS. 50 µL of 1:150.000 diluted anti-IgG1 horseradish peroxidase (HRP) antibody in 1x DPBS + 1 % BSA (Bethyl, Cat. No. A90-105P) was incubated for 1 h at RT before detection with 100 µL / well 3,3',5,5'-tetramethylbenzidine (TMB) substrate (BD Bioscience, Cat. No. 555214). Colorimetric reaction was stopped after 30 min at RT using 50 µL / well 1 M H_3PO_4. For analysis, absorbance summation of NP_2-bound and NP_{23}-bound IgG1 was normalized to the plate-specific sum of standard absorbance measurements inspired by Hartman et al. 2019[135].

3.4.5 BCR amplicon sequencing

Determination of the somatic hypermutation frequency of Roquin knockout GCBs upon NP-CGG_{30-39} immunization at day 14 post-injection was inspired by Heise et al. 2017[134].
In brief, splenocytes of NP-CGG_{30-39} mice were enriched for GCBs using a MACS-based kit and then sorted for naïve ($CD11b^-$, $CD3\varepsilon^-$, $CD11c^-$, $CD138^-$, $B220^+$, $CD19^+$, $CD95^-$, $CD38^+$, IgD^+) and GCBs ($CD11b^-$, $CD3\varepsilon^-$, $CD11c^-$, $CD138^-$, $B220^+$, $CD19^+$, $CD95^+$, $CD38^-$, IgD^-). RNA of sorted cell populations was extracted, quantified by Qubit and transcribed into cDNA. In order to determine mutational load of V_H186.2 gene rearrangements, semi-nested PCRs using locus-specific primers were performed followed by agarose gel visualization. Gel extracted PCR products were purified and used for subsequent 500 bp paired-end Illumina MiSeq amplicon sequencing.

RNA extraction and concentration determination

RNA was isolated using the AllPrep DNA / RNA Micro Kit (Qiagen, Cat. No. 80284) according to the manufacturers' instructions in an RNAse-free environment using RNAse-free laboratory equipment and reagents. RNA was finally eluted in a volume of 14 µL. RNA concentration of 1 µL sample RNA was determined using the Qubit RNA high-sensitivity (HS) kit (Thermo Fisher Scientific, Cat. No. Q32852) according to the manufacturers' instructions, thereby acquiring new standards for each day of measurement. RNA was stored at -80 °C until further usage.

cDNA generation

4 µL of input RNA were used for cDNA generation using SMARTScribe Reverse Transcriptase (Takara Cat. No. 639538) according to the manufacturers' instructions and recommendations of additional required materials. Incubation at 42 °C was done for 90 min. Cγ1-cDNA primer (5'-CATGGAGTTAGTTTGGGCAG-3) was taken from Heise et al. 2017[134].

Semi-nested PCR amplification and sequencing

Settings of the first round of PCR are illustrated in table 9 and 10, settings of the second round are described in table 11 and 12. Primer sequences were taken from Heise et al. 2017 and are listed in table 13[134]. To avoid later sequence allocation errors in the flow-cell of the MiSeq Illumina sequencer due to highly similar PCR amplicon products, frameshifts were introduced by adding 1 – 5 nt to the original PCR primers (highlighted in bold in table 13) and using different PCR primers per experiment. Furthermore, Illumina overhang sequences were added (5'-GTGACTGGAGTTCAGACGTGTGCTCTTCCGATCT-3' to Cγ1-PCR primers and 5'-ACACTCTTTCCCTACACGACGCTCTTCCGATCT-3' to V_H186.2 nested PCR primers). Final PCR products were loaded onto 1.5 % agarose gels with a least one empty lane between samples to avoid cross-contamination. PCR amplicons were purified using the QIAquick Gel Extraction Kit (Qiagen, Cat. No. 28706).

Reagent	Stock concentration	Final concentration	Volume (µL)
Q5 Reaction buffer	5x	1x	10 µL
dNTPs	10 mM	200 µM	1 µL
Primer V_H186.2 leader	10 µM	0.5 µM	2.5 µL
Primer Cγ1-PCR +0	10 µM	0.5 µM	2.5 µL
Template DNA			2 µL
Q5 Hot Start High-Fidelity Polymerase		0.02 U / µL	0.5 µL
Q5 High GC Enhancer	5x	1x	10 µL
dH_2O			21.5 µL

Table 9: Setup of semi-nested PCR 1

Cycle No.	Temperature	Duration	Repetition of cycles
1	95°C	2 min	
2	95°C	30 sec	20 cycles
	70°C	30 sec	
	72°C	1.5 min	
3	72°C	5 min	
4	4°C	∞	

Table 10: PCR program of semi-nested PCR 1

Reagent	Stock concentration	Final concentration	Volume (µL)
Q5 Reaction buffer	5x	1x	10 µL
dNTPs	10 mM	200 µM	1 µL
Primer V_H186.2 nested +0 or +1 or +3 or +4	10 µM	0.5 µM	2.5 µL
Primer C_γ1-PCR +0 or +1 or +2	10 µM	0.5 µM	2.5 µL
Template DNA			3 µL
Q5 Hot Start High-Fidelity Polymerase		0.02 U / µL	0.5 µL
Q5 High GC Enhancer	5x	1x	10 µL
dH_2O			20.5 µL

Table 11: Setup of semi-nested PCR 2

Cycle No.	Temperature	Duration	Repetition of cycles
1	95°C	2 min	
2	95°C	30 sec	30 cycles
	70°C	30 sec	
	72°C	1.5 min	
3	72°C	5 min	
4	4°C	∞	

Table 12: PCR program of semi-nested PCR 2

Primer name	Primer sequence
C_γ1-PCR +0	5'-ATCCAGGGGCCAGTGGATAGAC-3'
C_γ1-PCR +1	5'-**A**ATCCAGGGGCCAGTGGATAGAC-3'
C_γ1-PCR +2	5'-**AT**ATCCAGGGGCCAGTGGATAGAC-3'
V_H186.2 leader	5'-AGCTGTATCATGCTCTTCTTGGCA-3'
V_H186.2 nested +0	5'-CATGCTCTTCTTGGCAGCAACAG-3'
V_H186.2 nested +1	5'-**G**CATGCTCTTCTTGGCAGCAACAG-3'
V_H186.2 nested +3	5'-**TGCG**CATGCTCTTCTTGGCAGCAACAG-3'
V_H186.2 nested +4	5'-**CTGCG**CATGCTCTTCTTGGCAGCAACAG-3'

Table 13: Primers used for semi-nested PCRs

Sequencing and bioinformatic analyses

Sample library preparation was performed by Rupert Öllinger from the laboratory of Prof. Roland Rad, TranslaTUM and samples were sequenced using paired-end 250 bp sequencing on the MiSeq Illumina sequencer on a 500 bp cartridge. 10-20 % PhiX virus spike-in controls were used to enable correct cluster reading of the highly repetitive PCR amplicon sequencing reads. Bioinformatic analyses was done in collaboration with Olga Baranov and Thomas Engleitner from the laboratory of Prof. Roland Rad, TranslaTUM and is already described in Weber et al. 2019[136]. In summary, *MIGEC* was used for demultiplexing and *MiXCR* was used for read alignment and clone assembly. Read mapping via *MiXCR* was performed using the special B cell aligner KAligner2. Analysis of mutation frequencies was restricted to reads with unique V region sequence which was recognized as heavy-chain region IgHV1-72 and obtained a mean sequencing quality > 20. For clonality analyses, the in-house developed pipeline CloNet was executed.

3.5 *In vitro* analyses

3.5.1 A20 cell culture

A20 cell identity

A20 cells are a murine B cell lymphoma cell line established and initially described by Kim et al. 1979 and further characterized by Feng et al. 2017[137,138]. They resemble GCB cells *in vitro* and are positive for B220, CXCR4, CD86, CD95, IgG, CD45.2, IRF4 and BCL6 and negative for cell markers including GL7 and CD38 as detectable by flow cytometry. A20 bulk cells in our hands showed a ~1:1 ratio of $CD19^+$ and $CD19^-$ expressing cells. A20 suspension cells were cultured at 37 °C, 5 % CO_2 and diluted to 100.000 cells / mL – 200.000 cells / mL for cell passaging.

A20 CDE WT cell line generation

A20 cells were manipulated through electroporation by Chia-I Lien, a PhD student in our laboratory using constructs that have been cloned and reported previously in MEF cells by David Riess[82]. Schematics of the constructs are presented in Fig. 32A and detailed vector maps are shown in Suppl. Fig. 13-15.

Essentially, vectors "*Nfκbid* CDE WT" (Suppl. Fig. 13) and "*Nfκbid* mutated CDE" (Suppl. Fig. 14) encode a dual-fluorescence reporter construct applicable to detect Roquin 1 expression levels. Thereby, a pGK promotor drives the transcription of an eGFP fluorochrome which is coupled 3' to the WT or mutated version of the *Nfκbid* tandem constitutive decay element (CDE) stem-loop structure. *Nfκbid* CDE WT is known to be recognized and regulated by Roquin 1 whereas the mutated version is not bound by Roquin 1 at the hairpin structure. It has been shown during this PhD project, that both elements cannot be detected by Roquin 2 (data not shown). In addition, vectors encode for another cassette composed of pEF1α promotor and the second fluorochrome mNeptune which allows mNeptune expression independent of the Roquin status inside the target cells. In summary, Roquin 1 downregulation or depletion in eGFP-*Nfκbid* CDE WT containing A20 cells results in less RNA-binding activity and degradation of the eGFP-*Nfκbid* CDE WT transcript visible by an increase of eGFP fluorescence intensity. On the contrary, eGFP fluorescence are not affected efficiently by an Roquin 1 knockout in eGFP-*Nfκbid* mutated CDE containing cells. mNeptune intensities are supposed to serve as internal control since they should not be affected by any scenario described.

A neomycin resistance cassette was employed to select target cells with stable genomic integration of the vectors "*Nfκbid* CDE WT" or "*Nfκbid* mutated CDE" for 10 days using 500 µg / mL G418. Parallel electroporation of a hyperactive *piggyBac* transposase encoded on a separate plasmid (Suppl. Fig. 15) was necessary to enable the stable integration event. Selected A20 cells modified by the piggyBac transposase together with the *Nfκbid* CDE WT or *Nfκbid* mutated CDE containing plasmid were named "A20 CDE WT" or A20 CDE mut", respectively.

3.5.2 Electroporation

For A20 cell manipulations, Cas9 ribonucleoprotein (RNP) complexes containing crRNA-tracrRNA guide RNA and Cas9 enzyme were electroporated using CRISPR-Cas9 reagents and protocols from IDT together with the Neon transfection system.
In brief, target crRNAs as listed in table 14 were coupled to tracrRNA (Alt-R® CRISPR-Cas9 tracrRNA, Cat. No. 1072532) before complex formation with Cas9 proteins (Alt-R® S.p. Cas9 Nuclease V3, Cat. No. 1081058). Afterwards, Cas9-sgRNA RNPs were delivered together with purified carrier DNA (Alt-R® Cas9 Electroporation Enhancer, Cat. No. 1075915) to 350.000 A20 cells diluted in resuspension buffer R using the 10 µL Neon kit (Invitrogen, Cat. No. MPK1025). In case the 100 µL Neon kit (Invitrogen, Cat. No. MPK10025) was used instead, all reagents including cell numbers were upscaled linearly. Electroporation conditions were tested in the laboratory before and optimal cell viability together with maximal electroporation efficiency could be achieved using 1350 V for 20 ms and 2 pulses. To enhance cell fitness and align different cell cultures, A20 cells were transferred to fresh medium in a cell density of 500.000 cell / mL the day before electroporation treatment.

crRNA target	crRNA sequence
Rc3h1	5'-ACTGAGCAGGGTATACACGG -3'
Rc3h2	5'-GTTGTCCTTGGGTCATTCGG -3'
LacZ	5'-AACGGCGGATTGACCGTAAT-3'

Table 14: crRNA sequences used for RNP complex formation

3.5.3 Single-cell clone (SSC) generation

To identify successful genome editing by electroporated Cas9-RNP complexes, genomic DNA of manipulated and control A20 cell cultures was isolated 4 - 10 days after treatment using the QIAamp DNA micro or minikit (Qiagen, Cat. No. 56204 / 51304) depending on cell numbers harvested. Following this, 400-600 bp surrounding the sgRNA cut-side at exon 12 of Roquin 1 or exon 11 of Roquin 2 were PCR amplified according to tables 15-17. PCR products were loaded onto SYBR-safe stained 2 % agarose gels, were gel purified by the QIAquick Gel Extraction Kit and were sent for sequencing to Eurofins together with either forward (fwd) or reverse (rev) primers. Received nucleotide (nt) sequences were loaded into the ICE analysis platform of Synthego to identify insertions and deletions. Successfully edited A20 bulk cell cultures could subsequently be used for SSC generation by dilution series in U-bottom 96-well plates according to the instructions of IDT. This was followed by another round of genomic indel screening as well as RT-qPCR and western blot verification of the target protein knockout. In case of A20 CDE WT Roquin1/2 double knockout SSCs, A20 CDE WT Roquin 2 knockout SSCs were electroporated with sgRc3h1 as described above and sorted for GFP^{hi} cells instead of using serial dilutions for SSC generation. Sorting for GFP^{hi} cells led to 6 out of 6 fully screened Roquin 1/2 double knockout clones.

Reagent	Stock concentration	Final concentration	Volume (µL)
Phusion HF buffer	5x	1x	10 µL
dNTPs	10 mM	200 µM	1 µL
Primer fwd	10 µM	1 µM	5 µL
Primer rev	10 µM	1 µM	5 µL
Template DNA			50 ng
High-Fidelity Phusion Polymerase (Thermo Scientific, Cat. No. F530S)	2 U / µL	0.02 U / µL	0.5 µL
dH_2O			Add up to 50 µL

Table 15: PCR amplification of CRISPR/Cas9 manipulated A20 cells for indel analyses

Cycle No.	Temperature	Duration	Repetition of cycles
1	98°C	30 sec	
2	98°C	15 sec	30 cycles
	60°C	30 sec	
	72°C	30 sec	
3	72°C	5 min	
4	4°C	∞	

Table 16: PCR program used for indel analyses

PCR target	Primer orientation	Primer sequence	PCR product size
Rc3h1	fwd rev	5‘-ATGTGTGTCCCGCTTTGTCC-3‘ 5‘-CAGCTAGCAGCGTGGAAAGT-3‘	503 bp
Rc3h2	fwd rev	5‘-CGCAGCAGTATGGACCAGTT-3‘ 5‘-GCCATGCAAAGGGCAAGTAA-3‘	543 bp

Table 17: PCR primers used for indel analyses

3.5.4 Western Blot

Protein isolation

For protein extraction, A20 cell pellets were lysed using 150 µL of Protein Isolation Buffer (Miltenyi Biotech, Cat. No. 130-091-125) per 5 Mio of A20 cells. Lysis suspensions were vortexed vigorously and incubated on ice for 5 min before cell debris was spin down for 10 min at full speed, 4 °C. Protein supernatants were transferred to pre-cooled eppis and stored until further usage at -80 °C. Freeze-thaw cycles of proteins were avoided. Protein concentrations were determined by the detergent compatible protein assay from BioRad (BioRad, Cat. No. 5000111) according to the manufacturers' instructions.

SDS-PAGE

For gel separation, equivalent protein amounts (40 - 60 µg) were loaded to NuPAGE 3 – 8 % TrisAcetate gels (Thermo Fisher Scientific EA03785BOX) using accompanying buffers and reagents according to the manufacturers' instructions. For optimal separation of the two Roquin proteins (Roquin 1 126 kDa, Roquin 2 132kDa), gels were run at 60 V for 20 min and afterwards at 140 V until the 100 kbp band of the PageRuler Plus Prestained Ladder (Thermo Fisher Scientific, Cat. No. 26619) ran out completely.

Western Blot

Proteins were transferred in self-made transfer buffer to 0.45 µm PVDF membranes (Merck, Cat. No. IPVH00010) for 90 min at 0.6 A. Unspecific binding was blocked with 5 % milk in 1x TBS + 1:1000 Tween-20 (TBS-T) for 30 min, RT. Afterwards, proteins were incubated with primary anti-mouse monoclonal Roquin antibody from rat (Clone 3F12, 1:10 in 5 % milk TBS-T) over night (ON), 4 °C. After two washing steps in TBS-T for 5 min at RT each, secondary anti-rat IgG-HRP from donkey (GE Healthcare, Cat. No. NA935V) was added for 30 min, RT. Blots were washed again and subsequently developed in chemiluminescent HRP substrate (Fisher Scientific, Cat. No. PI34096). Anti-mouse myosin IIa (230 kDa; Cell signaling technologies, Cat. No. 3403T) was used as loading control and was incubated for 1 h, RT in 5 % BSA (Cytiva, Cat. No. SH30574.02) in TBS-T after stripping the membrane for 10 min, RT. Anti-rabbit IgG-HRP from donkey (GE

Healthcare, Cat. No. NA934V) was incubated together with the membrane for 30 min, RT and blots were developed using equivalent HRP substrate solutions.

3.5.5 Quantitative real-time PCR (qRT-PCR)

qRT-PCRs enabled the detection of Roquin 1 and Roquin 2 transcription levels of Roquin manipulated A20 cells as well as gene expression levels after stimulation. For this purpose, RNA of respective samples was isolated and RNA concentrations determined as already described. 650 ng of RNA were transcribed into cDNA using the Maxima H Minus cDNA Synthesis Mastermix with dsDNAse (Thermo Scientific, Cat. No. M1681) according to the protocol of the manufacturer. Controls without reverse transcriptase or without RNA input were included. PCR amplification of 2 µL input cDNA was facilitated by the PowerUP SYBR Green Master mix (Thermo Scientific, Cat. No. 15360929) following the recommended standard cycling mode for primer T_m > 60°C. Samples were measured in technical duplicates or triplicates. 500 ng of each primer were applied per reaction with primer sequences listed in table 18 and taken partially from Feng et al. 2018[137].

PCR target	Orientation	Primer sequence	PCR product size
Rc3h1	fwd rev	5'-AAC CAG CAT TGG GCA TGT-3' 5'-CTT CAT CAC GTT TGG TGA CCT-3'	83 bp
Rc3h1	fwd rev	5'-ACCTGAGTCCAGAGAACGGTA-3' 5'-GGCCATTATTTCCTTCCGCC-3'	172 bp
Rc3h2	fwd rev	5'-TTG GCA CTC TAC TTA AAA CCA CTA AG-3 5'-TCG CAT AGC TCT GAC ACG AC-3	143 bp
HPRT	fwd rev	5'-CTTGCTGGTGAAAAGGACCTCTC-3 5'-GAAGTACTC ATTATAGTCAAGGGCA-3	112 bp
IRF4	fwd rev	5'-TCCGACAGTGGTTGATCGAC-3 5'-TCACGATTGTAGTCCTGCTT-3	124 bp
BCL6	fwd rev	5'-TTCGGATTCTAGCTGTGAG-3 5'-GTGGACAGTCTTGTGGCTG-3	181 bp
PAX5	fwd rev	5'-ACCACGGAACCCATCAAG-3 5'-CAAGTCTCGGCCTGTGAC-3	168 bp

Table 18: PCR primers used for qRT-PCR analyses

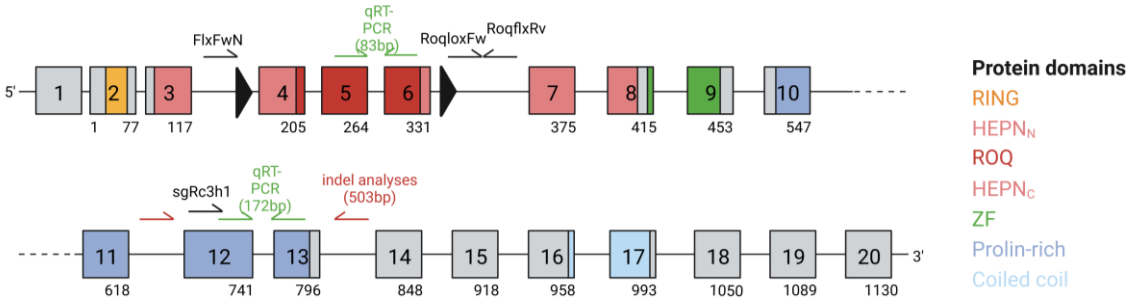

Figure 4: Schematic Roquin 1 exon-intron structure
Shown are the 20 exons of Roquin 1 (ENSMUSG00000040423) together with the amino acids that they account for (e.g., exon 4 constitutes amino acid 118 – 205). Only a rough consensus of protein domain boundaries is shown her, given the variation of their annotations between studies and organisms[75,87,88,92,98]. LoxP sites inserted into mice together with the corresponding genotyping primers FlxFwN, RoqloxFw, RoqflxRv are depicted (see chapter 3.3.3). In addition, primers used for qRT-PCR analysis (see chapter 3.5.5) shown in green and primers used for SSC verifications (see chapter 3.5.3) shown in red surrounding the sgRNA used for Cas9-sgRNA RNP electroporation (see chapter 3.5.2) are highlighted.

3.5.6 Stimulations

For *in vitro* A20 cell stimulations, GCB-like stimuli αIgG1 (Thermo Fisher Scientific, Cat. No. 16-5098-85) and αCD40 (BioCell, Cat. No. BE0016-2, Clone FGK4.5/ FGK45) were employed as already described in Feng et al. 2018[137]. A20 cells were stimulated using a cell density of 1 Mio cells / mL for 2 h, 6 h or 24 h, respectively. Stimulation reaction was titrated to be maximal with 10 µg / mL αIgG1 + 10 µg /mL αCD40 after 24 h, however increase in IRF4 levels as well as BCL6 downregulation was already visible after 6 h using both stimuli. Modest stimulation at both time-points was achieved using 2.5 µg / mL αIgG1 + 2.5 µg / mL αCD40. Stimulation efficiency was determined by flow cytometry as well as qRT-PCR. FOB stimulations were performed in cooperation with Dr. Andreas Gewies and Dr. Thomas O'Neill in the laboratory of Prof. Daniel Krappman using 0.5 µg / mL αCD40 (Invitrogen Cat.No. 16-0402-85, Clone HM40-3), 1.0 µg / mL or 10 µg / mL αIgM, 0.1 µg / mL or 10 µg / mL LPS and 0.1 µM CpG.

3.5.7 RNA sequencing

Sample preparation

The impact of Roquin knockouts on the transcriptome of A20 cells was evaluated by RNA-sequencing (RNAseq). An overview of samples is given in table 19.

In brief, 4 biological replicates of A20 CDE WT SSC carrying stable Roquin 1 knockouts were sequenced with (Samples No. 2, 3) or without (Samples No. 1) stimulation using

2.5 µg / mL αCD40 + 2.5 µg / mL αIgG1as modest stimulation reagents. LacZ SSCs (Samples No. 4-6) served as controls and Roquin 2 SSCs (Samples No. 8, 14, 16) were compared to determine Roquin 1 versus Roquin 2 specific effects. Additionally, stable Roquin 1/2 double knockout SSCs (Samples No. 7) were compared to induced Roquin 1/2 double knockout (Samples 9-16). Induction was thereby enabled by electroporation of Roquin 2 SSCs with Cas9-sgRc3h1 complexes and sorting of reporter GFP^{hi} (successful Roquin 1 knockout) and GFP^{lo} (Roquin 2 knockout only cells) cell fractions 30 h or 54 h after electroporation (Samples No. 9-12). 48 h after electroporation, αIgG1 + αCD40 stimuli were added to half of the electroporated Roquin 2 SSCs cultures and sorting for GFP^{hi} and GFP^{lo} populations was repeated after 6 h or 24 h, respectively (Samples No. 13-16).

No.	A20 CDE WT SSC	Electro-poration sgRNA	Time after electro-poration	Stimulation duration	Sorted popu-lation
1	Rc3h1 KO SSC 9 / 10 / 23 / 25	-	-	-	-
2	Rc3h1 KO SSC 9 / 10 / 23 / 25	-	-	6 h	-
3	Rc3h1 KO SSC 9 / 10 / 23 / 25	-	-	24 h	-
4	LacZ SSC 12 / 13 / 14 / 17	-	-	-	-
5	LacZ SSC 12 / 13 / 14 / 17	-	-	6 h	-
6	LacZ SSC – 12 / 13 / 14 / 17	-	-	24 h	-
7	Rc3h 1/2 KO SSC 6A / 6B / 6C / 7A / 7B	-	-	-	-
8	Rc3h2 KO SSC 6 / 7 / 21 / 22	-	-	-	-
9	Rc3h2 KO SSC 6 / 7 / 21 / 22	sgRc3h1	30 h	-	GFP^{hi}
10	Rc3h2 KO SSC 6 / 7 / 21 / 22	sgRc3h1	30 h	-	GFP^{lo}
11	Rc3h2 KO SSC 6 / 7 / 21 / 22	sgRc3h1	54 h	-	GFP^{hi}
12	Rc3h2 KO SSC 6 / 7 / 21 / 22	sgRc3h1	54 h	-	GFP^{lo}
13	Rc3h2 KO SSC 6 / 7 / 21 / 22	sgRc3h1	54 h	6 h	GFP^{hi}
14	Rc3h2 KO SSC 6 / 7 / 21 / 22	sgRc3h1	54 h	6 h	GFP^{lo}
15	Rc3h2 KO SSC 6 / 7 / 21 / 22	sgRc3h1	72 h	24 h	GFP^{hi}
16	Rc3h2 KO SSC 6 / 7 / 21 / 22	sgRc3h1	72 h	24 h	GFP^{lo}

Table 19: A20 RNAseq sample overview

RNA isolation and concentration measurement of listed samples was done as described previously. High RNA quality was confirmed with a fragment analyzer using the RNA 6000 Pico Kit (Agilent, Cat. No. 5067-1513).

Bioinformatic analysis

3'-polyA library generation was performed by Rupert Öllinger in the laboratory of Prof. Roland Rad, TranslaTUM and UMI-tagged samples were sequenced twice as 50 – 70 bp single-end reads on a MiSeq Illumina Sequencer (400 Mio reads per cartridge). UMI-filtered sequencing reads were processed by an in-house script developed by Dr. Sabrina Bortoluzzi using the DESeq2 package of R (version 4.1.2). For PCA visualization, data was rlog transformed and filtered for 10 % of the genes that accounted for the highest variation between samples. For DGE analysis and heatmap plotting, a cut-off GeneCount > 50 was set leading to a loss of genes less than 5 %. Statistical analysis was conducted by likelihood-ratio testing (LRT) and genes were selected dependent on the data set by an adjusted p-value (padj) of 0.05 or 0.001. Pathway enrichment analysis was performed using EnrichR and MSigDB Hallmark database with pathways filtered for significance using a padj < 0.05. Two pairwise comparisons were calculated in R using limma statistical testing in collaboration with Thomas Engleitner in the laboratory of Prof. Roland Rad. Genes were considered significant upon a padj < 0.05.

3.5.8 Mass-spectrometry

Sample preparation, sample measurement, protein identification and protein quantification were performed in collaboration by Julia Merger, TranslaTUM.

LC-MS/MS sample preparation

Cells were lysed in 8 M Urea in 50 mM Tris-HCl pH = 7.5 and sonicated for 5 min. 2 µL 100 trifluoroacetic acid (TFA) was added to each sample to hydrolyze DNA and the pH subsequently adjusted to 8.5 with 3 M Tris solution. 20 µg protein was used as input. Disulfide bonds were reduced with 10 mM DTT for 45 min at 30 °C, followed by alkylation of cysteines with 55 mM 2-chloracetamide (CAA) for 30 min at RT and 1:5 dilution with digestion buffer (2 mM CaCl2 in 50 mM Tris-HCl, pH 8.5). Trypsin [1:50 (wt / wt) enzyme-to-protein ratio] was added, and proteins were digested at 37 °C ON. The next day, samples were acidified with formic acid (FA) to pH < 3. Stage tip peptide purification was performed using in-house build C18 tips with five C18 discs. Stage tips were equilibrated consecutively with 250 µl 100 % ACN, 250 µl elution solution (50 % ACN, 0.1 % FA) and 250 µl washing solution (0.1 % FA) at 1000 g. Sample were loaded on the column and spun 5 min at 500 g, followed by reapplication of the flow through. Subsequently the stage tips

were washed three times with washing solution. Finally, the peptides were eluted with two times 40 µl elution solution. Peptide eluates were vacuum dried and resuspended in 0.1 % FA prior to liquid chromatography-coupled mass spectrometry (LC-MS/MS) analysis.

LC-MS/MS data acquisition

LC-MS/MS analysis was performed on an Eclipse mass spectrometer (Thermo Fisher Scientific) coupled on-line to a Dionex Ultimate 3000 RSLCnano system. The liquid chromatography setup consisted of a 75 µm x 2 cm trap column and a 75 µm x 40 cm analytical column, packed in-house with Reprosil Pur ODS-3 3 µm particles (Dr. Maisch GmbH). Peptides were loaded onto the trap column using 0.1 % FA in water at a flow rate of 5 µL / min and separated using a 110 min linear gradient from 4 % to 32 % of solvent B (0.1 % (v/v) formic acid, 5 % (v/v) DMSO in acetonitrile) at 300 nL / min flow rate. nanoLC solvent A was 0.1 % (v/v) formic acid, 5 % (v/v) DMSO in HPLC grade water. The Eclipse mass spectrometer was operated in data independent acquisition (DIA) and positive ionization mode. DIA was performed with one full MS event followed by 40 MS / MS windows in one cycle resulting in a cycle time of 3 s. The full MS settings included an automatic gain control (AGC) target value of 100 % in the 360 – 1,300 m / z range with a maximum injection time of 50 ms and a resolution of 120,000 at m / z 200. 40 variable DIA precursor windows ranged from 368 m / z (lower boundary of 1st window) to 1,179 m / z (upper boundary of 40th window). Precursor ions were fragmented by HCD and a normalized collision energy of 30 %. MS / MS spectra were acquired with an AGC target value of 1000 % for the precursor window with a maximum injection time of 54 ms and a resolution of 30,000 at m / z 200.

LC-MS/MS data analysis

DIA-NN version 1.8.1 (PMID31768060) was used to generate an in-silico predicted spectral library composed of the mouse proteome (UniprotKB reference proteome, UP000000589) and common contaminants (MaxQuant contaminants.fasta) with trypsin as digestion enzyme and one missed cleavage specified. Subsequently the acquired raw files were processed in library-free mode using DIA-NN default settings and the match between runs function enabled.

3.6 Data analysis software

Flow cytometry data was analyzed with FlowJo (version 10). Cell number calculations were done in Excel. Thereby, total cell numbers were calculated based on percentages of lymphocytes multiplied with manually counted cell numbers per organ. For bone marrow, cell numbers of one tibia and one femur are given. Legendplex analyses were performed using the kit associated dongle-based software. Graphs were generated using GraphPad Prism (version 9). Figure presentation was done by affinity designer and BioRender. ImageStudio was used to depict and quantify western blot images (version 5.2). Indel analysis of A20 SSCs was enabled by the online Synthego platform. Bioinformatic analysis were done using RStudio (version 4.1.2) and Perseus (version 2.0.6).

4 Results

Previous studies performed in our laboratory and others indicated a crucial role of Roquin proteins within the B cell compartment[2,81]. Furthermore, the importance of Roquin in T_{FH} cells suppressing uncontrolled GC expansion and arising ANA production is widely accepted[3,68,76]. However, the B cell intrinsic function of Roquin during terminal B cell development has not yet been addressed in detail. As part of this PhD thesis, the role of Roquin 1 and Roquin 2 during GC reactions (chapter 4.1), SHM (chapter 4.2), APC formation and CSR (chapter 4.3) were investigated using CD19Cre and Cγ1Cre mouse models as well as *in vitro* A20 cell cultures (chapter 4.4).

4.1 Influence of Roquin on GC formation *in vivo*

4.1.1 Splenomegaly and expansion of B and T cell compartments in immunized CD19Cre Roquin knockout mice

The formation of GCB cells needs to be experimentally triggered by immunizations as specific pathogen-free housed mice are isolated from most natural occurring foreign organisms during their whole life time[139]. In general, the type of antigen, its dose and route of administration as well as the availability of downstream detection assays influences the quality of the biological readout. Thus, two types of antigens (SRBCs and NP-CGG) were employed in parallel during this project addressing different readouts of GC biology.

CD19Cre Roquin knockout mice were injected 10^8 SRBCs at an age ranging from 8 to 13 weeks (average 11 weeks). Their organs were analyzed 10 days after immunization at the peak of GC reaction. SRBCs elicit a T cell dependent immune response even in the absence of adjuvant and are commonly used since the 1960's[140]. SRBCs trigger a rather strong GCB reaction with high clonal diversity[24].

Assessed genotypes of CD19Cre or later Cγ1Cre mediated Roquin knockout mouse models allowed to monitor the gene-dosage effect of Roquin proteins in B cells:

(I) $Cre^{I/+}$ $Rc3h1^{F/F}$ $Rc3h2^{F/F}$ (later also referred to as Roquin 1/2 double KO mice),

(II) $Cre^{I/+}$ $Rc3h1^{F/F}$ $Rc3h2^{F/+}$ (Roquin 1 homo Roquin 2 het KO mice)

(III) $Cre^{I/+}$ $Rc3h1^{F/F}$ (Roquin 1 KO mice)

$Cre^{I/+}$ $Rc3h2^{F/F}$ animals were not analyzed since previous studies reported a strong compensatory role of Roquin 1 in the absence of Roquin 2 leading to no detectable phenotypic changes[82,83]. PBS or antigen-injected control animals were mostly $Cre^{I/+}$, but also partially contained animals with loxP-flanked Roquin 1 or Roquin 2 alleles without Cre expression. To visualize that there was no detectable difference between Cre-containing and Cre-less controls, both groups are shown individually for the detection of SRBC specific serum antibodies.

SRBC immunized CD19Cre Roquin KO mice recapitulate the splenomegaly (~2 fold elevated in size on average) as already seen in unimmunized CD19Cre $Rc3h1^{F/F}$ (~1.5 fold) or CD19Cre $Rc3h1^{F/F}$ $Rc3h2^{F/F}$ (~2 fold) animals together with the accompanying increase in splenocytes which was found to be most pronounced in Roquin 1/2 double KO mice (Fig. 5A, 5B and Suppl. Fig. 1A). In concordance with previous findings, elevated total splenocyte numbers can partially be explained by a moderate expansion of B cell numbers at least in CD19Cre $Rc3h1^{F/F}$ and CD19Cre $Rc3h1^{F/F}$ $Rc3h2^{F/+}$ mice (Fig. 5C). Nonetheless, the proportions of Roquin depleted B cells are reduced in all analyzed organs compared to controls hinting towards the developmental defect seen before by Dr. David Riess in unimmunized Roquin 1/2 double KO animals (see introduction). In addition, the T cell compartment including $TCR\beta^+$, $TCR\beta^+$ $CD4^+$ T cells, $TCR\beta^+$ $CD4^+$ $FoxP3^-$ and $TCR\beta^+$ $CD4^+$ $FoxP3^+$ (T_{reg}) are elevated in proportions and numbers in particular in CD19Cre $Rc3h1^{F/F}$ mice (Fig. 6). Although only recorded for a limited number of mice, $CD8^+$ T cells seem to be less affected by loss of Roquin in B cells (Fig. 6). However, published work demonstrated a 3 to 4-fold increase in effector memory like $CD8^+$ T cells ($CD44^{hi}$ $CD62L^{lo}$) in CD19Cre $Rc3h1^{F/F}$, which was recapitulated in CD19Cre $Rc3h1^{F/F}$ $Rc3h2^{F/F}$ animals. A more detailed staining would be needed to address the differentiation of naïve ($CD44^-$ $CD62L^+$), effector memory like and central memory like ($CD44^+$ $CD62L^+$) T cells in immunized CD19Cre mice as well. In line with this, the myeloid compartment was neglected here, but has been shown before to contribute to the observed splenomegaly[81,82]. Overall, no difference between unimmunized and immunized controls is detectable.

Apart from the spleen, lymph nodes contain more total cells in all three Roquin KO genotypes, too, however none of these changes reaches statistical significance. Total cell numbers of gut-associated lymphoid tissues (GALT), meaning mesenteric lymph nodes and peyer's patches, are unchanged in Roquin 1 KO and Roquin 1 homo Roquin 2 het KO mice, however less peyer's patches can be found in Roquin 1/2 double KO mice as already reported before (Suppl. Fig. 1B).

Taken together, the described perturbances in immunized CD19Cre Roquin KO animals match in direction and extent those seen in unimmunized animals validating the reproducibility of the obtained results and extending them to the so far not reported CD19Cre Rc3h1$^{F/F}$ Rc3h2$^{F/+}$ genotype.

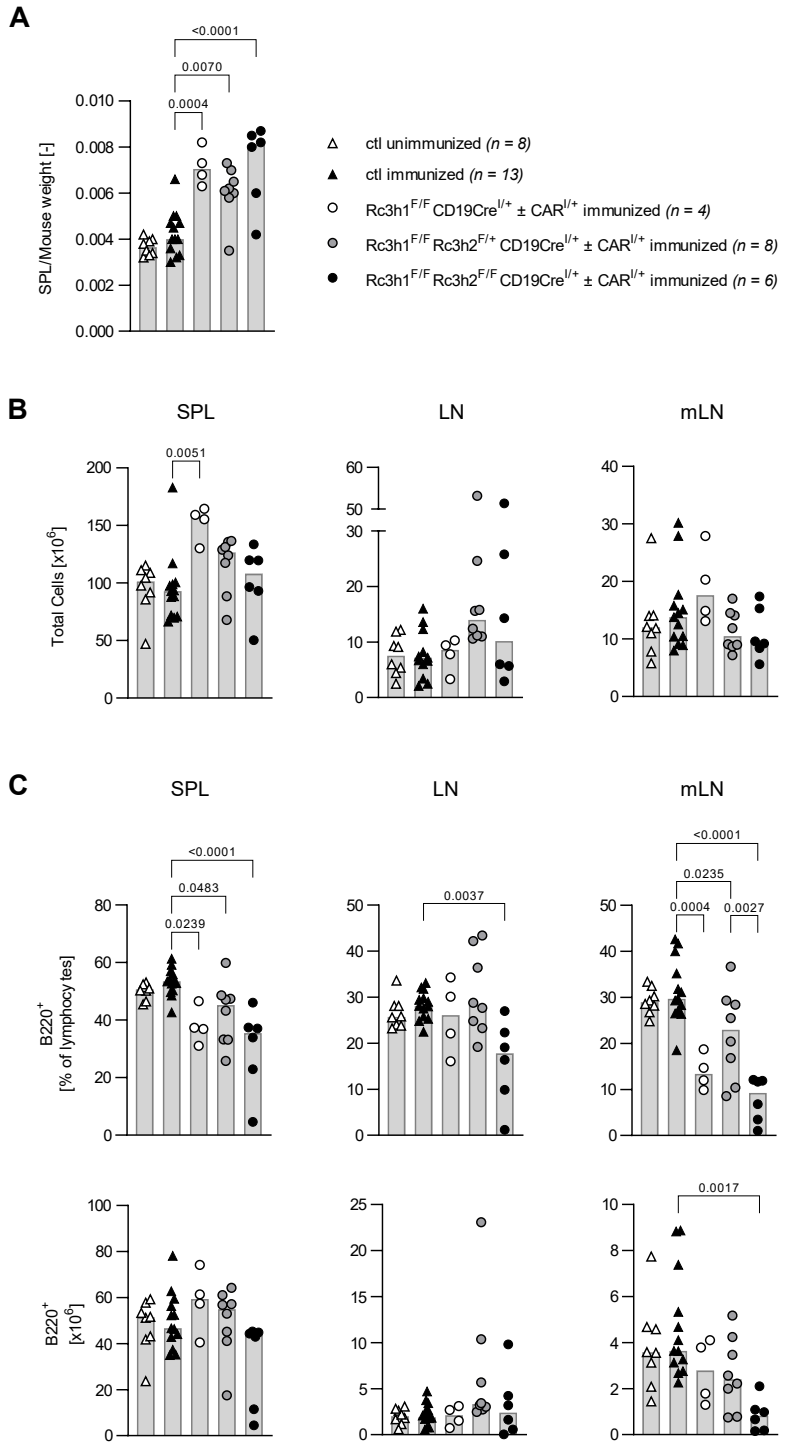

Figure 5: Enlargement of spleens upon SRBC immunization after 10 days in CD19Cre Roquin knockout mice and changes in B220⁺ B cell fractions.
(A) Spleen weight relative to mouse body weight. (B) Total lymphocyte cell numbers in indicated organs. For bone marrow, 1 femur and 1 tibia were considered for total cell number calculation. (C) B220⁺ B cell percentages and cell numbers in respective organs. Data are cumulative from 4 independent experiments. Bars show median values with each symbol representing a mouse. Statistical significance was determined by one-way ANOVA and most relevant p values, mainly compared to immunized controls, are shown. SPL, spleen; LN, lymph nodes; mLN, mesenteric lymph nodes

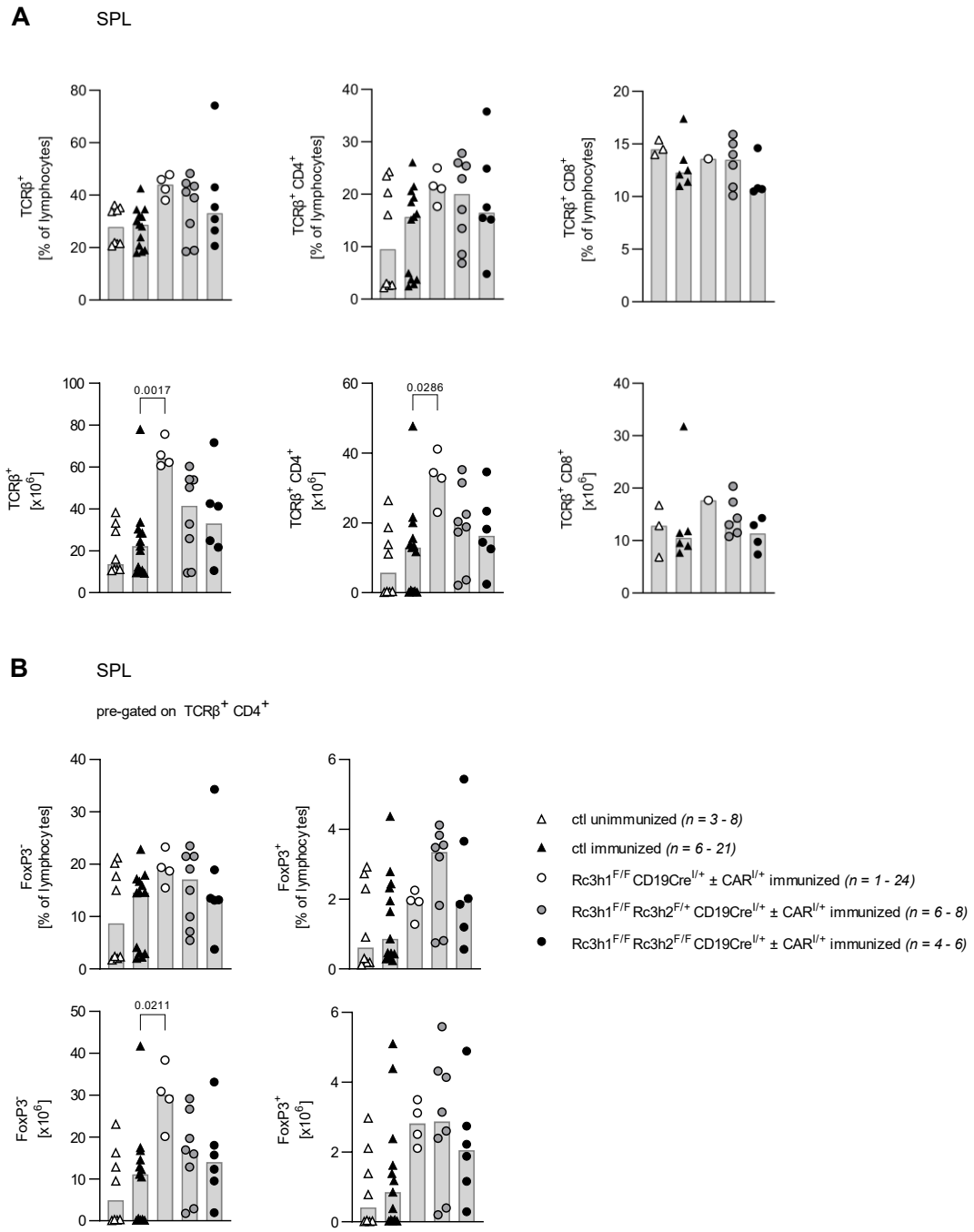

Figure 6: T cell subsets upon SRBC immunization after 10 days in CD19Cre Roquin knockout mice. (A) T cell subset percentages and numbers in spleen. (B) FoxP3 positive and negative CD4+ T cell percentages and numbers. Data are cumulative from 4 independent experiments, respectively. Bars show median values with each symbol representing a mouse. Statistical significance was determined by one-way ANOVA and p values compared to immunized controls are shown. SPL, spleen

4.1.2 CD19Cre mediated loss of both Roquin proteins impedes GC reactions

One of the main objectives during this project was to dissect the role of Roquin 1 and 2 in late B cell development, specifically during GCB and APC differentiation. Independent of the mouse model used, GCB cells were assessed by flow cytometry using the surface markers $B220^{+}$ $CD138^{-}$ $CD95^{hi}$ $CD38^{lo}$ $GL7^{+}$ for their identification (see gating strategy in Fig. 7A). Intracellular BCL6 expression levels were further monitored for a proper distinction between GCBs and naïve $B220^{+}$ cells especially in the absence of a vast and easily recognizable GCB population. Initially, GCB formation was analyzed in a CD19Cre background followed by more in-depth analysis in Cγ1Cre Roquin depleted animals.

In mice with CD19Cre-mediated ablation of Roquin proteins, it was most remarkable to see that GCBs are completely absent in Roquin 1/2 double KO animals even upon induction of a strong immune response via SRBC injection in all secondary lymphoid organs (Fig. 7B). The potency of the immunization reagent and technique was proven by the fact that immunized and unimmunized controls differ by 10-fold in their median GCB percentages, by 8-fold in their GCB total cell numbers in spleen as well as almost 2-fold in their GCB total cell numbers in lymph nodes. Thereby, GCB percentages and numbers of Roquin 1/2 double KO animals range even below those of unimmunized controls with the latter containing low basal GCB levels induced by the clean, but still non-sterile environment of the mice. This indicates a major perturbance of GCB formation recognized here at day 10 due to the introduced genetic lesions.

In strong contrast, Roquin 1 KO mice present with a definite elevation of GCB cell production while Roquin 1 homo Roquin 2 het KO mice show an intermediate phenotype with a reduction, but not complete collapse of the GCB compartment. Roquin 1 homo Roquin 2 het KO spleens obtain 3-fold reduced GCB percentages and numbers compared to controls (0.2 Mio cells vs. 0.6 Mio cells) hinting towards an affected GCB maturation balancing the reverse effects of their Roquin 1 KO or Roquin 1/2 double KO equivalents. These data fit to previous observations of Dr. David Riess showing a significant upregulation of $B220^{+}$ PNA^{+} $CD95^{+}$ $CD38^{lo}$ $CD19^{+}$ GCBs in spleens, mesenteric lymph nodes and peyer's patches of Mb1Cre $Rc3h1^{F/F}$ and a minor downregulation in Mb1Cre $Rc3h1^{F/F}$ $Rc3h2^{F/+}$ mice[82]. Trends seen in spleens are recapitulated in lymph nodes, however mesenteric lymph nodes are less severely affected.

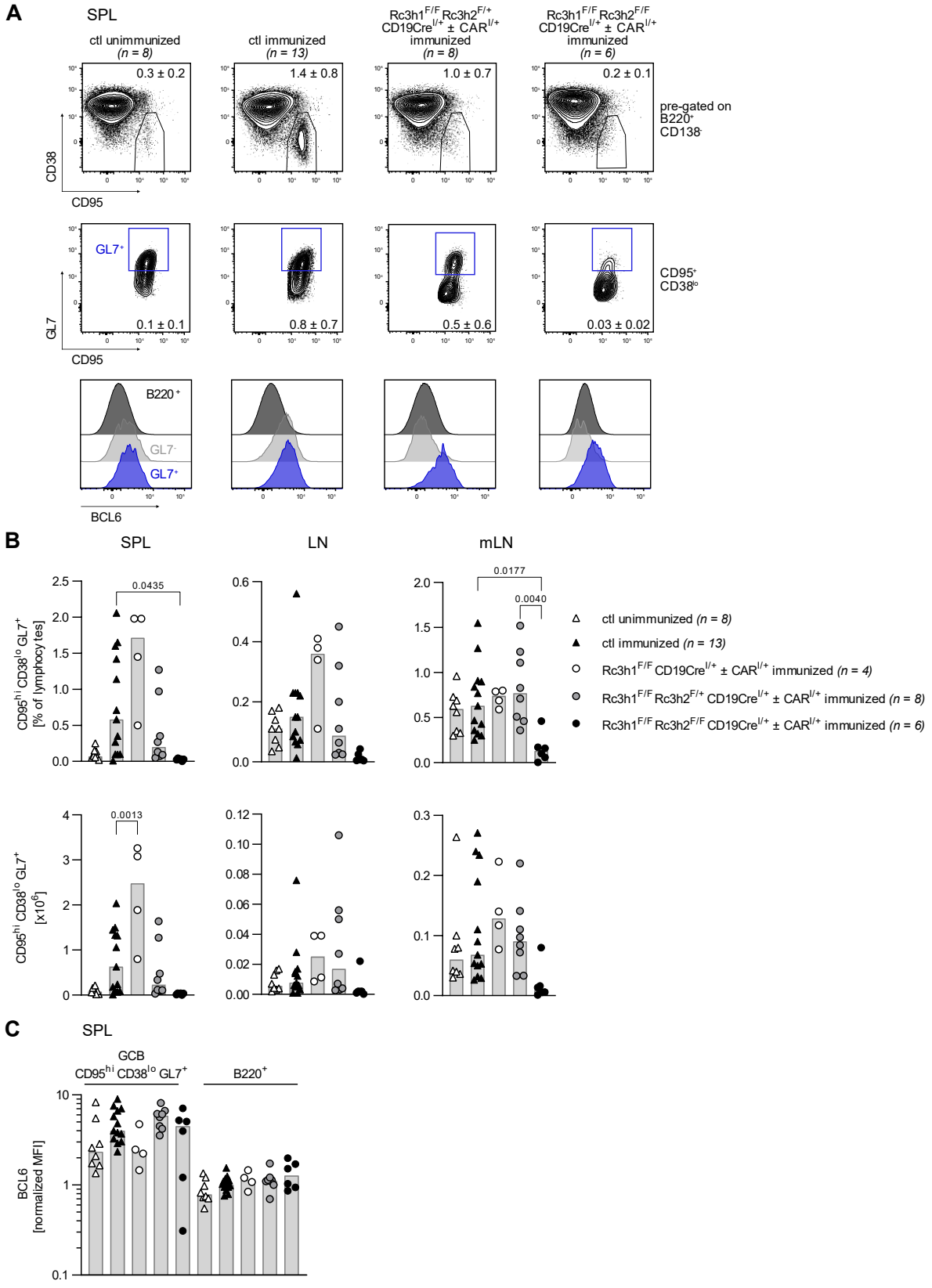

Figure 7: GCBs upon SRBC immunization after 10 days in CD19Cre Roquin knockout mice.
(A) Representative flow cytometry plots of GCBs in spleen. Percentages correspond to mean ± SD of GL7$^+$ GCBs within the lymphocyte population. (B) GCB percentages and numbers. (C) BCL6 expression levels of GCBs in comparison to B220$^+$ B cells exemplarily shown for spleen. MFI values are normalized per experiment to B220$^+$ cells of immunized controls. Data are cumulative from 4 independent experiments. Bars show median values with each symbol representing a mouse. Statistical significance was determined by one-way ANOVA and p values of most relevant comparisons are shown. SPL, spleen; LN, lymph nodes; mLN, mesenteric lymph nodes; B B220$^+$; GCB B220$^+$ CD38^{lo} CD95^{hi} GL7$^+$

4.1.3 Splenomegaly and expansion of B and T cell compartments in immunized Cγ1Cre Roquin knockout mice

The observation that GCBs cannot be formed upon CD19Cre mediated knockout of both Roquin 1 and Roquin 2 motivated us to dissect the role of Roquin proteins in the GC reaction further. CD19Cre Roquin KO mice suffer from a B cell maturation defect which also negatively impacts the naïve B cell compartment and thus could affect all subsequent developmental stages including GCB cells. Thus, it is not the optimal setting to address the influence of Roquin singularly on GCBs. To circumvent this issue, Roquin floxed alleles were introduced into mice containing an alternative Cre recombinase, namely Cγ1Cre.

Cγ1Cre mouse models are a highly useful tool to study protein knockouts specifically in the GC reaction and APC differentiation. In these mice, an IRES-Cre has been inserted 3' attached to the last Cγ1 exon enabling loxP-flanked gene deletion upon transcription of the Cγ1 locus. Thereby, transcription of the IgG1 locus is not necessarily determining a final CSR to IgG1 as well. Thus, also Cre-active GCBs of all other isotypes can be detected. Cre activity was published to reach 25 - 50 % of GCBs at day 4 and 85 – 95 % at day 10 after immunization with either SRBCs or NP-CGG[47,141].

In this study, Cγ1Cre animals harboring conditional Roquin alleles were immunized using SRBCs. Their organs were harvested again at day 10 after injection at an age of 8 - 16 weeks (average 12 weeks). Because there is no available antibody recognizing selectively Roquin 1 or Roquin 2 with sufficient sensitivity for flow-cytometry analysis and because the studied cell populations are rare which greatly impedes western-blot analysis, Cre-mediated recombination was tracked indirectly by the bright tdTomato fluorescent reporter (dTOM). dTOM has been inserted into the Rosa26 locus and is driven by a CAG promotor after excision of the 5' loxP-stop-loxP cassette[131,142]. Spontaneous germline deletions of dTOM or Roquin alleles caused by Cγ1Cre were excluded by the genotyping protocol.

Cγ1Cre Roquin KO mice present with significantly enlarged spleens albeit differences are less prominent than in CD19Cre Roquin KO mice (Fig. 8A and Suppl. Fig. 2A). For example, median spleen weight differences between Roquin 1/2 double KO mice and immunized controls are 42 mg in a Cγ1Cre background, but 118 mg for respective CD19Cre containing genotypes. Nevertheless, this shows that, at least in part, splenomegaly of mice with Roquin deficiency in B cells is caused by late B cell maturation events. Increased spleen weights are reflected in total cell numbers which are also enhanced with similar trends between genotypes in lymph nodes of Cγ1Cre Roquin KO mice (Fig. 8B). Other than in CD19Cre animals, GALT tissues and bone marrow are not affected by the depletion of Roquin in a Cγ1Cre background with regards to total cell numbers (Suppl. Fig. 2C). Loss of peyer's patches in Roquin 1/2 double KO CD19Cre mice does not occur anymore in a Cγ1Cre background (Suppl. Fig. 2B).

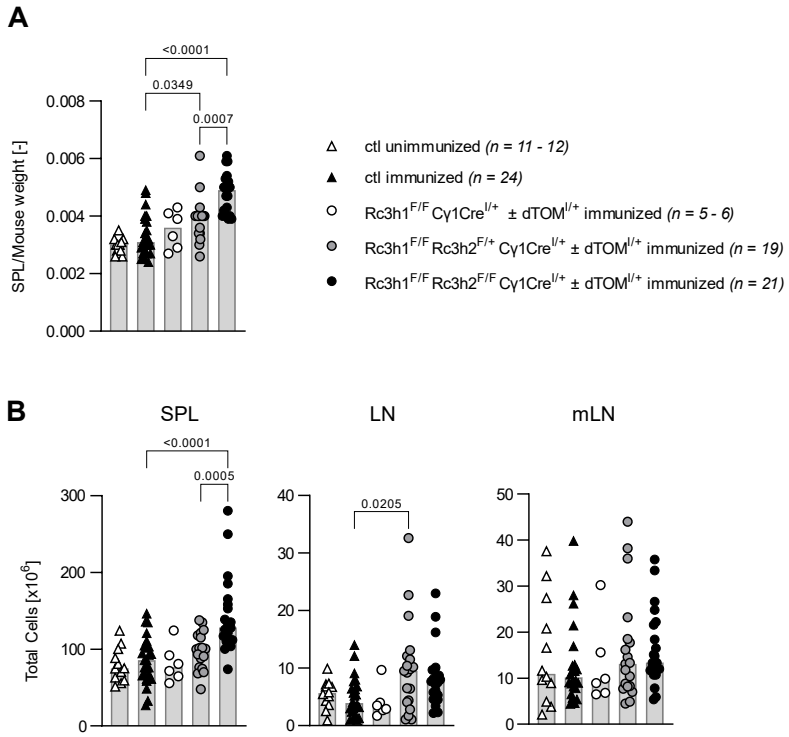

Figure 8: Enlargement of spleens upon SRBC immunization after 10 days in Cγ1Cre Roquin knockout mice.
(A) Spleen weight relative to mouse body weight. (B) Total lymphocyte cell numbers for indicated organs. Data are cumulative from at least 3 independent experiments. Bars show median values with each symbol representing a mouse. Statistical significance was determined by one-way ANOVA and p values of most relevant comparisons are shown. SPL, spleen; LN, lymph nodes; mLN, mesenteric lymph nodes

Similar to CD19Cre mice, GCB-specific ablation of Roquin causes B cell extrinsic effects on the T cell compartment contributing to the observed splenomegaly (Fig. 9). TCRß$^+$ T cell percentages are slightly elevated between 3 – 5 % in Roquin KO genotypes with Roquin 1 KO mice showing the greatest increase. CD4$^+$ T cell percentages are enriched in Roquin 1 homo Roquin 2 het KO and Roquin 1/2 double KO animals compared to immunized controls while percentages of CD8$^+$ T cells are unaffected and only numbers are elevated due to the splenomegaly in those animals. Again, FoxP3$^+$ T_{reg} proportions are significantly amplified within CD4$^+$ T cells with all Roquin KO genotypes showing a similar expansion. FoxP3$^+$ T_{reg} numbers in Roquin 1/2 double KO mice are even 4-fold enriched compared to immunized controls. A more detailed characterization based on the additional surface markers CXCR5$^-$ CD25^{hi} hints towards a similar trend at least in Roquin 1 homo Roquin 2 het KO and Roquin 1/2 double KO animals, although more biological replicates are still needed to support this dataset (Suppl. Fig. 3). FoxP3$^-$ T cell percentages are almost unchanged upon loss of Roquin and only a minor elevation of TCRß$^+$ CD4$^+$ FoxP3$^-$ CXCR5^{hi} PD1^{hi} T_{FH} T cells in Roquin 1 KO and Roquin 1/2 double KO mice can be seen, even though the PD1 staining intensity is not optimal (Suppl. Fig. 3). Within CD4$^+$ as well as CD8$^+$ T cells, the ones showing an effector memory like phenotype (CD44$^+$ CD62L$^-$) are augmented with Roquin 1/2 double KO mice showing the greatest deviation from immunized controls (Fig. 10). CD4$^+$ central memory like T cells (CD44$^+$ CD62L$^+$) are also enriched at the expense of naïve T cells (CD44$^-$ CD62L$^+$) although this effect does not reach significance.

In summary, B cell extrinsic effects occur even upon developmentally late Cγ1Cre-mediated depletion of Roquin and resemble in type the ones seen before in CD19Cre mice. Among Roquin KO animals, loss of both Roquin 1 and Roquin 2 presents with the highest impact on the T cell compartment.

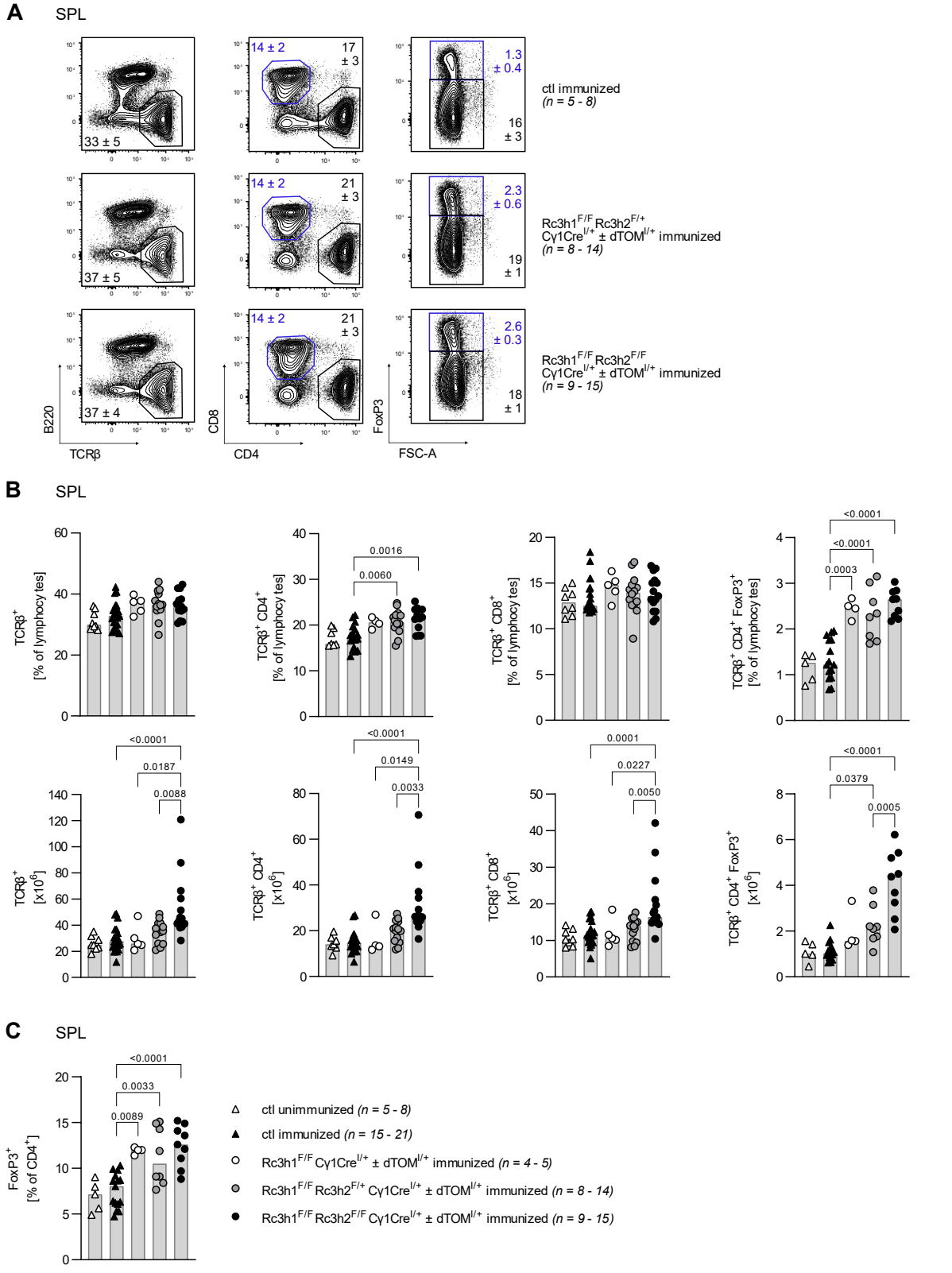

Figure 9: T cells upon SRBC immunization after 10 days in Cγ1Cre Roquin knockout mice.
(A) Representative flow cytometry plots of T cell subsets pre-gated on living lymphocytes in spleen. Percentages correspond to mean ± SD of gated populations within the lymphocyte population. (B) T cell subset percentages and numbers. (C) Fraction of FoxP3$^+$ T cells withing the TCRß$^+$ CD4$^+$ lymphocyte population. Data are cumulative from at least 5 independent experiments, respectively. Bars show median values with each symbol representing a mouse. Statistical significance was determined by one-way ANOVA and p values of most relevant comparisons are shown. SPL, spleen

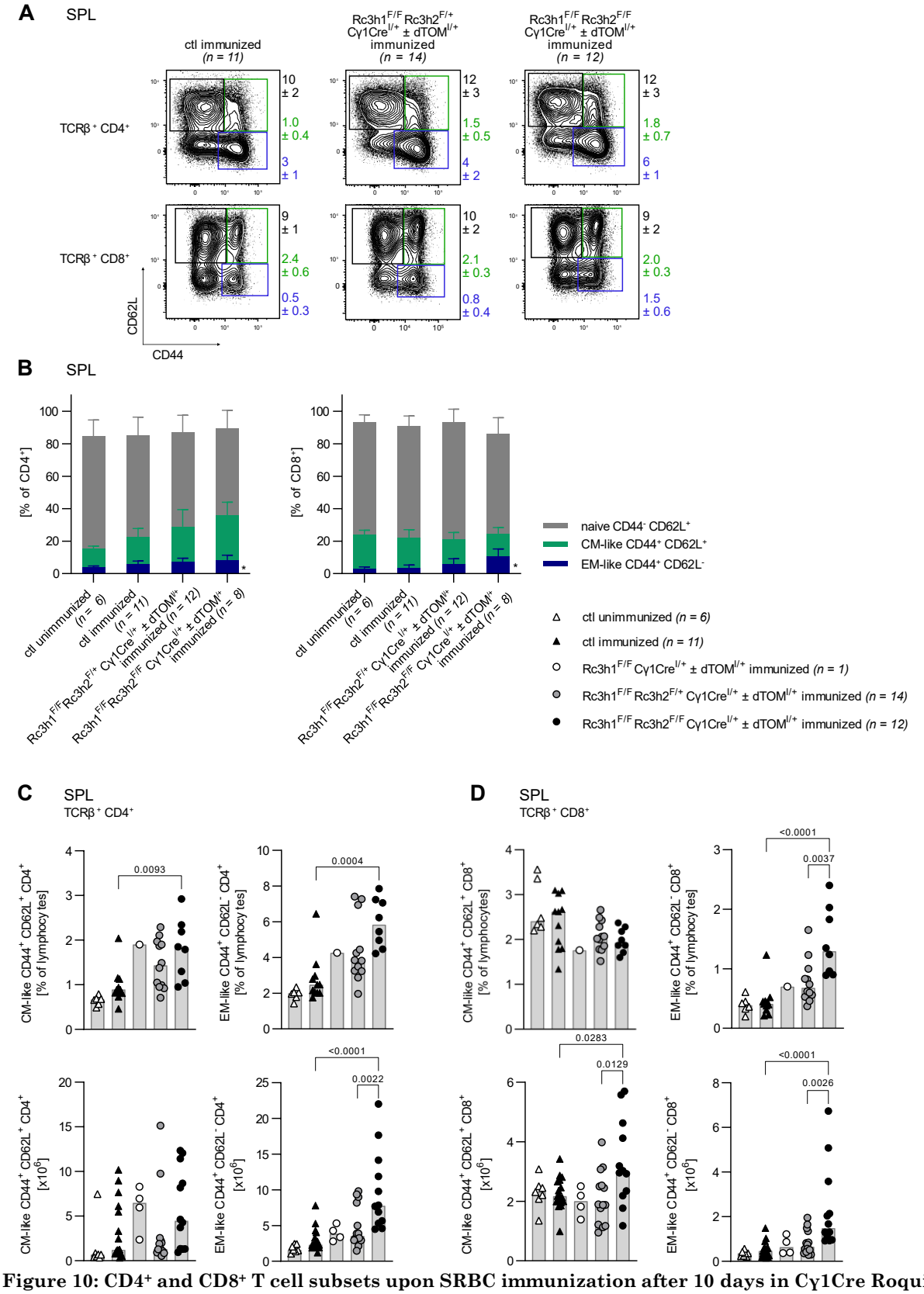

Figure 10: CD4⁺ and CD8⁺ T cell subsets upon SRBC immunization after 10 days in Cγ1Cre Roquin knockout mice.

(A) Representative flow cytometry plots of T cell subsets pre-gated on TCRß⁺ CD4⁺ or TCRß⁺ CD8⁺ T cells in spleen. Percentages correspond to mean ± SD of gated populations within the lymphocyte population. (B) T cell subset percentages as fraction of TCRß⁺ CD4⁺ or TCRß⁺ CD8⁺ T cells. (C) CM-like and EM-like CD4⁺ T cell subset percentages and numbers. (D) CM-like and EM-like CD8⁺ T cell subset percentages and numbers. Data are cumulative from 4-6 independent experiments, respectively. Bars show median values with each symbol representing a mouse. Statistical significance was determined by one-way ANOVA and p values of most relevant comparisons are shown. SPL, spleen; EM-like effector memory like; CM-like central memory like

In line with Cre recombination being initiated earliest after antigen activation, non-stimulated B220$^+$, CD21$^+$ CD1d$^+$ CD23$^-$ IgD^{lo} MZB and CD21^{lo} CD1d^{lo} IgD^{hi} FOB percentages of Cγ1Cre Roquin KO mice are unaffected in spleen, mesenteric lymph nodes, bone marrow and peyer's patches (Fig. 11, 12 and Suppl. Fig. 4). Expansion of B220$^+$ or FOB cell numbers in spleen and lymph nodes contribute to the increase of total cells in these organs with Roquin 1/2 double KO animals showing strongest enrichments. B220$^+$ percentages and cell numbers of immunized Cγ1Cre controls reflect those seen in corresponding CD19Cre animals. MZB percentages are in line with the literature for C56BL/6[17].

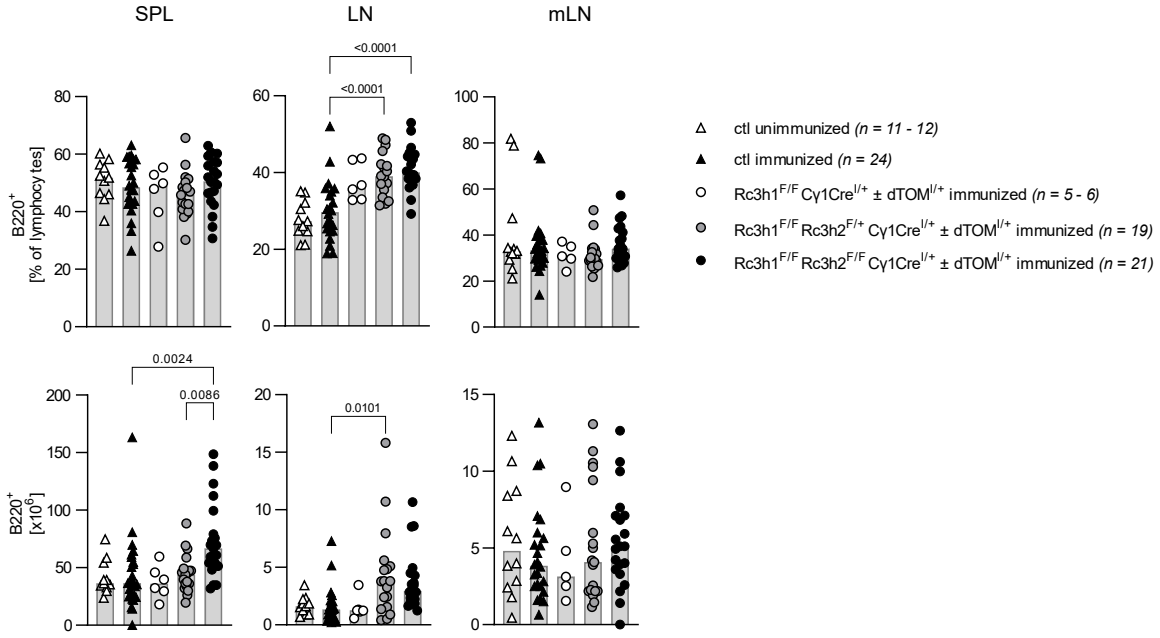

Figure 11: B220$^+$ cells upon SRBC immunization after 10 days in Cγ1Cre Roquin knockout mice. B220$^+$ proportions and numbers. Data are cumulative from at least 7 independent experiments. SPL, spleen; LN, lymph nodes; mLN, mesenteric lymph nodes

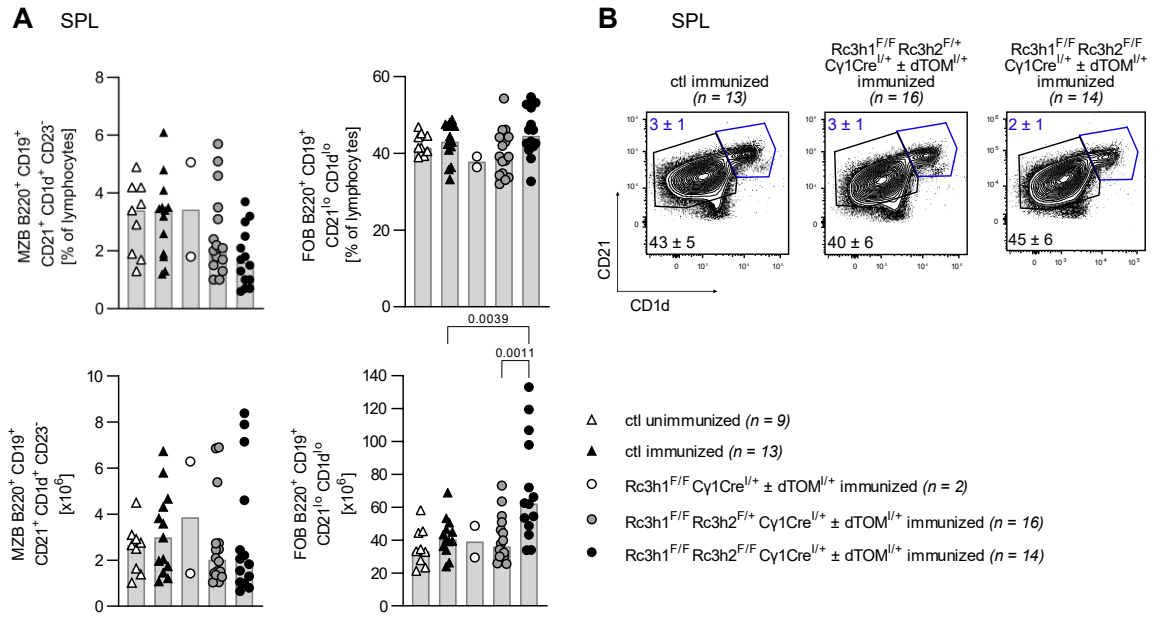

Figure 12: MZB and FOB upon SRBC immunization after 10 days in Cγ1Cre Roquin knockout mice. (A) MZB and FOB percentages and numbers. (B) Representative flow cytometry plots of MZB and FOB in spleen pre-gated on B220$^+$ CD19$^+$ lymphocytes. Percentages correspond to mean ± SD within the lymphocyte population. Data are cumulative from at least 7 independent experiments. SPL, spleen; MZB B220$^+$ CD19$^+$ CD21$^+$ CD1d$^+$ CD23$^-$; FOB B220$^+$ AA4.1$^-$ CD19$^+$ CD21^{lo} CD1d^{lo}

4.1.4 Roquin proteins regulate GCB expansion in Cγ1Cre mice

Roquin 1/2 double KO CD19Cre mice have been shown to be devoid of GCBs upon SRBC immunization. This could be a result of accumulating B cell deficits during development or could imply an essential role of Roquin proteins specifically during GCB formation. To differentiate between those two scenarios, GCBs were evaluated further in mice with a Cγ1Cre-based deletion of Roquin alleles.

Nicely, these analyses reveal a gene-dosage dependent effect of Roquin 1 and Roquin 2 recapitulating the lack of GCBs observed in Roquin 1/2 double KO CD19Cre mice (Fig. 14). While the B cell specific depletion of Roquin 1 leads to an increase of GCB cell numbers by ~2-fold in spleen and lymph nodes, compensatory mechanisms executed by Roquin 2 are essential to protect GC reactions from a total collapse. Roquin 1 homo Roquin 2 het KO GCBs are protected from elimination and even outperform control GCBs in lymph nodes suggesting that even the presence of a single Roquin 2 allele is sufficient for cell survival. BCL6 expression levels are significantly upregulated in Roquin 1 homo Roquin 2 het KO or Roquin 1/2 double KO GCBs (~4-fold in both genotypes) compared to controls. Increased BCL6 expression was already observed in a CD19Cre background, however only ~1.5-fold

in Roquin 1 homo Roquin 2 het KO mice and ~1-fold in Roquin 1/2 double KO GCBs compared to respective controls hinting towards a regulation upon acute Roquin ablation during the GC reaction (Fig. 7C). Overall, trends in GCB percentages are reflected also by cell numbers. To my knowledge, these are the first mice to date which demonstrate the indispensable function of Roquin proteins in GCB biology.

To characterize Roquin ablated GCBs in more detail, their DZ/LZ pattern was analyzed via flow cytometry revealing the characteristic centroblast:centrocyte ratio of 2:1 at day 10 after immunization in all analyzed secondary lymphoid organs (Fig. 13)[143]. This shows that Roquin proteins are not required to build up a DZ/LZ polarization. The data could also be recapitulated in CD19Cre animals (data not shown).

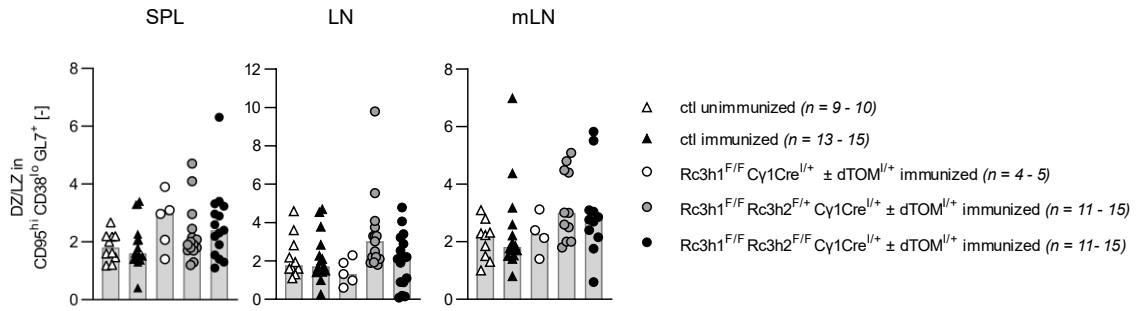

Figure 13: DZ/LZ ratios upon SRBC immunization after 10 days in secondary lymphoid organs of Cγ1Cre Roquin knockout mice.
DZ/LZ ratios in respective organs. Data are cumulative from at least 2 independent experiments. Bars show median values with each symbol representing a mouse. Statistical significance was determined by one-way ANOVA. SPL, spleen; LN, lymph nodes; mLN, mesenteric lymph nodes; DZ B220^{+} CD38^{lo} CD95^{hi} GL7^{+} CXCR4^{hi} CD86^{lo}; LZ B220^{+} CD38^{lo} CD95^{hi} GL7^{+} CXCR4^{lo} CD86^{hi}

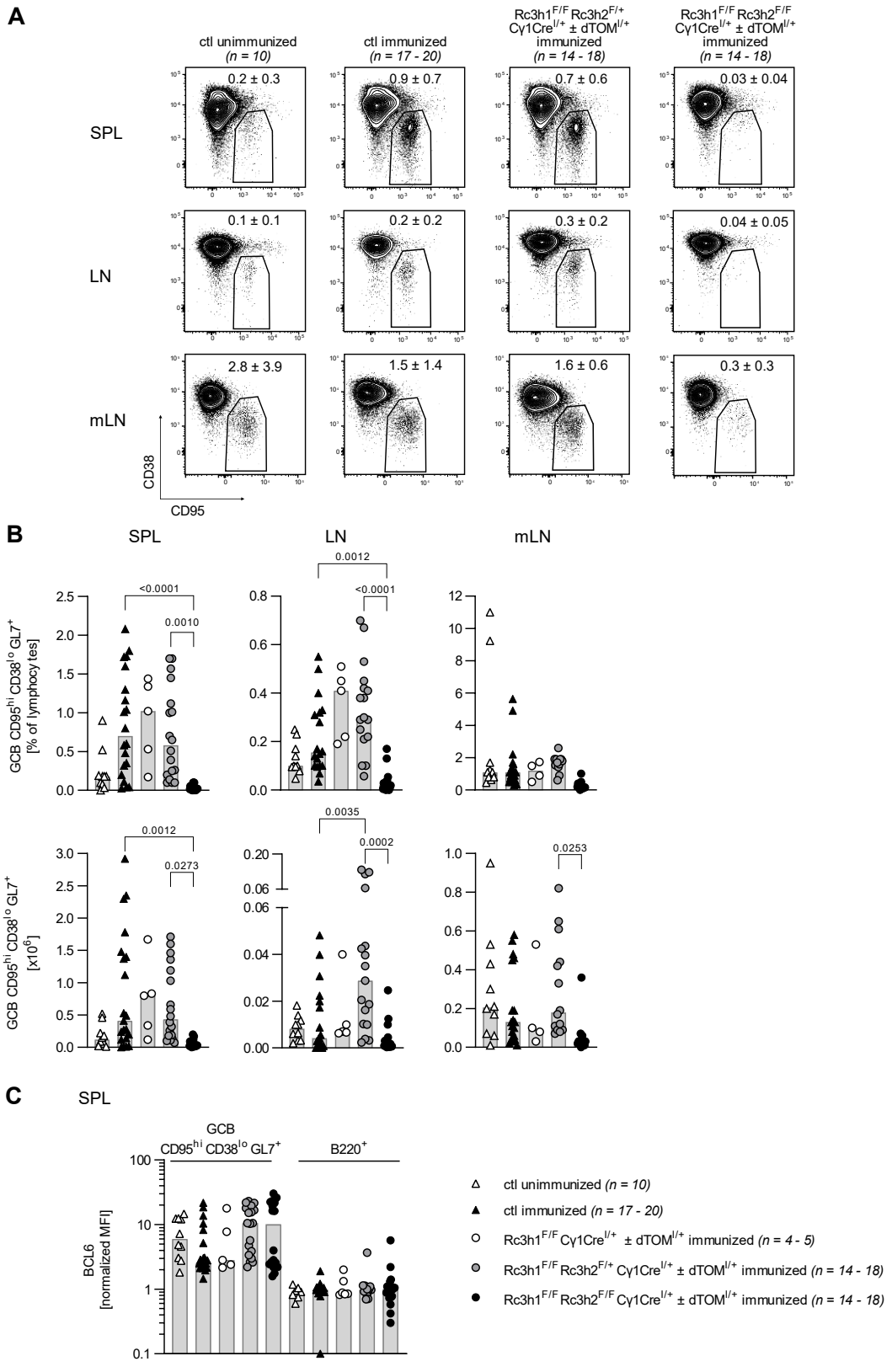

Figure 14: GCBs upon SRBC immunization after 10 days in Cγ1Cre Roquin knockout mice.
(A) Representative flow cytometry plots of GCBs in respective organs pre-gated on B220$^+$ lymphocytes. Percentages correspond to mean ± SD of GCBs within the lymphocyte population. (B) GCB percentages and numbers. (C) BCL6 expression levels of GCBs in comparison to B220$^+$ B cells exemplarily shown for spleen. MFI values are normalized per experiment to B220$^+$ cells of immunized controls. Data are cumulative from 8-9 independent experiments. Bars show median values with each symbol representing a mouse. Statistical significance was determined by one-way ANOVA and p values of most relevant comparisons are shown. SPL, spleen; LN, lymph nodes; mLN, mesenteric lymph nodes; B B220$^+$; GCB B220$^+$ CD38^{lo} CD95^{hi} GL7$^+$

4.1.5 High Cγ1Cre recombination efficiency and selectivity in immunized Roquin knockout mice

Cre activity allows tissue-specific deletion of loxP-flanked target genes. However, Cre-mediated recombination is known to be less than 100% in any biological system applied, and can eventually result in undesirable deletions already in the germline. The efficiency and selectivity of Cre-induced excision depends on the strength and stringency of the promotor driving Cre expression and the accessibility of the target gene locus. Thus, Cre activity needs to be re-validated in every individual setting.

As described before, the extent of Roquin 1/2 ablation was estimated in Cγ1Cre containing mice by the reporter fluorochrome dTOM. This revealed, that Cγ1Cre activity is very well restricted to GCBs and APCs since there is no detectable dTOM reporter expression in circulating $B220^+$ B cells, MZB or FOB of spleen, lymph nodes or mesenteric lymph nodes (Fig. 15A). Due to the brightness of the fluorophore, dTOM positive and negative populations are clearly separated as shown exemplarily for spleen in Fig. 15C and Suppl. Fig. 5.

Whenever a clear distinction between GCBs and non-GCBs is possible already by the cell surface markers $B220^+$ $CD38^{lo}$ $CD95^+$ only, those gated GCBs are majorly (> 70 %) dTOM positive as seen for immunized control animals. However, only $B220^+$ $CD38^{lo}$ $CD95^+$ $GL7^+$ B cells are bona-fide BCL6 expressing GCB cells in Roquin 1/2 double KO animals (Fig. 15B). Thus, all subsequent analysis of Roquin 1/2 double KO GCBs without the addition of the GL7 antibody probably overestimate the size of the GCB cell compartment. Similar percentages of $dTOM^+$ control (median 88 %), Roquin 1 homo Roquin 2 het KO (median 94 %) and Roquin 1/2 double KO $GL7^+$ GCBs (median 80 %) indicate that Roquin ablated cells are not counter-selected.

$IgG1^+$ APCs of all genotypes are largely $dTOM^+$ indicative of an efficient Cre-mediated recombination upon CSR from IgM to IgG1. In half of the immunized control animals, IgM^+ APCs are $dTOM^-$ meaning Cre transcription as well as CSR did not occur (yet). However, in Roquin 1 homo Roquin 2 het KO or Roquin 1/2 double KO animals, Cre transcription and dTOM re-arrangement occurred in all IgM^+ APCs even though they did not class-switch. This might hint towards an increased transcription of the Cγ1 locus, but

defective subsequent steps to ultimately induce CSR or an advantage of Roquin-deficient plasmablasts.

Overall, Cre recombination of the dTOM allele and thus most likely also of Roquin 1 and Roquin 2 target genes resembles previous reports by Casola et al. and shows that Roquin deficient cells are not strongly counter-selected within the populations analyzed[47].

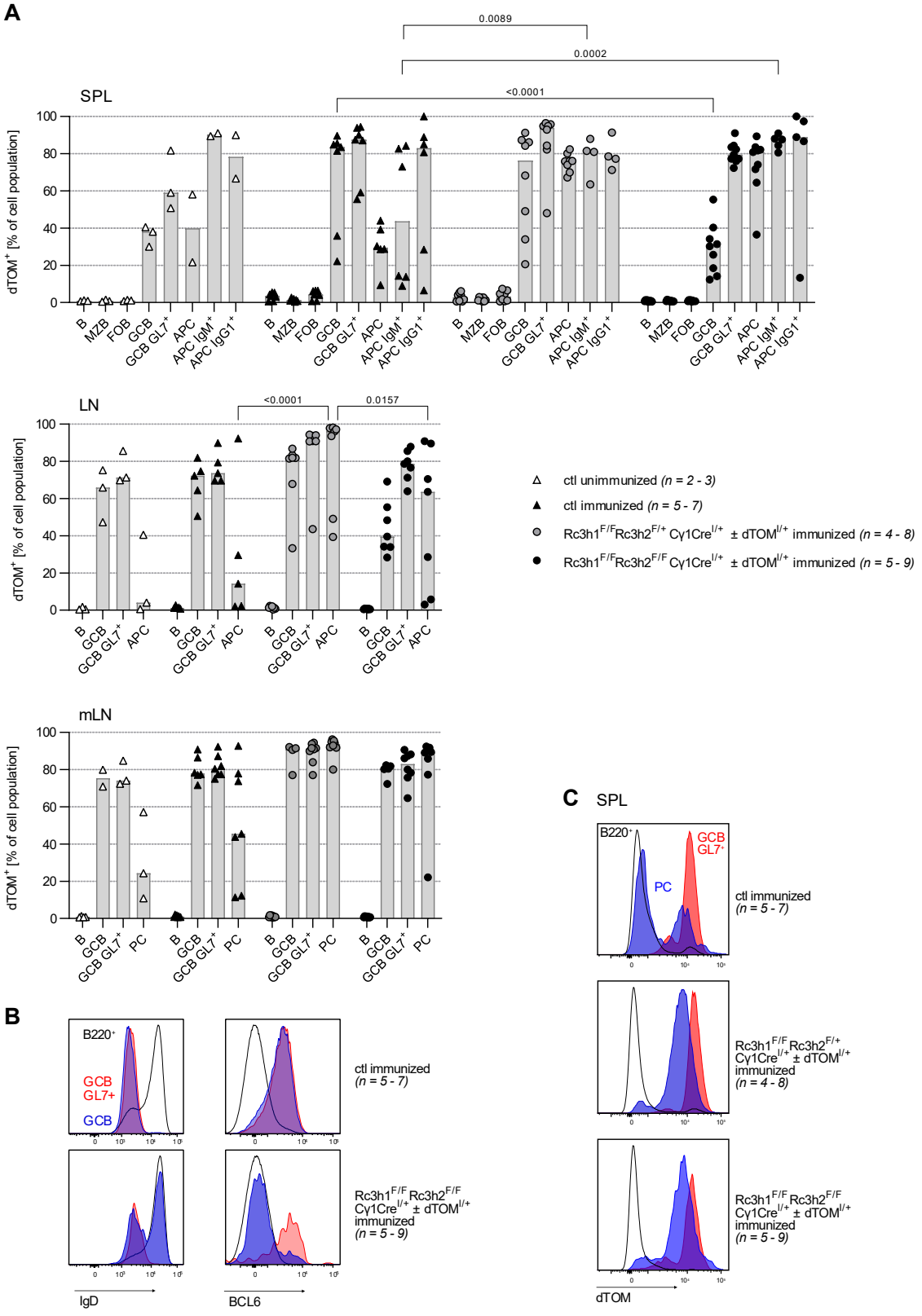

Figure 15: dTOM expression efficiency in B cell populations of different organs upon SRBC immunization after 10 days in Cγ1Cre Roquin knockout mice.
(A) dTOM percentages in different B cell subsets and mouse organs. (B) Representative flow cytometry histograms of IgD and BCL6. (C) Representative flow cytometry histograms of dTOM in three different genotypes. Data are cumulative from at least 3 independent experiments. Bars show median values with each symbol representing a mouse. Statistical significance was determined by one-way ANOVA and p values of most relevant comparisons are shown. SPL, spleen; LN, lymph nodes; mLN, mesenteric lymph nodes; B B220^{+} CD38^{+} CD95^{lo}; MZB B220^{+} CD19^{+} CD21^{+} CD1d^{+} CD23^{-}; FOB B220^{+} AA4.1^{-} CD19^{+} CD21^{lo} CD1d^{lo}; GCB B220^{+} CD38^{lo} CD95^{hi}; GCB GL7^{+} B220^{+} CD38^{lo} CD95^{hi}; APC CD138^{+} IRF4^{+} B220^{lo}

4.1.6 Roquin knockout does not abolish naïve B cell activation

Further experiments intended to better understand the disruption of the GCB equilibrium upon loss of Roquin. Manifold checkpoints and cellular pre-requisites determine GC formation with one of them being the need of B cells to get activated by cognate antigen which induces migration and proliferation. The ability of Roquin KO B cells to upregulate activation surface markers was addressed by flow cytometry looking at CD69, CD25, CD80, CD86, BAFFR and MHCII. In the following, I briefly introduce these proteins:

CD69

CD69 is an early activation marker which is transiently upregulated after stimulation. Upon cellular activation, CD69 homodimers are detectable on the surface even before CD25. CD69 expression has been linked, at least in T cells, to the surrounding oxygen levels with hypoxia, as it is also found in GC follicles, enhancing CD69 transcription through HIF1α signaling[144–146].

CD25 (IL2 receptor alpha)

CD25 is the central subunit of the high affinity IL2 receptor. Its expression is linked to cell activation of peripheral B cells, too. CD25 is upregulated *in vitro* upon TLR ligand (e.g., LPS) and anti-Ig stimulation. Isolated $CD25^+$ B cells express higher levels of CXCR5 and CXCR4 allowing them to migrate more efficiently to the T cell zone or DZ than $CD25^-$ B cells[147,148].

CD80 and CD86

CD80 and CD86 are both costimulatory molecules binding to CD28 or CTLA-4 on $CD4^+$ T cells. CD86 is only weakly expressed on resting B cells, but both proteins are upregulated upon activation. They are essential for GCB formation as $CD86^{-/-}$ $CD80^{-/-}$ mice are deficient of GCBs and impaired to class switch upon immunization[149,150].

BAFFR

BAFF is a cytokine of the TNF superfamily and a fundamental survival signal provided by many cell types, including T_{FH} and FDCs. BAFF is acting differentiation-dependent through two possible receptors: BAFFR or TACI. BAFFR expression intensities were measured to be highest in the follicle surrounding mantle zone which is composed of activated IgM^+ IgD^+ B cells, although BAFFR could also be detected in the DZ or LZ. This

suggests that BAFFR is crucial for antigen activated B cell maturation at the earlier stages of the GC reaction whereas TACI becomes more relevant during APC development[151,152]. Second, BAFF is mandatory for proper FDC network formation and therefore impacts antigen presentation[153]. Third, BAFF deficient ($BAFF^{-/-}$ mice), BAFFR deficient or BAFFR defective (A/WySnJ) mice are still capable to generate GC follicle structures, however these are reduced in size, less frequent and cannot be maintained as long as in WT conditions. Present GCs of A/WySnJ mice are not impaired in affinity maturation or apoptosis, but appear to be less proliferative as measured by Ki67. Hence, BAFF signaling also through BAFFR is required for GC maintenance both B cell intrinsically and extrinsically[151,154].

MHCII

MHCII antigen presentation is particularly decisive for early B cell selection by T_{FH} and higher MHCII densities on the surface are correlated with an advantage in entering the GC compartment. Once the GC is fully established, including DZ/LZ structures, even cells with low MHCII expression are capable to produce high-affinity antibodies[155].

Activation marker expression levels in CD19Cre-mediated Roquin KO mice

Naive $B220^{+}$ B cells of SRBC immunized Roquin KO CD19Cre animals appear hyperactivated based on their increased expression of CD86 in all three genotypes compared to controls (Fig. 16A). Furthermore, CD69 levels are slightly elevated in Roquin 1/2 double KO mice, although the effect is lost in Roquin 1 KO or Roquin 1 homo Roquin 2 het KO mice. However, data of CD25 and CD69 in Roquin 1 KO B cells are derived of only one mouse and thus cannot be used to make a generally valid statement. MHCII and BAFFR levels are moderately upregulated, but this trend fails to reach significance. In line with the here presented findings, *ex vivo* isolated B cells of non-immunized Roquin 1/2 double KO mice were found by Dr. David Riess to upregulate MHCII, CD69 and CD86 to similar extents (1.4 – 1.6).

Activation marker expression levels in Cγ1Cre-mediated Roquin KO mice

As expected, naïve B cells of Cγ1Cre mice are unchanged in their activation status between genotypes whereas GCBs overall express increased levels of the assessed surface molecules (Fig. 16B-D). For technical reasons, GCBs are determined here by CD38 and CD95 only which led to a $MHCII^{hi}$ and $MHCII^{lo}$ population in Roquin 1/2 double KO mice possibly due to a contamination with non-GCBs accounting for the $MHCII^{lo}$ proportion (Fig. 16D). Thus, MFI values presented here are extracted from $CD38^{lo}$ $CD95^{hi}$ $MHCII^{hi}$ cells (Fig. 16C). CD86 expression intensities are enhanced in all Roquin KO animals compared to controls. In addition, CD80, CD25 and BAFFR levels are moderately elevated in the one Roquin 1 KO mouse analyzed. Other than that, differences are marginal and most likely do not play important biological roles.

In conclusion, loss of Roquin does not inhibit upregulation of essential activation markers necessary to promote their survival and T cell recognition. On the contrary, there is a trend for hyperactivation, seen here and in previous studies, via increased CD86 expression particularly in Roquin 1/2 double KO mice.

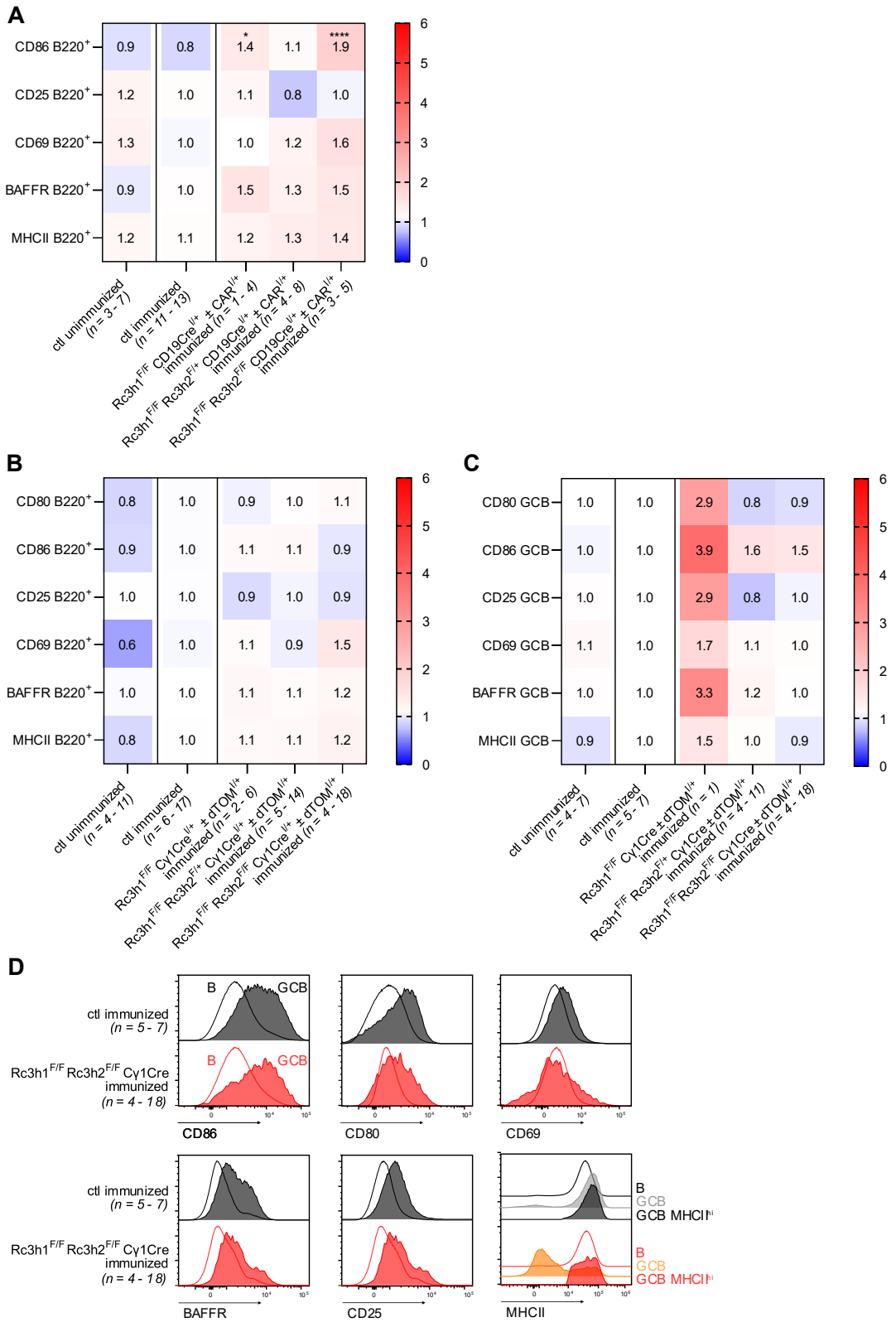

Figure 16: Activation of B and GCB cells upon SRBC immunization after 10 days in Roquin knockout and control B cell lineages in spleen.
(A) Heatmap of protein MFI values normalized per experiment to B220+ cells of immunized CD19Cre control animals. Data are cumulative from 4 independent experiments. (B) Heatmap of protein MFI values normalized per experiment to B220+ cells of immunized Cγ1Cre control animals. Data are cumulative from 9 independent experiments. (C) Heatmap as in (B) but shown for GCB cells. Animal numbers per genotype are indicated. Values are geometric means and statistical significance was determined by one-way ANOVA. (D) Representative flow cytometry histogram of CD86, CD80, BAFFR, CD69, MHCII and CD25 expression levels in GCBs and B220+ B cells of immunized Cγ1Cre control animals and Roquin 1/2 double KO mice. SPL, spleen; B B220+; GCB B220+ CD38lo CD95hi; * $p \leq 0.05$; ** $p \leq 0.01$; *** $p \leq 0.001$; **** $p \leq 0.0001$

Given the fact, that Roquin depleted B cells can induce an activation signature, their capability to proliferate upon stimulation was assessed in a next step *ex vivo* and *in vitro*.

Ex vivo, cell cycle stages were visualized by DAPI staining comparing dTOM$^+$ and dTOM$^-$ CD95^{hi} CD38^{lo} GCBs (Fig. 17). Neither obvious trends nor significant differences in the proportion of G2/S cycling cells are detectable between the genotypes suggesting equal division rates. Fluctuations in signals might be balanced out by addition of more biological replicates which should definitely be added for unimmunized controls. Future Ki67 staining or BrdU incorporation assays could be performed to support these initial results. Overall, cell cycling rates are consistent with previously published findings. Descatoire et al. for example report that in Cγ1Cre$^{I/+}$ YFP$^{I/+}$ mice immunized with human red blood cells, 6.26 % ± 0.81 % of splenic CD19$^+$ CD95$^+$ IgD$^-$ GCBs cycle in G2/M phase and 5.67 % ± 1.55 % cycle in S phase based on DAPI and EdU staining[156].

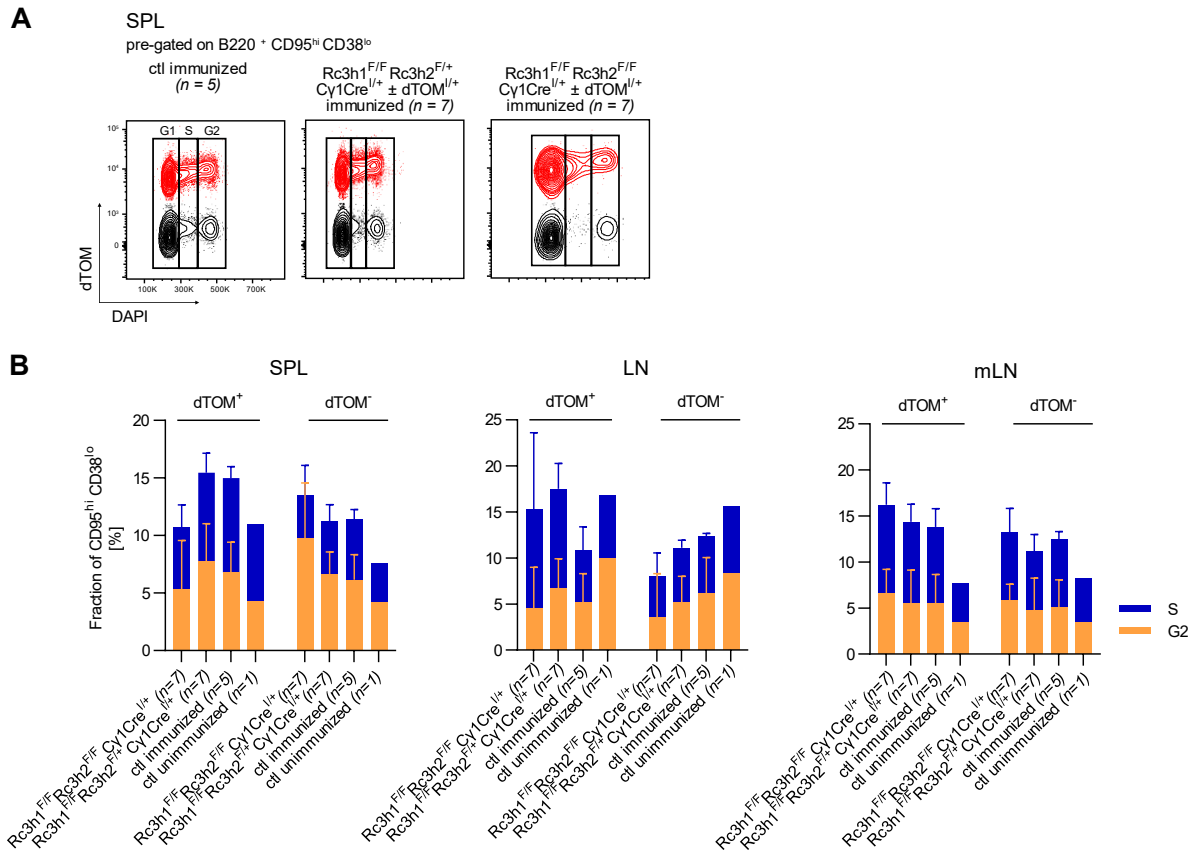

Figure 17: Proliferation of GCBs upon SRBC immunization after 10 days in Cγ1Cre Roquin knockout mice.
(A) Representative flow cytometry plots of B220$^+$ CD95^{hi} CD38^{lo} GCBs gated for their cell cycle status using DAPI. dTOM$^+$ and dTOM$^-$ cells were sub-gated into G1, S, G2 using the same gating positioning. (B) Cycling cells in dTOM$^+$ and dTOM$^-$ GCBs of indicated organs. Data are cumulative from 2 independent experiments. SPL, spleen; LN, lymph nodes; mLN, mesenteric lymph nodes

In vitro, isolated FOB cells of non-immunized CD19Cre animals were treated with B cell mitogens for 2 - 3 days measuring their proliferation via CFSE. The following mitogens or combination of mitogens were used: αIgM^{low} (1 µg / mL), αIgM^{hi} (10 µg / mL), αCD40 (0.5 µg / mL), αCD40 (0.5 µg / mL) + αIgM^{low} (1 µg / mL), LPS^{low} (0.1 µg / mL), LPS^{hi} (10 µg / mL) and CpG (0.4 µg / mL).

Day2

Surprisingly, at day 2 Roquin 1/2 double KO FOBs divided significantly more in contrast to the other genotypes upon all stimuli applied except for αIgM (Fig. 18A and 18B). Noteworthy proliferation in control, Roquin 1 KO or Roquin 1 homo Roquin 2 het KO cells is only detectable to a similar extent for the strong stimuli LPS^{hi} and CpG acting as TI antigens through TLR4 and TLR9, respectively. αIgM^{lo} treated cells suffered from BCR-induced cell death with most drastic effects in Roquin 1/2 double KO cells (6 % viability in αIgM^{lo} compared to 25 % in the untreated condition)[157]. Viability for the conditions αCD40 + αIgM^{lo} (55 - 65 %), LPS^{lo} (55 - 75 %), LPS^{hi} (75 - 85 %), CpG (83 -87 %) were similar between genotypes and thus are not shown.

Day3

By day 3 under strong stimulating conditions such as LPS^{hi}, CpG and αIgM^{hi} the differences in proliferation potential between the genotypes was lost (Fig. 18C). Upon weaker stimuli, Roquin 1/2 double KO cells still divided the most. In addition, Roquin 1 KO and Roquin 1 homo Roquin 2 het KO cells also outperformed control cells. Addition of αIgM^{lo} to αCD40 enhanced proliferation only to a minor extent. Viable cells were almost absent in wells incubated with αIgM^{lo} in all four genotypes (< 8 %). Roquin 1/2 double KO cells seem to be most sensitive towards αIgM provoked apoptosis as αIgM^{hi} treated cells maintained low levels of viability whereas cells from the other genotypes slightly recovered from day 2 until day 3.

In summary, FOB cells are very well able to induce proliferation upon activation, which is a requirement for GC initiation. Thereby, Roquin 1 KO and Roquin 1 homo Roquin 2 het KO cells behave more similar to WT cells as opposed to Roquin 1/2 double KO cells which substantially proliferate more. These data match experiments from Dr. David Riess showing an enhanced proportion of S/G2/M cycling cells (Ki67^{+} DRAQ^{hi}) in Roquin 1/2 double KO mature bone marrow B cells compared to CD19Cre$^{I/+}$ controls[82]. However, it is important to consider that this assay was done only once using two biological replicates and should therefore be repeated in the future.

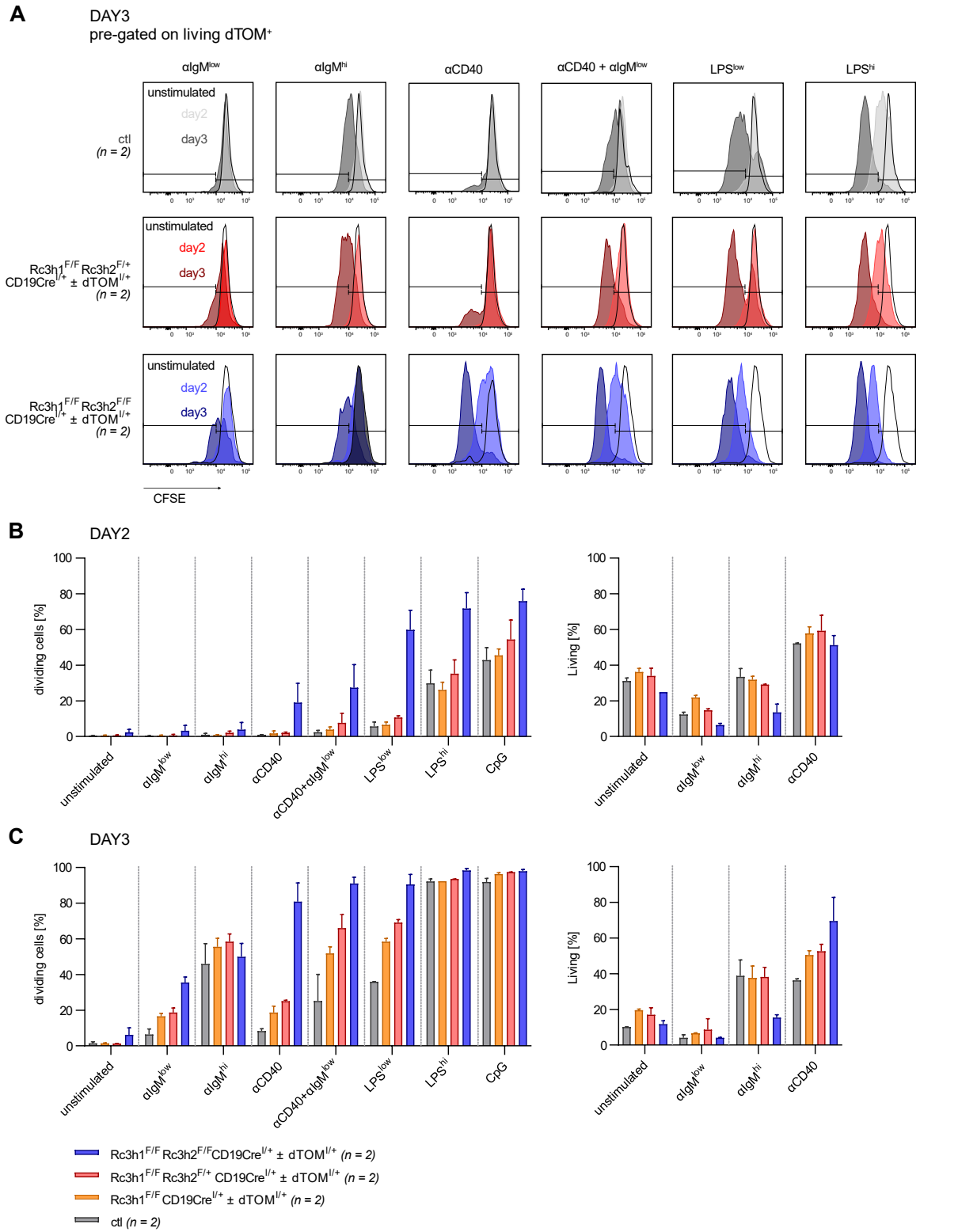

Figure 18: Proliferation of Roquin knockout follicular B cells.
(A) CFSE detection of proliferation of splenic follicular B cells isolated by the AutoMACS MZ and FO B cell isolation kit from Miltenyi. Each plot shows CFSE stainings of unstimulated cells at day 2 after seeding together with histograms of cells stimulated for either 2 or 3 days with the indicated stimuli. $CFSE^+$ (non-dividing cells) and $CFSE^-$ (dividing cells) gates are based on the unstimulated condition and are kept identical over all samples. (B) Percentages of dividing and living cells ($CFSE^-$ as shown in (A)) after 2 days of culture in the respective stimuli. (C) Same as in (B) but shown for day 3 after seeding. Data are derived from one experiment and are cumulative for two mice per genotype. Bars and numbers show mean ± SD values. Statistical significance was determined by one-way ANOVA and p values of most relevant comparisons are shown. αIgM^{low} 1 µg / mL, αIgM^{hi} 10 µg / mL, αCD40 0.5 µg / mL, LPS^{low} 0.1 µg / mL, LPS^{hi} 10 µg / mL, CpG 0.4 µg / mL

4.1.7 Roquin might be essential for the nucleation of GC follicles

The observations made so far demonstrate that Roquin 1 limits the GC response. However, Roquin protein effector functions are to some extent needed either to begin or sustain GC follicular structures. To better understand if Roquin 1/2 proteins are required for GCB cells, GCB progression was monitored over time.

Hence, in order to identify if Roquin 1/2 double KO GC either cannot be initiated starting from day 4 after immunization or cannot be maintained from day 4 up to day 10, SRBC immunized mice were opened at consecutive timepoints. Measurements at day 4 and day 7 could only be performed once so far and are thus a first indicator needing further investigation. Interestingly though, GCB cells already lack at early timepoints in Roquin 1/2 double KO mice hinting towards a crucial role of Roquin alleles at the very early stages of GC nucleation (Fig. 19). Moreover, Roquin 1 homo Roquin 2 het KO animals display a strong elevation of GCBs in percentages and numbers at day 7 which either could be derived from an experimental bias or could indicate a burst of GC formation from day 4 to day 7. Already at day 4 after immunization, > 75 % of GCBs are $dTOM^+$ in all Roquin KO genotypes with equal percentages at day 7 which demonstrates that counterselection is not the reason for absent GCBs in the context of Roquin 1/2 double KO cells (data not shown). It will be very informative to expand this dataset in the future.

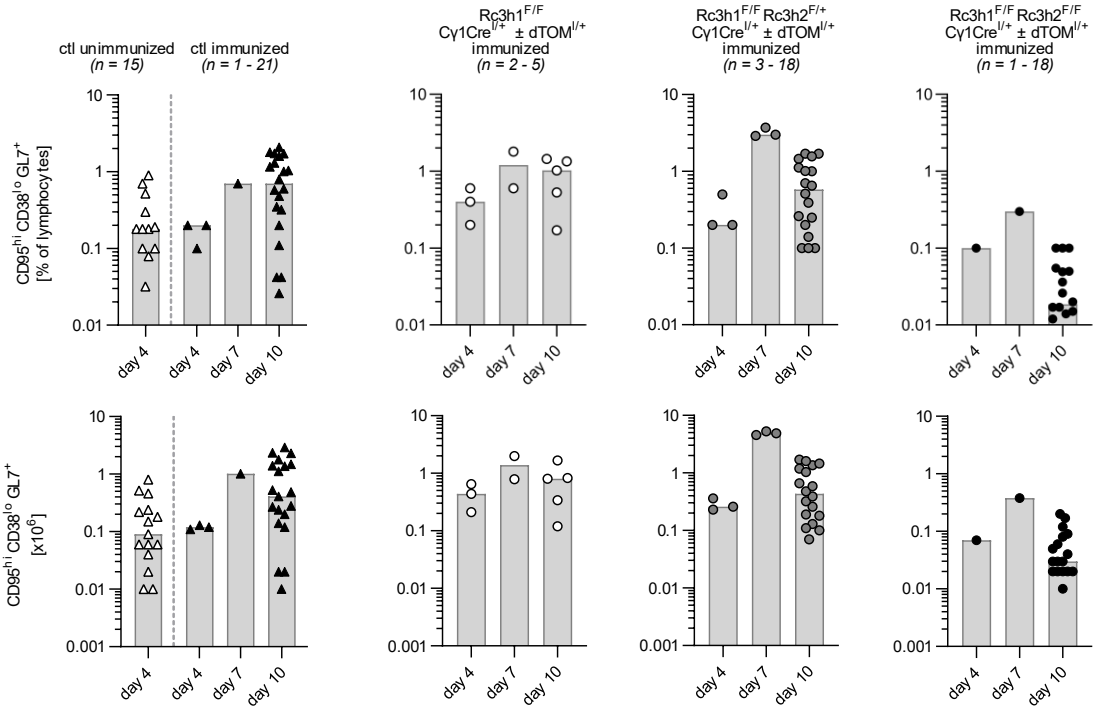

Figure 19: Preliminary data on GCB formation upon SRBC immunization after 4 or 7 days in Cγ1Cre Roquin knockout mice.
GCB cell percentages and numbers of Cγ1Cre Roquin knockout spleens 4-, 7- or 10-days after immunization. Bars show median values with each symbol representing a mouse. Data from day 4 and day 7 derive of only one experiment each. Data from day 10 are identical to data already shown in Fig. 14.

4.1.8 The effect of Roquin on GCB development is seen with different antigens

Immunizations of mice which are otherwise kept in an as sterile as possible environment, are an efficient system to induce an immune reaction selectively with or without the help of T cells. This allows to dissect TI and TD responses of the adaptive immune system experimentally while both would occur simultaneously in a natural infectious environment. Several immunization reagents have been established over time to elicit specifically a TD immune activation. They differ in their antigen structure and thus result in varying characteristics of the response. Alternative to SRBC immunization, hapten-carrier conjugates are commonly used as TD immunization reagents. Here, the hapten 4-hydroxy-3-nitrophenyl-acetyl coupled 30 - 39 times to the chicken gamma globulin protein (NP-CGG_{30-39}) in alum was additionally employed. The NP hapten has the special ability to induce clonally highly restricted, heteroclitic antibody formation which is well-characterized in C56BL/6 mice and suitable to study affinity maturation[158]. SHM mutation frequency thereby accumulates over the time of an ongoing GC reaction beginning most likely by day 7 and peaking at day 14 after immunization[39,159].

To study the impact of the loss of Roquin proteins on affinity maturation, blood serum of Cγ1Cre cohorts was gathered before immunization with NP-CGG_{30-39} (d0) followed by weekly collections (d7, d14, d21, d28, d35) until organ harvest either at day 14 or day 35. Cγ1Cre mice euthanized at day 14 were between 9 and 14 weeks of age (average 11.5 weeks) and animals analyzed at day 35 were slightly older between 13 and 17 weeks (average 15 weeks).

As expected, NP-CGG in alum immunizations resulted in reduced GCB responses compared to SRBC immunizations. Overall, the previously described results with SRBC immunization could be reproduced and the impact of Roquin 1 and Roquin 2 loss on GC formation across the different genotypes was confirmed (Fig. 20).

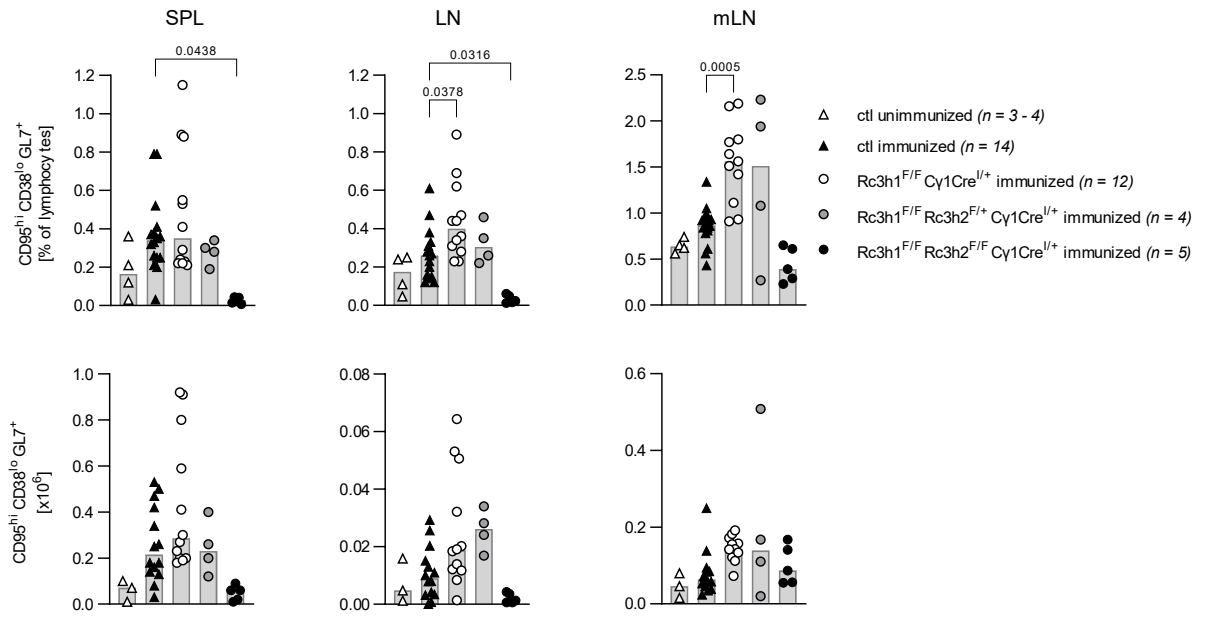

Figure 20: GCBs upon NP-CGG$_{30-39}$ immunization after 14 days in Cγ1Cre Roquin knockout mice. GCB percentages and numbers at day 14 after immunization in indicated organs. Data are cumulative from 7 independent experiments. Bars show median values with each symbol representing a mouse. Statistical significance was determined by one-way ANOVA and p values of most relevant comparisons are shown. SPL, spleen; LN, lymph nodes; mLN, mesenteric lymph nodes

4.1.9 Less GCBs are antigen-specific upon loss of Roquin

From the technical point of view, NP immunizations have the benefit that NP-binding cell populations can be monitored via flow cytometry using NP or NIP, an NP analogue coupled to fluorescent dyes. Here, GCBs and APCs were monitored for their antigen-specificity at day 14 after immunization. This shows that on average 18 % (spleen), 12 % (lymph nodes) or 12 % (mesenteric lymph nodes) of the GCBs were NP-specific in control mice, respectively, which is in range with published results (Fig. 21). Microscopic imaging performed by Jacob et al. in the 90's suggests that 28 % of foci formed between day 2 and day 6 after NP-CGG injection and 32 % of PNA$^+$ GCs by day 14 are λ1$^+$ cells and therefore most likely a response to the NP immunization which causes a bias towards otherwise highly rare λ1 light chain usage. However, only a fraction of 95 % (foci) or 55 % (PNA$^+$ GCs) thereof was also found to bind the cross-reactive 4-hydroxy-5-iodo-3-nitrophenyl (NIP) NP-analogue, thus reducing the theoretical amount of NP$^+$ follicles in these studies[38].

Roquin 1 KO mice obtain similar total numbers of NP$^+$ GCBs, however the fraction of NP-binders within the GC compartment is reduced by ~2-fold compared to control

counterparts (Fig. 21C). Although Roquin 1 homo Roquin 2 het KO mice obtain similar numbers of total GCBs, their numbers of antigen-specific GCBs are diminished and only 3 % of their GCBs are also NP positive. This suggests that both in Roquin 1 KO and Roquin 1 homo Roquin 2 het KO mice either less naïve B cells react and get activated by the immunogen to subsequently enter the GC reaction or these antigen-specific B cells cannot be maintained within the GC reaction until day 14. This effect is also present in the absence of all Roquin alleles resulting in a fraction of ~3 % out of the GCB pool which is NP^+ in spleen, 0.2 % in lymph nodes and 2 % in mesenteric lymph nodes on average.

In the APC compartment no significant differences in the fraction of NP-binders are present in spleen (Fig. 22D). 2 % of APCs are stained NP positive in controls, 2.5 % in Roquin 1 KO mice and 1 % in both Roquin 1 homo Roquin 2 het KO or Roquin 1/2 double KO animals. It cannot be distinguished whether these NP-specific APCs derived from the GC reaction or are of extrafollicular origin. However, in all Roquin KO genotypes, the fraction of $IgG1^+$ cells within the NP-binding APCs is reduced and similar trends were detected in the proportion of $IgG1^+$ cells within the NP-binding GCBs suggesting an extrafollicular origin of NP^+ APCs at least in Roquin 1/2 double KO mice. Interpretation of this data needs be done carefully as staining of $IgG1^+$ NP^+ APCs is based on small cell numbers (< 100 per mouse) and no IgM staining was performed. Overall, control mice contain a ratio of NP^+ GCBs to NP^+ APCs of ~10:1 whereas Roquin 1/2 double KO mice contain a ratio of ~1:2 (Fig. 22D).

APC percentages and numbers in the bone marrow 35 days after immunization were unchanged between genotypes (Suppl. Fig. 6). Monitoring of their NP status was unfortunately difficult since less than 30 NP^+ cells per sample could be recorded. In general, APC formation upon NP-CGG immunization is in line with SRBC immunization results which will be discussed later.

In summary, loss of Roquin alleles results gene-dosage dependently in a reduction of the proportion of antigen-recognizing GCBs among total GCBs per genotype (Fig. 21C). With the data at hand, it cannot be finally concluded how this affects the number of antigen-specific APCs particularly derived from GC sites although the loss of $IgG1^+$ NP^+ APCs in Roquin deficient mice suggest a dominating role of the extrafollicular pathway. However, the APCs compartment as a whole (follicular and extrafollicular) does not seem to be constrained in its capability to recognize NP upon loss of Roquin proteins.

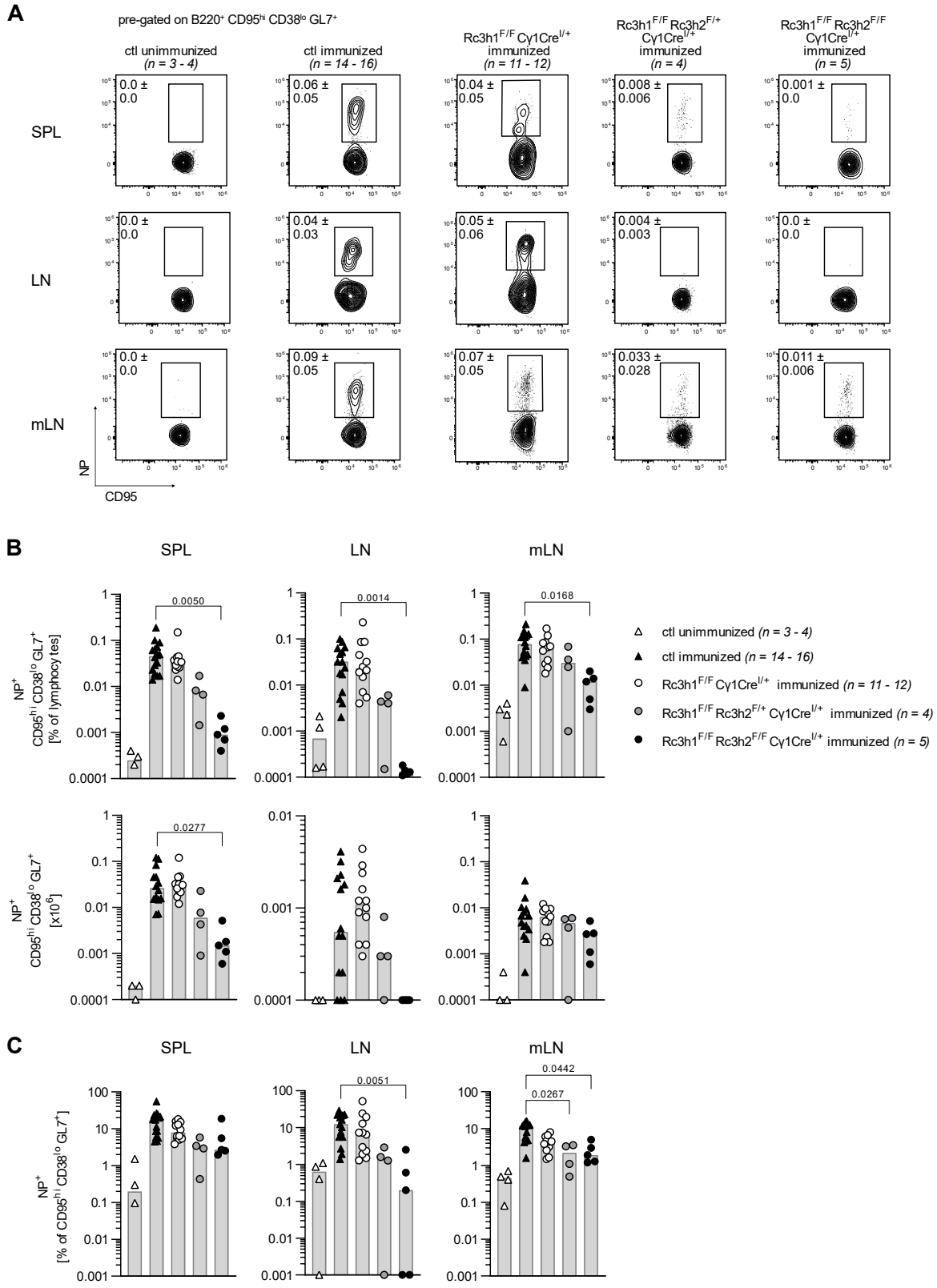

Figure 21: NP specific GCBs upon NP-CGG$_{30-39}$ immunization after 14 days in in Cγ1Cre Roquin knockout mice.

(A) Representative flow cytometry plots of NP$^+$ germinal center B cells in different organs. (B) NP$^+$ germinal center B cells percentages and numbers. (C) Fraction of NP$^+$ cells within the germinal center B cells population. Data are cumulative from 7 independent experiments. Bars show median values with each symbol representing a mouse. Statistical significance was determined by non-parametric Kruskal Wallis testing and p values of most relevant comparisons are shown. SPL, spleen; LN, lymph nodes; mLN, mesenteric lymph nodes

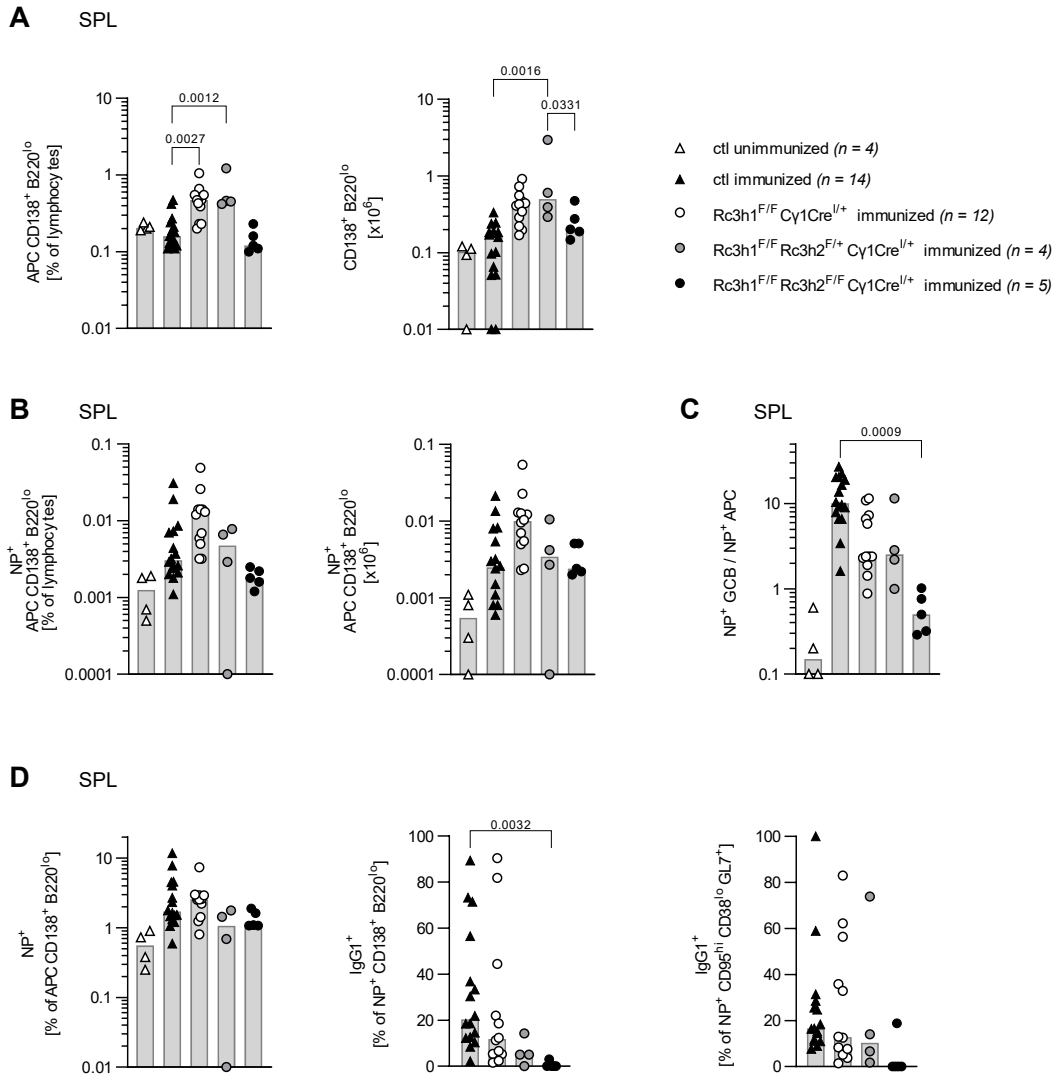

Figure 22: NP specific APCs upon NP-CGG$_{30-39}$ immunization after 14 days in Cγ1Cre Roquin knockout mice.
(A) APC percentages and numbers at day 14 after immunization in spleen. Statistical significance was determined by one-way ANOVA and p values of most relevant comparisons are shown. (B) NP$^+$ APCs percentages and numbers. (C) Ratio of NP$^+$ GCB as shown in Fig. 21B and NP$^+$ APC as shown in Fig. 22B. (D) Fraction of NP$^+$ cells within the APC population and fraction of IgG1$^+$ cells within the NP$^+$ APC or NP$^+$ GCB population. Data are cumulative from 7 independent experiments. Bars show median values with each symbol representing a mouse. Statistical significance was determined by non-parametric Kruskal Wallis testing and p values of most relevant comparisons are shown. SPL, spleen

4.2 Influence of Roquin on somatic hypermutation

4.2.1 Roquin knockout cells fail to affinity maturate

The highly clonal restricted antibody repertoire elicited by NP-haptens is a major advantage when studying immunization-caused immune effects. Primary anti-NP antibodies are predominantly constituted by Igλ light chains which are found only in 1 % of the regular immunoglobulin repertoire. Investigators published that in NP immunized animals, over 90 % of antigen-binding foci and approximately 55 % of GCs can be positively stained for Igλ in spleen sections[38]. The diversity of heavy chain recombination is minimized, too, upon NP encounter with heavy chains being predominantly composed of the IgG1 isotype and in more rare cases being IgM or IgG2b[160]. In addition, the heavy chain V region (V_H) V_H186.2 of the J558 gene family is dominantly expressed in NP recognizing immunoglobulins after NP immunization. Even though other V_H segments of the J558 gene family including V102, V23, VC1H4, V165.1, CH10, V3, V24.8 and V593 can be detected at day 6 after immunization in the immunoglobulin repertoire of a primary immune response as well, their proportion within the APC immunoglobulin pool declines drastically until day 14 unlike the V_H186.2 clonotype[161].
During this project, the amount of NP-specific IgG1 antibodies was analyzed in blood sera of C_γ1Cre Roquin KO mice over time. Thereby, total antigen-recognizing IgG1 titers are measured by ELISA using a NP_{23}-BSA coating while the proportion of high-affinity antibodies can be evaluated by serum incubation with NP_2-BSA coated plates.

NP-binding IgG1 is not detectable in Roquin 1/2 double KO cells due to their incapability to form an efficient GCB cell response and of course is also absent in non-immunized controls which never received any NP antigen (Fig. 23A). High-affinity NP_2-binding antibodies are first observable at day 14 with no major differences between Roquin 1 KO or Roquin 1 homo Roquin 2 het KO genotypes and immunized controls. However, from day 21 onwards, the production of high-affinity IgG1 drops significantly compared to controls with Roquin 1 homo Roquin 2 het KO mice being even more affected than Roquin 1 KO animals. The proportion of NP_2 binding IgG1 within total IgG1 blood serum levels (NP_2/NP_{23}) is significantly lower in Roquin 1 homo Roquin 2 het KO mice at late

time points (day 28 and day 35) (Fig. 23B). The spread of the individual data points can be seen in Suppl. Fig. 7. In summary, this ELISA analysis suggests that loss of Roquin 1 negatively affects the generation of affinity matured antibodies and that the presence of both Roquin 2 alleles, instead of only one allele, can partially rescue the defect. Perturbances can be recognized earliest after 3 weeks once the GC reaction is already finished hinting towards the ongoing selection of high-affinity APCs.

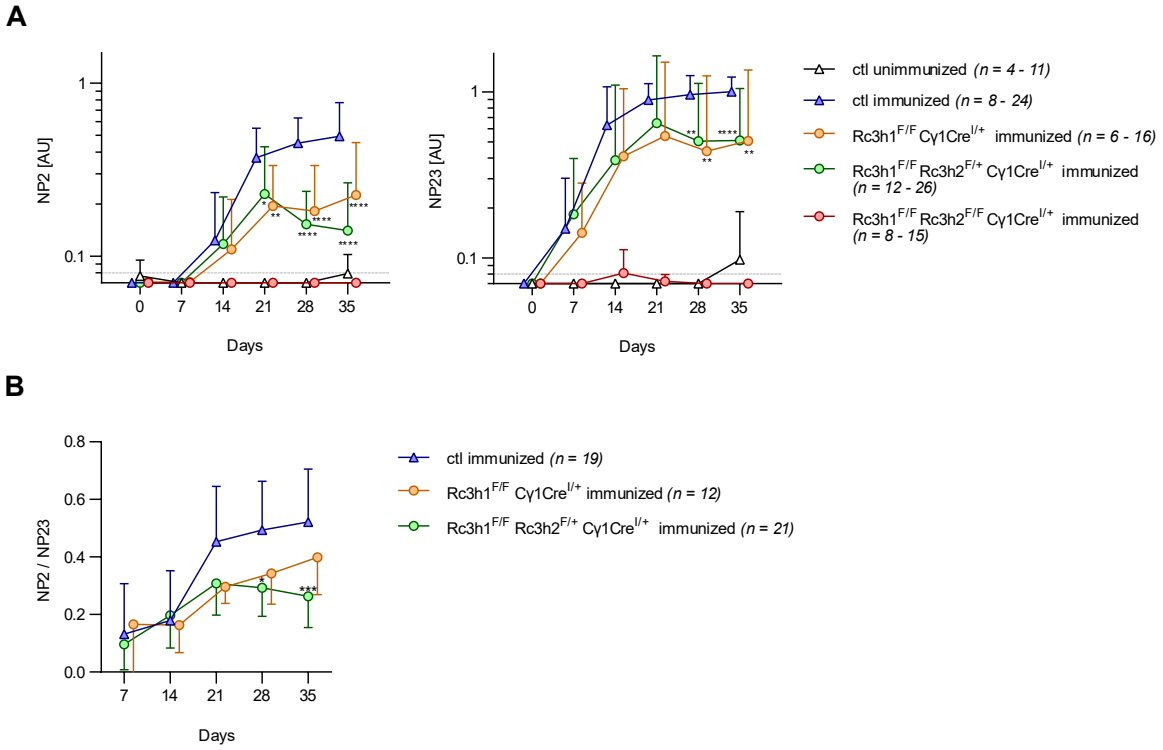

Figure 23: NP-specific IgG1 production in Cγ1Cre Roquin knockout mice until five weeks after NP-CGG$_{30-39}$ immunization.
(A) NP_2-binding high-affinity IgG1 antibodies of blood sera collected at indicated time-points before (0 days) or after (7, 14, 21, 28, 35 days) immunization with NP-CGG$_{30-39}$. Absorption values of six dilutions were summarized, substracted by blank values and normalized to plate-specific standard absorption measurements. Detection threshold of 0.08 is indicated. Data points are only plotted if all six dilutions could be measured and absorption summation values below threshold levels were set to 0.07. Each symbol represents the geometric mean ± SD. (B) Same as in (A), but shown for NP_{23}-binding low-affinity IgG1 antibodies. (C) Ratio of NP_2 to NP_{23}-binding IgG1 levels. Data points are plotted independent of the number of dilutions measured, but restricted to samples with NP_{23}-IgG1 normalized absorption values > 0.08. Data are cumulative from 4 independent ELISA experiments. Statistical significance was determined by two-way ANOVA and p values are shown. * $p \leq 0.05$; ** $p \leq 0.01$; *** $p \leq 0.001$; **** $p \leq 0.0001$

Besides the identified restriction to IgG1 constant regions within the BCR of NP-challenged mice, also VDJ rearrangements were discovered to be selected specifically to produce high-affinity antibodies. Out of 107 potentially productive V genes, the IgHV 1-72 allele 1 (J558 gene family, VH186.2, www.imgt.org/IMGTrepertoire) and out of 10 productive D segments, the IgHD 1-1 allele 1 (also called DFL16.1) can primarily be found, even if not exclusively, in anti-NP antibodies. From the four available J genes, JH2 is preferred[162–165]. Besides the defined usage of VDJ junctions, a tryptophan to leucin exchange at position 33 (W33L) of the VH186.2 segment is a hallmark of affinity maturation upon NP-CGG immunization. This mutation increases the affinity for NP by ~10-fold[166]. W33L mutations are located in the CDR1 region with additional mutations also accumulating in the antigen contact regions CDR1 - 3. According to literature, 90 - 95 % of mutations are single nucleotide substitutions, although deletions and insertions also occur in reduced amounts, too[39,159]. In parallel, clonal competition also reduces the availability of low-affinity gene segments other than VH186.2, DFL16.1, JH2 in spleen and bone-marrow APCs at later timepoints of the immune response[62].

To quantify the mutational load of BCR sequences in Roquin KO animals, GCBs were isolated via MACS and flow cytometry sorting 14 days after immunization. Next, their RNA was isolated, transcribed into cDNA and amplified by two rounds of semi-nested PCRs using primers targeting the VH186.2 and the Cγ1 heavy chain region. The original protocol by Heise et al. suggests further vector cloning and sequencing from bacterial colonies[134]. However, we made use of the advances of next-generation sequencing instead which allows to analyze thousand BCR amplicon sequences from a single mouse thereby improving upon former hybridoma assays or bacterial amplification of cloned BCR products in time and coverage[37,134].

BCR sequences of 6 control animals, three Roquin 1 KO and four Roquin 1 homo Roquin 2 het KO mice were analyzed. Due to the absence of adequate GCBs in Roquin 1/2 double KO mice, this genotype had to be excluded from the experiment. Between 30.000 - 140.000 reads were sequenced per mouse and on average > 97 % of those sequences could be aligned. Reads were further filtered for high quality, successful alignment to the IgHV 1-72 allele, and unique V sequences to rule out clonal replication of reads biasing the further analysis. After these filtering steps, between 9.000 and 100.000 reads per mouse remained and on average 23.000 could be examined.

First, the frequency of mutations per read per base pair (bp) was determined which can further be categorized into substitutions, deletions and insertions. The overall mutational rate is significantly diminished in Roquin 1 KO ($2.7 * 10^{-2}$ mutations/bp/read) or Roquin 1 homo Roquin 2 het KO mice ($3.3 * 10^{-2}$ mutations/bp/read) within the V_H186.2 region compared to controls ($4.9 * 10^{-2}$ mutations/bp/read) (Fig. 24B). As expected, substitutions dominate over deletions or insertions making up 86 % of all mutations in controls, 98 % in Roquin 1 KO and 91 % in Roquin 1 homo Roquin 2 het KO mice. Insertions are neglectable accounting for less than 0.5 % of all mutations (data not shown).

Importantly, W33L mutations (nucleotide triplet exchange from TGG to TTG at position 33 in the CDR1) are significantly reduced upon ablation of Roquin compared to controls (Fig. 24A). Nucleotide triplets other than TTG correspond mostly to the germline encoded TGG, however another 35 different combinations are detectable. Nevertheless, they make up only a minor fraction of nucleotide triplets (~5 % in controls, ~1 % in Roquin 1 KO and ~6 % in Roquin 1 homo Roquin 2 het KO). Considering the whole V_H186.2 amplicon, amino acid position 33 is the major hotspot for mutations in control BCR sequences with no other site, even within the CDR1 or CDR2, being mutated as frequently (Fig. 24B). This pattern is abolished in Roquin KO genotypes where other positions such as position 31 predominate, however still no other position reaches the mutational frequency of > 12 % as seen for position 33 in control BCRs. The same is true at the nucleotide level (Suppl. Fig. 8A). Looking more closer at individual nucleotides, the second position of the germline TGG triplet (position 23 within the CDR1, see Suppl. Fig. 8A) is affected the most with almost 50 % of the guanines being exchanged in $C\gamma1Cre^{I/+}$ mice, but only ~20 % in Roquin 1 KO or Roquin 1 homo Roquin 2 het KO sequences. The drastic decrease by ~3.5-fold of affinity-enhancing W33L sequences strongly argues towards an essential role of Roquin 1 for affinity maturation.

Beyond the W33L hotspot mutation, BCRs with a high amino acid modification content (more than 3 mutations per read) are found in the CDR1 regions of control animals which is also reflected by a high burden of nucleotide exchanges (Fig. 25 and Suppl. Fig 8B). Remarkably, there are CDR1 reads with more than a quarter of their nucleotides being mutated (e.g., 6-10 mutations within the 24-nucleotide long CDR1). Even though they are a minor fraction of the total pool, it is worth mentioning that these reads are absent in Roquin 1 KO CDR1 sequences. Similarly, V_H186.2 sequences with an elevated number of nucleotide mutations (27-127 within the 294-nucleotide long V_H186.2) are reduced by > 20-fold in Roquin 1 KO GCBs and > 8-fold in Roquin 1 homo Roquin 2 het KO GCBs

(Fig. 25B). Hence, whereas Roquin 1 KO and Roquin 1 homo Roquin 2 het KO BCRs do not differ in their ability to acquire W33L mutations, Roquin 1 KO sequences have a higher tendency to lose reads with particularly increased mutational load compared to Roquin 1 homo Roquin 2 het KO KOs. This is connected to the observed clonality described in the following chapter and can further be associated with the proportion of non-silent mutations, meaning mutation leading to an amino acid exchange (Fig. 24B), related to the total amount of nucleotide mutation within the V_H186.2 sequence (NS / Total) (Suppl. Fig. 9). While $C\gamma1Cre^{I/+}$ control mice present with a ratio of non-silent to total mutations of 2.88 which is similar to the ratio found in Roquin 1 homo Roquin 2 het KO mice (NS / Total = 3.00), this ratio is reduced by ~1/3 in Roquin 1 KO mice (NS / Total = 2.08). Still both Roquin KO genotypes contain a reduced amino acid modification rate in comparison to control mice with an average of 1.03 in $C\gamma1Cre^{I/+}$ mice, but only 0.69 in Roquin 1 KO or 0.68 in Roquin 1 homo Roquin 2 het KO animals (Fig. 25A). Transitions are more prominently detected in Roquin 1 KO mice, but transversions dominate in Roquin 1 homo Roquin 2 het KO mice (Fig. 25C).

Taken together, the obtained results reveal an essential role of Roquin 1 for the emergence of affinity matured antibodies in blood sera and SHM within the V_H186.2 BCR sequences of NP-injected animals.

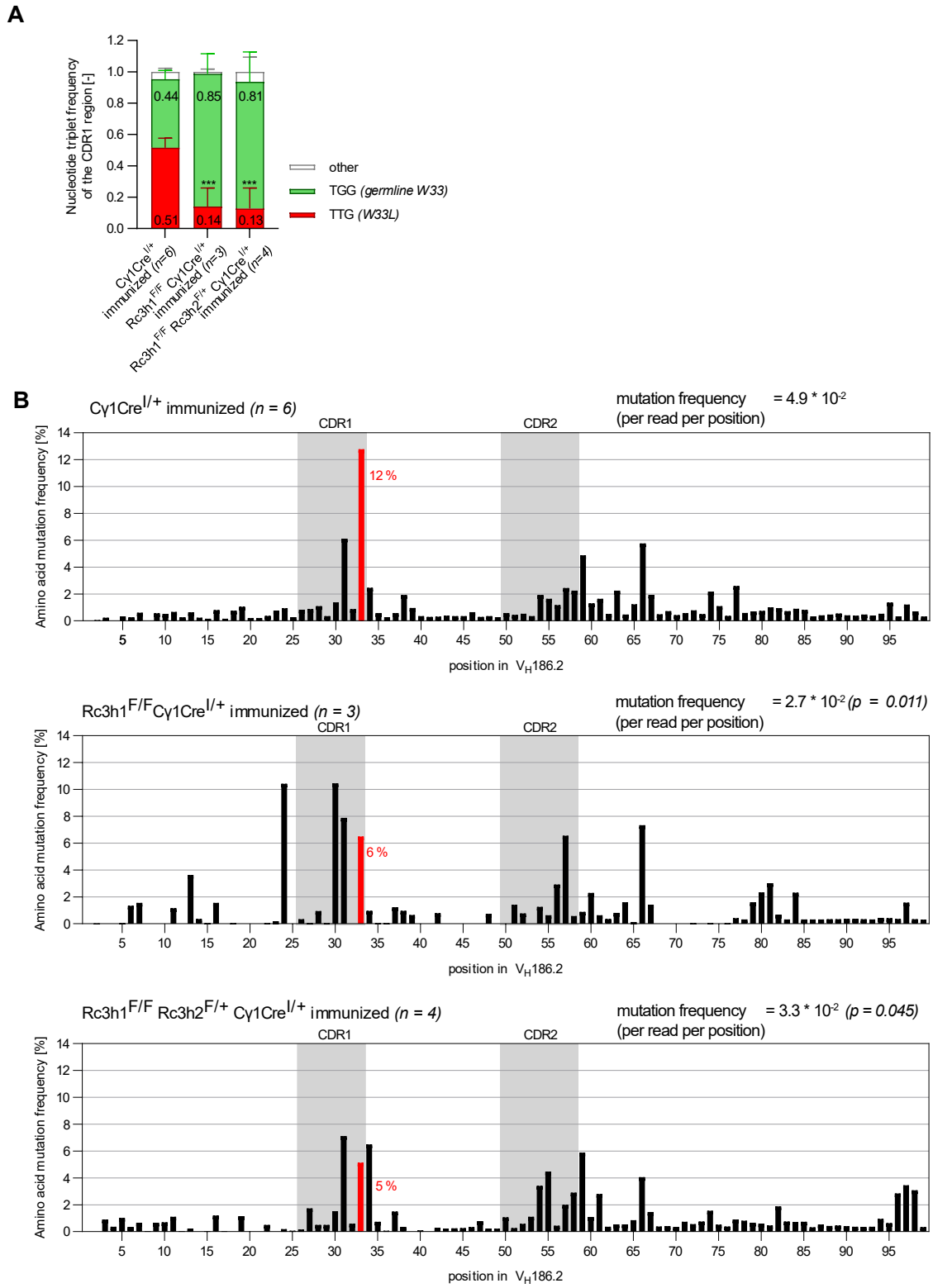

Figure 24: W33L exchange rate and overall amino acid exchange upon NP-CGG$_{30-39}$ immunization after 14 days in Cγ1Cre Roquin knockout mice.
(A) Fraction of TTG nucleotide triplets resulting in a W33L conversion at the hotspot position 23 of the CDR1. Statistical significance was determined by unpaired t-test *** $p \leq 0.001$. Percentages are based on ~17.000 – 124.000 reads per mouse. (B) Percentages of amino acid changes (substitutions, insertions, deletions) at a distinct position of the V_H186.2 per genotype. Highlighted position 33 (shown in red) corresponds to the W33L hotspot mutation site upon affinity maturation of immunized animals. Percentages are mean values. Reads were filtered for unique V sequences (> 10.000 per mouse), a mean sequencing quality above 20 and successful recognition of the Ig_HV 1-72 during alignment. Frequencies were normalized to the total amount of filtered reads per sample. Data are cumulative from 4 independent immunization experiments combined into one sequencing analysis. Statistical significance was determined by one-way ANOVA and p values are indicated.

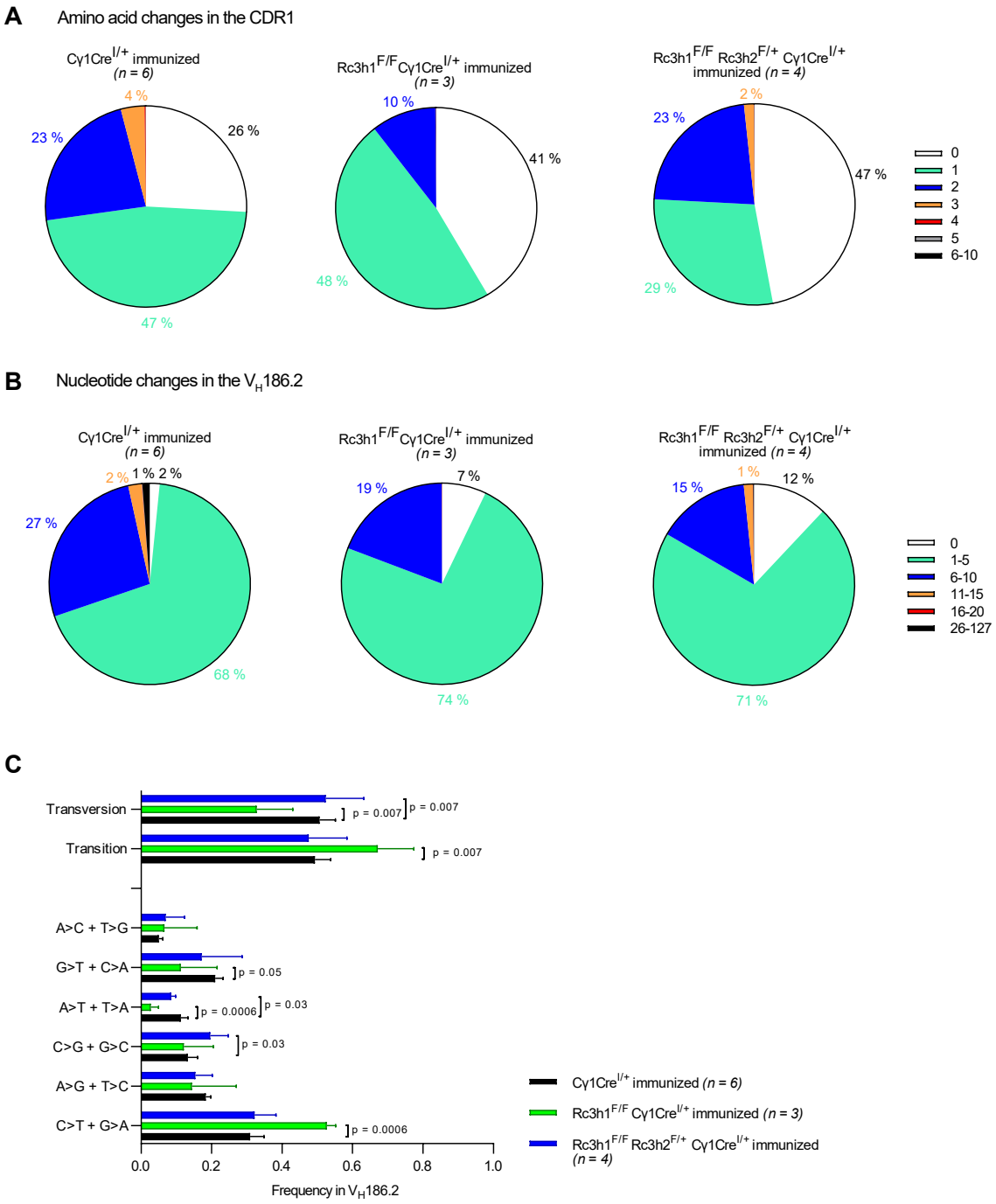

Figure 25: Mutations in the CDR1 or V_H186.2 region of Ig_HV 1-72 amplified BCR sequences upon NP-CGG$_{30-39}$ immunization after 14 days in Cγ1Cre Roquin knockout mice.
(A) Percentages of amplified reads containing 1-10 amino acid changes (substitutions, insertions, deletions) in the CDR1 region of the Ig_HV 1-72 region per read per genotype. (B) Percentages of amplified reads containing 1 - 127 nucleotide mutations in the V_H186.2 region per read per genotype. (C) Transversion and transition frequencies in the V_H186.2 region. Reads were filtered for unique V sequences (> 10.000 per mouse), a mean sequencing quality above 20 and successful recognition of the Ig_HV 1-72 during alignment. Frequencies were normalized to the total amount of filtered reads per sample. Data are cumulative from 4 independent immunization experiments combined into one sequencing analysis. Statistical significance was determined by an unpaired t-test.

4.2.2 BCR sequencing reveals higher clonality upon Roquin knockout

Besides the in-depth analysis of filtered unique V_H186.2 receptor sequences as described before, total reads were also employed for clone detection. Clonality was determined via the junction of VDJ in the CDR3 of the Ig heavy chain of the BCR. Given the high combinatorial possibilities for this re-arrangement, a certain combination can be very likely be considered unique[37,167]. Computational analysis enables the assembly of a clonal network aggregating reads with shared VDJ isotypes and in addition connecting sequences of high similarity, e.g., with only one nucleotide difference, which evolved from each other. Fig. 26 visualizes these clonal populations captured per mouse. As can be seen at first glance, control mice contain a finely structured composition of a multitude of individual clones with on average two dominating, colored clones containing ≥ 10 % of the total reads. Oppositely, Roquin 1 KO BCRs are reduced ~ 10-fold in numbers of detectable clones with 2 - 5 dominating clones. Roquin 1 homo Roquin 2 het KO mice follow the same trend, but at least contain on average 58 clones with a maximum of 3 main clones. The effect is independent of the amount of GCB cells sorted. Hence, the V_H186.2 specific BCR repertoire is drastically reduced upon Roquin ablation and intraclonal diversity is substantially diminished.

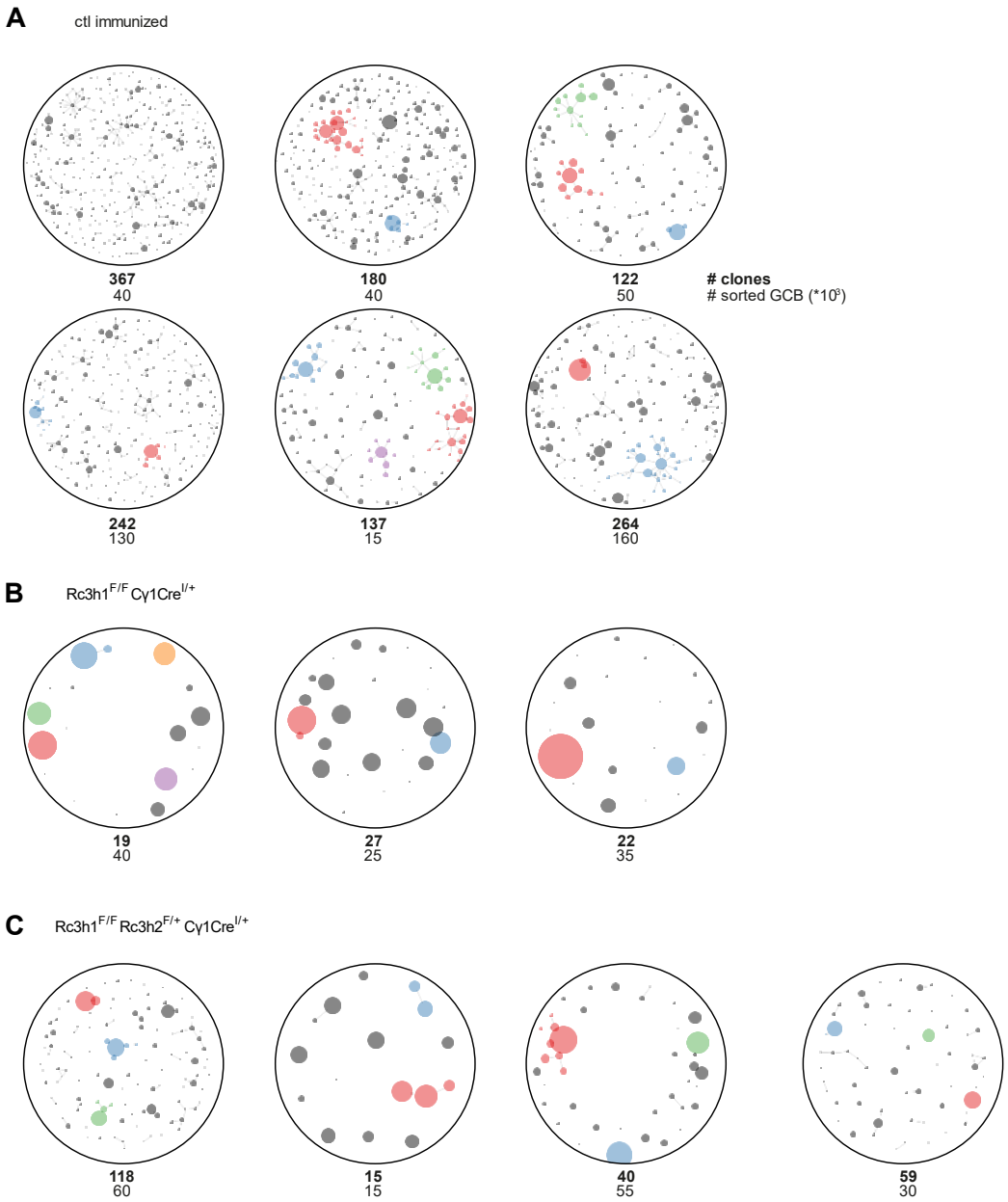

Figure 26: Clonality Plots based on genotype upon NP-CGG$_{30-39}$ immunization after 14 days in Cγ1Cre Roquin knockout mice.
Clonality analyses are based on the in-house developed bioinformatic tool *CloNet* as described in Weber et al. 2019[168]. Each clone is detected via its CDR3, meaning unique VDJ re-arrangements and is represented by a dot once at least 5 reads were assigned to the respective clone. The size of the dot relates to the number of associated reads with colored clones containing ≥ 10 % of all reads. Clones differing only by 1 bp in sequence are linked to each other thereby visualizing the grading of SHM within a given clone and sample. Total number of detected clones and total number of sorted GCBs is indicated.

4.3 Influence of Roquin on APC formation and class-switching *in vivo*

The analysis of GC reaction in SRBC immunized Roquin ablated Cγ1Cre mice verified an impact of Roquin on GC generation. Subsequent NP-CGG immunizations furthermore showed the dependence of SHM on the presence of Roquin 1. SHM is a hallmark of the GC response and facilitates the generation of high-affinity immunoglobulins which are then massively produced and secreted by GC-derived APCs. However, APCs can also emerge independent of the GC reaction. Hence, I assessed the influence of absent or elevated GCB levels in Roquin KO mice on the generation of APCs in a next step. Furthermore, I analyzed their immunoglobulin repertoire shedding light on the capability of Roquin KO animals to undergo CSR.

4.3.1 Roquin knockout perturbs the generation of antigen-specific class-switched antibodies upon SRBC immunization

Complementary to the measurement of antigen-specific antibodies in NP-CGG immunized Cγ1Cre animals, gathered blood sera of SRBC immunized CD19Cre or Cγ1Cre cohorts can equally be utilized to determine their SRBC-recognizing antibody content. IgM, IgG1 and Igκ were therefore measured by flow cytometry following the protocol of McAllister et al.[133]. The assay enables to record antibody titers with high confidence by using sera dilution series in combination with FMO controls and staining B220 as negative control (Fig. 27A). However, the readout of the assay is qualitative, not quantitative and although antibodies need to be specific enough to bind the SRBCs per se, high- and low-affinity antibodies cannot validly be discriminated.

SRBC specific antibodies in CD19Cre Roquin KO mice

Unimmunized controls served as negative controls independent of the mouse strain and the staining antibody (Fig. 27A). CD19Cre control mice present with a decent MFI shift when stained for SRBC-specific Igκ antibodies. More specifically, their titers were measured to be higher for IgG1 antibodies than IgM reflecting an ongoing GC reaction which favors IgG^+ over IgM^+ GCBs although IgM^+ B cells are, once entered to the GC,

equally capable to undergo SHM generating high-affinity antibodies (Fig. 27B)[46,163]. Except for one outlier in immunized controls IgM measurements, controls containing conditional Roquin alleles, but no CD19Cre ($Rc3h1^{F/F}$ $Rc3h2^{+/+ \text{ or } F/+ \text{ or } F/F}$) behave identical to Cre controls ($CD19Cre^{I/+}$ $Rc3h1^{+/+}$ $Rc3h2^{+/+}$) justifying their compilation in other analysis. In comparison to CD19Cre controls, sera of Roquin 1 KO and Roquin 1 homo Roquin 2 het KO animals contain slightly reduced mean levels of SRBC-specific total Igκ and IgG1 antibodies while IgM antibodies are elevated especially in Roquin 1 homo Roquin 2 het KO animals. Sera of Roquin 1/2 double KO cells contain low levels of Igκ antibodies and those found are mostly of an IgM isotype indicative of a reduction in total antigen-specific antibodies in those mice.

SRBC specific antibodies in Cγ1Cre Roquin KO mice

Relative to the CD19Cre cohort, the reduction of Igκ titers of Roquin KO genotypes is less pronounced compared to their control counterpart (Fig. 27C). This result can be correlated to the previously described measurement of NP-specific antibodies in blood sera of Cγ1Cre mice which equally showed little differences between genotypes at early time-points (e.g., comparing day 14 in NP immunizations with day 10 for SRBC treatments). Furthermore, it demonstrates that even though GCBs are virtually absent in Roquin 1/2 double KO mice, still a fraction of antigen-detecting antibodies are produced hinting towards extrafollicular APCs as their source. IgG1 measured MFIs are widely spread along the axis and only a small trend, if at all, of diminished IgG1 in Roquin 1/2 double KO mice is recognizable compared to immunized controls. However, IgM antibody titers are significantly elevated in Roquin 1/2 double KO sera correlating with the hypothesis that these antibodies are derived of an extrafollicular immune response. No significant differences between Roquin 1 KO or Roquin 1 homo Roquin 2 het KO titers and the ones from immunized controls can be measured.

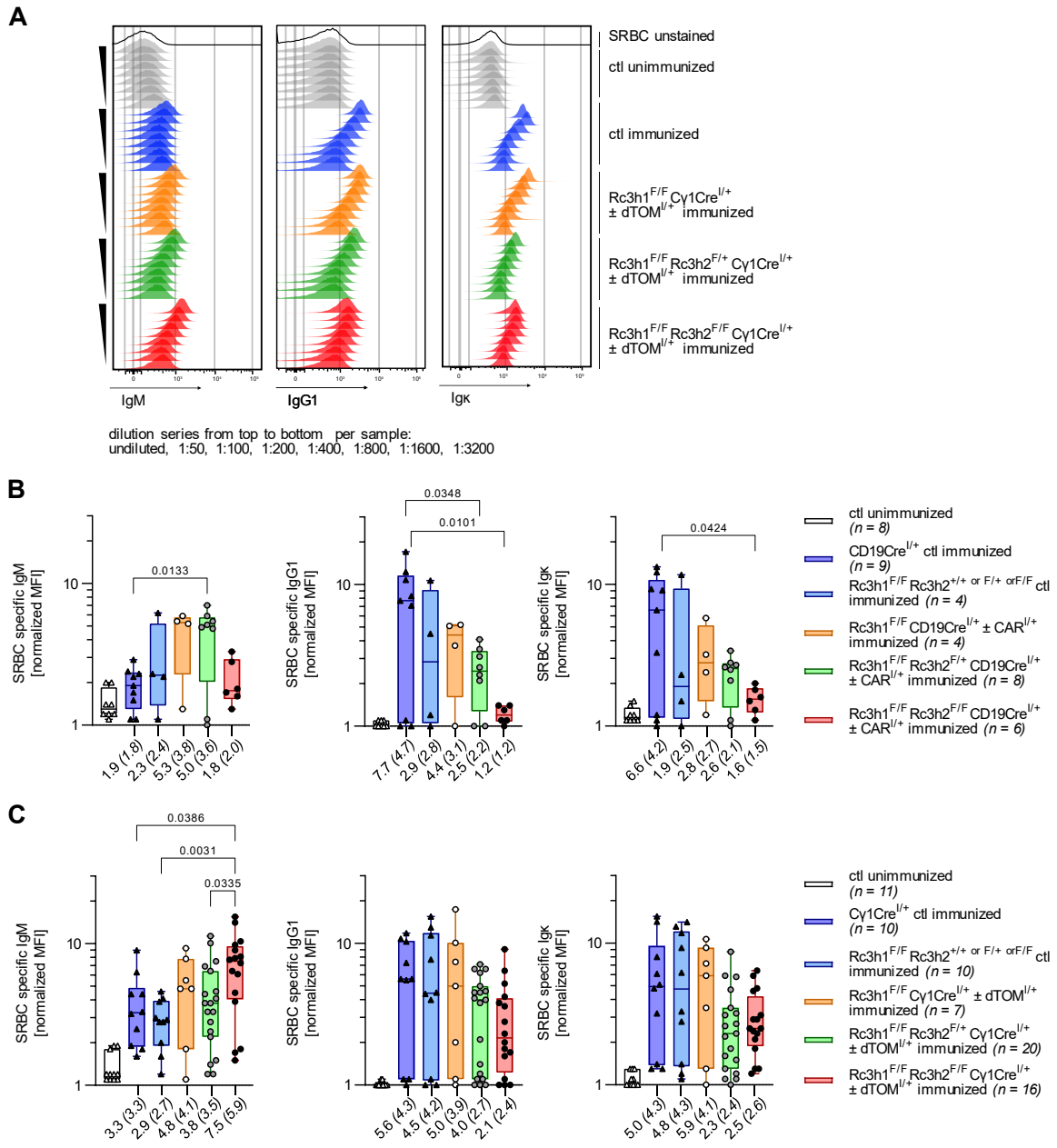

Figure 27: SRBC-specific immunoglobulin production upon SRBC immunization after 10 days in Roquin knockout mice.
(A) Representative flow cytometry histograms of SRBC-specific IgM, IgG1 and Igκ of undiluted and diluted sera in respective genotypes. Dilution factor is indicated. (B) SRBC specific immunoglobulin levels in 1:50 diluted blood sera of CD19Cre Roquin knockout mice plotted as MFI values normalized to SRBC unstained controls. Numbers at the x-axis are median values. Geometric means are additionally given in italic and brackets. Blood sera were collected in 4 independent experiments and were evaluated for antigen specific immunoglobulin levels in one experiment. (C) As shown in (B) for Cγ1Cre Roquin knockout mice. Blood sera were collected in 9 independent experiments and were evaluated for antigen specific immunoglobulin levels in two independent experiments. Statistical significance was determined by one-way ANOVA and p values are indicated.

4.3.2 Loss of Roquin reshapes the APC compartment

The production of high-affinity, antigen-specific antibodies is shaped by the APC compartment. In SRBC immunized animals, first extrafollicular, still dividing plasmablasts become visible 3 days after the injection even before the emergence of GCBs at day 4. Already 1 day after GC formation, plasmablasts can exit the GC reaction although memory B cell formation is favored as an output of early GCs. During the ongoing immune response, plasmablasts mature into non-dividing plasma cells and low-affinity APCs are displaced by higher-affinity APCs which ultimately migrate out of secondary lymphoid organs and enter the bone marrow through the blood stream from day 10 onwards. Except for their timing of emergence, their ability to divide and their affinity of antibodies, there are up to date no unique markers distinguishing plasmablasts from short-lived or long-lived plasma cells. However, researchers try to differentiate plasmablasts from plasma cells by intermediate instead of high expression levels of B220, CD19 or BLIMP-1 which is not always a straightforward approach considering also the rarity of these cells[41,55,67,169]. Hence, APCs were defined more general during this thesis as $CD138^{+}$ $IRF4^{+}$ $B220^{lo}$ cells showing elevated levels of BLIMP-1 and downregulation of CD19 compared to $B220^{+}$ cells (Fig. 29A). At the time-point analyzed, no difference in BLIMP-1 expression levels could be detected between APCs of the different genotypes and the resolution of the staining did not allow for a further reliable sub-gating on BLIMP-1^{hi} or BLIMP-1^{lo} cell populations (Suppl. Fig. 10A).

In CD19Cre mice immunized with SRBCs and opened at day 10 after the treatment, APCs are, as expected, up to 2-fold elevated in percentage and numbers in immunized controls compared to unimmunized controls in all secondary lymphoid organs (Fig. 29B). There is a pronounced increase in Roquin 1 KO or Roquin 1 homo Roquin 2 het KO APCs compared to immunized controls and even Roquin 1/2 double KO mice display a slightly enlarged APC compartment in all analyzed organs. These phenotypes are again independent of the immunization method used as they can be re-capitulated in NP-CGG treated animals as well (Fig. 22). Furthermore, there is a moderate, albeit not significant, increase in IRF4 expression in both APCs and naïve B cells of Roquin 1/2 double KO mice.

A higher proportion of Roquin 1 KO APCs are class-switched compared to immunized controls suggesting that loss of Roquin 1 alone enhances the process of CSR (Fig. 28). Especially IgG2c, IgG2b and IgG3 APC proportions are elevated at the expense of IgA

producing APCs. Roquin 1 homo Roquin 2 het KO APCs contain similar proportions of $IgG3^+$ and IgA^+ APCs compared to Roquin 1 KO APCs, but otherwise resemble more immunized control animals. For technical reasons, IgG2c was not determined in Roquin 1 homo Roquin 2 het KO mice. An alternate composition of the immunoglobulin repertoire can be caused by differing signaling events and results in divergent effector functions. IgG2c, IgG2b and IgG3 contribute to proinflammatory immune responses while IgG1 and IgE rather limit these proinflammatory reactions. IgM and IgA maintain mucosal immunity as both antibodies can migrate through epithelial layers. They also serve additional regulatory functions sustaining immune homeostasis and preventing autoimmunity[59]. Based on this broad classification, Roquin 1 homo Roquin 2 het KO and especially Roquin 1 KO mice obtain a more proinflammatory immunoglobulin phenotype.

Most strikingly, Roquin 1/2 double KO APCs are mostly stained IgM^+ intracellularly with only a neglectable fraction of APCs being class-switched. Together with the fact that GCBs are lost in this genotype, all APCs are most likely of an extrafollicular origin. The pronounced absence of any class-switched APCs suggests that the presence of at least one Roquin 2 allele is necessary to enable the generation of class-switched APCs. This result complements studies of our laboratory of Dr. Maike Kober in unimmunized CD19Cre Roquin 1/2 double KO mice which likewise were devoid of $IgG1^+$ $CD138^+$ $B229^{lo}$ cells in spleen and bone marrow (unpublished data).

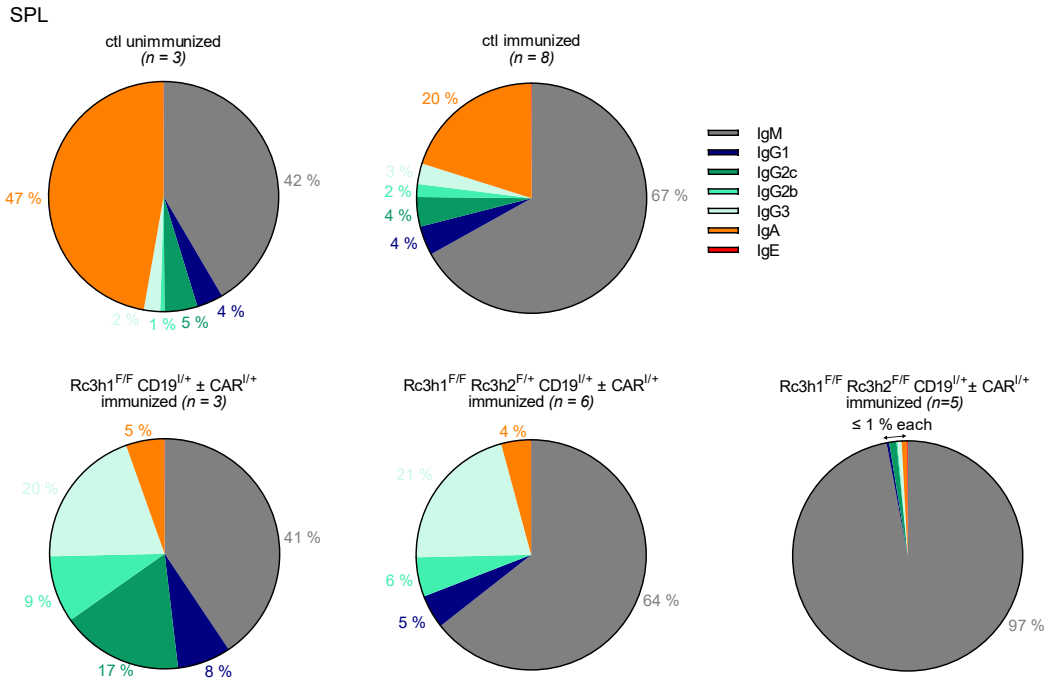

Figure 28: **Immunoglobulin proportions of class-switched APCs upon SRBC immunization after 10 days in CD19Cre Roquin knockout mice.**
Proportions of immunoglobulins in CD138^{+} IRF4^{+} B220^{lo} APCs in spleen of mice with indicated genotypes. Percentages correspond to the median of immunoglobulins within the APC population. Data are cumulative from 4 independent experiments, respectively. SPL, spleen

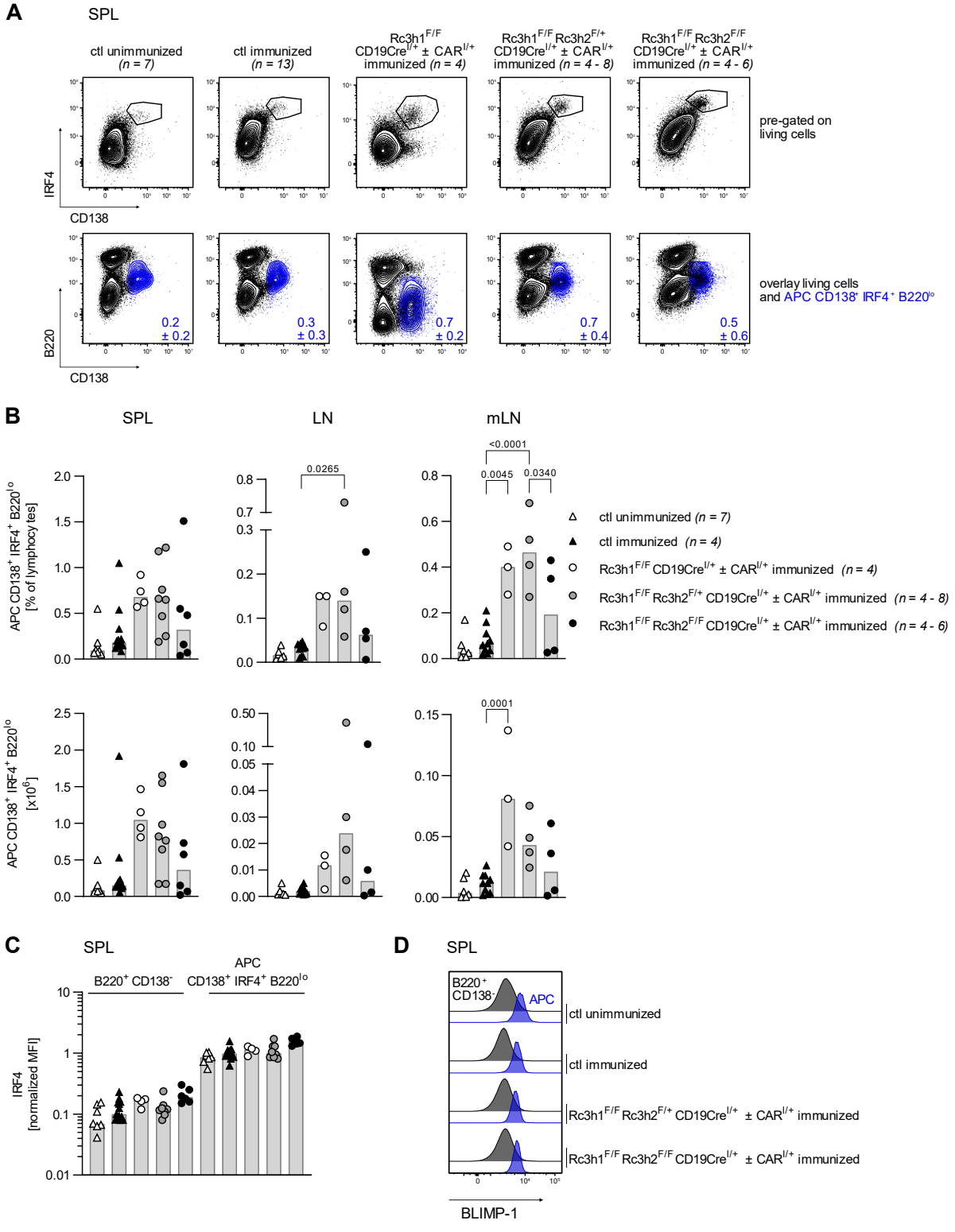

Figure 29: APCs production upon SRBC immunization after 10 days in CD19Cre Roquin knockout mice.

(A) Representative flow cytometry plots of APCs in spleen. Percentages correspond to mean ± SD of APCs within the lymphocyte population. (B) APC percentages and numbers in respective organs. Data are cumulative from 4 independent experiments. (C) IRF4 expression levels of GCBs in comparison to $B220^+$ $CD138^-$ B cells exemplarily shown for spleen. MFI values are normalized per experiment to APC cells of immunized controls. (D) Representative histograms of BLIMP-1 protein expression levels of $B220^+$ $CD138^-$ B cells and APCs in spleen. Bars show median values with each symbol representing a mouse. Statistical significance was determined by one-way ANOVA. SPL, spleen; LN, lymph nodes; mLN, mesenteric lymph nodes; B $B220^+$ $CD138^-$; APC $CD138^+$ $IRF4^+$ $B220^{lo}$

Cγ1Cre Roquin KO mice replicate the APC phenotype of the CD19Cre cohort with regard to the enrichment of Roquin 1 homo Roquin 2 het KO APCs in secondary lymphoid organs at day 10 after SRBC immunization (Fig. 30 and Suppl. Fig. 10). Roquin 1 KO mice equally present with higher APC percentages and numbers in spleen, but contain similar cell numbers in lymph nodes and mesenteric lymph nodes compared to immunized controls suggesting a less severe variation of APC formation in the presence of two instead of only one WT Roquin 2 allele. Higher amounts of APCs in Roquin 1 homo Roquin 2 het KO mice in the periphery translates into slightly elevated levels in the bone marrow. Surprisingly, even though GCBs are missing in Roquin 1/2 double KO mice, no major differences of APC proportions and numbers can be detected compared to immunized controls in all organs analyzed.

As expected, the immunoglobulin repertoire is more diverse in spleens of immunized control mice compared to unimmunized animals, because of the favored selection of IgG immunoglobulins over IgM in the induced GC reaction (Fig. 31A and Suppl. Fig. 11A). Percentages of IgG2b$^+$ and IgG3$^+$ APCs are increased, although not significantly, in Roquin 1 KO and Roquin 1 homo Roquin 2 het KO APCs compared to immunized controls. In those mice, the fraction of IgG1$^+$ APCs is significantly elevated while especially IgM$^+$ cells are deprived. Together with the obtained results of CD19Cre animals, this hints towards a repressive role of Roquin proteins for switching to IgG isotypes. As seen before, the absence of both Roquin 1 and Roquin 2 eliminates extensive class-switching leading to the loss of IgG1$^+$ APCs. Overall, trends remain when gated more restrictively on dTOM$^+$ APCs thereby excluding the small proportion of ~7 % dTOM$^-$ APCs in Roquin 1 homo Roquin 2 het KO mice and ~17 % dTOM$^-$ APCs in Roquin 1/2 double KO mice (Suppl. Fig. 11C). The bone marrow is mainly populated by IgA$^+$ APCs most likely deriving from immune responses in the GALT and probably does not yet contain many SRBC-specific APCs only 10 days after immunization. Besides IgA, the immunoglobulin repertoire resembles the ones in spleen (Fig. 31B and Suppl. Fig. 11B).

To summarize, loss of GCBs in Roquin 1/2 double KO mice does not prohibit the generation of APCs neither in a CD19Cre nor a Cγ1Cre genetic background. On the contrary, APC proportions and numbers are at least equal to immunized controls. They are devoid of class-switched populations. Roquin 1 KO or Roquin 1 homo Roquin 2 het KO upon Cγ1Cre favors plasmocytic development and increases the rate of class-switching especially to IgG1.

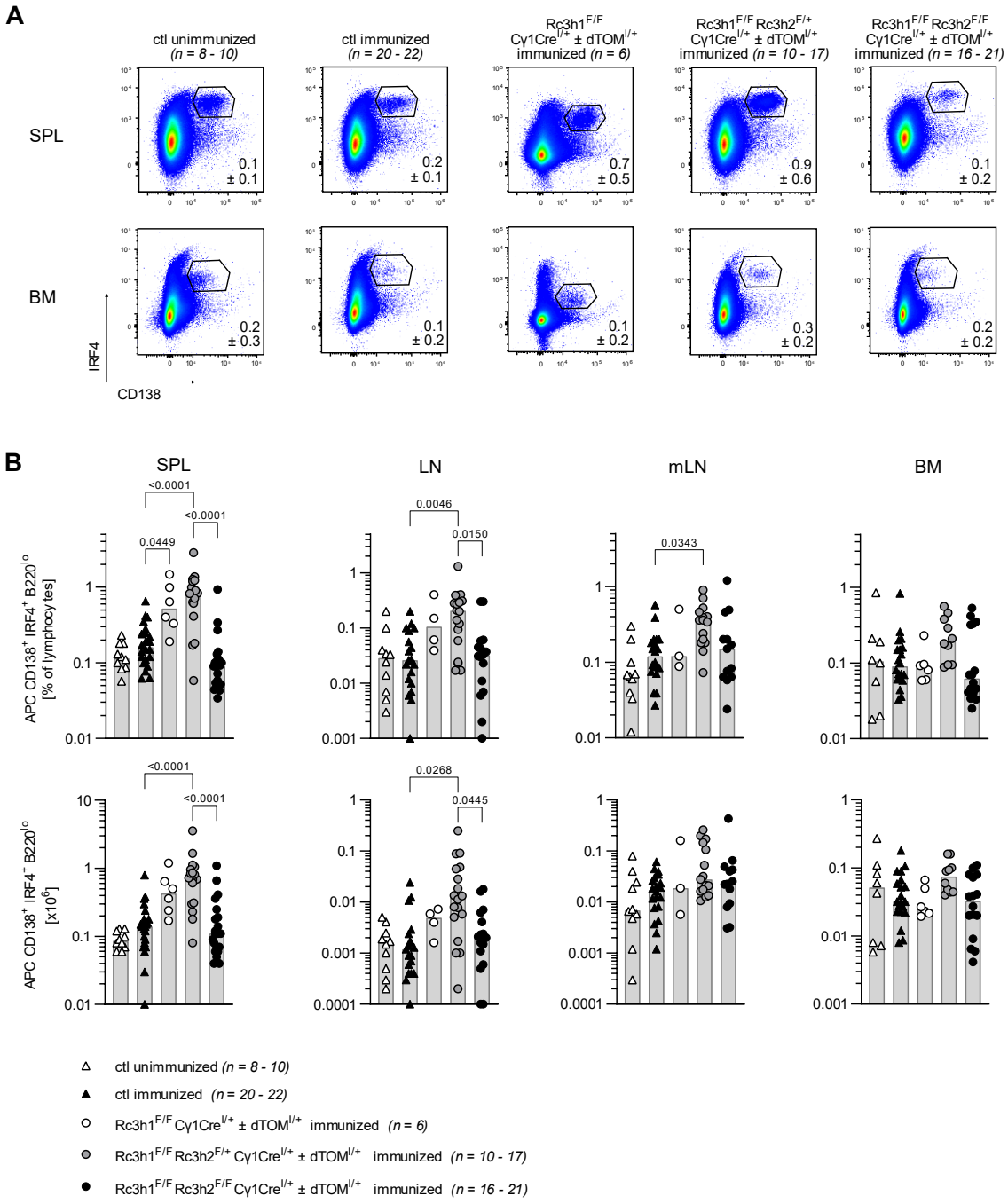

Figure 30: APCs upon SRBC immunization after 10 days in Cγ1Cre Roquin knockout mice.
(A) Representative flow cytometry plots of APCs in respective organs pre-gated on living lymphocytes. Percentages correspond to mean ± SD of APCs within the lymphocyte population. (B) APC percentages and numbers. Data are cumulative from 7 (BM) and 9 (SPL, LN, mLN) independent experiments, respectively. Bars show median values with each symbol representing a mouse. Statistical significance was determined by one-way ANOVA and p values of most relevant comparisons are shown. SPL, spleen; LN, lymph nodes; mLN, mesenteric lymph nodes; BM, bone marrow; APC CD138$^+$ IRF4$^+$ B220^{lo}

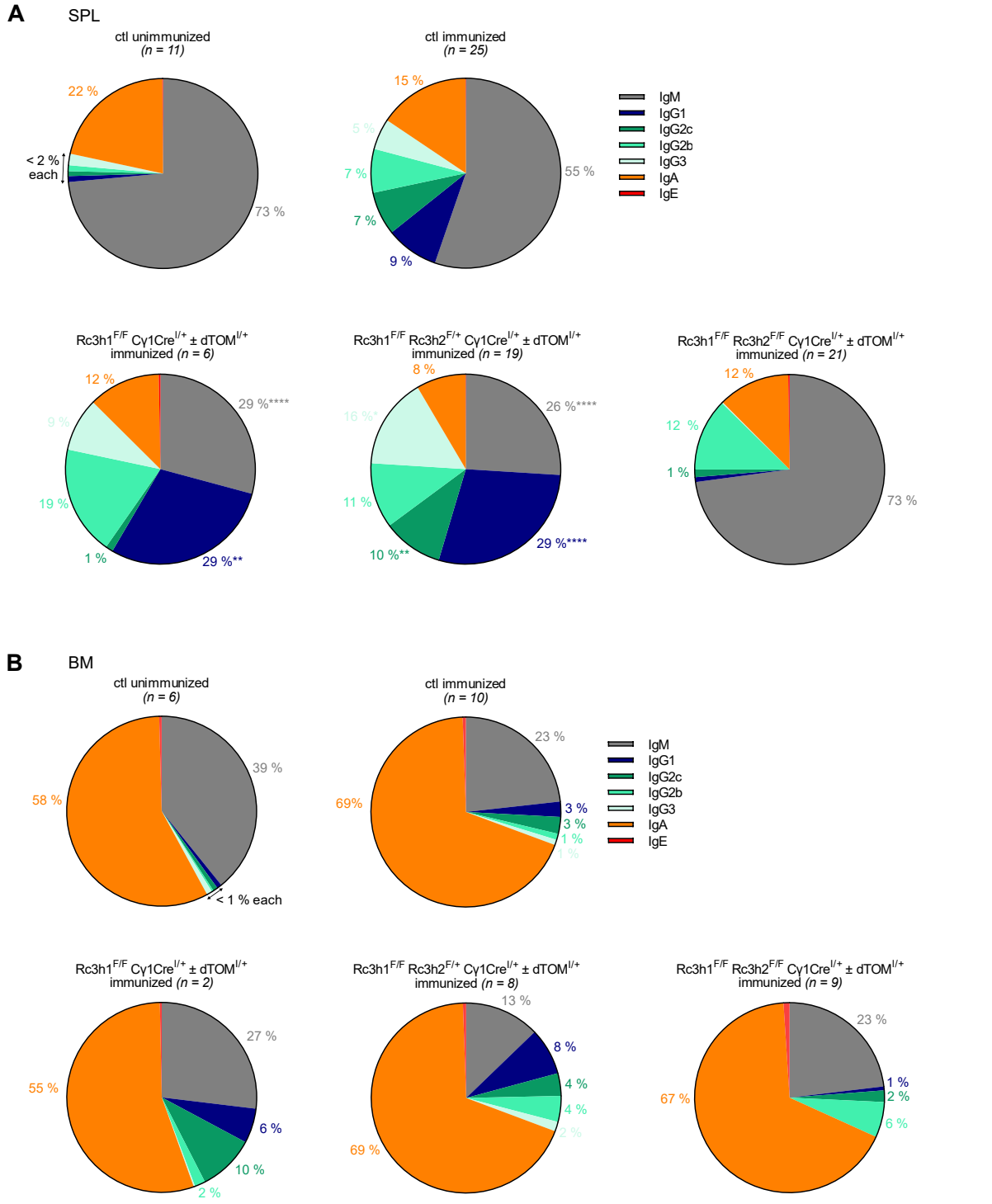

Figure 31: Immunoglobulin proportions of class-switched APCs upon SRBC immunization after 10 days in CD19Cre Roquin knockout mice.
(A) Immunoglobulin proportions of APCs in spleen. (B) Same as in (A) but data shown for bone marrow. Data are cumulative from 3 (BM) and 9 (SPL) independent experiments, respectively. Statistical significance was determined by one-way ANOVA and p values comparing Roquin knockout animals versus immunized ctl animals are shown. SPL, spleen; BM, bone marrow, * $p \leq 0.05$; ** $p \leq 0.01$; *** $p \leq 0.001$; **** $p \leq 0.0001$

4.4 *In vitro* studies

In vitro studies were performed in order to better understand the underlying molecular mechanisms of Roquin proteins during GC reaction. The GC-like cell line A20 represents a valuable tool during this project especially since Roquin 1/2 double KO cells are virtually absent *in vivo* and thus cannot be isolated for further *ex vivo* examinations. A20 cells are derived from a murine lymphoma of BALB/c mice and resemble primary GCBs in their expression of CD95, EphrinB1 and BCL6 even though they are $GL7^-$ and cannot be classified explicitly as DZ or LZ GCB-like cells ($CXCR4^+$ $CD86^+$). A20 are IgG^+ and can be induced to undergo SHM. CD40L treatment in the presence or absence of additional BCR stimulation via αIgG results in the upregulation of IRF4 and simultaneous downregulation of GC markers including BCL6, IRF8 and PAX5. Thus, although complete differentiation into APCs, e.g., via induction of BLIMP-1, cannot be induced in these highly proliferative transformed cells, initial post-GC differentiations steps can still be triggered[137,170].

First, A20 Roquin 1 or Roquin 2 single knockout or Roquin 1/2 double knockout single-cell clones (SSC) were established and characterized via flow cytometry and western blot (chapter 4.4.1). Next, the introduction of a Roquin 1 knockout on a Roquin 2 knockout background was monitored over time using a fluorescence reporter system (chapter 4.4.2). Then the capability to stimulate these SSC was measured (chapter 4.4.3 and 4.4.4). Last, transcriptomic changes upon Roquin knockout were assessed (chapter 4.4.5).

4.4.1 Establishment of Roquin knockout GC-like cell lines

A20 cells were modified by Chia-I Lien in our laboratory to stably express Roquin 1 dual-reporter constructs as visualized in Fig. 32A. Thereby, WT Nfκbid CDE containing plasmids (for plasmid card see Suppl. Fig. 12-14) report Roquin 1 expression levels via eGFP whereas mutations of the Nfκbid CDE sequence abolish Roquin 1 binding and thus can be employed as negative control. Reporter positive A20 cell lines were named “A20 CDE WT” or “A20 CDE mut”. Electroporation of A20 CDE WT cells with Cas9-sgRc3h1 complexes results in a ~5-fold upregulation of eGFP indicating loss of Roquin 1. A20 CDE mut express elevated eGFP levels at steady state and eGFP MFIs do not change majorly upon Roquin 1 targeting (Fig. 32B and 32C). Manipulation of A20 cells by the reporter plasmids did not lead to alterations of GCB marker expressions (Fig. 32D).

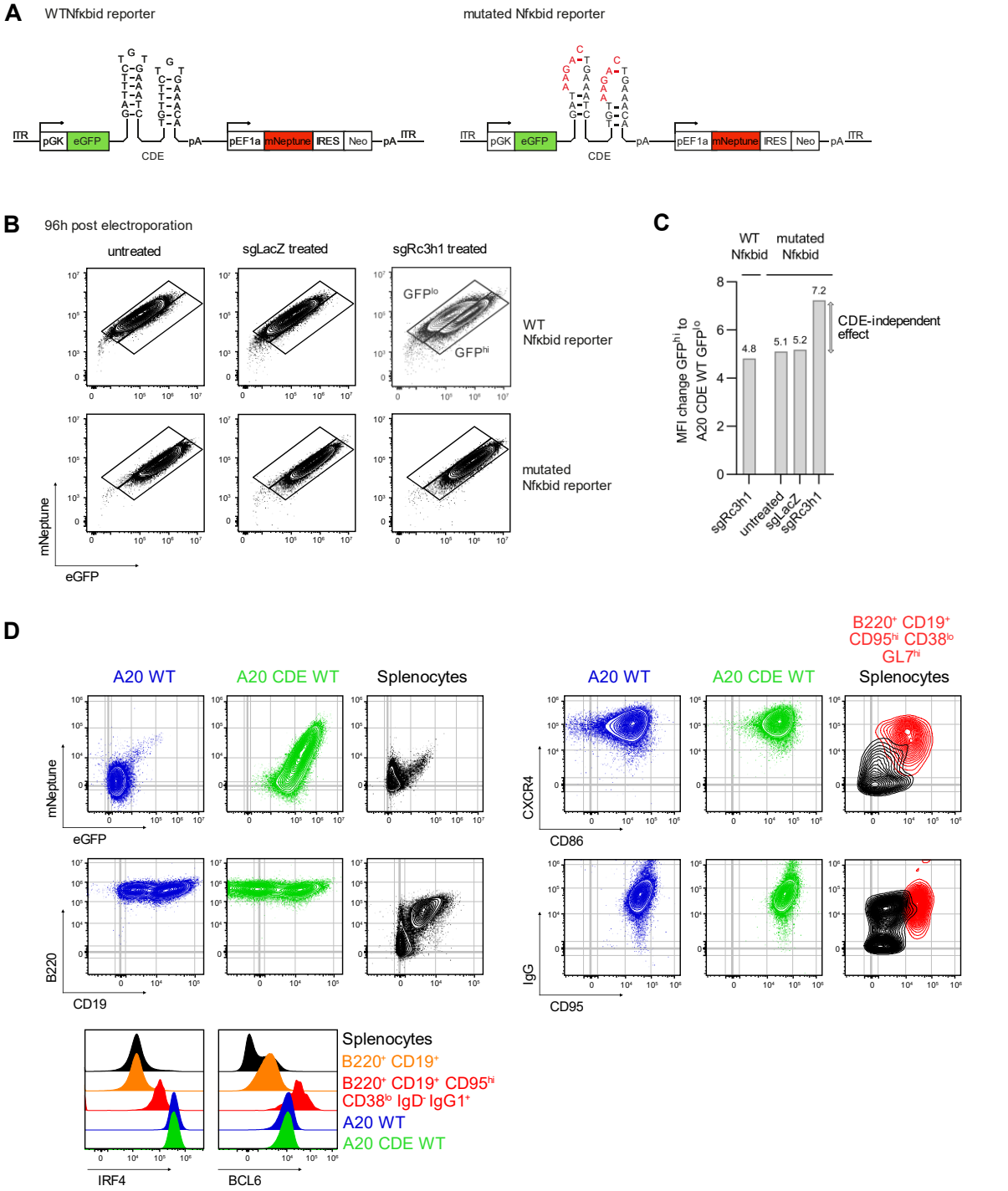

Figure 32: Dual-Nfκbid reporter visualizing Roquin 1 expression levels in A20 cells.
(A) Scheme of the WT and the mutated Nfκbid reporter containing inverted terminal repeats (ITR) for PiggyBac transposase mediated, stable genomic integration and two cassettes driven by pGK or pEF1α promotor, respectively. eGFP expression is dependent on Roquin 1 expression levels due to the association with the tandem *Nfκbid* CDE. In the mutated reporter version, crucial nucleotides of the CDE element were modified to inhibit Roquin 1 binding. mNeptune expression is independent of Roquin 1 regulation. A cloned 3'neomycin cassette allows for antibiotic resistance selection of cells with integrated reporter sequences. Images were taken and modified from Dr. David Riess[82]. (B) Representative flow cytometry plots of dual-reporter containing A20 cells electroporated with RBPs carrying sgRNAs targeting LacZ (sgLacZ) or Roquin 1 (sgRc3h1) or A20 cells left untreated. Images are pre-gated on living lymphocytes and taken 96 h after electroporation. (C) Quantification of the eGFP MFI changes shown in (B) normalized to the GFP^{lo} MFI of untreated CDE WT reporter containing A20 cells. (D) Flow cytometry plots visualizing marker expression levels of A20 containing the WT Nfκbid reporter (A20 CDE WT, shown in green) in comparison to A20 cells without reporter (shown in blue), *ex vivo* splenocytes (shown in black) or *ex vivo* B cell populations (shown in red)[171]. pA poly-A tail; IRES internal ribosome entry site

Overall, A20 cells are a heterogenous cell line based on $CD19^{hi}$ and $CD19^{-}$ expression levels. SSCs were not kept in G418 antibiotic selective pressure and partially lost mNeptune reporter expression while eGFP expression stayed stable over time of culturing (Suppl. Fig. 16). The molecular mechanism for the reporter silencing was not investigated.

Next, Roquin knockouts were introduced by Cas9-sgRNA electroporation and subsequent single-cell cloning resulting in four Roquin 1 knockout (named SSC 9, 10, 23, 25), four Roquin 2 knockout (SSC 6, 7, 21, 22) and four sgLacZ treated negative control clones (SSC 12, 13, 14, 17). Roquin 1/2 double knockouts were induced by treatment of Roquin 2 SSCs (either SSC 6 or 7) with Cas9-sgRc3h1 complexes and subsequent single-cell sorting of reporter GFP^{hi} cells (final SSC 6A, 6B, 6C, 7A, 7B).

Single knockouts were verified on the DNA level by PCR amplifications of sgRNA surrounding products followed by sequencing analysis of indels. Thereby, clone specific homo- or heterozygous deletions and insertions were detected with all of them causing frameshift mutations (Suppl. Fig. 15A and 15B). Downregulation of transcripts was additionally proven via RT-qPCR (Suppl. Fig. 15C) and most importantly, single and double knockouts were confirmed at the protein level by western blot analysis (Fig. 33A and 33B). SSCs were further characterized by flow cytometry revealing no significant changes for protein levels of B220, IgG, CD95, BCL6, IRF4 and CD86 in Roquin 1 or Roquin 2 single knockout clones compared to LacZ controls. However, Roquin 1/2 double knockout cells display a more than 2-fold increase in IRF4, BCL6 and CD86 expression levels (Fig. 33C) which nicely reflects *ex vivo* analysis of Roquin 1/2 double KO Cγ1Cre mice (shown in Fig. 15C and 16B) and Roquin 1/2 double KO CD19Cre mice (shown in Fig. 29C and 16A). All SSCs are $eGFP^{+}$, however with different intensities due to the broad range of eGFP expression levels already in the founder A20 CDE WT cells (Fig. 32D). Similarly, CD19 expression varied between clones reflecting the heterogeneity of the original population (Suppl. Fig. 16). The mNeptune cassette, meant to be a non-regulated, cell internal control fluorochrome, turned out to be unstable in culture and got irreversibly downregulated in some SSCs upon withdrawal of the selective pressure by G418 antibiotics. In summary, Roquin knockout A20 cell lines were successfully generated which allowed further studies on their capability to react on BCR stimulations.

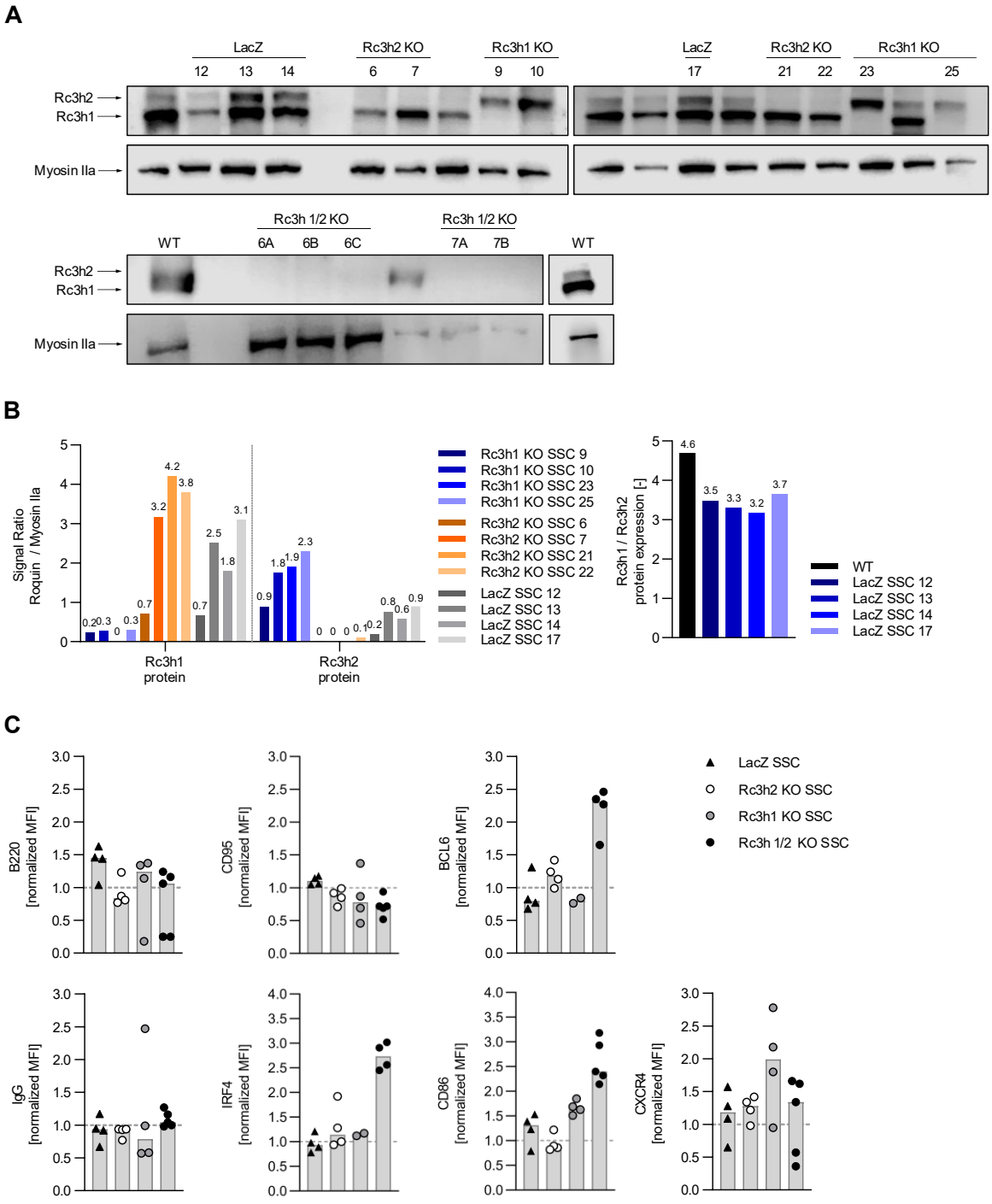

Figure 33: Roquin knockout single-cell clone generation in A20 cells.
(A) Western Blot of numbered single cell clones (SSCs) treated with sgRNAs targeting LacZ, Roquin 1 or Roquin 2 (top). Western Blot of numbered Roquin1/2 double knockout (KO) clones as well as wildtype (WT) A20 cells (bottom). Roquin 1/2 double KO SSCs 6A, 6B and 6C are derived of the Roquin 2 knockout SSC 6 through electroporation with a Cas9-sgRNA RBP complexes targeting endogenous Roquin 1. Roquin 1/2 double KO SSCs 7A and 7B were generated identically treating Roquin 2 SSC 7. (B) Quantification of western blot images shown in (A). (C) Protein expression levels of SSCs normalized to A20 CDE WT assessed by flow cytometry. Bars show median values. Each dot represents one clone.

4.4.2 Characterization of A20 cell lines by time-course and proliferation experiments

The simultaneous knockout of Roquin 1 and Roquin 2 has a detrimental effect on GCBs *in vivo*. Nevertheless, A20 CDE WT Roquin 1/2 double knockout SSCs could readily be established hinting towards comprehensive compensatory mechanisms of the *in vitro* cell culture to the severe introduced perturbations. This is not an obvious result since my efforts to generate stable Roquin deficient cells already failed in another B cell line due to poor survival upon the Roquin 1/2 double knockout (data not shown). To circumvent that long-term adaptations of stable Roquin 1/2 double knockout SSCs cause manifold transcriptional changes which do not reflect the physiology of Cγ1Cre induced Roquin knockouts *in vivo* anymore, Roquin 1/2 double knockouts were also generated transiently by induction of Roquin 1 deletions in Roquin 2 deficient SSCs. Therefore, Roquin 2 SSCs were electroporated with Cas9-sgRc3h1 and Roquin 1 ablation was monitored via the eGFP reporter system.

Initial time-course experiments using all four available Roquin 2 SSCs were performed to assess the timing of the Roquin 1 deletion (Fig. 34). An upregulation of eGFP is detectable first after 24 h with a distinct population being visible after 36 h. The reaction peaks at day 3 with ~60 % $eGFP^+$ cells. Afterwards, the frequency of $eGFP^+$ cells declines steadily and is reduced by half until day 10. 42 days after electroporation, no $eGFP^+$ cells are present in the culture anymore. This data suggests that although a Roquin 1/2 double knockout can be induced without immediate cell death, Roquin 1/2 double knockout cells cannot survive when kept long-term in a competitive environment together with single Roquin 2 knockout A20 cells. This continuous counterselection could result from deficiencies in proliferation and metabolism or increased apoptosis and could reflect a counterselection also occurring *in vivo*, albeit to a lesser extent, as Roquin 1/2 double knockout cells *in vivo* are completely absent in the GC state.

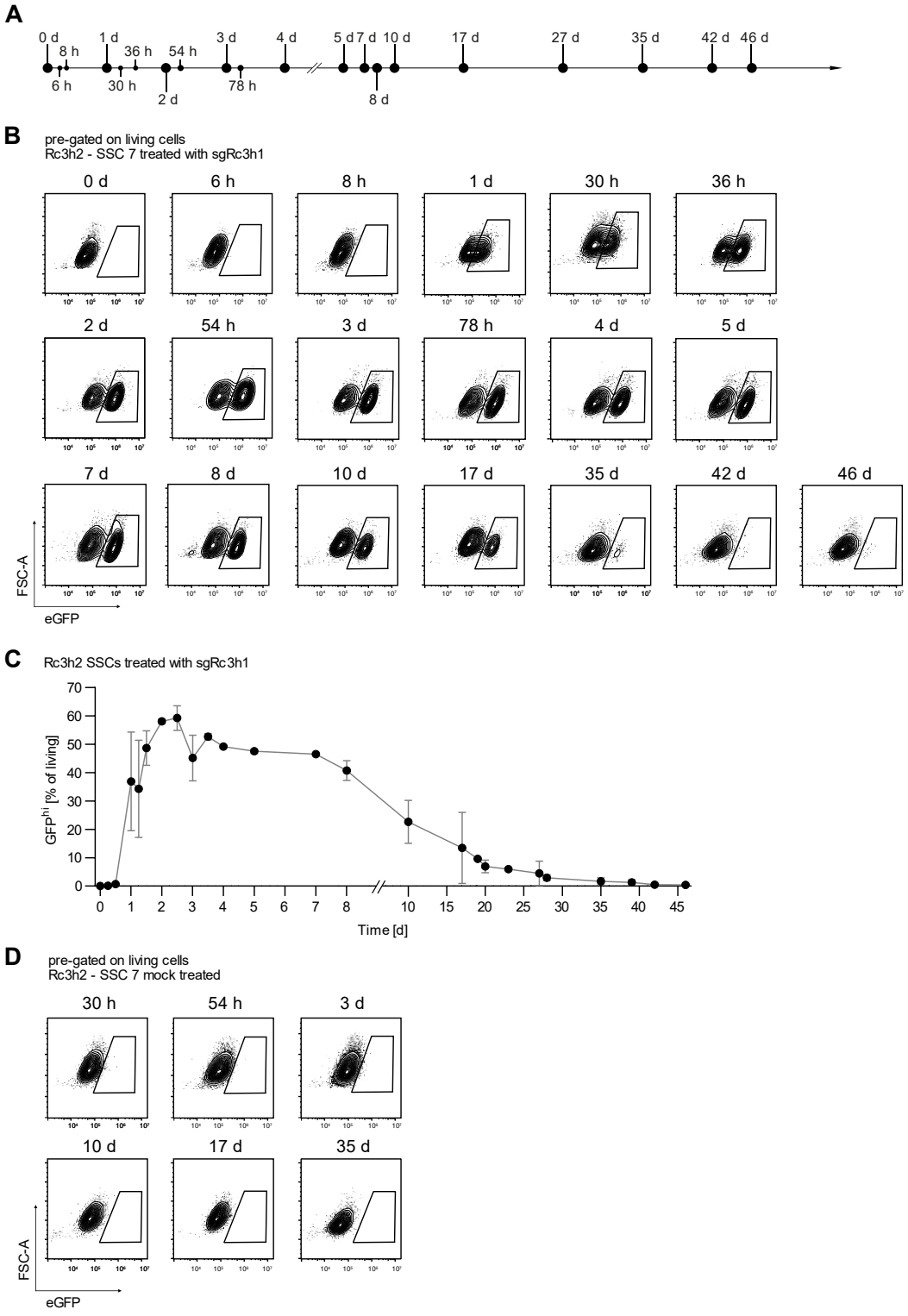

Figure 34: Time course to monitor Roquin 1 knockout efficiency in Roquin 2 SSCs.
(A) Timeline showing time-points at which Roquin 2 SSCs 6, 7, 21 and 22 were analyzed for eGFP expression indicating Roquin 1 knockout efficiency after electroporation with Cas9-sgRc3h1 RBP complexes. (B) Representative flow cytometry plots of eGFP expression in sgRc3h1 treated Roquin 2 SSC 7 A20 cells over time. (C) Quantification of plots shown in (B) including 3 additional biological replicates. Data points show mean values ± SD. Data are cumulative from 3 independent experiments. (D) Representative flow cytometry plots of eGFP expression in mock treated Roquin 2 SSC 7 A20 cells. Mock treated cells were electroporated in the respective electroporation buffer and cell densities, however without addition of Cas9 RBP complexes. They were employed to determine GFP^{hi} populations in sgRc3h1 treated samples. Time-points are shown here only exemplarily.

Regarding this finding, Roquin 1 knockout SSCs or Roquin 1/2 double knockout SSCs were mixed 1:1 with eGFP$^-$ WT A20 cells and their metabolic capacity was challenged by reducing glucose levels in their culturing media from a standard of 2 g / L to 0.1 g / L or 0 g / L. Cells were counted and splitted every 2 - 3 days thereby seeding identical cell densities throughout the experiments. The content of eGFP$^+$ Roquin ablated cells was recorded by flow cytometry, their proliferation status was determined using DAPI staining and the frequency of pro-apoptotic cells was measured by AnnexinV.

Already within 12 days of culture, the fraction of initial ~50 % eGFP$^+$ cells reduced drastically upon mixed cultures with Roquin 1/2 double knockout SSCs independent of the glucose levels inside their media (Fig. 35A and Suppl. Fig. 17A and 17B). In contrary, the proportion of single Roquin 1 or single Roquin 2 knockout SSCs were much less affected over time. Especially cells cultured without any glucose suffered after three passages (day 7) from apoptosis as measured by an increase of manually counted trypanblue$^+$ or stained PF840$^+$ cells which prohibited any further culturing beyond day 12 (Fig. 35C and Suppl. Fig. 17C). Low concentrations of glucose were sufficient to rescue A20 cells from massive cell death although their expansion was slowed down (less viable cells counted in comparison to 2 g / L treated wells). However, these trends were independent of the respective Roquin genotype. Furthermore, no trends in the frequency of AnnexinV$^+$ cells were detectable over time, between culturing conditions or genotypes (data not shown). Staining of DNA via DAPI revealed a decrease of proliferating (S / G2 cell cycle stage) cells over time, again independent of the genetic status of the cells and independent of the glucose concentration in the culturing media, too (Fig. 35B).

In summary, the counterselection of Roquin 1/2 double knockout cells in competition with WT cells could be reproduced in an alternative experimental setup. Additionally, it could be shown that the presence of only one Roquin protein acts protectively in A20 cells irrespective whether this protein is Roquin 1 or Roquin 2. However, the underlying reasons still need to be identified since deprivation of glucose did not reveal a major deficit of Roquin 1/2 double knockout cells over WT cells suggesting that they are not majorly impaired in their aerobic glycolysis or oxidative phosphorylation energy consumption pathways.

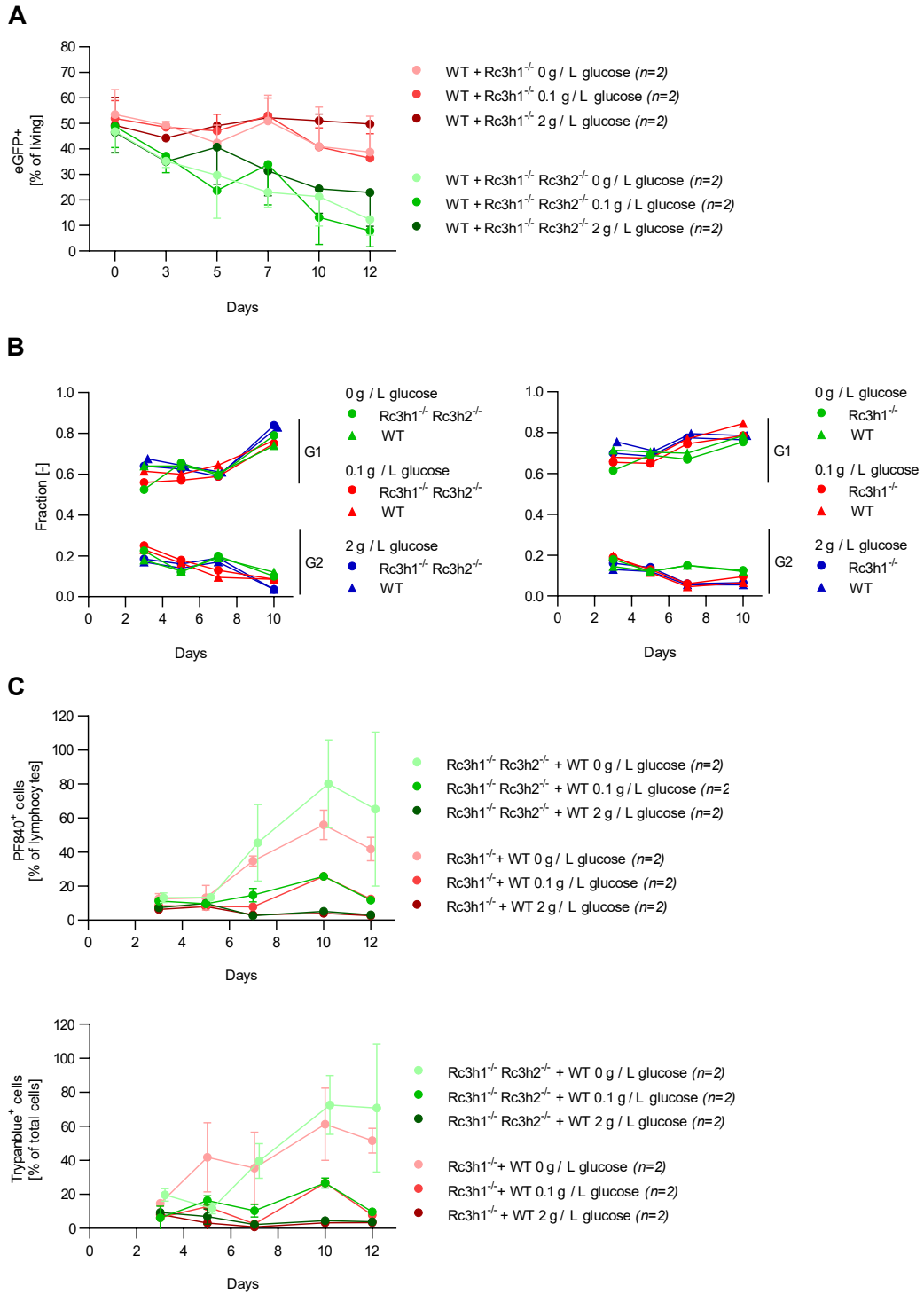

Figure 35: Competition assay challenging Roquin knockout SSC growth in presence with WT cells in different media compositions.
(A) Fraction of Roquin knockout cells (eGFP+) in a Roquin knockout and wildtype A20 mixed culture over time in 0 g / L, 0.1 g / L or 2 g / L glucose containing media. (B) Fraction of cycling (G2) and non-cycling (G1) cells within eGFP+ (Roquin knockout) or eGFP- (WT) populations over time. (C) Percentage of dead cells in mixed cultures over time determined via PF840 flow cytometry staining and trypanblue manual cell counting irrespective of the cell genotype. Data points show mean values ± SD. Data are cumulative from 2 biological replicates measured in one experiment.

4.4.3 Characterization of A20 cell lines by stimulation experiments

With the aim to assess Roquin mediated effects on the transcriptome at steady state and upon activation of BCR signaling, TD stimulation was mimicked *in vitro* by the addition of αCD40 and αIgG to A20 CDE WT cultures (Fig. 36). Thereby, 2 h of stimulation does not lead to a pronounced upregulation of IRF4 protein in contrary to the results shown by Feng et al.[137] However, longer stimulation of 6 h or 24 h achieved a robust IRF4 upregulation on the protein and mRNA level upon αIgG treatments comparable to results from the literature. This effect was independent of the manufacturer of stimuli reagents. Overall, αCD40 was a mild stimulus other than the published CD40L of fibroblast co-cultures[137]. Simultaneously to IRF4 upregulation, BCL6 protein and mRNA levels are decreased in stimulated A20 CDE WT cells compared to unstimulated cells, with αCD40 + αIgG addition showing the strongest effect. Thereby, 6 h of stimulation seem to be sufficient for maximal BCL6 protein downregulation since prolonging the stimulation up to 24 h does not lead to a further decrease. αIgG dependent downregulation of PAX5 mRNA additionally verified the potency of the applied stimulation. The latter was already shown previously to not be inducible via CD40L[137].

Interestingly, Roquin reporter activity detected by flow cytometry increased 3 - 6-fold upon BCR stimulation while the internal mNeptune control changes only insignificantly hinting towards a downregulation of Roquin 1 in these cells (Fig. 36B). However, Roquin 1 transcript levels appear almost completely stable suggesting a post-transcriptional regulation (Fig. 36C).

Taken together, suitable stimulation conditions for A20 CDE WT cells could be established together with a read-out based mostly on BCL6 and IRF4 expression. For subsequent RNAseq analysis, both stimuli were further titrated down to final 2.5 µg / mL αCD40 + 2.5 µg / mL αIgG (data not shown) to trigger a TD-like activation while prohibiting overactivation of the cells which might override potential genotype-related effects similarly to the already described *ex vivo* stimulations of FOB. Reduced stimuli concentrations thereby still enable the evaluation of stimulation efficiency by monitoring IRF4, BCL6 and eGFP.

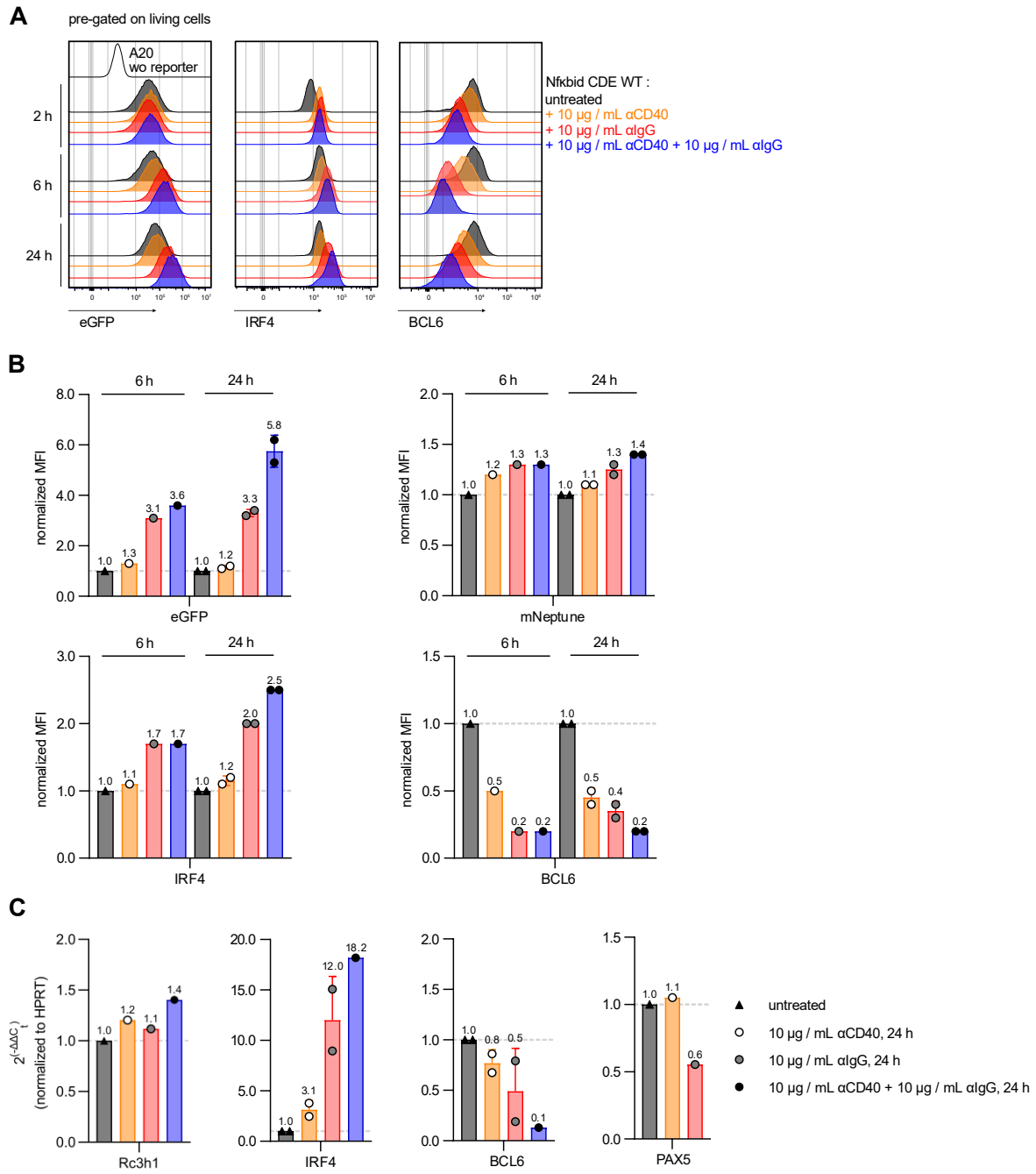

Figure 36: Stimulation of wildtype Nfκbid reporter containing A20 cells.
(A) Flow cytometry histograms showing eGFP, IRF4 and BCL6 expression levels after 2 h, 6 h and 24 h of respective stimulation conditions. (B) Quantification of protein expression levels as shown in (A). MFI values are normalized per time-point and protein to A20 CDE WT cells. Bars show mean values ± SD with each symbol representing one sample. (C) RT-qPCR mRNA transcription levels gathered from cell samples shown in (A) and (B) after 24 h of stimulation. Bars show mean values ± SD with each symbol representing the mean of technical triplicates. Data are cumulative from 2 independent experiments.

4.4.4 MALT-1 dependency of Roquin regulation in A20 cells

Roquin 1 and Roquin 2 were reported to be cleaved by the paracaspase MALT-1 after TCR stimulation using either PMA / ionomycin or CD3 / CD28 stimuli. MALT-1 is part of the CBM complex together with CARMA-1 and BCL10. MALT-1 functions either as scaffolding protein enabling canonical NFκB pathway induction by recruitment of E3 ubiquitin ligases and subsequent IKK activation or as arginine-specific paracaspase degrading negative NFκB regulators as well as mRNA stability controlling RBPs. MALT-1 cleavage occurs at Arg510 in Roquin 1 and Roquin 2 and additionally in Arg579 in Roquin 1 and is ablated in the presence of the MALT-1 inhibitor S-Mepazine. The strength of TCR activation thereby relates to the amount of Roquin cleavage in $CD4^+$ T cells as shown by stimulation of OT-II T cells with varying OVA peptide concentrations[114,172].

To show whether MALT-1 inhibition can also result in cleavage of Roquin 1 in the context of BCR activated A20 cells, A20 CDE WT or A20 CDE mut cells were treated with either S-Mepazine or another MALT-1 inhibitor MLT-985 for 24 h in the absence or presence of αCD40 and αIgG. Both inhibitors were kindly provided by Prof. Daniel Krappmann. Indeed, BCR-induced downregulation of Roquin 1 protein levels (visualized by upregulation of the eGFP reporter) was abolished in A20 CDE WT cells upon blocking the MALT-1 enzymatic activity independent of the applied inhibitor (Fig. 37). As expected, the negative control A20 CDE mut showed almost constant eGFP levels in all conditions with only a slight increase of signal in strongly activated B cells without MALT-1 inhibitor which is a CDE-independent effect. These results show a MALT-1 dependent cleavage of Roquin 1 in GCB-like cells induced by BCR activation. Future validation of the data by western blot visualization of the Roquin cleavage products should be performed.

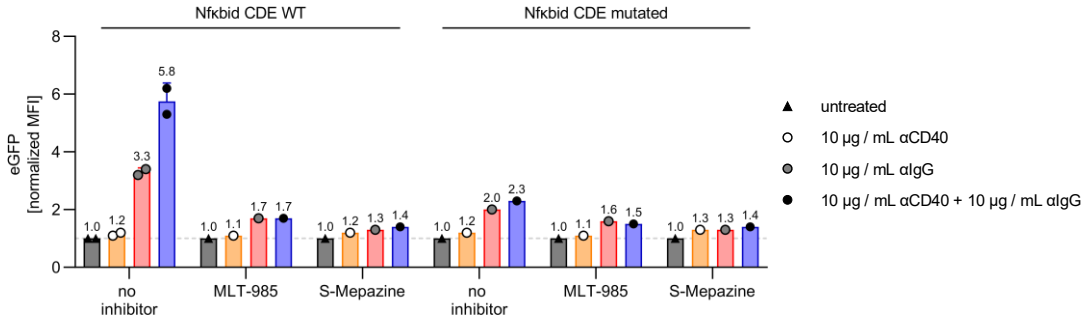

Figure 37: MALT-1 inhibition of stimulated wildtype Nfκbid reporter containing A20 cells.
(A) Normalized MFI values of eGFP levels in living A20 cells containing WT or mutated Nfκbid reporter after 24 h of stimulation with indicated stimulation reagents. In addition to the stimuli, cells were treated with either 2 µM of the MALT-1 inhibitor MLT-985 or 20 µM of S-Mepazine for the duration of the experiment. Bars show mean values ± SD with each symbol representing one sample. Data are derived of one experiment and were proven by Chia-I Lien with same experimental settings.

4.4.5 Experimental setup of the transcriptomic and proteomic analysis of Roquin knockout A20 cells

Having established single Roquin-deficient GC-like cell lines which can be activated in a defined experimental setting by αCD40 + αIgG to mimic *in vivo* TD antigen stimulation, the next aim of this project part was to analyze transcriptomic and proteomic changes upon Roquin knockout that might explain the observed *in vivo* phenotype and hints towards potential target genes that are promising to address in future studies.

In total, the RNA of 73 samples was harvested and sent for bulk 3'-RNAseq. This included 4 - 5 biological replicates per condition obtained in 1 - 2 independent experiments. The whole workflow is visualized in Fig. 38A. In addition, 34 cell pellets were prepared in one experiment and sent for mass-spectrometry analysis. For a clear presentation, samples can be grouped into four categories as follows:

(I) Untreated cells at their steady state

Bulk WT A20 cells and A20 CDE LacZ SSCs were combined during later analysis for the unstimulated "ctl" group. Single Roquin 1 or Roquin 2 knockout SSCs or Roquin 1/2 double knockout SSCs were harvested after 1 - 2 days of culturing without stimulation at equal cell densities. These samples were analyzed for their transcriptomes and proteomes.

Genotype before treatment	Electroporation	Timepoint after electroporation	Stimulation duration	Genotype after treatment
WT *(n = 1)*	-	-	0 h	-
CDE WT sgLacZ *(n = 4)*	-	-	0 h	-
Rc3h2$^{-/-}$ *(n = 4)*	-	-	0 h	-
Rc3h1$^{-/-}$ *(n = 4)*	-	-	0 h	-
Rc3h1$^{-/-}$ Rc3h2$^{-/-}$ *(n = 5)*	-	-	0 h	-

Table 20: Sample group 1

(II) Induced Roquin 1/2 double knockout clones without stimulation

Complementary to stable Roquin 1/2 double knockout SSCs, Roquin 1 knockouts were induced by Cas9-sgRc3h1 electroporation in Roquin 2 knockout SSCs. Roquin 1-deficient eGFP^{hi} populations and Roquin 1-expressing eGFP^{lo} populations were separated by

sorting 30 h or 54 h after the knockout induction. These samples were gathered for transcriptomic analysis only.

Genotype before treatment	Electroporation	Timepoint after electroporation	Stimulation duration	Genotype after treatment
Rc3h2$^{-/-}$ *(n = 4)*	Cas9-sgRc3h1	30 h	0 h	Rc3h2$^{-/-}$ (GFP^{lo})
Rc3h2$^{-/-}$ *(n = 4)*	Cas9-sgRc3h1	30 h	0 h	Rc3h1$^{-/-}$ Rc3h2$^{-/-}$ (GFP^{hi})
Rc3h2$^{-/-}$ *(n = 4)*	Cas9-sgRc3h1	54 h	0 h	Rc3h2$^{-/-}$ (GFP^{lo})
Rc3h2$^{-/-}$ *(n = 4)*	Cas9-sgRc3h1	54 h	0 h	Rc3h1$^{-/-}$ Rc3h2$^{-/-}$ (GFP^{hi})

Table 21: Sample group 2

(III) Stimulated SSCs

Roquin 1 knockout or LacZ SSC were stimulated in equal cell densities using 2.5 µg / mL αCD40 + 2.5 µg / mL αIgG for 6 h or 24 h, respectively, to address Roquin 1 dependent transcriptomic and proteomic changes in activated A20 cells.

Genotype before treatment	Electroporation	Timepoint after electroporation	Stimulation duration	Genotype after treatment
CDE WT sgLacZ *(n = 4)*	-	-	6 h	-
Rc3h1$^{-/-}$ *(n = 4)*	-	-	6 h	-
CDE WT sgLacZ *(n = 4)*	-	-	24 h	-
Rc3h1$^{-/-}$ *(n = 4)*	-	-	24 h	-

Table 22: Sample group 3

(IV) Induced Roquin 1/2 double knockout SSCs with stimulation

Lastly, induced Roquin 1/2 double knockout clones were activated by 2.5 µg / mL αCD40 + 2.5 µg / mL αIgG to enable a comparison to stimulated Roquin 1 single knockout clones. Therefore, stimulation reagents were added 48 h after the electroporation. Sorting of eGFP^{hi} or eGFP^{lo} populations was then conducted 6 h or 24 h later, meaning 54 h or 72 h after the electroporation, respectively. These samples were gathered for transcriptomic analysis only.

Genotype before treatment	Electroporation	Timepoint after electroporation	Stimulation duration	Genotype after treatment
Rc3h2$^{-/-}$ *(n = 4)*	Cas9-sgRc3h1	54 h	6 h	Rc3h2$^{-/-}$ (GFP^{lo})
Rc3h2$^{-/-}$ *(n = 4)*	Cas9-sgRc3h1	54 h	6 h	Rc3h1$^{-/-}$ Rc3h2$^{-/-}$ (GFP^{hi})
Rc3h2$^{-/-}$ *(n = 4)*	Cas9-sgRc3h1	72 h	24 h	Rc3h2$^{-/-}$ (GFP^{lo})
Rc3h2$^{-/-}$ *(n = 4)*	Cas9-sgRc3h1	72 h	24 h	Rc3h1$^{-/-}$ Rc3h2$^{-/-}$ (GFP^{hi})

Table 23: Sample group 4

Fig. 38B exemplarily illustrates the eGFP separation of induced Roquin 1/2 double knockout SSCs with and without stimulation. Mock treatment (= electroporation without RNP complexes) was solely used to proper set $eGFP^{hi}$ gates for sorting. Stimulation efficiency was verified by BCL6, IRF4, CD80 and CD86 flow cytometry analysis (Fig. 38C and Suppl. Fig. 18A). Knockout efficiency was exemplarily examined by RT-qPCR (Suppl. Fig. 18B). RNAseq normalized counts for Roquin 1, Roquin 2 and the reporter CDE Nfκbid were compared between all samples and were in line with the expected knockouts demonstrating the efficiency of the sample preparation approach (Suppl. Fig. 19).

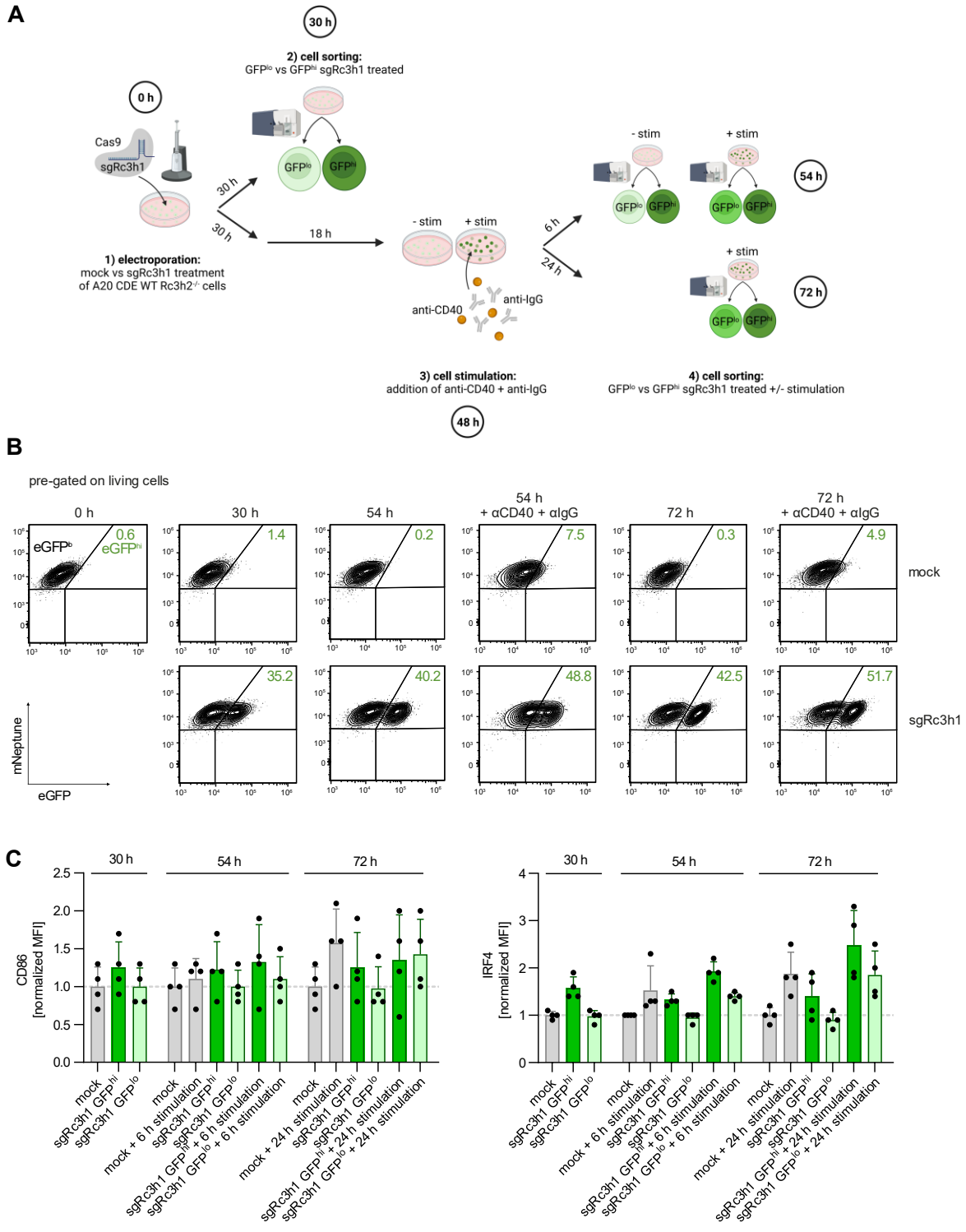

Figure 38: RNAseq sample preparation of resting and stimulated SSCs with induced Roquin 1 knockout.

(A) Schematics presenting the workflow of RNAseq sample preparation. (B) Representative flow cytometry plots of Roquin 2 SSC 7 at indicated time-points after electroporation with sgRc3h1 Cas9-RBP complexes or mock treatment. Percentages indicate the proportion of GFP^{hi} cells of living A20 CDE WT cells in the shown sample. Gating used for final cell sorting of GFP^{lo} and GFP^{hi} populations was based on mock treated cells with same stimulation status. On contrary, gating here is shown based on mock treated, unstimulated cells to demonstrate the shift in GFP expression levels due to stimulation with αIgG and αCD40. (C) Protein expression levels of CD86 and IRF4 at indicated time-points and treatments normalized to mock treatment per timepoint and experiment. Bars show mean values ± SD. Data are cumulative for 4 biological replicates and 2 independent experiments.

4.4.6 Transcriptomic and proteomic analysis of Roquin knockout A20 cells

To enable a detailed analysis of the transcriptome and proteome of A20 Roquin knockout SSCs comparing diverse knockout and stimulation conditions, samples were grouped as outlined before. Thereby, different stimulation conditions were separated as transcriptomic and proteomic changes were triggered most by αIgG1 + αCD40 with 6 h stimulated samples clustering distinct from non-stimulated or 24 h stimulated samples in principal component analysis (PCA) independent of the cell genotype or analysis (Fig. 39). No batch effects between independent experiments, RNA preparation dates, sequencing runs or mass-spectrometry measurements were detected.

Differential gene expression analysis was performed by an in-house script using the DESeq2 package and LRT test for clustering in R Studio for heatmap visualizations. LRT test results were verified by a collaborating laboratory using the Limma package and multiple sample testing in R Studio. Overall, Limma analysis resulted in less significantly regulated transcripts due to more stringent filtering and other than LRT testing enabled the evaluation of Log_2FoldChanges necessary for comparison of transcriptomic data with proteomic data. Consequently, in individual cases the results of the LRT analysis, visualized in heatmaps, and the results of the Limma analysis, visualized in scatter plots together with proteome data, are minimally different.

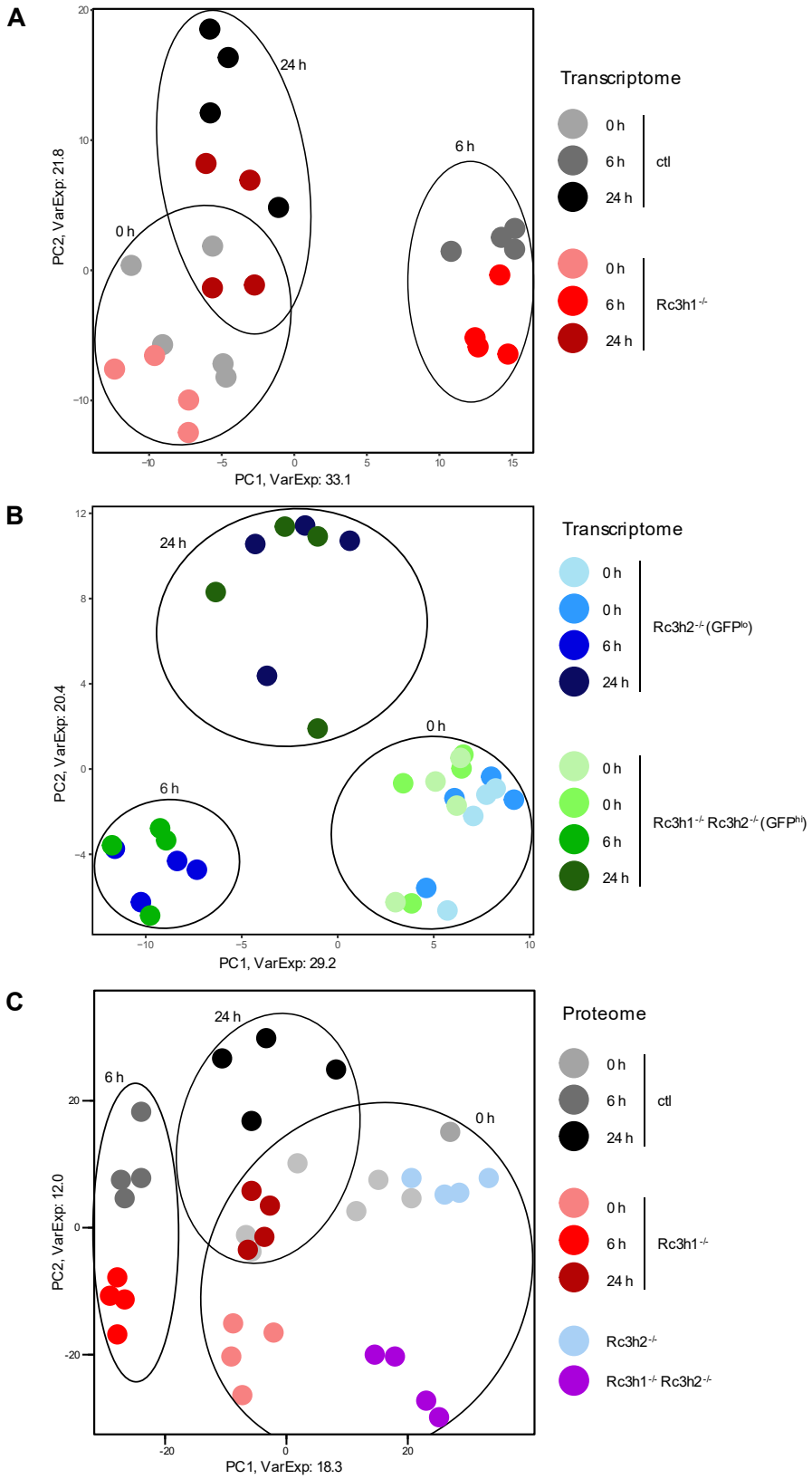

Figure 39: Principal component analysis of A20 Roquin knockout SSCs.
(A) PCA analysis of Roquin 1 KO SSCs transcriptomes (shown in red) in comparison to LacZ SSCs transcriptomes (shown in grey). (B) PCA analysis of transcriptomes of Cas9-sgRc3h1 electroporated Roquin 2 SSCs sorted for GFP^{lo} (shown in blue) and GFP^{hi} (shown in green). Stimulation duration is indicated. Unstimulated samples were gathered 30 h after electroporation (0 h in light blue / green) or 54 h after electroporation (0h in darker blue / green). (C) PCA analysis of proteomes of unstimulated, 6 h or 24 h stimulated SSCs.

Expression of Roquin targets was assessed in transcriptomes and proteomes of A20 SSCs. To my knowledge, there is until today no published validation of Roquin target genes in B lymphocytes differentiating Roquin 1 and Roquin 2. Thus, 96 differentially regulated Roquin 1 targets were retrieved using the annotation of Leppek et al. with the addition of ZC3H12A, IL6, REL and Nfκbia (Suppl. Table 1)[92]. Thereby, it needs to be considered that Leppek et al. experimentally determined these target genes by co-immunoprecipitations from LPS stimulated RAW264.7 macrophages and evaluated only some of their hits in NIH 3T3 cells. Thus, this target list is most likely biased due to cell-type mediated differences in the transcriptome and there is a certain likelihood that I miss Roquin 2 targets and targets specifically related to the B cell lineage in this analysis. Ongoing work in our laboratory to specifically assess Roquin 1 and Roquin 2 targets in A20 cells will improve the current analysis presented here in the future. In addition to Roquin target genes, transcript and proteome levels of well characterized markers of the GCB or PC fate, genes involved in AID-mediated CSR, BCR or CD40 signaling were assessed. Lists of relevant marker genes were created from literature search (Suppl. Table 9)[42,44,55,64,173,174].

(I) Comparison of Roquin 1 and Roquin 2 knockouts in stable cell lines at steady state

Unstimulated Roquin 1/2 double knockout SSCs display a heavily modified gene signature in comparison to single knockout or control SSCs (Fig. 40C). Pathway enrichment analysis of transcriptomes revealed a major upregulation of pathways related to cellular stress, DNA damage response, cell cycle arrest and apoptosis containing partially overlapping proteins (“p53 pathway”, “apoptosis”, “hypoxia”, “unfolded protein response”, “UV response up”) and downregulation of cell cycle related pathways (“E2F targets”, G2-M checkpoint”, “Myc targets”, “mitotic spindle”) and metabolism related pathways (“OXPHOS”, “Glycolysis”) (Fig. 40B). Proteins upregulated in the “TNFα-signaling via NF-κB” pathway are listed in Suppl. Table 2 and in sum also hint towards a pro-apoptotic regulation. 15 out of 100 Roquin targets were detected to be significantly regulated with 12 of them being upregulated in Roquin 1/2 double knockout SSCs compared to controls or single Roquin knockout clones. This included well-known Roquin targets such as Nfκbid and Nfκbiz. As Roquin 1/2 double knockout SSCs could be generated, it can be speculated that pro-apoptosis drivers are counterbalanced by cell cycle and metabolism adaptation in these A20 cells. However, their selection disadvantage when mixed with WT A20 cells as described earlier could be related to the enhanced stress, apoptosis as well as decreased cell cycle signature observed in Roquin 1/2 double KO transcriptomes. Most likely a more

detailed monitoring than the conducted PF840 and AnnexinV staining at only two-day intervals would be required to capture this imbalance in mixed *in vitro* cell culture experiments.

Analysis of Roquin 1/2 double knockout SSC proteomes resulted in 246 significantly upregulated and 157 significantly downregulated proteins compared to control SSCs (Fig. 41A). Upregulated proteins participate, as already described for respective transcriptomes, in pro-apoptotic signaling pathways such as "TNFα-signaling via NF-κB" and "p53 pathway" whereas proteins of cell cycle related pathways ("mitotic spindle", G2-M checkpoint") are significantly downregulated. In addition, proteins involved in fatty acid metabolism were found to be upregulated (Fig. 41C). Roquin targets were significantly enriched upon Roquin 1/2 double knockout SSCs (1D annotation enrichment, FDR = 0.026, score = 0.18)[175]. Connecting transcriptome and proteome measurements results in a total of 158 genes with significant expression changes both at the transcript as well as the protein level (Fig. 41D). Among those, the Roquin targets IRF4, Nfκbid and FBXO33 were detected. Their relevance is described in brief in the following. Mean protein intensities of Roquin targets measured by mass-spectrometry are given in Suppl. Fig. 20. Hits with protein intensities < 18 were considered with care and protein intensity differences between samples as well as the number of peptides detected per protein were evaluated closely.

IRF4 (Interferon regulatory factor 4)

IRF4 is a transcription factor with a bimodal role during late B cell development. On the one hand, low IRF4 expression in naïve B cells is essential for GC initiation via BCL6 and OBF1 (encoded by *Pou2af1*) and promotes AID expression when transiently expressed. IRF4 expression is absent in proliferating GC centroblasts reasoning that IRF4 is dispensable for GC maintenance. On the other hand, high and prolonged IRF4 expression results in APC formation via BLIMP-1 induction and reduced AID activity as seen by an increase of IgM^+ cells[176]. Thus, IRF4 is essential for CSR. $C\gamma1Cre^{I/+}$ $IRF4^{F/F}$ mice almost completely lack $IgG1^+$ APCs and are reduced in their antigen-specific serum IgG1 titers[177]. Increased IRF4 protein expression was already detected *in vivo* in CD19Cre Roquin 1/2 double KO APCs (Fig. 29C) and was additionally validated by flow-cytometry in Roquin 1/2 double knockout A20 cells (Fig. 33C). IRF4 protein intensities measured by mass-spectrometry were > 18 in all samples. In conclusion, Roquin-mediated dysregulation of IRF4 levels could influence the commitment of naïve B cells to the GCB or APC fate[176–178].

FBXO11 and 33 (F-box only protein 11 and 33)

F-box proteins are part of the E3 ubiquitin ligase complex SCF (F-BOX, SKP1, CUL1, RBX1) recognizing substrates including BCL6 leading to their ubiquitylation and proteasomal degradation. Cγ1Cre$^{I/+}$ FBXO11$^{F/F}$ mice obtain elevated levels of GCBs with higher DZ/LZ ratios, normal SHM and CSR, but disturbed GC exiting. FBXO11 mediated BCL6 degradation upon BCR signaling is thus necessary to terminate the GC program and enter an APC cell fate[27,179]. Studies in CD19Cre$^{I/+}$ FBXO11$^{F/F}$ mice further revealed deficiencies in αCD40 + IL4 induced CSR to IgG1 upon FBXO11 knockout. In addition, FBXO11 was shown to enhance CD40 expression levels by inducing BCL6 degradation. Enhanced CD40 surface levels are necessary to induce CD95 upregulation in Daudi cell lines[180]. Much less is known so far about the family member FBXO33 especially in the context of B cell development. During my studies in A20 cells, FBXO33 protein intensities in control samples were in average 16.4 and in Roquin 1/2 double knockout SSCs 18.7, meaning FBXO33 proteins were enriched ~4-fold in Roquin 1/2 double knockout SSCs compared to controls. Even though protein intensities were not high in general, FBXO33 protein identification was based on 3 – 11 peptides allowing a reliable quantification of the protein. Nevertheless, due to the low protein intensities in mass-spectrometry measurements, a verification e.g., via western blot should be performed in addition. Roquin-mediated regulation of FBXO33 could be related to the enhanced BCL6 expression levels monitored in Roquin 1/2 double knockout SSCs (Fig. 33C) as well as the increased BCL6 protein levels detected in GCBs of Cγ1Cre or CD19Cre Roquin 1/2 double KO mice (Fig. 7C and 14C) and is hence a highly interesting candidate to evaluate further.

Nfκbid

Nfκbid deficient mice fail to produce adequate levels of especially extrafollicular plasma cells upon TD immunization probably due to disturbed TACI, IRF4 and BLIMP-1 induction[181,182]. In line with previous studies, Roquin proteins mediate NFκB signaling in A20 cells, among others via Nfκbid, however the net outcome of this regulation is hard to predict due to the complexity of NFκB regulation inside the cell.

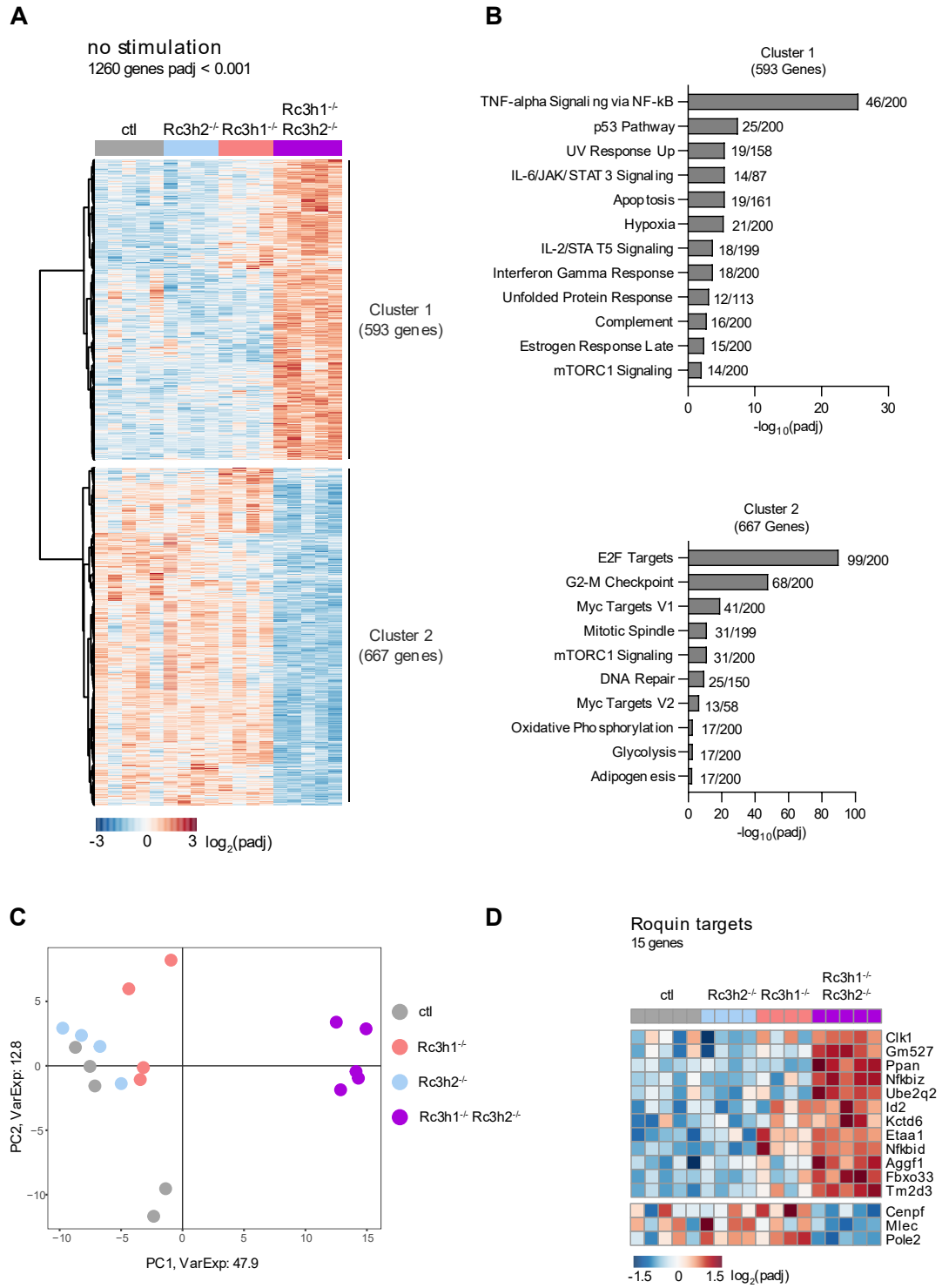

Figure 40: Transcriptomic analysis of Roquin 1/2 double knockout SSCs at steady state.
(A) Heatmap of significantly regulated genes using a GeneCutoff > 50 and padj < 0.001 in unstimulated SSCs. (B) MSigDB Hallmark pathway enrichment of significant genes as plotted in (A) filtered for padj < 0.05. Pathways which contain more than 10 genes are plotted. Numbers indicate the overlap of identified genes as proportion to the total gene number of the respective pathway. (C) PCA analysis of Roquin knockout SSCs at steady state. (D) Heatmap of significantly regulated Roquin targets included in (A).

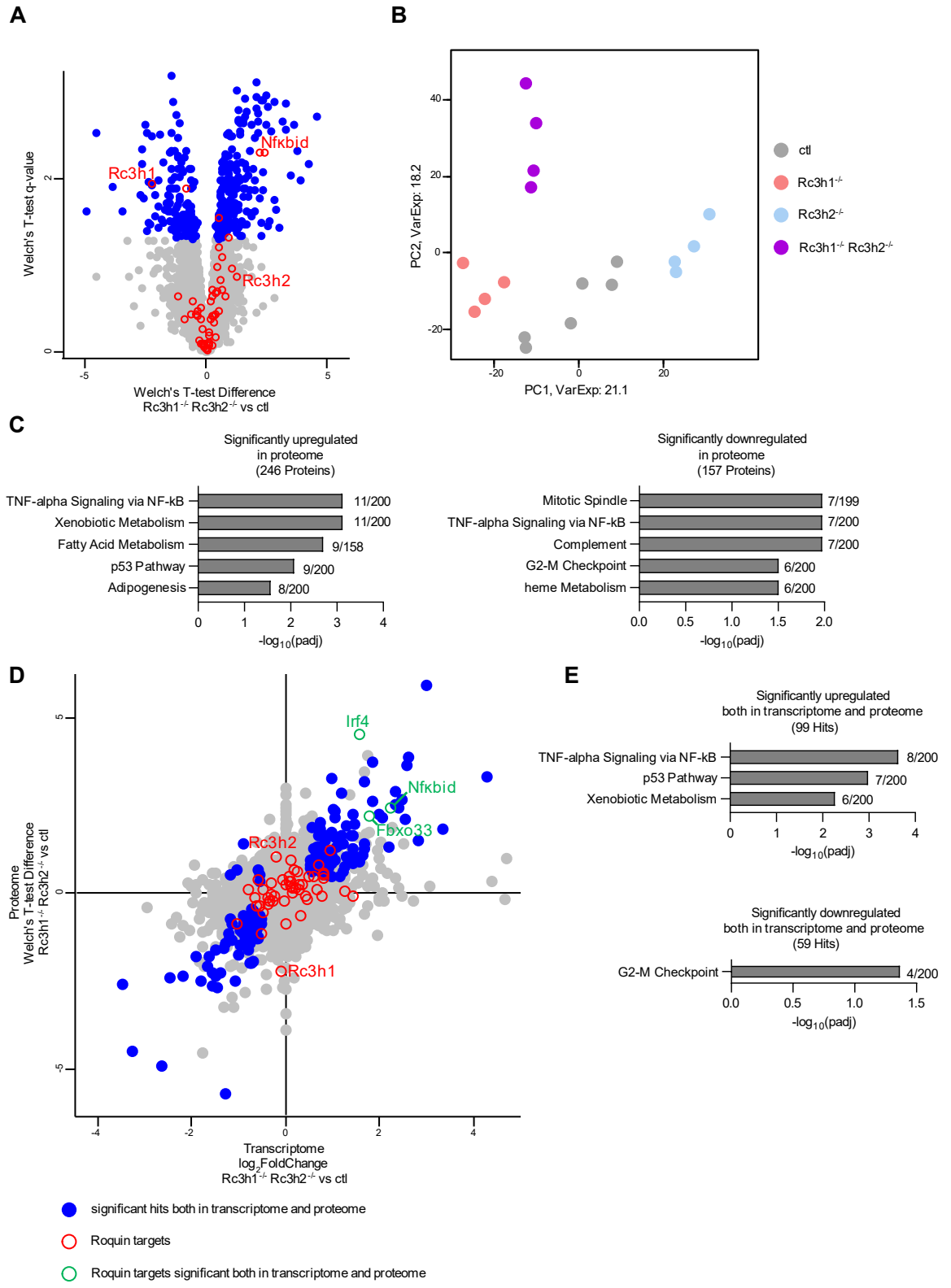

Figure 41: Proteomic analysis of Roquin 1/2 double knockout SSCs at steady state.
(A) Proteomic analysis of Roquin 1/2 double knockout SSCs compared to ctls. Significant hits are shown in blue, Roquin targets are highlighted in red. (B) PCA analysis of SSCs at steady state measured by mass-spectrometry. (C) MSigDB Hallmark pathway enrichment of significant genes highlighted blue in (A) filtered for padj < 0.05. Numbers indicate the overlap of identified genes as proportion to the total gene number of the respective pathway. (D) Scatter plot visualizing combined hits of transcriptome and proteome analysis. Significance of transcriptomic samples was determined by padj < 0.05 and $|\log_2\text{FoldChange}| > 0.5$. Significance of proteomic samples was determined by a both-sided Welch's T-test using FDR = 0.05 and S0 = 0.1. Hits significant in both transcriptomic and proteomic analyses are highlighted in blue or green color. Hits significant in only one of the two analyses are not highlighted. (E) MSigDB Hallmark pathway enrichment of significant genes highlighted blue in (D) filtered for padj < 0.05.

Vast transcriptomic changes in Roquin 1/2 double knockout SSCs mask more subtle differences between Roquin 1 and Roquin 2 single knockout SSCs when included in the analysis. However, 92 genes are significantly upregulated and 52 genes are downregulated upon Roquin 1 single knockout compared to controls (Fig. 42A). ~70 % of the upregulated genes, but only ~21 % of the downregulated genes overlap with previous transcriptome analysis including Roquin 1/2 double knockout SSCs (Fig. 40A). As expected, and in accordance with *in vivo* data, the transcriptomic profile of Roquin 2 knockout SSCs is highly similar to controls. Genes found in differentially regulated pathways overlap almost 100 % (only one gene difference) with the ones found in Roquin 1/2 double knockout SSCs compared to controls (Fig. 42B). Only one Roquin target, namely Nfκbid, was upregulated in transcriptomes of all biological replicates of $Rc3h1^{-/-}$ compared to $Rc3h2^{-/-}$ or controls (data not shown). Comparison of Roquin 1 knockout proteomes to controls showed a significant regulation of 6 proteins whose function is given in Suppl. Table 3. Thereof, only Smox is an overlapping hit between transcriptome and proteome analysis. This suggests that loss of Roquin 1 already drives the upregulation of, among others, pro-apoptotic genes albeit to much lesser extent as seen in Roquin 1/2 double knockout SSCs.

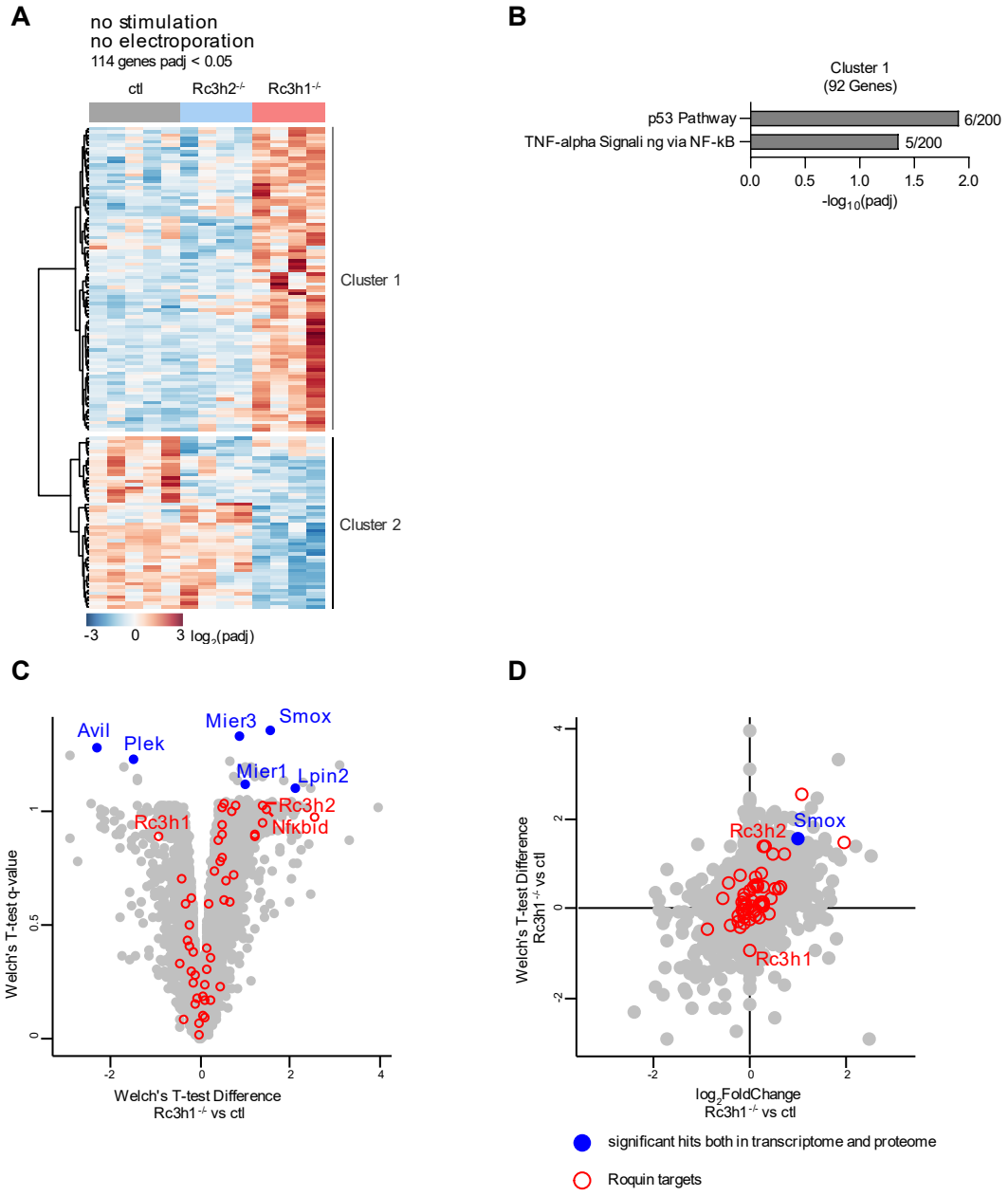

Figure 42: Transcriptomic and proteomic analysis of unstimulated Roquin 1 knockout SSCs. (A) Heatmap of significantly regulated genes using a GeneCutoff > 50 and padj < 0.05 in unstimulated Roquin knockout SSCs transcriptomes. (B) MSigDB Hallmark pathway enrichment of significant genes as plotted in (A) filtered for padj < 0.05. Cluster 2 contained only 52 genes. Pathway analysis using cluster 2 therefore could not retrieve a significantly regulated pathway with more than 5 genes involved. Numbers indicate the overlap of identified genes as proportion to the total gene number of the respective pathway. (C) Proteomic analysis of Roquin 1 knockout SSCs compared to ctl. Significant hits are shown in blue, Roquin targets are highlighted in red. (D) Scatter plot visualizing combined hits of transcriptome and proteome analysis. Significance of transcriptomic samples was determined by padj < 0.05 and $|\log_2\text{FoldChange}| > 0.5$. Significance of proteomic samples was determined by a both-sided Welch's T-test using FDR = 0.05 and S0 = 0.1. The hit significant in both transcriptomic and proteomic analyses is highlighted in blue. Hits significant in only one of the two analyses are not highlighted.

(II) Comparison of Roquin 2 and induced Roquin 1/2 double knockout clones at steady state

Roquin 1/2 double knockout induction via electroporation was performed to assess an immediate response of A20 cells to the complete loss of Roquin proteins which could resemble an acute loss of Roquin, similar to a Cγ1Cre-mediated ablation *in vivo*. As expected, early transcriptomic changes upon induction are not as pronounced as permanent Roquin 1/2 double knockout adaptation and only 18 or 40 genes were differentially regulated, respectively (Fig. 43).

Significantly downregulated transcripts upon acute induction of the Roquin 1/2 double knockout could almost all be detected in steady state Roquin 1/2 double knockout SSCs, too (Fig. 43D). Their function is given in Suppl. Table 4. Among them, OBF-1 is a highly interesting candidate for future validation.

OBF-1 (OCT-Binding Factor 1)

OBF-1 is a B cell specific transcriptional coactivator encoded by *Pou2af1*. OBF-1 interacts with the transcription factors OCT-1 and OCT-2 on octamer motif containing promotors such as immunoglobulin promoters in B lymphocytes[183]. OBF-1$^{-/-}$ mice completely lack GCs in response to NIP-OVA immunizations and are impaired in their ability to produce NIP-specific IgG1[103]. OBF-1 was shown to positively regulate GC hallmark gene expression levels (e.g., *Bcl6*, *Aicda*, *Foxo1, Cxcr4*) while it negatively modulates PC differentiation related genes such as *Irf4*[184,185]. Downregulation of OBF-1 due to the loss of Roquin proteins might initiate a PC cell fate while prohibiting GC entry or survival and could correlate with the upregulation of IRF4 transcripts and proteins in Roquin 1/2 double knockout SSCs and the downregulation of BCL6 proteins in Roquin 1 deficient SSCs after 24 h of stimulation compared to controls as shown later in Fig. 46.

32 transcripts were found to be significantly upregulated upon induced Roquin 1/2 double knockout with 19 of them already found in Roquin 1/2 double knockout steady state clones and 13 genes being unique to this dataset (Fig. 43E). Their function is listed in Suppl. Table 5. Most strikingly, they included the surface molecules CD9 and CD137L and the cytokine IL10.

CD9

CD9 is a glycoprotein and was proposed as a marker to distinguish $CD9^{hi}$ MZB from $CD9^{lo}$ FOB. Furthermore, CD9 expression is absent in GCBs, but is upregulated again in GC-derived isotype switched plasma cells as well as MZ-derived IgM^+ plasma cells[186]. Monitoring of CD9 expression levels of B lymphocyte populations *in vivo* should be conducted to validate the upregulation seen *in vitro* in Roquin deficient A20 cells.

TNFSF9 (Tumor necrosis factor ligand superfamily member 9)

TNFSF9, also called CD137L or 4-1BBL, is preferentially expressed in GCBs and plays a role in preventing GC B cell lymphomagenesis. RNA sequencing of *ex vivo* GCBs of NP-CGG in alum immunized $CD137L^{-/-}$ mice revealed a significant upregulation of transcription factors essential for GC reactions such as *Ciita*, *Bcl6*, *Bach2* and *SpiB* as well as *Aicda* compared to WT controls suggesting that CD137L acts as a suppressor of GCB survival and SHM[187]. Hence, CRISPR/Cas9 targeting of TNFSF9 should be performed in the future to study the effect of TNFSF9 ablation on BCL6 and AID expression levels in Roquin depleted A20 cells.

IL10

IL10, together with IL21 is a cytokine triggering plasma cell development by repressing PAX5 and BCL6. Thereby, IL10 is particularly required for late APC maturation while IL21 favors early APC differentiation processes from centroblasts[188]. During this PhD project, splenic FOB from CD19Cre Roquin 1/2 double KO mice and respective control mice were isolated and cultured for 18 h. Culture supernatants were harvested and measured for their cytokine content via LEGENDplex. Among 13 cytokines analyzed, IL10 concentrations differed most between the genotypes. CD19Cre Roquin 1/2 double KO FOBs produced ~18-fold more IL10 in the absence of additional stimuli and ~150-fold more IL10 upon addition of 10 µg / mL LPS in comparison to controls. Roquin 1 homo Roquin 2 het KO FOBs still secreted ~7-fold more IL10 in untreated and ~13-fold more IL10 in LPS treated samples compared to controls (data not shown). Thus, both Roquin proteins are potent regulators of IL10 transcript levels *in vitro* and in addition modulate IL10 secretion *ex vivo*.

In summary, sequencing of electroporated Roquin 2 SSCs allowed the assessment of transcriptomic changes upon acute ablation of Roquin 1 in A20 cells in a time-dependent manner. The analysis revealed that IL10 cytokine expression levels are modified early-on upon loss of Roquin 1. In addition, CD9 and CD137L were detected as new candidate target genes to be included in future *in vivo* validation experiments.

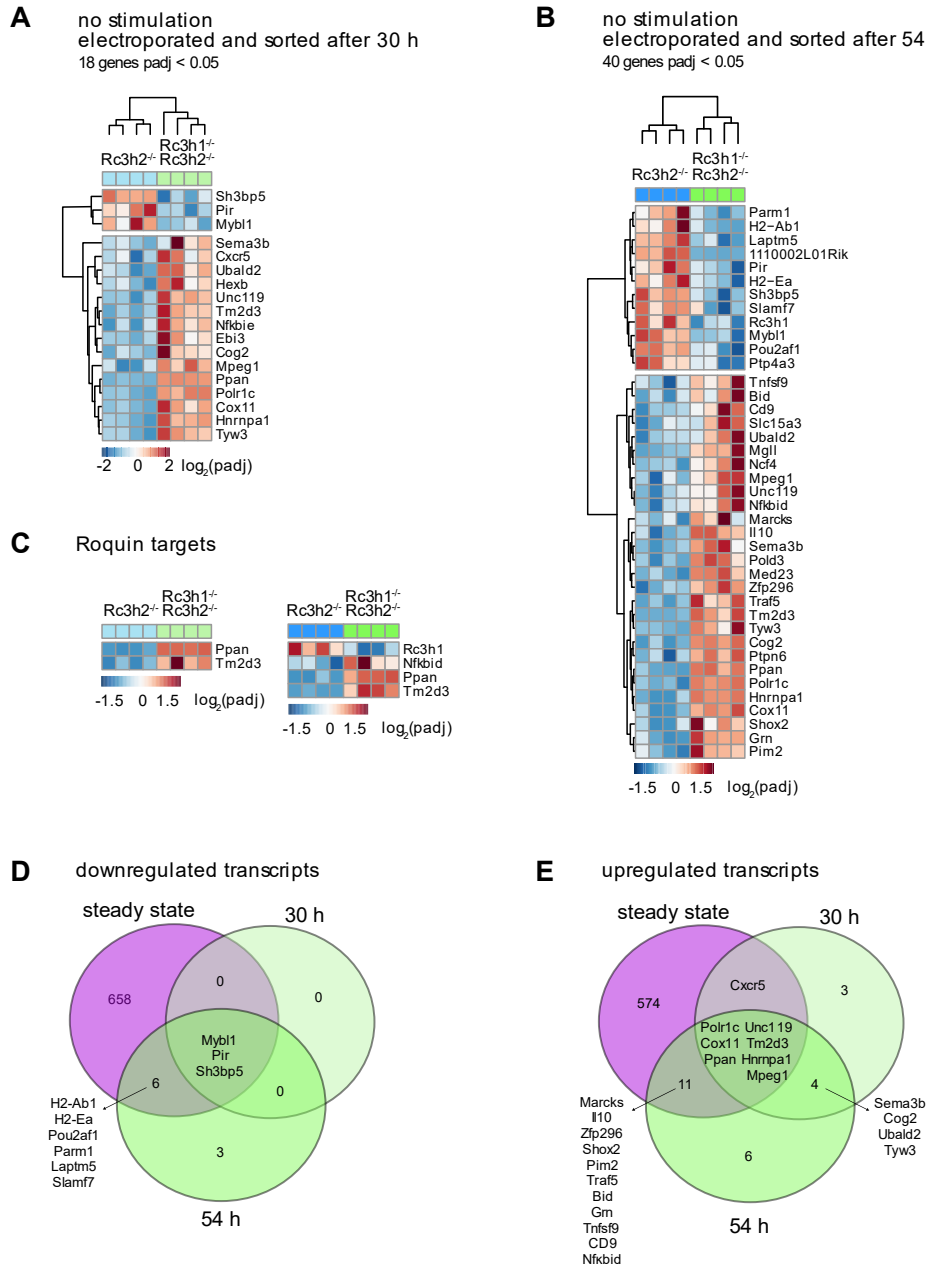

Figure 43: Transcriptomic analysis of unstimulated, sorted Roquin knockout SSCs.
(A) Heatmap of significantly regulated genes using a GeneCutoff > 50 and padj < 0.05 in unstimulated Roquin knockout SSCs sorted for GFP^{lo} (Rc3h2$^{-/-}$) and GFP^{hi} (Rc3h1$^{-/-}$ Rc3h2$^{-/-}$) 30 h after electroporation. (B) Heatmap of significantly regulated genes using a GeneCutoff > 50 and padj < 0.05 in unstimulated Roquin knockout SSCs sorted for GFP^{lo} (Rc3h2$^{-/-}$) and GFP^{hi} (Rc3h1$^{-/-}$ Rc3h2$^{-/-}$) 54 h after electroporation. (C) Heatmap of significantly regulated Roquin targets included in (A) and (B). (D) Venn diagram visualizing the overlap of significantly downregulated genes as shown in Fig. 40A, Fig. 43A and Fig. 43B. (E) Same as in (D) but shown for significantly upregulated genes.

(III) Comparison of Roquin 1 and Roquin 1/2 double knockouts upon stimulation

A20 SSCs were stimulated using αIgG + αCD40 to mimic *in vivo* activation cues such as BCR signaling and T cell help and thereby evaluate the impact of loss of Roquin proteins to the response of activated A20 cells. After 6 h of stimulation, 68 transcripts and 78 proteins were found to be significantly upregulated in Roquin 1 knockout SSCs compared to controls with 4 of them being detected in both analyses. Their function is given in Suppl. Table 6. Among them, CD70 was detected to be highly enriched at the protein level (~23-fold) (Fig. 44F).

CD70

CD70 is the ligand of the TNFR family member CD27 and is transiently expressed on activated immune cells including T and B cells. Studies by Arens et al. demonstrated that transgenic expression of CD70 (CD70-tg) in *ex vivo* $CD27^{-/-}$ B cells promoted their cell cycle measured by CFSE upon anti-CD70 mAb treatment[189]. This might correlate with the enhanced cell cycle progression seen in *ex vivo* CD19Cre Roquin 1 KO FOBs upon stimulation with αCD40 ± αIgM (Fig. 18). Changes in CD70 expression levels of Roquin deficient GCBs could impact the CD70-CD27 signaling axis between B and T cells *in vivo*. T cell specific CD70-tg mice are impaired in their capability to produce GCBs during an immune response and CD70-tg T cells trigger GCB apoptosis through a FAS-dependent mechanism[190]. B cell specific CD70-tg expression is known to negatively influence plasma cell differentiation and favors IgM over IgG1 immunoglobulin secretion[189]. Considering the pronounced upregulation of CD70 protein detected in A20 Roquin 1 knockout SSCs compared to controls and the vast implications this might have on B-T cell interactions *in vivo*, I suggest to assess CD70-dependent signaling effects by flow-cytometry in the future.

124 transcripts and 35 proteins were significantly downregulated in Roquin 1 knockout SSCs compared to controls with 8 of them being detected in both analyses. Among those 8 proteins, IL4I1 and CIITA protein expression levels differed the most from controls (~6-fold IL4I1 and ~4-fold CIITA) (Fig. 44F).

IL4I1 (IL-4 induced gene-1)

IL4I1 proteins were detected with a mean protein intensity of 19.3 in Roquin 1 knockout SSCs and 21.8 in controls, resulting in a ~6-fold decrease of protein expression upon loss of Roquin 1. Thereby, 8 – 25 IL4I1 peptides were used for protein identification and

quantification. IL4I1 is a L-phenylalanine oxidase which converts amino acids and in addition dampens BCR-induced proliferation signaling through the mTOR signaling pathway. IL4I1$^{-/-}$ mice present with higher proportions of plasma cells during a primary immune response and increased antigen-specific IgM serum titers[191]. Thus, the role of IL4I1 on plasma cell formation in Roquin deficient mice should be evaluated more closely in the future.

CIITA (Class-II transactivator)

CIITA is a transcriptional coactivator of MHCII expression including expression of H2-Aa, H2-Ab and H2-DM. Dynamic regulation of MHCII surface expression is essential to enable selection and affinity maturation of GCBs while they cycle between dark and light zone of the GC reaction[192]. CIITA gets repressed via BLIMP-1 during the transition into plasma cells leading concomitantly to MHCII downregulation[193,194]. CIITA proteins were detected with a mean protein intensity of 16.3 in Roquin 1 knockout SSCs and 18.4 in controls, resulting in a ~4-fold decrease of protein expression upon loss of Roquin 1. 2 – 8 CIITA peptides were recorded in stimulated samples. In consent with the role of CIITA being a major regulator of MHCII, also H2-Aa and H2-Ab1 transcripts and proteins were significantly downregulated in Roquin 1 knockout SSCs. Roquin dependent repression of CIITA and thereby influences on MHCII antigen presentation might modify the ability to receive T cell help and therefore enter the GC reaction or might diminish the capability of affinity maturation within the GC *in vivo*. H2-Aa or H2-Ab1 specific staining could confirm these results by flow-cytometry.

Pathway enrichment analysis of 6 h stimulated samples revealed an upregulation of cell cycle related genes ("G2-checkpoint" and members of the "p53 pathway") suggesting a hyperactivation of Roquin 1 knockout SSCs driving an excessive cell cycle progression program upon stimulation (Fig. 44B). Again, this could be linked to the pronounced proliferation of Roquin 1 deficient FOBs stimulated *ex vivo* (Fig. 18). Transcripts of the "p53 pathway" gene signature included TNFSF9, which was also found as top 5 hit to be upregulated ~4-fold in proteomes of Roquin 1 knockout A20 SSCs compared to controls. Thus, TNFSF9 is significantly regulated at the transcript and proteome level upon loss of Roquin 1 alone or both Roquin 1 and Roquin 2 independent of the activation status of the cell (Fig. 43E and 44E).

Genes involved in the "mTORC1 signaling" pathway were downregulated upon loss of Roquin 1 in 6 h stimulated samples (Fig. 44B). 4 out of 9 pathway members relate to

transport (STARD4), negative regulation (INSIG1) or biosynthesis (SC5D, HMGCR) of cholesterol. They partially overlap with genes of the "cholesterol homeostasis" pathway which additionally includes FDPS necessary for lipid metabolism. Considered together with the perturbance of metabolism related pathways seen in unstimulated Roquin 1/2 double KO SSCs, this might hint towards a role of Roquin proteins in the metabolism of GCBs. Behrens et al. provided already evidence for a participation of Roquin proteins in cellular metabolism in $CD4^+$ T cells showing that mitochondrial respiration and glycolytic capacities are enhanced upon simultaneous loss of both Roquin 1 and Roquin 2 compared to controls[112]. Furthermore, Weisel et al. observed that the metabolism of GCBs varies significantly from naïve or activated B cells. While GCBs were shown to rely only minimally on glycolysis and significantly performed less OXPHOS compared to activated B cells, they instead actively metabolized endogenous and exogenous fatty acids to meet their energy demands[195]. Disturbances of fatty acid metabolism related genes by the ablation of Roquin proteins could therefore be one explanation for the observed loss of GCBs in Roquin 1/2 double KO mice. Seahorse assays evaluating fatty acid oxidation in Roquin depleted A20 SSCs will be useful experiments to dissect this in more detail. Seahorse analysis of OXPHOS in A20 SSCs already verified the downregulation of OXPHOS related genes in unstimulated Roquin 1/2 double knockout SSCs and revealed a reduction in basal respiration, maximal respiration and spare respiratory capacity in those cells compared to controls or single knockout clones although changes did not reach statistical significance (Suppl Fig. 21).

Upon 24 h of stimulation, 221 proteins were significantly upregulated with 32 of them overlapping with the ones found in 6 h treated samples (Fig. 45). Additionally, 159 proteins were found to be downregulated with 24 of them overlapping with the 6 h stimulation dataset. CD70 was detected again as the most differentially regulated gene upon loss of Roquin 1 and pathway analysis verified the results already described for 6 h activated A20 SSCs.

In summary, stimulation of A20 SSCs and analyses of subsequent transcriptomic and proteomic changes revealed a deregulated response of Roquin 1 depleted cells to αIgG + αCD40 induced activation compared to controls. CD70, IL4I1 and CIITA were identified as interesting candidates for future validation experiments modifying GCB proliferation, GCB selection and plasma cell differentiation according to literature. Furthermore, Roquin proteins were shown to play a role in A20 metabolism.

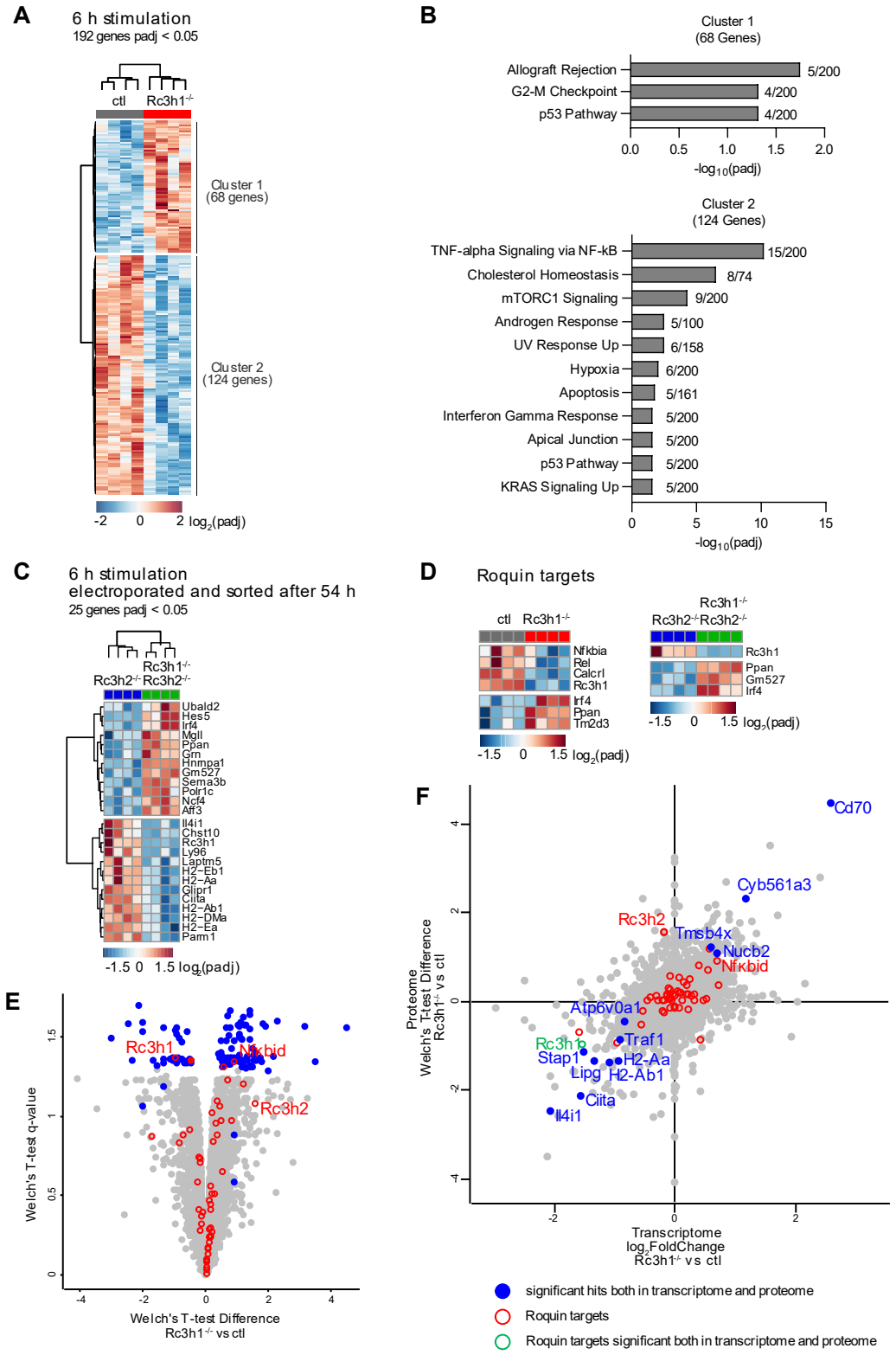

Figure 44: Transcriptomic analysis of 6 h stimulated Roquin knockout SSCs.
(A) Heatmap of significantly regulated genes of stable cell line SSCs after 6 h of stimulation using a GeneCutoff > 50 and padj < 0.05. (B) MSigDB Hallmark pathway enrichment of significant genes as plotted in (A) filtered for padj < 0.05. Numbers indicate the overlap of identified genes as proportion to the total gene number of the respective pathway. (C) Heatmap of significantly regulated genes of GFP^{lo} (Rc3h2$^{-/-}$) and GFP^{hi} (Rc3h1$^{-/-}$ Rc3h2$^{-/-}$) SSCs sorted 54 h after electroporation and stimulated for 6 h using a GeneCutoff > 50 and padj < 0.05. (D) Heatmap of significantly regulated Roquin targets included in (A) and (C). (E) Proteomic analysis of samples shown in (A). Significant hits are shown in blue, Roquin targets are highlighted in red. (D) Scatter plot visualizing combined hits of transcriptome and proteome analysis. Significance of transcriptomic samples was determined by padj < 0.05 and $|\log_2\text{FoldChange}| > 0.5$. Significance of proteomic samples was determined by a both-sided Welch's T-test using FDR = 0.05 and S0 = 0.1.

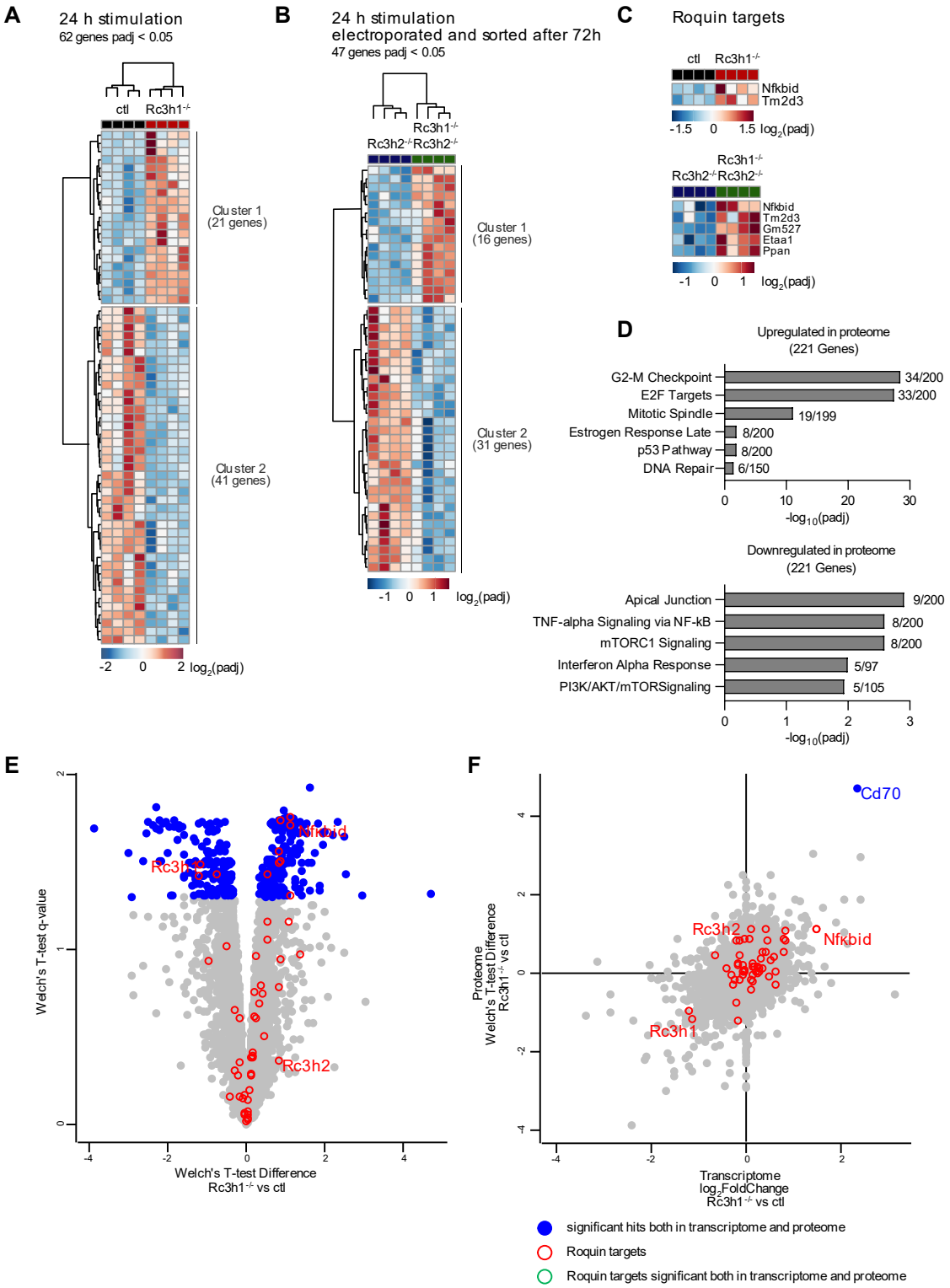

Figure 45: Transcriptomic analysis of 24 h stimulated Roquin knockout SSCs.
(A) Heatmap of significantly regulated genes of stable cell line SSCs after 24h of stimulation using a GeneCutoff > 50 and padj < 0.05. (B) Heatmap of significantly regulated genes of GFP^{lo} (Rc3h2$^{-/-}$) and GFP^{hi} (Rc3h1$^{-/-}$ Rc3h2$^{-/-}$) SSCs sorted 54h after electroporation and stimulated for 24h using a GeneCutoff > 50 and padj < 0.05. (C) Heatmap of significantly regulated Roquin targets included in (A) and (B). (D) MSigDB Hallmark pathway enrichment of significant genes as plotted in (E) filtered for padj < 0.05. Numbers indicate the overlap of identified genes as proportion to the total gene number of the respective pathway. (E) Proteomic analysis of Roquin 1 knockout SSCs compared to ctl. Significant hits are shown in blue, Roquin targets are highlighted in red. (F) Scatter plot visualizing combined hits of transcriptome and proteome analysis. Significance of transcriptomic samples was determined by padj < 0.05 and $|\log_2\text{FoldChange}| > 0.5$. Significance of proteomic samples was determined by a both-sided Welch's T-test using FDR = 0.05 and S0 = 0.1. The hit significant in both transcriptomic and proteomic analyses is highlighted in blue. Hits significant in only one of the two analyses are not highlighted.

4.4.7 Roquin target genes

Monitoring of Roquin target gene expression levels validated the efficiency of Roquin 1 ablation in A20 SSCs and enabled the detection of cellular mechanisms specifically regulated by Roquin in A20 cells. 53 Roquin targets were identified by mass-spectrometry and 28 Roquin targets were significantly regulated either at the transcript or protein level of Roquin 1/2 double knockout or Roquin 1 single knockout A20 cells compared to controls. A summary is given in Table 24. Their functions are described in Suppl. Table 7 with particular focus on B cell biology if not yet mentioned in the previous chapter.

Roquin target	**Steady state**		**Induced knockout**	**6 h stimulation**		**24 h stimulation**	
	Transcript	Protein	Transcript	Transcript	Protein	Transcript	Protein
Aggf1	↑						
Ap1s3							↓
Calcrl				↓			
Cenpf	↓						↑
Clk1	↑						
Etaa1	↑					↑	
Fam160b1		↑					
Fbxo33	↑	↑					
Gm527	↑			↑		↑	
Id2	↑						
Irf4	↑	↑		↑			↑
Kctd6	↑						
Mlec	↓						
Msl2							↑
Nfκbia		↓		↓			↓
Nfκbid	↑	↑	↑		↑	↑	↑
Nfκbiz	↑						
Nuf2							↑
Pole2	↓						
Ppan	↑		↑	↑		↑	
Pptc7		↑			↑		↑
Rel				↓			
Tfap4							↑
Tm2d3	↑		↑	↑		↑	
Ube2q2	↑						
Zbtb43							↑

Table 24: Significantly regulated Roquin target genes in transcriptomes and proteomes of Roquin 1/2 double knockout A20 cells (steady state / induced knockout) or Roquin 1 single knockout A20 cells (6 h / 24 h stimulation) compared to controls as shown in Fig. 40 – 45 and listed in alphabetical order.
Upregulation of Roquin targets in Roquin depleted SSCs compared to controls is indicated with black arrows, downregulation is indicated with blue arrows. Mass-spectrometry measurements were able to quantify proteins written in bold whereas proteins written in italic were not abundant enough to be identified.

ID2 (Inhibitor of differentiation protein 2)

ID2 is a negative regulator of transcription with low expression levels in all B lymphocytes except for plasma blasts. ID2$^{-/-}$ mice obtain a normal B cell development in the bone marrow, although they show reduced MZB levels[196]. Most importantly, ID2 together with ID3 negatively regulates AID by inhibition of PAX5 binding to AID promotor regions in activated B cells and is induced upon BLIMP1 expression meaning the induction of a plasmocytic cell maturation program. Its expression can be induced by TGFß1 leading to enhanced IgE class-switching[42,197]. Thus, regulation of ID2 by Roquin proteins might be relevant for class-switching capacities *in vivo*. However, ID2 proteins could not be identified even in mass-spectrometry measurements using an additional pre-fractionation of protein samples to detect ~1500 proteins more than in the measurements described within this thesis (data not shown). This is probably due to low abundance of the protein in A20 cells. Therefore, I suggest to perform simultaneous flow-cytometry-based detection of ID2 mRNA (PrimeFlow) and proteins to validate the role of ID2 in Roquin deficient GCBs in the future.

In summary, 7 out of 28 identified Roquin target genes act predominantly during cell division (CENPF, CLK1, ETAA1, NUF2, POLE2, PPAN, UBE2Q2) suggesting a crucial role of Roquin for cell cycling. This is in line with pathway analysis showing a deficiency in cell cycle related genes upon ablation of Roquin 1/2 in unstimulated SSCs and a hyperactivation of proliferation related processes upon stimulation in Roquin 1 deficient SSCs compared to controls both seen at the transcript and protein level. This is of particular interest as GC entry after B cell activation and GCB maintenance crucially rely on massive cell proliferation *in vivo*. However, differential regulation of these 7 Roquin target genes could only be detected at the transcript level and was not translated to the proteome suggesting that yet other direct or indirect targets are essential for Roquin dependent cell cycle modification.

4.4.8 Selected target gene expression in Roquin knockout A20 cells

In a subsequent step, the influence of Roquin proteins on a small set of well-known genes involved in GCB formation and APC development as well as CSR or BCR and CD40 signaling was examined. Other than the unsupervised pathway enrichment analysis, this is a biased approach only meant to explore mRNA and protein levels of the 149 genes which were chosen based on my literature search and are listed in Suppl. Table 9[42,44,55,64,174,198]. Significantly regulated transcripts and / or proteins of the distinct sample groups are shown in Fig. 46.

39 selected transcripts were significantly regulated in Roquin 1/2 double knockout SSCs compared to controls and single knockout clones (Fig. 46A). Thereof, H2-EA, H2-EB1, MRE11A, ICOSL, IL6RA, IL6ST, XBP1, IL10 and ID2 could not be detected by mass-spectrometry. Nevertheless, transcriptomic changes in IL6R can be connected to my data on IL6 cytokine secretion of Roquin deficient B cells which will be described in the following and together strongly suggest a major role of Roquin proteins during IL6 signaling.

IL6R

During this PhD project, *ex vivo* splenic FOBs of Roquin 1/2 double KO CD19Cre mice were shown to secrete 8-times more IL6 in the presence of LPS compared to $CD19Cre^{I/+}$ control cells whereas their IL6 secretion was unchanged in unstimulated samples (data not shown). IL6 is a proinflammatory cytokine and excessive IL6 production is linked to the development of inflammatory diseases[199]. IL6 expression is positively regulated by OCT2 and OBF-1 and is induced upon early B cell activation[200]. Hence, future experiments could aim to correlate OBF-1 expression with IL6R expression and IL6 secretion in naïve B cells, activated B cells and GCBs upon loss of Roquin proteins. B cell derived IL6 is capable to induce IL21 expression from $CD4^+$ T cells, drives T_{FH} formation which altogether enables GCB formation. IL6 also induces APC generation and IL6 transgenic mice suffer from splenomegaly, plasmacytosis and IgG1 hypergammaglobulinemia[199,201,202]. In addition, IL6 has been proposed to be involved in lipid metabolism[199]. In A20 cells IL6R mRNA is differentially expressed suggesting a change in IL6 sensing. Overall, Roquin proteins were shown to regulate IL6 signaling of A20 cells *in vitro* as well as in *ex vivo* naïve B cells.

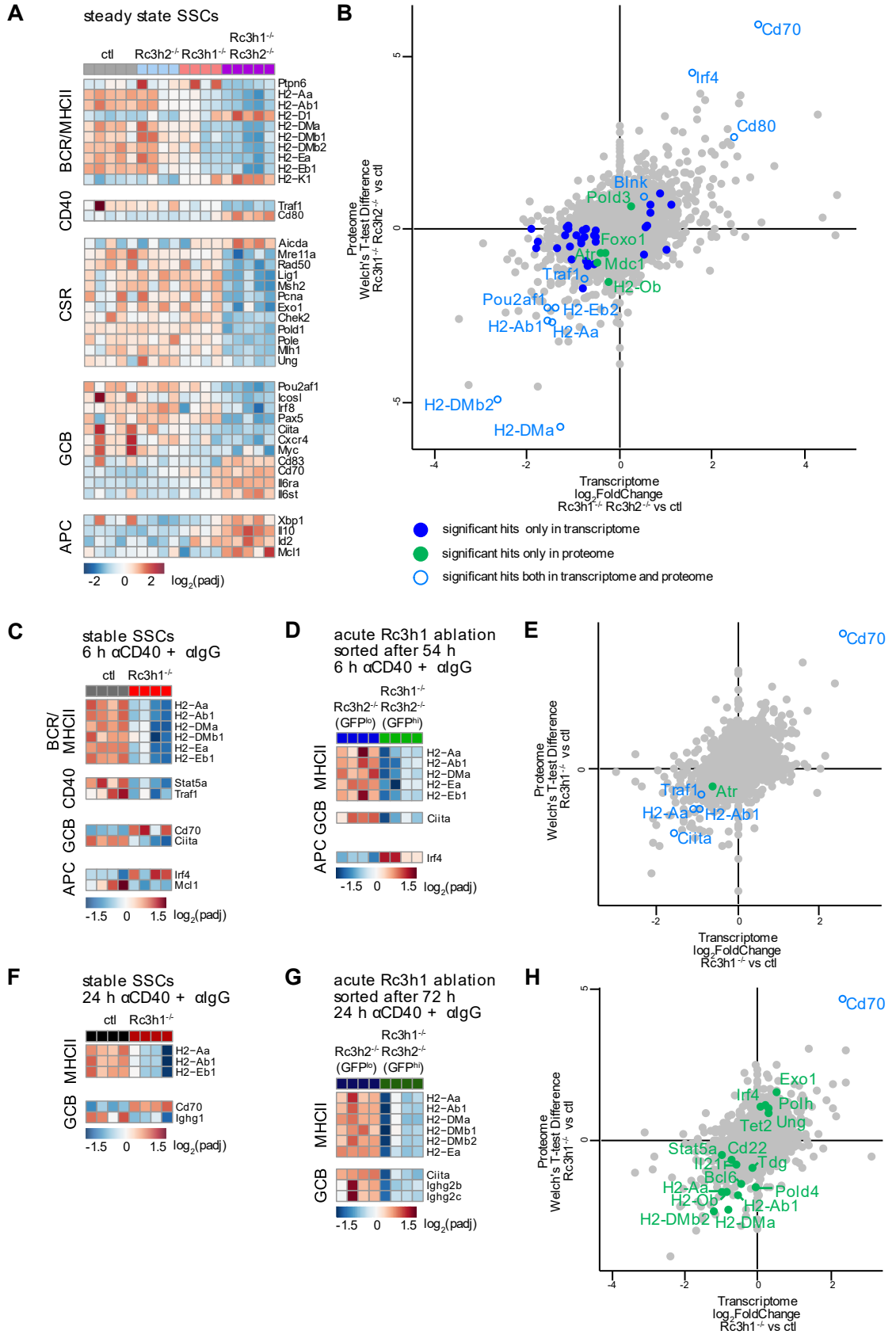

Figure 46: Selected target gene expression in Roquin knockout SSCs.
(A, C, D, F, G) Heatmap of significantly regulated genes of Roquin deficient SSCs compared to controls using a GeneCutoff > 50 and padj < 0.05. (B, E, H) Scatter plot visualizing combined hits of transcriptome and proteome analysis of stable SSCs with or without stimulation as shown in A, C and F. Significance of transcriptomic samples was determined by padj < 0.05 and | log2FoldChange | > 0.5. Significance of proteomic samples was determined by a both-sided Welch's T-test using FDR = 0.05 and S0 = 0.1.

Next, loss of both Roquin proteins in unstimulated A20 cells resulted in the downregulation of several transcripts involved in DNA damage repair mechanisms such as the ligase *Lig1*, the DNA polymerase delta auxiliary gene *Pcna* and components of the MRN complex involved in dsDNA break repair (double-strand break repair gene *Mre11*, DNA repair gene *Rad50*) and the DNA mismatch repair system (DNA mismatch repair gene *Msh2* and exonuclease *Exo1*) as well as upregulation of the activation-induced cytidine deaminase AID (encoded by *Aicda*). Protein expression was well detectable by mass-spectrometry for DNA repair proteins (mean protein intensities: LIG1 23.4, PCNA 26.1, RAD50 21.7, EXO1 16.8), however their transcriptomic changes did not translate into significant differences at the protein level.

AID

AID is essential for immunoglobulin class-switching and SHM and overexpression of AID was connected to pathologies such as lymphomagenesis resulting from AID off targeting or autoimmunity due to AID-induced mutations of immunoglobulins[203–205]. By contrast, deletion of AID in $AID^{-/-}$ mice or $AID^{-/-}$ B cells used in mixed bone marrow chimeric mice was shown to induce increased numbers and sizes of GC reactions after immunization due to diminished apoptosis[206]. Thereby, $AID^{-/-}$ B cells accumulate in the LZ of the GC and are impaired in their cell differentiation into plasma cells[207]. Transcriptomes of Roquin 1/2 double knockout A20 cells revealed a significant upregulation of *Aicda* compared to WT controls and a modest upregulation upon deletion of Roquin 1 only. However, AID could not be quantified well by mass-spectrometry (mean protein intensity = 16.6, 10 out of 38 samples without any detection of AID and 13 samples with an identification of AID based on only 1 peptide). Hence, AID protein levels should be evaluated via western blots to better understand the effect of Roquin ablation on AID expression in GCBs or GCB-like A20 cells in the future which might be crucial during SHM and regulation of GCB cell viability *in vivo*.

4 candidate genes were significantly upregulated (CD70, IRF4, CD80 and BLNK) and 7 candidate genes were significantly downregulated (TRAF1, OBF-1, H2-Aa, H2-Ab1, H2-DMa, H2-DMb2) both at the transcript and protein level in Roquin 1/2 double knockout clones compared to controls (Fig. 46B). Differential gene expression of CD70, IRF4, MHCII components and OBF-1 was described before and is independent of the stimulation status of Roquin deficient A20 cells (Fig. 46 C-H). In addition, the costimulatory molecule CD80 was found to be upregulated upon ablation of both Roquin 1 and Roquin 2 without stimulation compared to controls. Increased CD80 protein levels in Roquin 1/2 knockout

A20 cells compared to Roquin 2 deficient controls was also confirmed via flow-cytometry (Suppl. Fig. 18). De-regulated expression of CD80 could lead to perturbances to receive T cell help and thereby could diminish successful GCB entry *in vivo*[208]. Similarly, defects in antigen presentation due to downregulation of MHCII components H2-DMb1, H2-DMa and H2-Eb2 upon loss of Roquin proteins could also impair T cell help and GC initiation. Hence, their cellular protein expression should be verified by flow-cytometry using component specific antibodies for detection.

H2-DM

The nonclassical MHCII molecule H2-DM is required for stabilization of empty MHCII in the endosomes of B cells and exchange of the class II associated invariant chain-derived peptide (CLIP) with internalized, more stable binding antigen peptides. H2-DM$^{-/-}$ mice do not form GCB cells and respond delayed and less efficient to immunization with NP-OVA or NP-HEL in terms of NP_{23}-binding IgG1 production and are incapable to form high-affinity NP_2 IgG1$^+$ antibodies. In those mice also the CD4$^+$ T cell compartment is less pronounced. Thus, their T-B cell interaction is severely impaired which negatively influences the GC reaction. Nevertheless, class-switching can occur and DM-deficient APCs are capable to present antigen to a certain extent. Antigen presentation by the classical MHCII protein H2-A is reported to be H2-DM dependent whereas H2-E is less dependent on H2-DM[209,210].

In summary, A20 cells are a GC-like lymphoma cell line with limited capacity to mimic the complex differentiation program from non-activated naïve B cells into GCBs or APCs occurring *in vivo*. Nevertheless, A20 cell lines are a suitable *in vitro* model system to capture intrinsic transcriptomic and proteomic regulation upon loss of Roquin proteins.

Analysis results from A20 cell lines were in line with other experimental approaches as well as already published studies showing a significant influence of Roquin proteins on IL10, IL6 and NFκB signaling. Roquin-mediated modifications of these signaling pathways are highly likely to induce major changes in cellular interactions e.g., with T cells and thus will have a great impact on GCB development and differentiation *in vivo*. However, due to the complexity of cytokine-dependent effects on the cellular interplay and context dependent effects of NFκB signaling, it will be difficult to dissect their precise molecular mechanisms in the future.

Roquin proteins were shown to be essential for proliferation, apoptosis and metabolism of A20 cells. Loss of both Roquin proteins in the absence of activating stimuli led to the upregulation of apoptosis, stress- and anti-proliferative gene signatures causing their counterselection in a competitive environment with Roquin 1 expressing cells. Furthermore, ablation of Roquin proteins impaired the capability to perform OXPHOS and fatty acid oxidation. Roquin-deficient cells reacted hyperactivated upon treatment with growth-enhancing stimuli suggesting that Roquin proteins are necessary to suppress cellular activation responses.

With the aim to better understand the molecular mechanism of the phenotypes observed in Roquin-ablated mice, I identified 10 candidate genes in A20 cell lines, namely IRF4, FBXO33, OBF-1, CD9, TNFSF9, CD70, IL4I1, CIITA, ID2, AID and the MHC components H2-Aa, H2-Ab1, H2-DMa, H2-DMb1. They were published to play crucial roles during GC entry, plasmacytic differentiation and CSR and thus will be highly promising targets to study in the future. In our laboratory, Seren Bayguen established comprehensive protocols to genetically alter HoxB8 hematopoietic progenitor cells *in vitro* followed by adoptive transfer into irradiated mice and monitoring of B lymphocyte development. Therefore, I suggest to perform a targeted CRISPR / Cas9 screen in HoxB8 cells derived from Cγ1Cre Roquin deficient mice and monitoring of their B lymphocyte development upon transfer with and without additional immunization[171,211].

5 Discussion

Manifold studies mainly undertaken in mouse models have noticeably increased our current understanding of the cascade from B cell antigen encounter to antibody production since the discovery of GC structures and blood serum antibodies more than 100 years ago. However, GC biology is multifaceted and still many questions regarding B cell responses are unresolved. Filling those gaps in knowledge in the future is indispensable to efficiently diagnose and treat B cell derived malignancies as well as design efficient vaccination strategies[212]. PTGR facilitated by RBPs is more and more acknowledged to play an important role for immune regulatory processes. However, only a minor fraction of RBPs is already studied in the context of immune modulation[69]. Roquin 1 and Roquin 2 are two RNA-binding paralogues recognized for their essential function in T cell differentiation and their implications in the autoimmune disorder systemic lupus erythematosus[3]. Studies in our laboratory have addressed first the relevance of Roquin proteins during B cell maturation and have hinted towards a potential role also during late B cell development[82]. These preliminary data gave rise to my PhD project aiming to decipher the role of Roquin proteins in the GC reaction and APC differentiation.

5.1 Loss of Roquin destabilizes GC reactions

Research on Roquin in T cells showed a remarkable influence of Roquin proteins on T cell mediated immune homeostasis which B cell extrinsically also impacts GC biology. However, little is known about B cell intrinsic functions of Roquin proteins[82,213]. During my project, I thus performed a comprehensive characterization of pre-GC and GC B cells in conditional Roquin 1 and Roquin 2 depleted animals.

Roquin proteins are required for GC formation

By using mice with a GC-specific deletion of Roquin 1 and Roquin 2, I was able to verify that both Roquin proteins are absolutely required for GC formation *in vivo*. Loss of all Roquin alleles in Roquin 1/2 double KO Cγ1Cre animals completely inhibits the formation of a GC compartment especially in spleen and lymph nodes in response to immunizing agents such as SRBC or NP-CGG by day 10 or day 14, respectively. Loss of GCBs could be

related to an impairment of GC entry or GC maintenance. Studies by Heise et al. dissected the role of c-Rel on GC entry versus GC maintenance in $Rel^{F/F}$ Cγ1Cre mice by flow cytometry and histology analysis monitoring multiple time-points after SRBC immunization (day 4 to day 10)[214]. Mimicking their approach, I examined GCB formation capacities at day 4 and day 7 after SRBC injection by flow-cytometry. My preliminary data suggests that GCB development is already perturbed at early timepoints after immunization in Roquin 1/2 double KO mice indicating an impairment of GC entry upon Roquin protein ablation.

Roquin proteins are crucial regulators of B cell proliferation and metabolism

GCB formation is regulated by a complex network of cellular and soluble factors[215]. This includes cellular activation of naïve B cells by soluble antigen, antigen-presenting cells as well as T-B cell interactions. Antigen-stimulated B cells migrate into the follicle facilitated by a transcriptional program including upregulation of BCL6, the master transcription factor of GC development. GC formation is further driven by rapid cell cycling of B cells and their differentiation into centroblasts and centrocytes[30,216]. In order to investigate if these processes are compromised upon loss of Roquin proteins leading to the absence of GCBs, I assessed surface activation markers, expression levels of BCL6, proliferation capabilities and DZ/LZ polarization by flow-cytometry *ex vivo*. Furthermore, I studied the effect of Roquin protein ablation in A20 cell lines, a model *in vitro* system for GCBs.

These analyses did not reveal significant differences in the activation signature between Roquin-deficient and WT B cells *in vivo*. Instead, Roquin 1/2 double knockout B and GCB cells presented with a modest increase in CD86 expression levels compared to controls which could be confirmed in Roquin 1/2-ablated GC-like A20 cell lines and is in line with previous findings of Dr. David Riess in unimmunized Roquin 1/2 double knockout CD19Cre mice[82]. Hence, although Roquin protein ablation causes modest modifications of B cell activation, they do not seem to be strong enough to be causal for the drastic phenotype seen in Roquin 1/2 double KO animals. Furthermore, upregulation of BCL6 in GCBs was not negatively impacted upon loss of Roquin proteins and Roquin-deficient GCBs presented with an unbiased DZ/LZ polarization.

Assessment of proliferation capacities of isolated Roquin-deficient FOB cells as well as transcriptomic and proteomic analysis of Roquin knockout A20 SSCs revealed that Roquin proteins are essential regulators of B cell cycling. FOBs isolated of Roquin-ablated

CD19Cre mice proliferated drastically more than control FOBs with a particular bias upon αCD40 treatment. This effect was gene-dosage dependent with FOBs proliferating to a higher extent the more Roquin alleles were ablated. Concomitantly, Roquin 1/2 double knockout A20 SSCs presented with an upregulation of cell cycle regulated gene signatures upon αIgG + αCD40 stimulation compared to controls. Modification of cellular proliferation by Roquin proteins has been shown before by Zhao et al. and Lu et al. in T cells[117,118]. However, to my knowledge this is up to date the first study showing that Roquin proteins are essential to suppress proliferation upon cellular activation in B cells.

B cell proliferation requires the adjustment of cellular metabolism beforehand to meet the increased energetic needs of biomass synthesis. B cell metabolism is highly context-dependent and a rather new field of investigation. However, initial studies showed that GCB follicles are a hypoxic environment with limited availability of nutrients causing energetic stress. Regarding glucose metabolism, GCBs were found to have a higher glucose uptake rate and were more sensitive towards inhibition of glycolysis via 2-deoxy-D-glucose than non-GCB cells[217,218]. Studies by Weisel et al. further demonstrated that GCBs rather depend on fatty acid oxidation than glucose as their main source of energy which is unique compared to naïve B cells or *in vivo* activated B cells[195]. Within this project, pathway analysis of A20 transcriptomes revealed a downregulation of mTORC signaling, oxidative phosphorylation and glycolysis related genes and an upregulation of fatty acid metabolism related genes upon loss of both Roquin 1 and Roquin 2. Second, Roquin 1 deficient A20 SSCs failed to upregulate genes required for lipid metabolism upon stimulation. Third, Roquin 1/2-depleted A20 cells were deprived in their mitochondrial respiratory activity determined via seahorse assays. In summary, these data are a first hint towards an impairment of Roquin depleted GCB cells to properly metabolically adapt and to enter an adequate cellular growth and proliferation program upon activation which could be a reason for disturbed GC entry of Roquin 1/2 double KO B cells.

Roquin 1 fine-tunes GC development

Deciphering the role of Roquin proteins during GCB development is largely compromised in Roquin 1/2 double KO mice due to the almost complete absence of GCBs. In Roquin 1 homo Roquin 2 het KO mice, GC proportions were slightly upregulated or equal compared to control animals in a Cγ1Cre background. This shows that only one allele of Roquin 2 is sufficient to ensure GCB cell survival. Monitoring of dTOM reporter expression indicating Roquin-deficiency demonstrated that Roquin-ablated GCBs are not counter-selected with

> 80 % of GCBs being Roquin-deficient. Hence, Roquin 1 homo Roquin 2 het KO mice are suitable to investigate GCB characteristics at a minimal Roquin gene dosage. This allowed the identification of Roquin-mediated effects on SHM and affinity maturation as described in the following chapter.

In contrast to the complete loss of Roquin proteins in Roquin 1/2 double KO GCB cells, ablation of Roquin 1 only in Roquin 1 KO animals leads to an expansion of GCs in secondary lymphoid organs independent of the Cre recombinase employed. Thereby, GCBs were already enriched early after immunization by day 4 to day 7. This demonstrates that Roquin 1 impedes an overt immune response.

Loss of Roquin proteins in B cells causes B cell extrinsic perturbances *in vivo*

Perturbances in the B cell milieu entailed changes in the T cell compartment in spleens of Roquin-deficient mice. Roquin 1/2 double KO Cγ1Cre mice were shown to be enriched in TCRβ$^+$ CD4$^+$ cell proportions and total cell numbers and more specifically contained significantly elevated levels of regulatory TCRβ$^+$ CD4$^+$ FoxP3$^+$ T cells, CD4$^+$ CM-like and EM-like T cells, CD8$^+$ EM-like T cells as well as moderately enhanced T_{FH} cell proportions compared to control mice. Alterations in T cell populations of Roquin 1/2 double KO Cγ1Cre mice were in accordance with published results of unimmunized Roquin 1 KO CD19Cre mice[81,82] and my own analysis in immunized Roquin 1 single KO or Roquin 1/2 double KO CD19Cre mice. They showed the importance of Roquin proteins for the preservation of an immune equilibrium B cell intrinsically and extrinsically. Measurements of resulting effects on the blood or tissue cytokine environment could provide further valuable information about Roquin mediated B cell extrinsic effects. Myeloid cells such as macrophages and dendritic cells play an essential role for immune responses due to their ability to present antigen and are thus also crucial for GC reactions. Although not assessed during my studies, it is most likely that the myeloid environment is altered in Roquin-deficient mice, too.

In this PhD thesis, I reveal a fundamental role of Roquin proteins on GCB development both *in vivo* and *in vitro*. Studies on A20 cell lines and *ex vivo* isolated B cells provided evidence that Roquin proteins are involved in three out of four hallmarks of GCB development as proposed by Basso et al. - proliferation, inhibition of differentiation and genomic instability (the latter described in chapter 2)[219]. Molecularly, transcriptome and proteome analysis of Roquin-deficient A20 SSCs revealed 10 candidate genes which were

found to be significantly regulated by Roquin proteins and which play essential roles for adequate GC entry and B cell differentiation.

Future studies

Immunofluorescent staining of spleen or lymph node tissue sections could confirm whether the observed enlargement of the GCB compartment in Roquin 1 KO and Roquin 1 homo Roquin 2 het KO mice are due to an elevation of the number of GC reaction sites or the size of the individual GC structures. Second, to better link Roquin deficiency to cell cycle of naïve B cells and GCBs, my experiments monitoring CFSE intensities after stimulation or performing DAPI staining *in vivo* should be re-validated. Additional staining of proliferating cells via the application of EdU/BrdU of mice before organ harvest would further strengthen the current data set. Furthermore, B cell proliferation, GC entry and differentiation into APCs could be monitored in Nojima cultures comparing Roquin deficient and control CD19Cre B cells[220,221]. In order to better understand the impact of Roquin proteins on cellular metabolism crucial for GC entry and survival, measurements of the capacity of Roquin deficient A20 cells as well as *ex vivo* Roquin KO naive B cells and GCBs to oxidize fatty acids and consume glucose should be vastly expanded. Additionally, experiments monitoring the survival of Roquin deficient A20 cells in mixed cell cultures should be repeated using fatty acids as limiting nutrient source instead of glucose. Most importantly, validation of candidate genes identified in transcriptome and proteome analysis of Roquin-ablated A20 SSCs as well as CLIP-seq experiments should be performed with the goal to gather a molecular understanding for the loss of GCBs in Roquin 1/2 double KO mice.

5.2 Roquin is required for SHM

The process of affinity maturation is commonly studied using the immunizing hapten NP coupled to a carrier protein (e.g., CGG or KLH) due to its unique ability to induce a clonally restricted TD immune response which can nicely be monitored over time. Most characteristically, a tryptophan to leucin amino acid exchange at position 33 of the V_H186.2 gene region (W33L) increases the affinity of the antibody by 10-fold[222]. Hence, immunizations using carrier-coupled NP together with alum adjuvant have been widely used to study the kinetics and extent of affinity maturation and SHM.

Roquin proteins are needed to introduce affinity enhancing W33L mutations upon NP-CGG_{30-39} immunization

In C57BL/6 mice, W33L mutations in V_H186.2 sequences of isolated NP-specific GCBs were shown to accumulate within the first two weeks after immunization peaking at day 14 with ~50 % of W33L mutated V_H186.2 sequences. Beyond day 14, no significant changes were observed anymore in the proportion of W33L mutated V_H186.2 sequences supporting my experimental approach to assess W33L mutational load 14 days after NP-CGG_{30-39} immunization[223]. In comparison, Kober-Hasslacher et al. detected 40 % of W33L mutated V_H186.2 sequences in immunized $CD19Cre^{I/+}$ animals at the same time point after immunization[224]. Detection of W33L mutations is conventionally facilitated by hybridoma or cloning approaches to amplify BCR sequences of isolated GCBs. Thereby, sequencing of several hundreds of BCR heavy-chains already represents a considerable expenditure of time and money. During my PhD thesis, I hence aimed to take advantage of the technical progress of next-generation sequencing enabling the analysis of thousands of BCR sequences within one sequencing run instead. Due to my primer design, my analysis was limited to the V_H186.2 heavy chain in conjunction with a downstream $C\gamma1$ region. Still, this method should cover > 90 % of the BCR repertoire due the dominance of this rearrangement at the peak of the GC response to the carrier-coupled NP immunogen[38,162]. $C\gamma1Cre^{I/+}$ control animals were significantly enriched in sequences containing W33L mutations (51 % W33L mutated CDR1 sequences) compared to Roquin 1 KO BCRs (14 %) or Roquin 1 homo Roquin 2 het KO BCRs (13 %). This data strongly suggests that Roquin 1 is required for optimal affinity maturation.

Roquin proteins are necessary to produce high-affinity antigen-specific antibodies

Beyond the analysis of W33L mutational loads, the extent of affinity maturation in the GC reaction can be observed by the measurement of the abundance and affinity of NP-specific antibodies in blood sera of immunized animals. Studies on immunized C57BL/6 mice thereby demonstrated that the most pronounced increase in the titer of high-affinity NP-specific IgG1 occurs from day 7 until day 14 while titers plateau after day 21. This suggests that affinity maturation processes mainly take place until day 21[223]. $C\gamma1Cre^{I/+}$ control animals nicely recapitulated this progression of NP-specific IgG1 antibody titers. In contrast, immunized Roquin 1 KO mice had significantly less circulating high-affinity NP-specific IgG1 antibodies in their blood sera starting from day 21 and their levels of high-affinity antibodies within the pool of total NP-recognizing antibodies were significantly reduced by day 28, too. These effects were even more skewed upon additional deletion of one Roquin 2 allele in Roquin 1 homo Roquin 2 het KO animals. My data suggests that loss of Roquin proteins compromises the ability to produce NP-specific IgG1 antibodies in quantity and quality.

Roquin proteins shape the mutational spectrum of Ig heavy chains

Beyond mutations at position 33 of the V_H186.2 sequence, BCRs constantly accumulate mutations during an ongoing GC reaction especially in the epitope recognizing CDR1 and CDR2 regions. In line with the literature, I detected an average mutational frequency of ~5 amino acid mutations per V_H186.2 sequence in control mice[223]. Transitions and transversions were equally distributed in control animals and heavy chains with a particular high burden of nucleotide or amino acid mutations were identified. Besides position 33, mutations were widely spread between the CDR and the framework regions and within the pool of sequences analyzed, each position within the V_H186.2 was found to be mutated at least once. The mutation spectrum was however drastically changed in Roquin 1 homo Roquin 2 het KO and even more in Roquin 1 KO animals. In both genotypes, average mutation frequencies were pronouncedly decreased, reads with an accumulation of many mutations were lost and less positions within the heavy chain were mutated pointing towards a defect of SHM upon Roquin 1 ablation. Furthermore, I detected a bias in the frequency of transitions and transversions. Thus, the mutational spectrum in addition to the already described hotspot mutation W33L was negatively influenced by the loss of Roquin alleles.

Taken together, BCR sequencing clearly demonstrated a drastic impairment of SHM in Roquin 1 ablated GCBs. My analysis was thereby restricted to the simple carrier-coupled NP antigen. It would be interesting to investigate if more complex antigens, the challenge of the immune system with manifold diverse pathogens or a second challenge employing a boost immunization would cause a major failure of the high-affinity humoral immune response in Roquin 1 deficient mice.

Loss of Roquin proteins leads to a reduction of detectable antigen-specific GCBs

I discovered that NP^+ GCBs are drastically diminished in secondary lymphoid organs of Roquin deficient animals compared to controls while the fraction of NP^+ cells within APCs is not significantly changed between genotypes. This effect was measured to be Roquin gene dosage dependent since in Roquin 1 KO mice on average ~8 % of their GCBs were stained NP^+ while this fraction was reduced to ~3 % in Roquin 1 homo Roquin 2 het KO mice. In comparison, GCBs of control mice contained on average 18 % NP^+ cells which is in accordance with literature[38].

It has been shown that antigen-specificity is an important factor for GC recruitment by combining primed BCR sequences in transgenic mouse models with non-matching immunogens[34]. Following this line of argumentation, this would suggest that Roquin-deficient mice either contain less antigen-specific naïve B cells which can be recruited into the GC reaction or their pre-GC selection process is negatively impaired. The latter seems more probable when considering that APCs contain equal amounts of NP^+ cells in Roquin-ablated mice compared to controls. However, antigen-specificity is most likely not the only factor driving GC selection[34]. Thus, with the current dataset at hand, I cannot validly demonstrate or rule out a pre-GC selection deficit upon ablation of Roquin proteins. Furthermore, studies by Di Niro et al. also consider that BCRs of B lymphocytes might be antigen-specific, however with such a low affinity that they fail detection thresholds of standard procedures such as ELISpot, ELISA or flow cytometry[225,226]. According to the experimental approaches of Di Niro et al., future experiments could discriminate between antigen-unspecific BCRs from antigen-specific BCRs with very low affinity by sequencing the overall BCR repertoires at an early time-point (e.g., 7 days after immunization) and a late time-point (e.g., 21 days after immunization) and comparing the BCR repertoires of naïve B cells to GCBs and APCs. If the BCR repertoires would be narrower at the late time-point compared to the early time-point or would be narrower in GCBs and APCs compared to naïve B cells, then there

would be a sign of selection suggesting that BCR repertoires were antigen-specific but of low affinity rather than antigen-unspecific. Di Niro et al. further showed that SHM and affinity maturation occurs both during GC reaction as well as extrafollicular[227]. In summary, NP staining of GCBs might not be sufficient to determine antigen-specificity and might neglect a proportion of antigen-specific, but low affinity GCBs. Defects in SHM and affinity maturation upon loss of Roquin proteins might enhance this proportion of undetectable antigen-specific, but low affinity B lymphocytes compared to controls.

Clonal diversity is reduced upon loss of Roquin proteins

Deep sequencing of V_H186.2 PCR amplicons covering the VDJ junction as well as 5' ends of the Cγ1 heavy chain region and subsequent bioinformatic analysis revealed a surprising increase in B cell clonality especially in Roquin 1 KO BCRs, but also to a slightly minor extent in Roquin 1 homo Roquin 2 het KO BCRs.

30 years ago, Jacob et al. published that GCs are seeded by only 1 - 3 B cell precursors driving among others the long-held concept that individual GCs are pauciclonal[38]. However, the emergence of improved mouse models together with high-resolution imaging techniques enabled Tas et al. to challenge this concept showing that early GCs (day 6 after CGG alum injection) are highly polyclonal containing 50 - 200 clones. Furthermore, investigators showed that in a WT background, the development of a higher clonality at the expense of diversity is a stochastic process and monoclonal GC sites can co-exist with polyclonal GC sites in one lymph node. In their experiments, monoclonal GCs were less frequent than polyclonal GCs. In addition, SHM can lead to a clonal burst and thus dominance of a single clone within one GC reaction, but can occur at same efficiency in polyclonal GCs[34]. While these studies were designed to detect individual GC structures within the tissue and assess their mutational spectrum and clonality, the sequencing approach applied during my project only gives information about the amount of B cell clones participating in the whole immune response.

It can be suspected that the observed clonality in Roquin-deficient mice is connected to and maybe even a direct consequence of the failure of SHM which is meant to diversify BCR sequences. NP-CGG immune responses are per se dampened in their potential to induce diverse VDJ rearrangements which drastically limits interclonal competition and diversity[24]. Due to the lack of SHM in Roquin-ablated GCBs, also intraclonal competition is probably diminished. This could also account for the tree-like network of clone

connections in $C\gamma1Cre^{I/+}$ control animals which is mostly absent in Roquin-deficient mice. Additively, deprived diversity can also be connected to the idea of perturbed pre-GC selection which would equally result in a diminished repertoire of $V_H186.2$ expressing B cells within the GCB cell pool.

Taken together, during my studies I provided evidence for the essential role of Roquin proteins for SHM. Furthermore, my data indicate that Roquin proteins are required for effective affinity maturation. Pre-GC selection processes might be perturbed upon Roquin ablation resulting in a reduced amount of detectable antigen-specific B cell clones participating in the response of Roquin 1 KO and Roquin 1 homo Roquin 2 het KO mice. Overall, impairments before and during the GC reaction accumulate in low affinity antibodies making Roquin-deficient mice potentially more vulnerable towards foreign microbes. By the parallel analysis of Roquin 1 KO and Roquin 1 homo Roquin 2 het KO mice, I could show that both Roquin 1 and Roquin 2 are important regulators of the described processes.

Future studies

Future experiments to expand the given dataset (beyond the ones already described) could include RNA sequencing and mass-spectrometry analysis of sorted GCBs of immunized Roquin 1 KO and Roquin 1 homo Roquin 2 het KO mice versus controls to analyze transcriptomic and proteomic changes of genes involved in SHM and affinity maturation. The quantity of $IgG1^+$ or IgM^+ NP-specific APCs in the bone marrow should be assessed via ELISpot. Microdissections of single GC follicles in tissue sections and sequencing of their BCRs could enrich our knowledge about clonality effects in those animals at the level of individual GC reactions.

5.3 Roquin proteins are essential for CSR

To evaluate the impact of Roquin ablation on APC differentiation, I assessed CD138^{+} IRF4^{+} B220^{lo} APCs by flow cytometry *in vivo*. In addition, I determined their capacity to class-switch by intracellular staining as well as their capability to produce antigen-specific antibodies.

Roquin 1 prevents excessive APC formation

I discovered that APCs are enriched in Roquin 1 KO and Roquin 1 homo Roquin 2 het KO Cγ1Cre mice compared to controls independent of the applied TD antigen in secondary lymphoid organs. Thereby, I did not measure significant differences of the APC formation capacity between Roquin 1 KO and Roquin 1 homo Roquin 2 het KO Cγ1Cre mice hinting towards a minor role of Roquin 2 during APC differentiation processes. These data provide evidence that under wildtype conditions, Roquin 1 acts as an inhibitor of an overt plasmacytic response without vast changes in the absence of one Roquin 2 allele. Discrimination of follicular versus extrafollicular APC origin is not a trivial experimental task and thus was out of the scope of this project (see future studies).

In contrast to secondary peripheral organs of Roquin 1 KO and Roquin 1 homo Roquin 2 het KO Cγ1Cre mice, APC numbers and proportions were unchanged in the bone marrow 35 days after NP-CGG$_{30\text{-}39}$ immunization. This is in accordance with the generally held concept of a limited capacity of survival niches[228]. It will be interesting to evaluate in the future, whether long-lived, bone marrow APCs of Roquin-deficient animals are altered in their proportion of antigen-specific APCs compared to controls. This would complement my current dataset showing that the fraction of detectable antigen-specific APCs is unchanged between Roquin-ablated animals and controls.

Strikingly, loss of GCBs in Roquin 1/2 double KO mice did not lead to a concomitant loss and not even reduction of APCs. On contrary, Roquin 1/2 double KO CD19Cre or Cγ1Cre mice contain similar proportions and numbers of APCs compared to controls. By using Roquin-ablated A20 cell lines as an *in vitro* model system, I was able to monitor genetic perturbations upon simultaneous loss of Roquin 1 and Roquin 2 compared to controls and identified 10 candidate genes impacting plasmacytic development. Hence, future

validation experiments as proposed before will be able to shed light on the molecular mechanism of APC differentiation in Roquin-deficient mice.

Future studies

Up to date, a reliable distinction of extrafollicular and follicular plasma cells based on surface marker expression is not possible due to the transient nature of differentiation states impeding the analysis of the origin of Roquin 1 KO and Roquin 1 homo Roquin 2 het KO APCs by flow cytometry 10 - 14 days after immunization[61]. CSR precedes the lineage commitment of the extrafollicular or follicular response and unswitched as well as switched B cells can be found in both populations[45,57]. Thus, immunoglobulin production does not reliably allow to discriminate extrafollicular versus follicular plasma cells. Extrafollicular plasmablasts are produced rapidly within 3 days after antigen recognition to provide early, low affinity antibody titers as a first line of defense. Most of them undergo apoptosis within a week as spleen and bone marrow offer only a limited capacity of niches to foster long-term survival. By choosing an appropriate time point of monitoring, short-lived versus long-lived APCs can be differentiated. However, extrafollicular plasma cells are equally capable to colonize survival niches and thus exist in parallel to follicular plasma cells at late time-points[229]. Hence, to answer the question of APC origin in Roquin-deficient mice in the future, APC production needs to be tightly monitored in time (before and while the formation of GCs) together with an imaging-based approach to visualize their localization in the spleen (migration from the T cell zone into and from the GC follicle versus development in extrafollicular foci and movement towards the red pulp)[57]. Extrafollicular dominant responses have also been linked to a break-up of regular tissue architecture which could be evaluated by histology[41]. Furthermore, a follicular origin can be verified by the mutational load of respective BCR sequences as shown by Sze et al. who sequenced individual tissue dissected antigen-specific plasma cells[229].

My research on late B cell development focused on GCBs and APCs thereby neglecting memory B cell populations. Memory B cells develop either from activated naïve progenitors or emerge from GCBs with several studies suggesting that low BCR affinities and an unswitched BCR isotype favor memory B cell differentiation over APC production[24,60,223,230]. Three distinct memory B cell subsets can be distinguished based on CD80 and PDL2 surface expression levels which vary in their BCR mutational load, their cell fate decision upon secondary antigen challenge, their splenic localization and their BCR isotype[163,231–233]. Considering the vast impact of Roquin on SHM, I anticipate a

consequence of Roquin ablation on the memory B cell compartment as well which could be assessed by future flow-cytometry analysis.

Roquin proteins impact CSR

Molecularly, the process of CSR is dependent on AID and a multitude of DNA repair proteins. AID expression (e.g., via BATF) leads to the conversion of dC nucleotides into dU preferentially in the switch regions of the C_H locus. Next, dU are removed by DNA glycosylases (e.g., UNG, TTG) and ssDNA breaks are induced at the abasic sites by Ape endonuclease enzymes (APEX1, APEX2). Due to the vast amount of induced ssDNA breaks, base excision repair mechanisms (POLB, POLE, POLD1-4, XRCC1, LIG1) will only repair a proportion of lesions favoring the generation of dsDNA breaks whenever two ssDNA breaks remain in close proximity to each other. Mismatch repair mechanisms (MSH2, MSH6, MLH1, PMS1, PCNA, EXO1) lead additionally to the generation of further dsDNA incisions. DNA breaks are sensed by the MRN complex (MRE11, RAD50, NBN) recruiting DNA damage response proteins (e.g., ATM, PRKDC, TRP53BP1). The endonuclease Ercc1 generates blunt-end joints at the site of the dsDNA break and last, switch regions are recombined via nonhomologous end joining proteins (e.g., XRCC5, XRCC6, XRCC4, LIG4) leading to class-switching from IgM to IgG / IgA / IgE[44].

During this project, I assessed transcript levels of those genes involved in CSR in Roquin deficient A20 SSCs via RNA sequencing. This revealed an upregulation of AID in the absence of Roquin proteins while mRNAs of 11 repair proteins were found to be significantly downregulated in Roquin 1/2 double KO A20 SSCs compared to controls. These results suggest that while AID activity might be enhanced upon loss of Roquin proteins, AID induced DNA breaks probably cannot be efficiently repaired. This would lead to a general inability of Roquin ablated A20 cells to deal with DNA damage which would impair their survival during AID expression as well as during fast cell cycle progression. This could explain their inability to compete with WT cells in mixed long-term cultures. However, 7 out of those 11 repair proteins could be detected well by mass-spectrometry and even though some were found to be downregulated, their protein expression changes failed statistical significance. Mass-spectrometry analysis could not validly show AID expression changes due to low protein abundance. Hence, validation of my RNA sequencing results e.g., via monitoring of A20 SSC survival capabilities upon DNA damage induction should be performed in the future.

Even though transcript levels of essential CSR players can be evaluated, A20 cells are already IgG1$^+$ IgM$^-$ and thus immunoglobulin switching can only be investigated in a limited framework. Therefore, the influence of Roquin absence on CSR was evaluated further by intracellular immunoglobulin staining of APCs *in vivo*. Roco et al. showed that upon transfer of SW_{HEL} B cells into C57BL/6 mice > 60 % of extrafollicular plasmablasts (CD38^{lo} CD95^{lo} B220$^+$) are IgG1$^+$ at day 6.5 after HEL^{2x}-SRBC immunization indicating that a significant proportion of extrafollicular APCs is capable to undergo CSR[45]. However, in Roquin 1/2 double KO mice (either CD19Cre or Cγ1Cre), APCs are mostly IgM$^+$ and are completely devoid of class-switched IgG1. In contrast, Roquin 1 KO and Roquin 1 homo Roquin 2 het KO Cγ1Cre mice are significantly reduced in their proportions of IgM$^+$ APCs with a concomitant increase in especially IgG1$^+$ APCs, but also IgG2b$^+$ and IgG3$^+$ APCs. Hence, loss of Roquin 1 amplifies the amount of CSR if at least one allele of Roquin 2 is still present while loss of both Roquin proteins leads to a collapse of the class-switched APC compartment. To enrich the current knowledge about Roquin on CSR in the future, *ex vivo* CD19Cre Roquin ablated naïve B cells should be cultured in the presence of class-switch inducing stimuli (LPS, IL4, αCD40, IFNγ) for 3 - 4 days to measure the capability of diverse genotypes to undergo CSR *in vitro*[47].

Taken together, I could demonstrate that Roquin proteins affect the emergence of class-switched APCs and differentially regulate transcripts of essential DNA repair proteins.

To my knowledge, my PhD thesis is the first study deciphering the role of Roquin proteins during late B cell differentiation. Through comprehensive phenotypic analyses using diverse mouse models and immunization methods, I could demonstrate that Roquin proteins are indispensable for the formation of GCBs and class-switched APCs during a primary immune response. My findings emphasize a fundamental impact of Roquin proteins on cell cycling in B cells as already shown in literature for other immune cell types. In my model system, Roquin 1 protein expression was crucial to enable adequate SHM and affinity maturation in GCBs. In addition, I successfully established and characterized an *in vitro* GC-like cell line system which enabled me to gain a better molecular understanding of Roquin protein functions.

Supplementary Figures

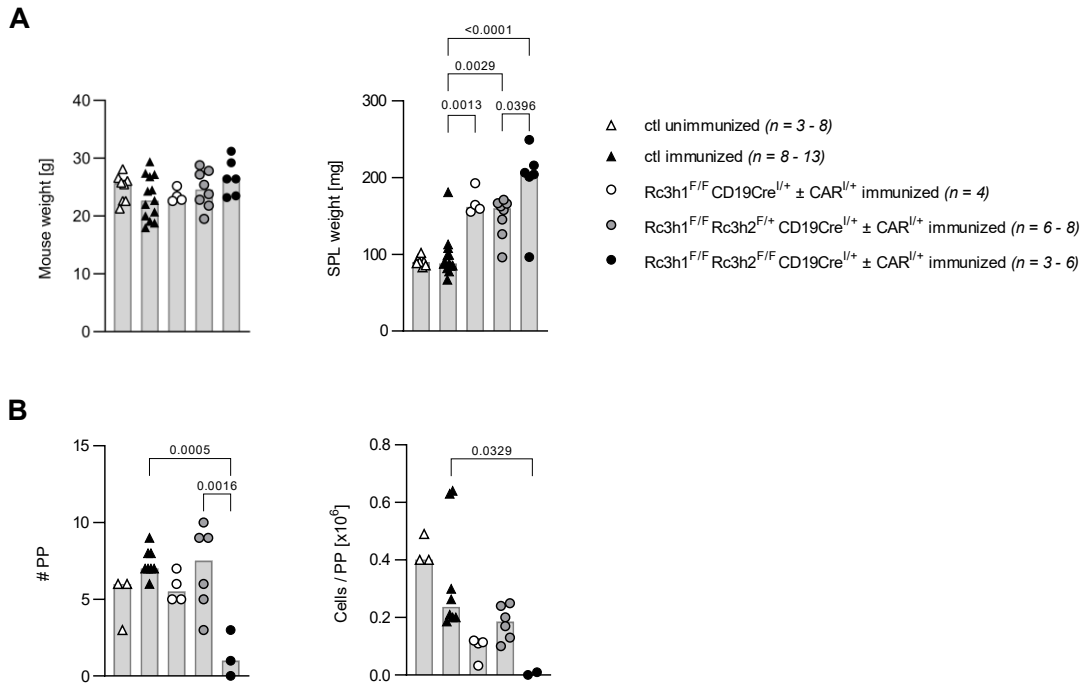

Supplemental Figure 1: Weights and peyer's patches upon SRBC immunization after 10 days in CD19Cre Roquin knockout mice.
(A) Mouse and spleen weights. (B) Total numbers of peyer's patches and total cell numbers per peyer's patch in Mio Bars show median values with each symbol representing a mouse. Statistical significance was determined by one-way ANOVA and p values of most relevant comparisons are shown. PP, peyer's patches

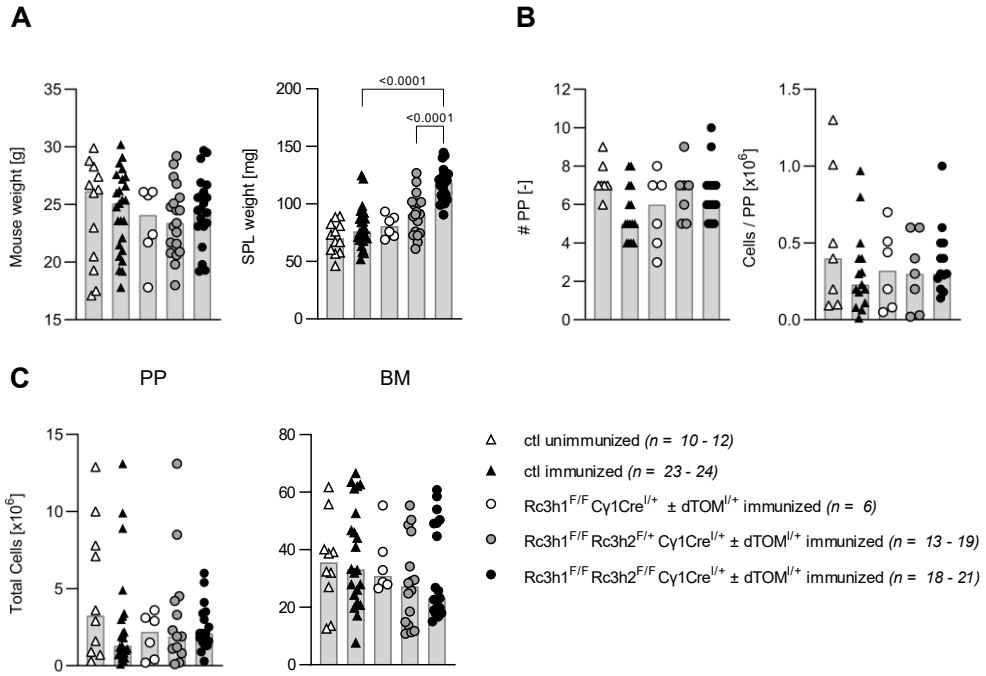

Supplemental Figure 2: Total cell numbers and organ weights upon SRBC immunization after 10 days in Cγ1Cre Roquin knockout mice.
(A) Mouse and spleen weights. (B) Total numbers of peyer's patches and total cell numbers per peyer's patch in Mio. (C) Total lymphocyte cell numbers for indicated organs. Bars show median values with each symbol representing a mouse. Statistical significance was determined by one-way ANOVA and p values of most relevant comparisons are shown. SPL, spleen; PP, peyer's patches; BM, bone marrow

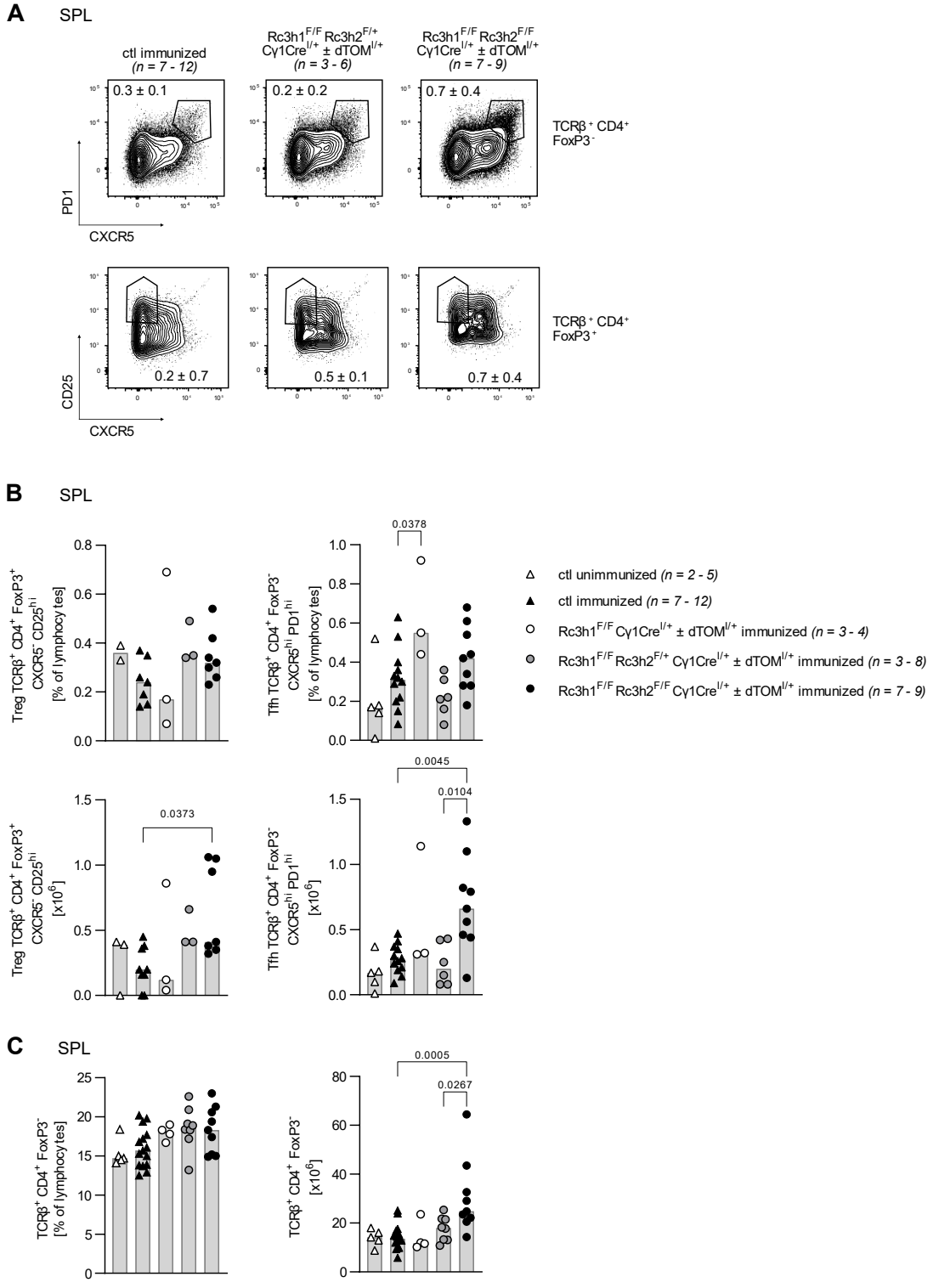

Supplemental Figure 3: T_{reg} and T_{FH} upon SRBC immunization after 10 days in Cγ1Cre Roquin knockout mice.

(A) Representative flow cytometry plots of T_{reg} and T_{fh} pre-gated on TCRβ$^+$ CD4$^+$ FoxP3$^+$ or TCRβ$^+$ CD4$^+$ FoxP3$^-$ T cells, respectively. Percentages correspond to mean ± SD of gated populations within the lymphocyte population. (B) T_{reg} and T_{fh} percentages and numbers. (C) Numbers and percentages of CD4$^+$ FoxP3$^-$ T cells. Data are cumulative from at least 3 independent experiments. Bars show median values with each symbol representing a mouse. Statistical significance was determined by one-way ANOVA and p values of most relevant comparisons are shown. SPL, spleen; T_{reg} regulatory T cell; T_{fh} follicular helper T cell

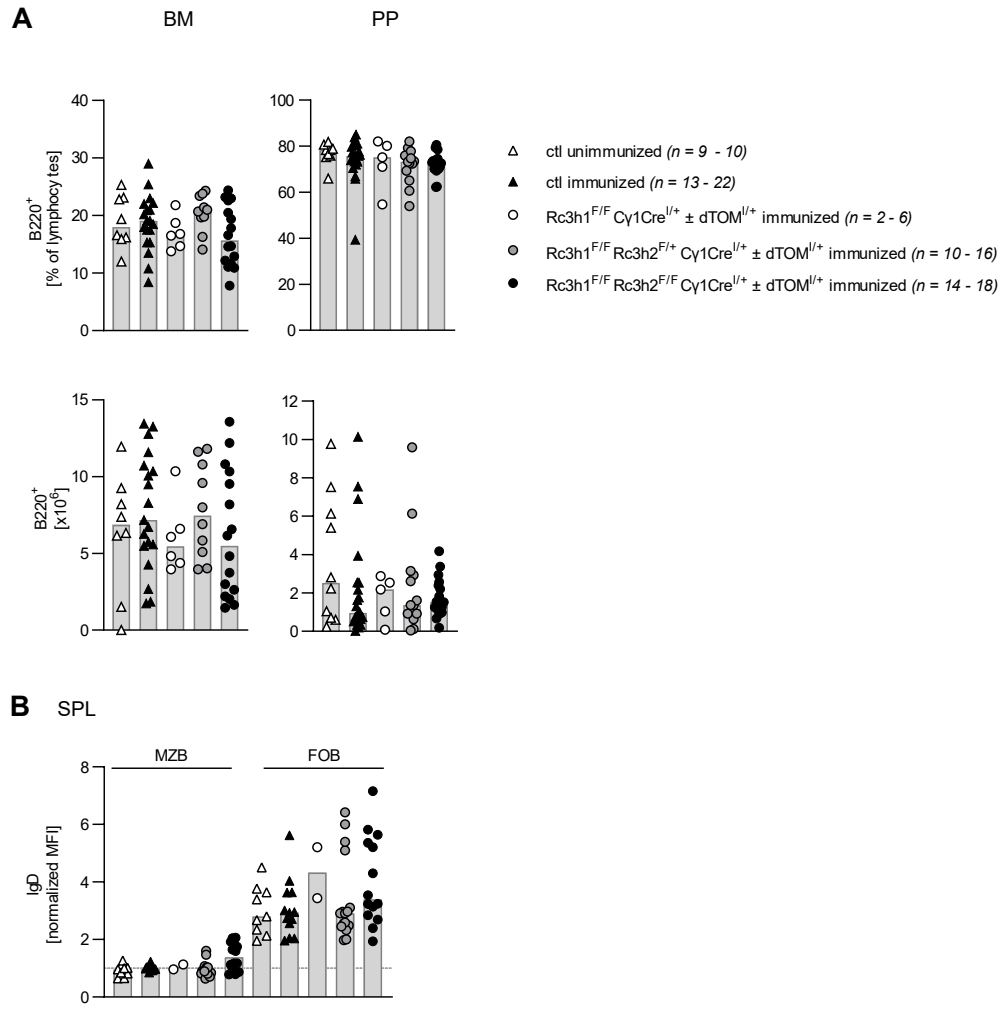

Supplemental Figure 4: B cells upon SRBC immunization after 10 days in Cγ1Cre Roquin knockout mice.
(A) $B220^+$ percentages and numbers in bone marrow and peyer's patches. (B) IgD protein expression levels of MZB and FOB. Data are cumulative from at least 7 independent experiments. SPL, spleen; BM, bone marrow; PP, peyer's patches; MZB $B220^+$ $CD19^+$ $CD21^+$ $CD1d^+$ $CD23^-$; FOB $B220^+$ $AA4.1^-$ $CD19^+$ $CD21^{lo}$ $CD1d^{lo}$

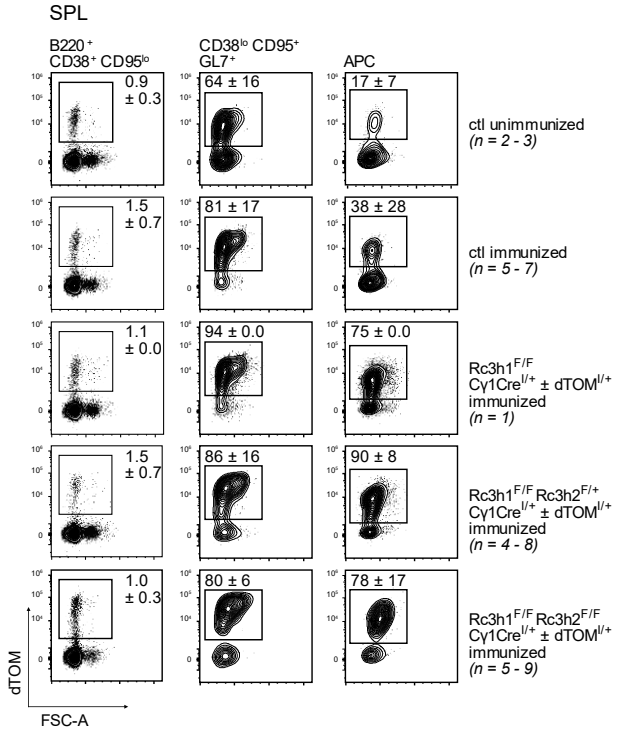

Supplemental Figure 5: dTOM+ cells upon SRBC immunization after 10 days in Cγ1Cre Roquin knockout mice.
Representative flow cytometry plots of dTOM+ cells within the population of B220+ CD38+ CD95lo B cells, GCB or APC in spleen. GCB B220+ CD38lo CD95hi GL7+; APC CD138+ IRF4+ B220lo

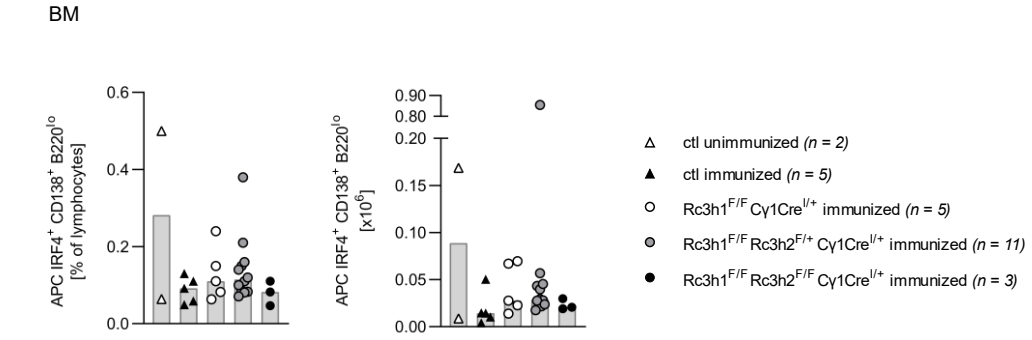

Supplemental Figure 6: APCs upon NP-CGG$_{30-39}$ immunization after 35 days in Cγ1Cre Roquin knockout mice.
APC proportions and numbers in bone marrow 35 days after immunization with NP-CGG. Data are cumulative from 4 independent experiments. Statistical significance was determined by two-way ANOVA. APC CD138+ IRF4+ B220lo

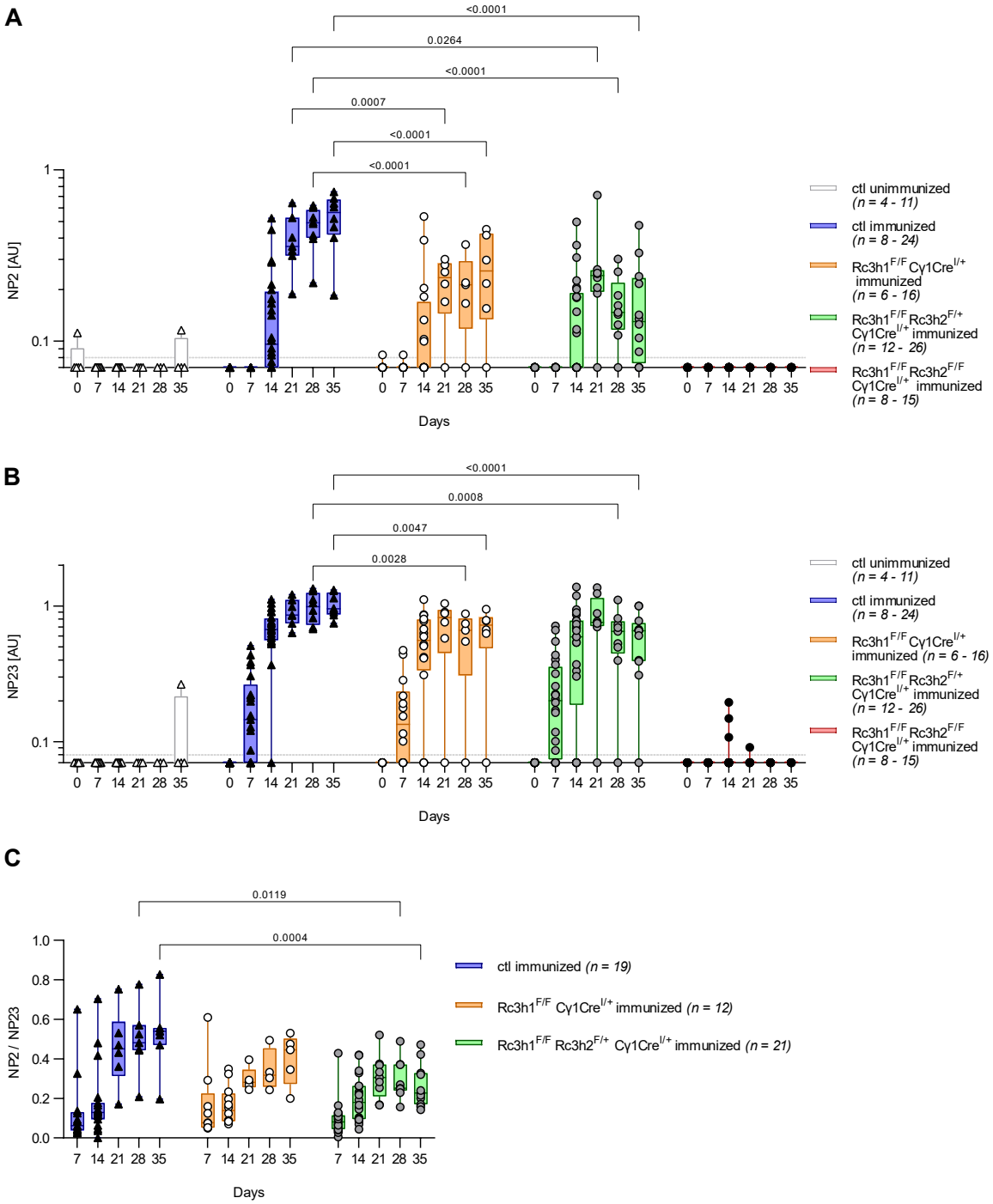

Supplemental Figure 7: NP-specific IgG1 production in Cγ1Cre Roquin knockout mice until five weeks after NP-CGG$_{30-39}$ immunization.
(A) NP_2-binding high-affinity IgG1 antibodies of blood sera collected at indicated time-points before (0 days) or after (7, 14, 21, 28, 35 days) immunization with NP-CGG$_{30-39}$. Absorption values of six dilutions were summarized, substracted by blank values and normalized to plate-specific standard absorption measurements. Detection threshold of 0.08 is indicated. Data points are only plotted if all six dilutions could be measured and absorption summation values below threshold levels were set to 0.07. (B) Same as in (A), but shown for NP_{23}-binding low-affinity IgG1 antibodies. (C) Ratio of NP_2 to NP_{23}-binding IgG1 levels. Data points are plotted independent of the number of dilutions measured, but restricted to samples with NP_{23}-IgG1 normalized absorption values > 0.08. Data are cumulative from 4 independent ELISA experiments. Each symbol represents one blood serum sample. Statistical significance was determined by two-way ANOVA and p values of most relevant comparisons are shown.

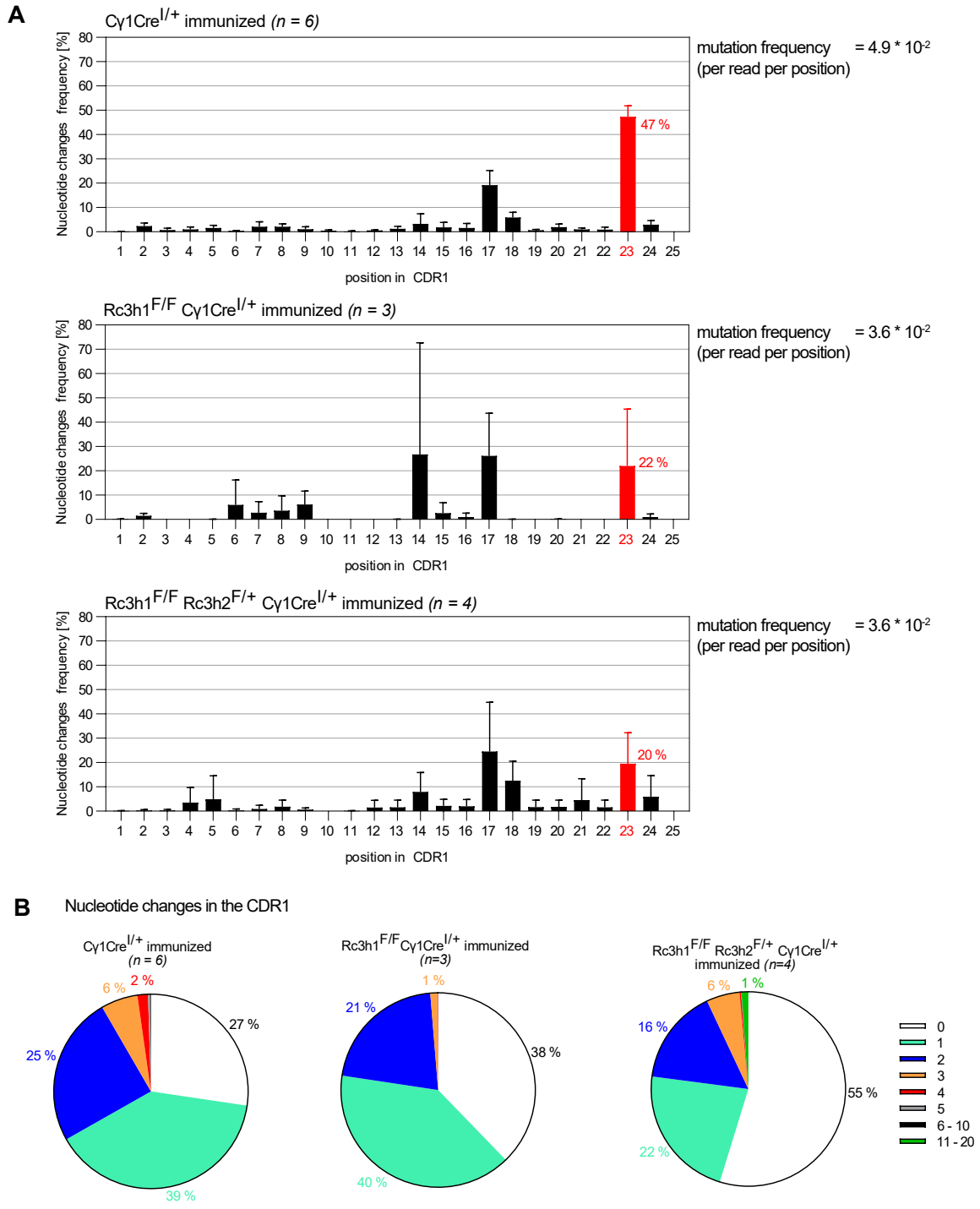

Supplemental Figure 8: Nucleotide mutation frequencies in the CDR1 region of Ig_HV 1-72 amplified BCR sequences upon NP-CGG_{30-39} immunization after 14 days in Cγ1Cre Roquin knockout mice.

(A) Percentages of nucleotide changes at a distinct position of the CDR1 per genotype. Highlighted position 23 (shown in red) corresponds to the W33L hotspot mutation site upon affinity maturation of NP-CGG immunized animals. (B) Percentages of amplified reads containing 1 - 20 mutations per read per genotype. Reads were filtered for unique V sequences (> 10.000 per mouse), a mean sequencing quality above 20 and recognition of the Ig_HV 1-72 during alignment. Frequencies were normalized to the total amount of filtered reads per sample. Data are cumulative from 4 independent immunization experiments combined into one sequencing analysis.

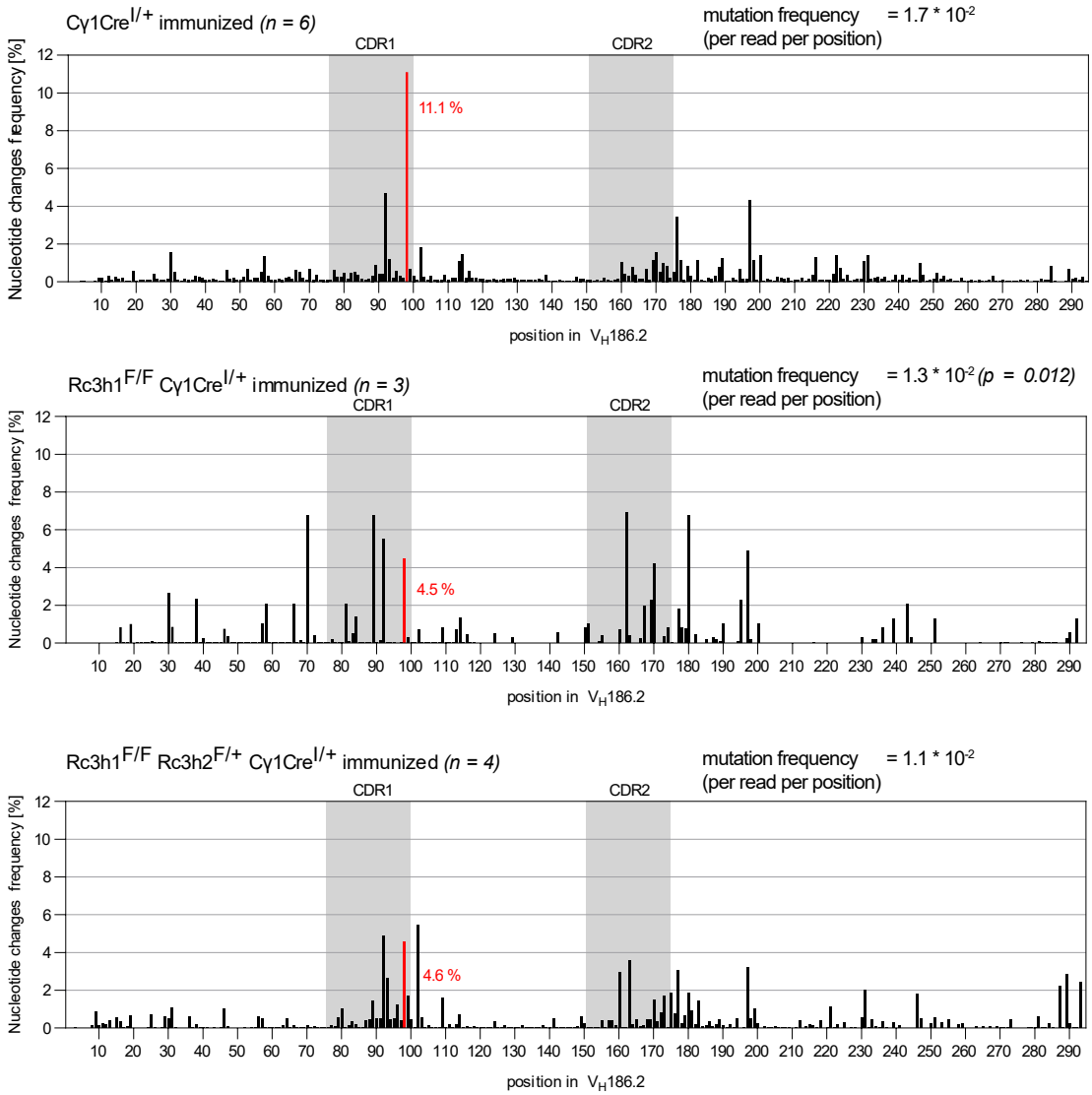

Supplemental Figure 9: Nucleotide mutation frequencies in the V_H186.2 region of Ig_HV 1-72 amplified BCR sequences upon NP-CGG_{30-39} immunization after 14 days in Cγ1Cre Roquin knockout mice.

Percentages of nucleotide changes at a distinct position of the V_H186.2 per genotype. Highlighted position 97 (shown in red) corresponds to the W33L hotspot mutation site upon affinity maturation of NP-CGG immunized animals. Reads were filtered for unique V sequences (> 10.000 per mouse), a mean sequencing quality above 20 and recognition of the Ig_HV 1-72 during alignment. Frequencies were normalized to the total amount of filtered reads per sample. Data are cumulative from 4 independent immunization experiments combined into one sequencing analysis.

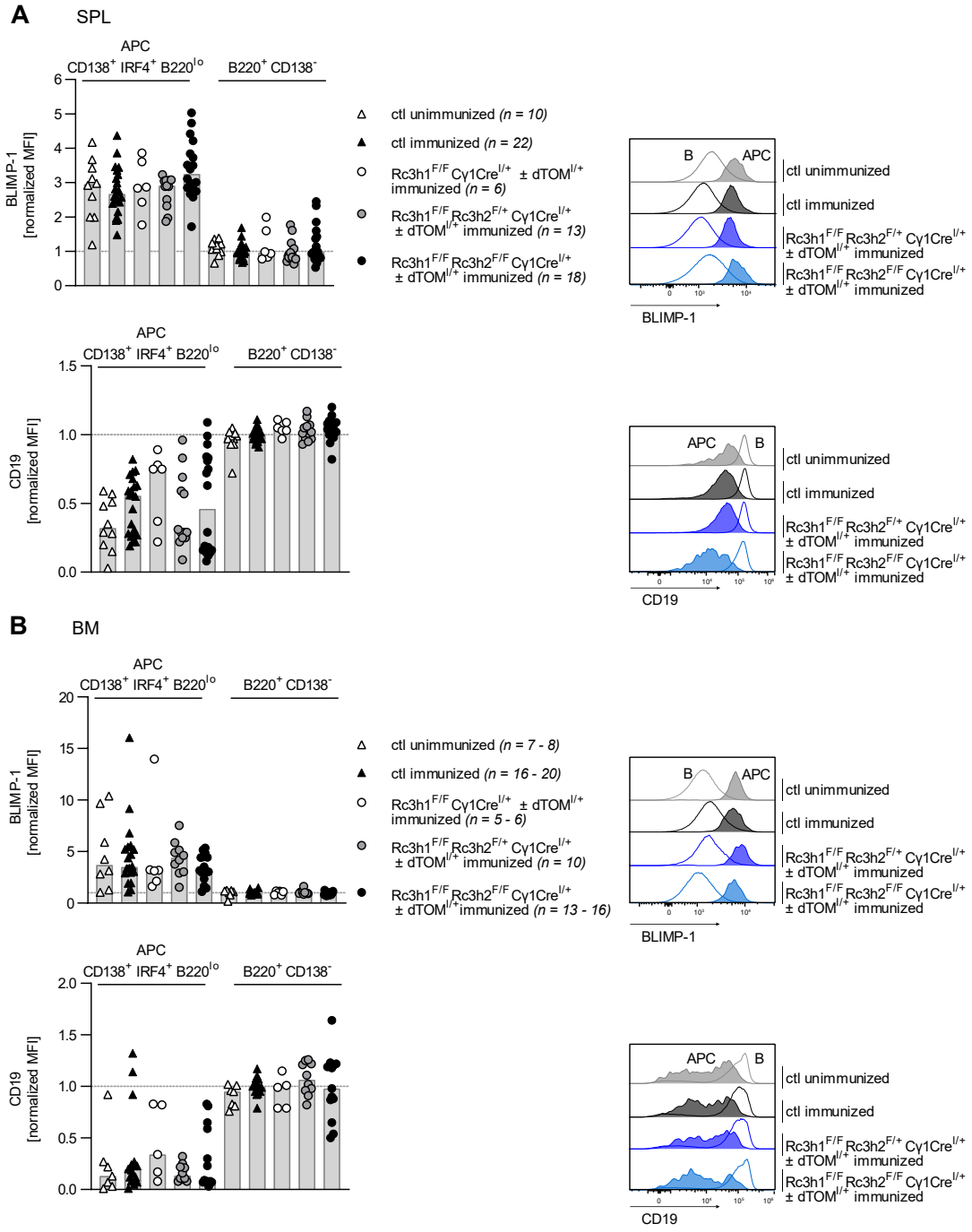

Supplemental Figure 10: Protein expression of BLIMP-1 and CD19 in APCs upon SRBC immunization after 10 days in Cγ1Cre Roquin KO mice.
(A) BLIMP-1 protein expression levels of antibody producing cells in comparison to B220$^+$ CD138$^-$ B cells shown as bar chart and representative flow cytometry histogram in spleen. MFI values are normalized per experiment to immunized controls. (B) Same as in (A) but data shown in bone marrow. Data are cumulative from 7 (BM) and 9 (SPL) independent experiments. Bars show median values with each symbol representing a mouse. SPL, spleen; BM, bone marrow; B B220$^+$ CD138$^-$; APC CD138$^+$ IRF4$^+$ B220^{lo}

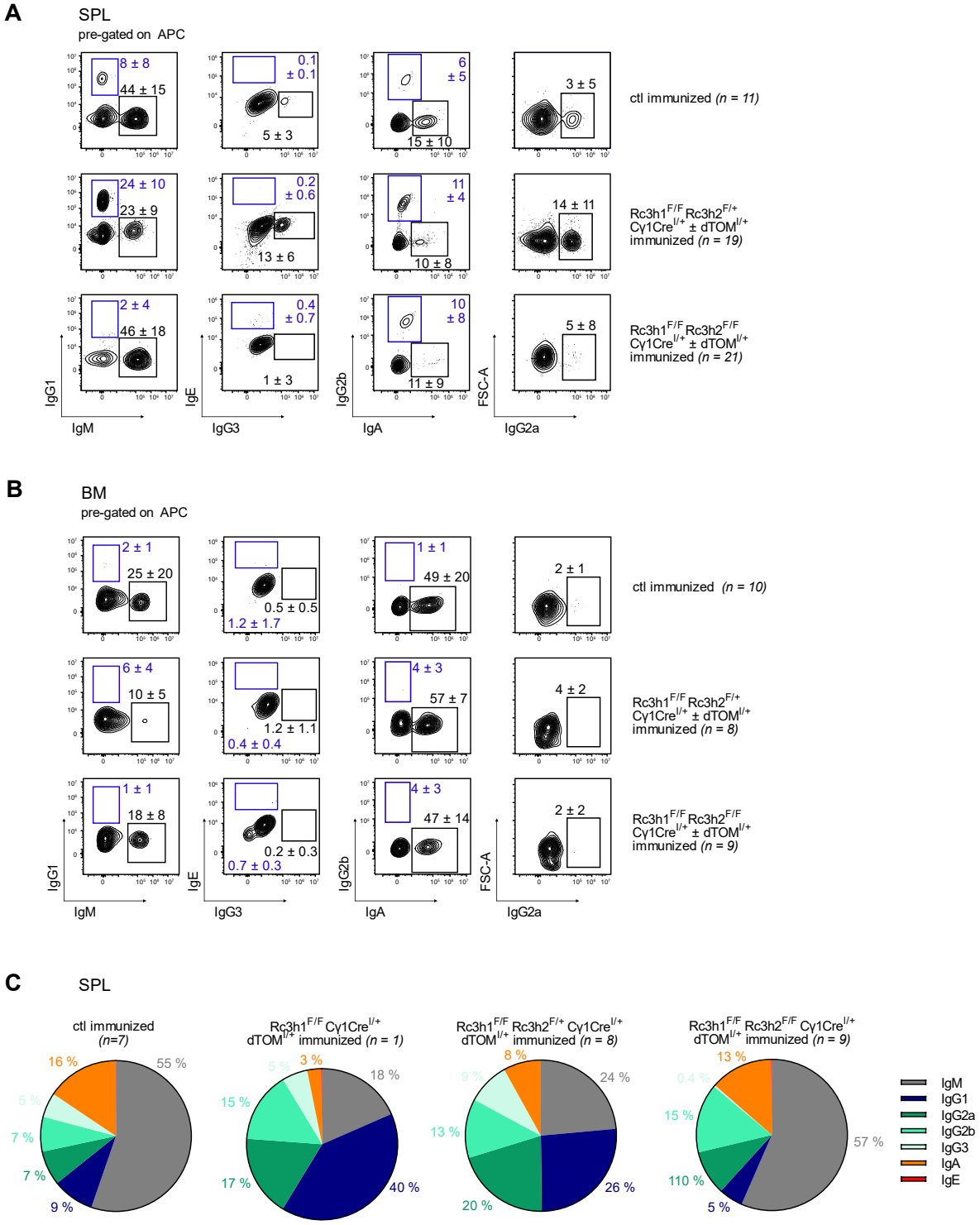

Supplemental Figure 11: Immunoglobulin proportions in APCs upon SRBC immunization after 10 days in Cγ1Cre Roquin KO mice.
(A) Representative flow cytometry plots of immunoglobulins pre-gated on CD138$^+$ IRF4$^+$ B220^{lo} APCs in spleen. Percentages correspond to mean ± SD of immunoglobulins within the APC population. (B) Same as in (A) but shown for bone marrow. (C) Immunoglobulin percentages of dTOM$^+$ APCs in spleen. Data are cumulative from 3 (BM) and 9 (SPL) independent experiments, respectively. SPL, spleen; BM, bone marrow; APC CD138$^+$ IRF4$^+$ B220^{lo}

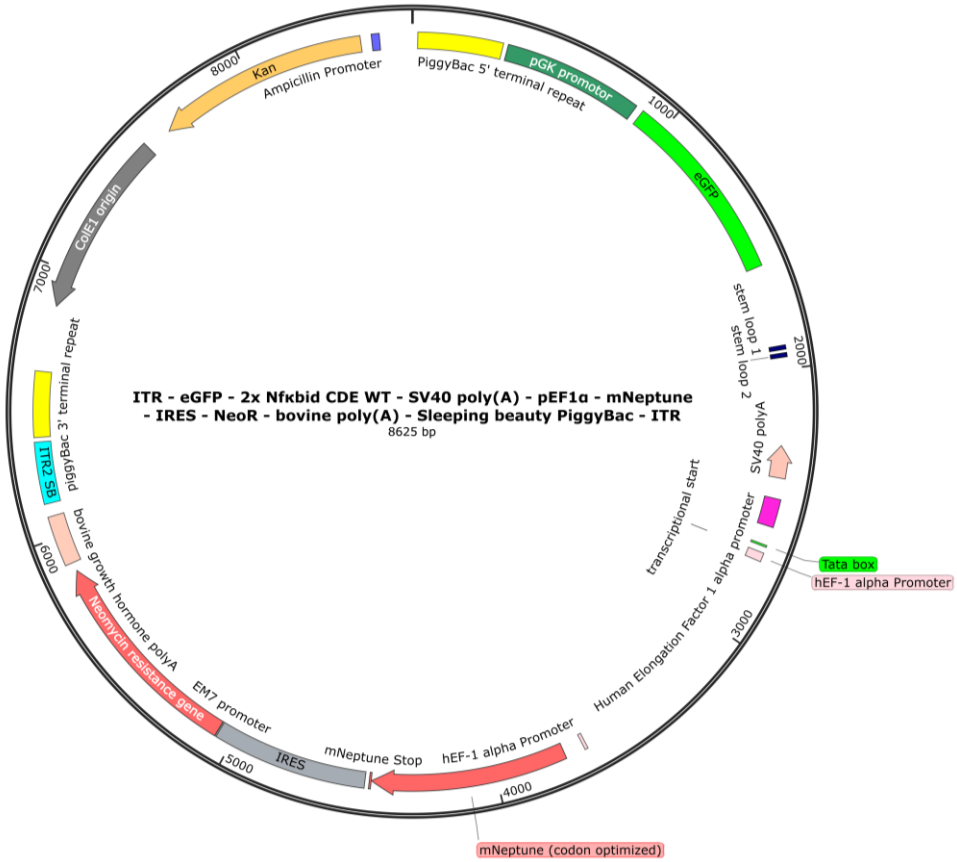

Supplemental Figure 12: Nfκbid CDE WT vector map used for A20 cell manipulation

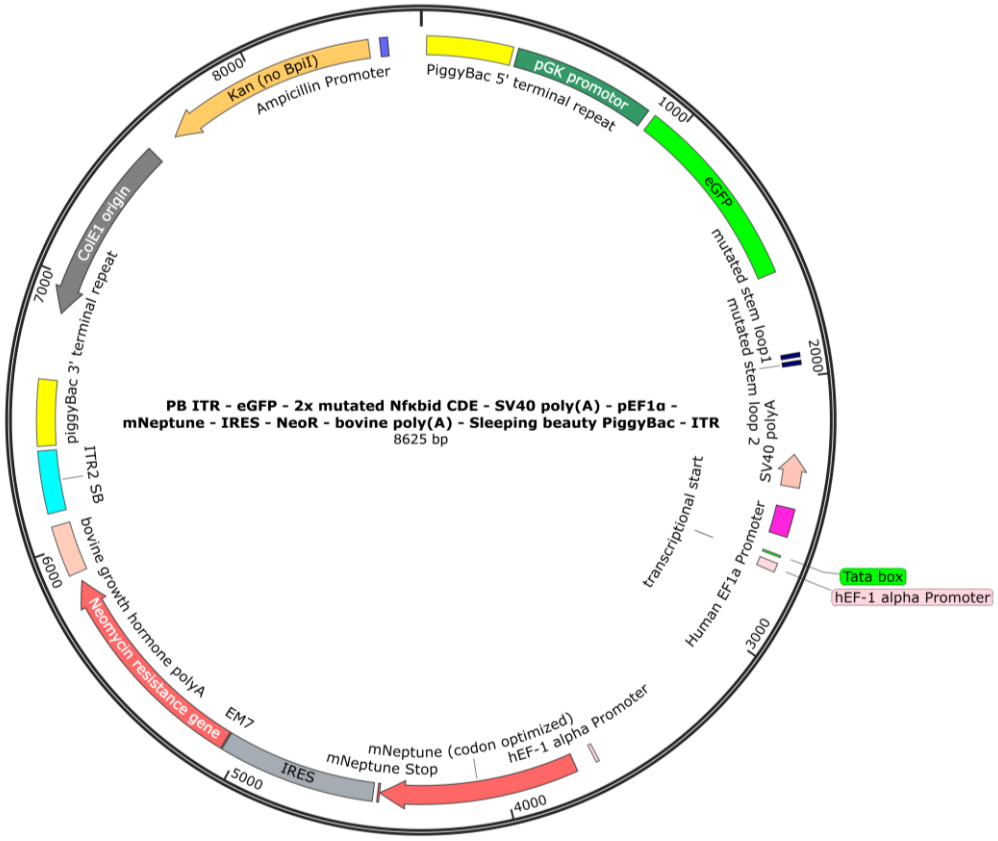

Supplemental Figure 13: Nfκbid mutated CDE vector map used for A20 cell manipulation

Supplemental Figure 14: Hyperactive *piggyBac* encoding plasmid used for A20 cell manipulations

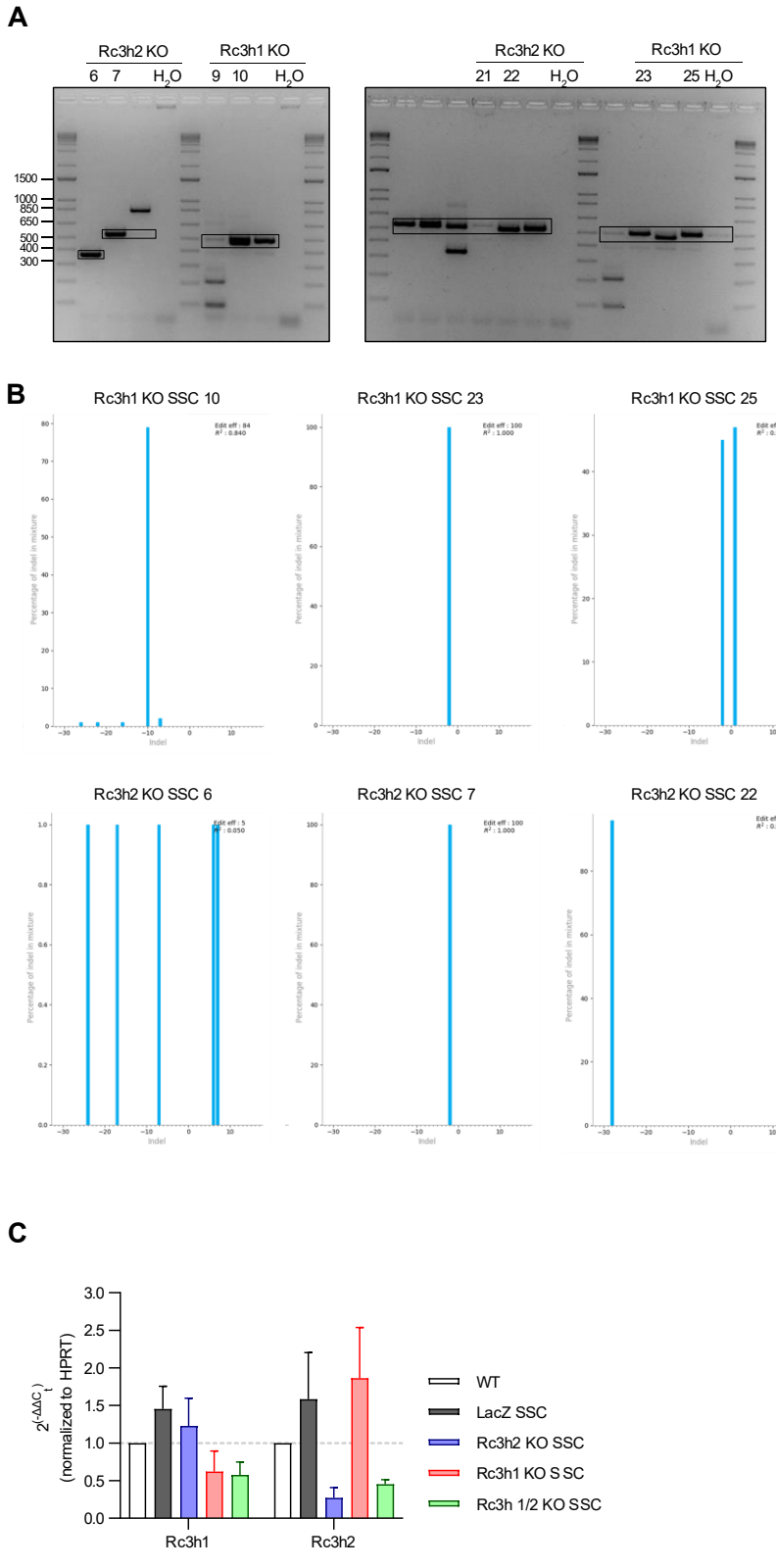

Supplemental Figure 15: Roquin knockout SSC generation in A20 cells.
(A) Agarose gel image visualizing PCR products of isolated genomic DNA using primers approx. 300 bp up- and dowsntream of the respective sgRc3h1 or sgRc3h2 cut-site. Indicated bands were cut, gel purified and used for further indel sequencing analysis. (B) Indel sequencing analysis results generated by Synthego online software for individual Roquin KO clones. (C) qRT-PCR analysis of Roquin 1 or Roquin 2 RNA levels in indicated SSCs normalized to bulk WT cells. Data are cumulative of 2 independent experiments. Bars show mean values ± SD.

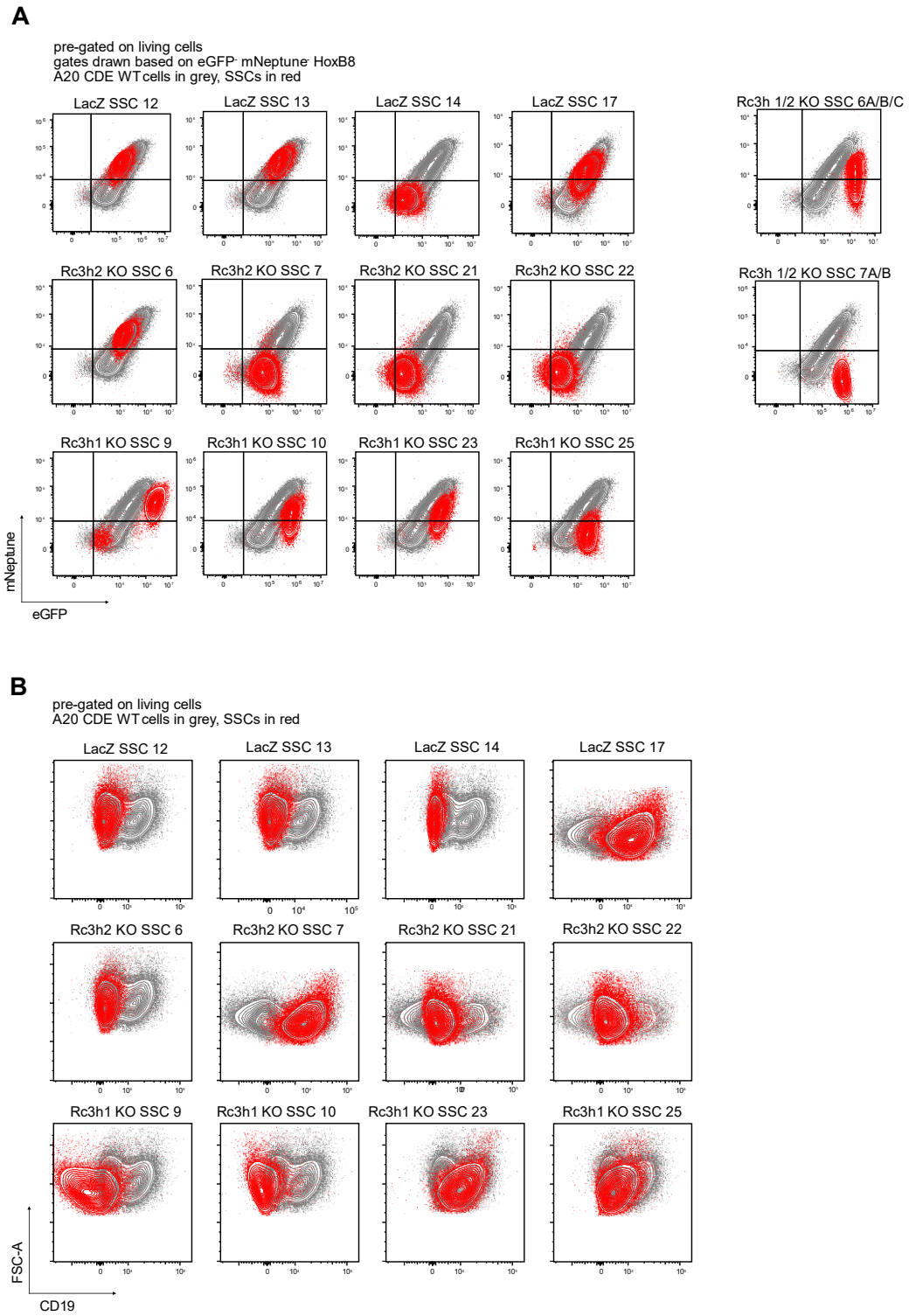

Supplemental Figure 16: Differences of eGFP, mNeptune and CD19 expression levels in Roquin knockout SSCs.
(A) Flow cytometry plots of mNeptune and eGFP in Roquin KO SSCs. (B) Same as in (A), but shown for CD19 expression levels.

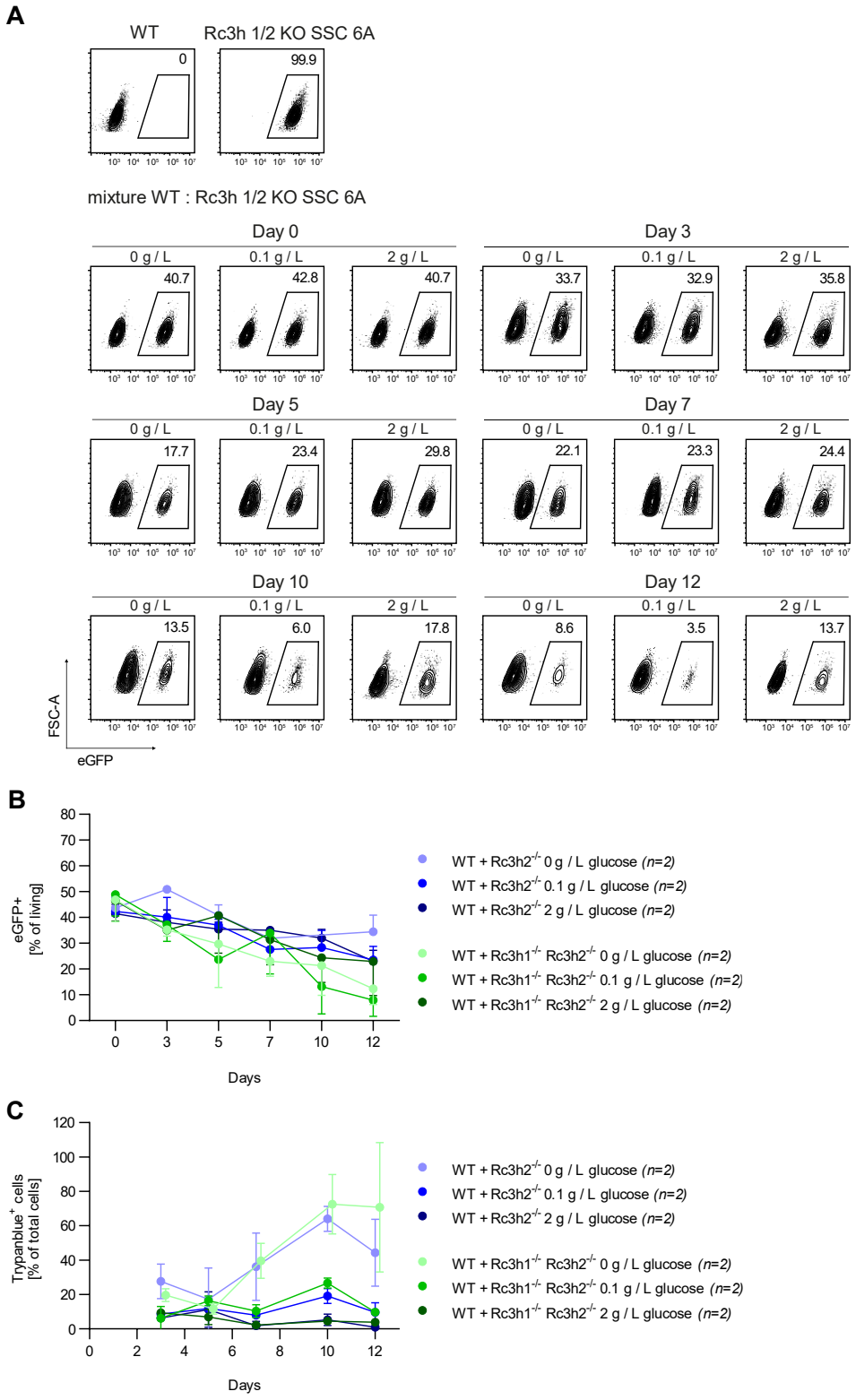

Supplemental Figure 17: Competition assay challenging Roquin knockout SSC growth in presence of WT cells in different media composition.
(A) Representative flow cytometry plots showing depletion of Roquin 1/2 double KO SSC 6A over time when mixed 1:1 with A20 WT cells and treated with different glucose-containing media. Percentages indicate the proportion of GFP^{hi} cells of living cells in the shown sample. (B) Fraction of Roquin knockout cells ($eGFP^{+}$) in a Roquin knockout and A20 WT mixed culture over time in 0 g / L, 0.1 g / L or 2 g / L glucose containing media. (C) Percentage of dead cells in mixed cultures over time determined via trypanblue manual cell counting irrespective of the cell genotype. Data points show mean values ± SD. Data are cumulative from 2 biological replicates measured in one experiment.

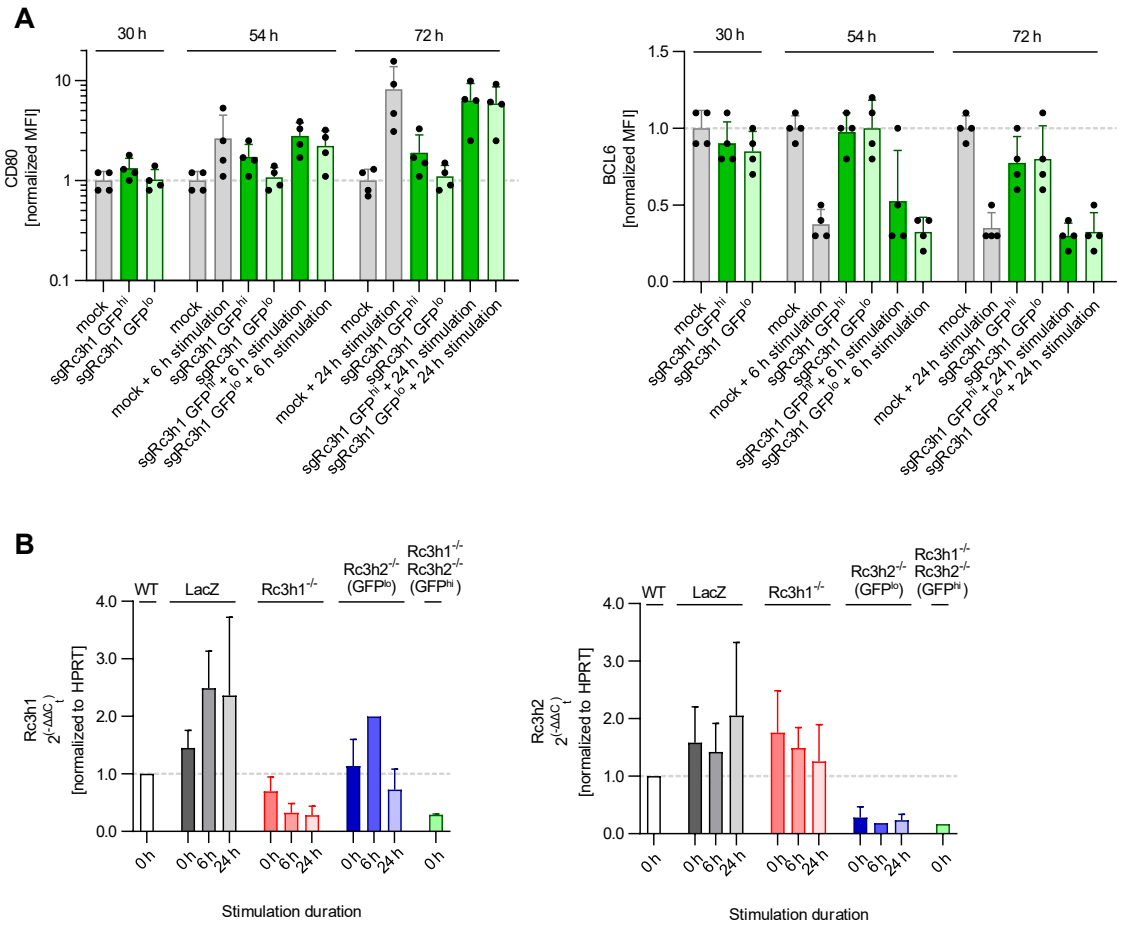

Supplemental Figure 18: RNAseq sample characterization.
(A) Protein expression levels of CD80 and BCL6 at indicated time-points and treatments normalized to mock treatment per timepoint and experiment. Bars show mean values ± SD. Data are cumulative for 4 biological replicates and 2 independent experiments. (B) Roquin 1 or Roquin 2 mRNA levels measured by RT-qPCR in stimulated and unstimulated LacZ SSCs, Roquin 1 SSCs, induced Roquin 1/2 double knockout clones sorted for eGFP^{lo} (Rc3h2$^{-/-}$) or eGFP^{hi} (Rc3h1$^{-/-}$ Rc3h2$^{-/-}$) normalized to WT bulk A20 cells. Bars show mean values ± SD. Data are cumulative for 1-4 biological replicates and 2 independent experiments.

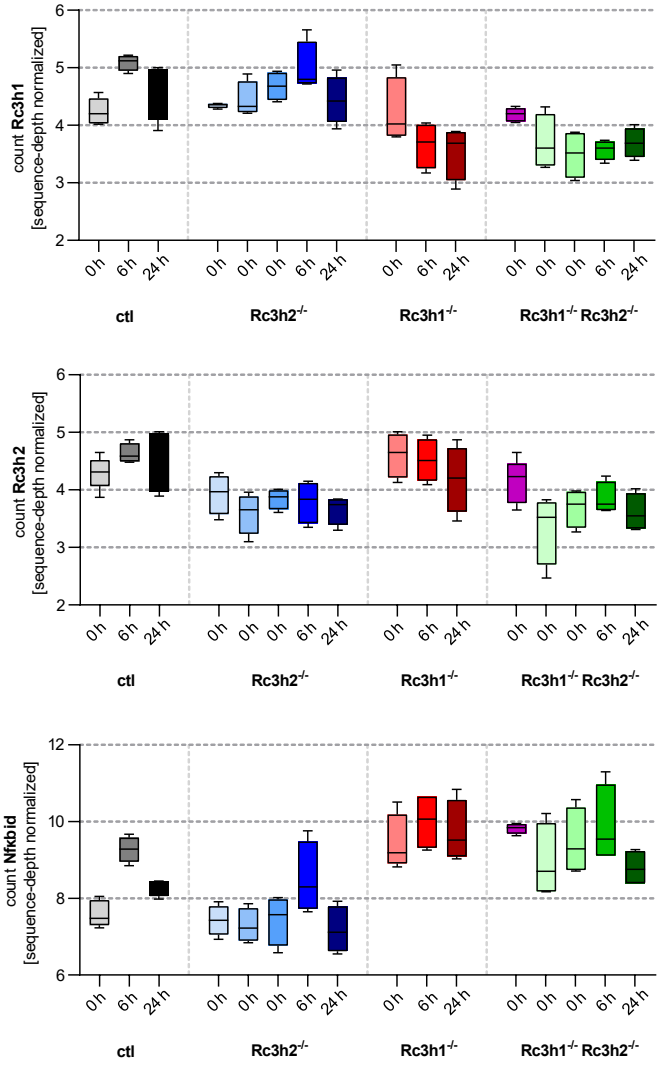

Supplemental Figure 19: RNAseq sample characterization.
Sequence depth normalized counts between all samples for Roquin 1 (top), Roquin 2 (middle) and Nfκbid (bottom).

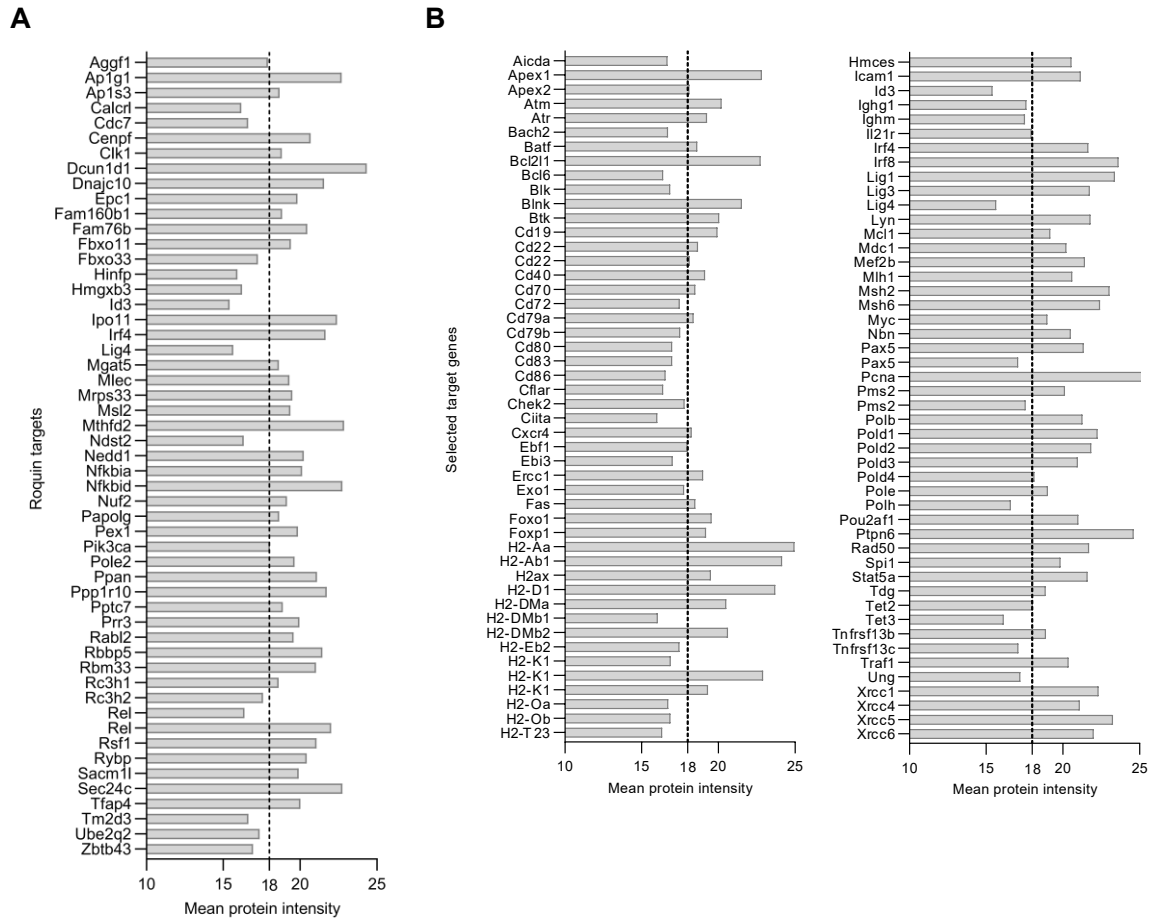

Supplemental Figure 20: Mean protein intensities of Roquin target genes and selected target genes in proteome analysis of A20 SSCs.
(A) Mean protein intensities of 53 Roquin target genes detected in proteome analysis of A20 SSCs in alphabetical order. Mean was calculated considering all samples analyzed independent of stimulation status or genotype. (B) Mean protein intensities of 96 selected target genes detected in proteome analysis of A20 SSCs in alphabetical order. Mean was calculated considering all samples analyzed independent of stimulation status or genotype.

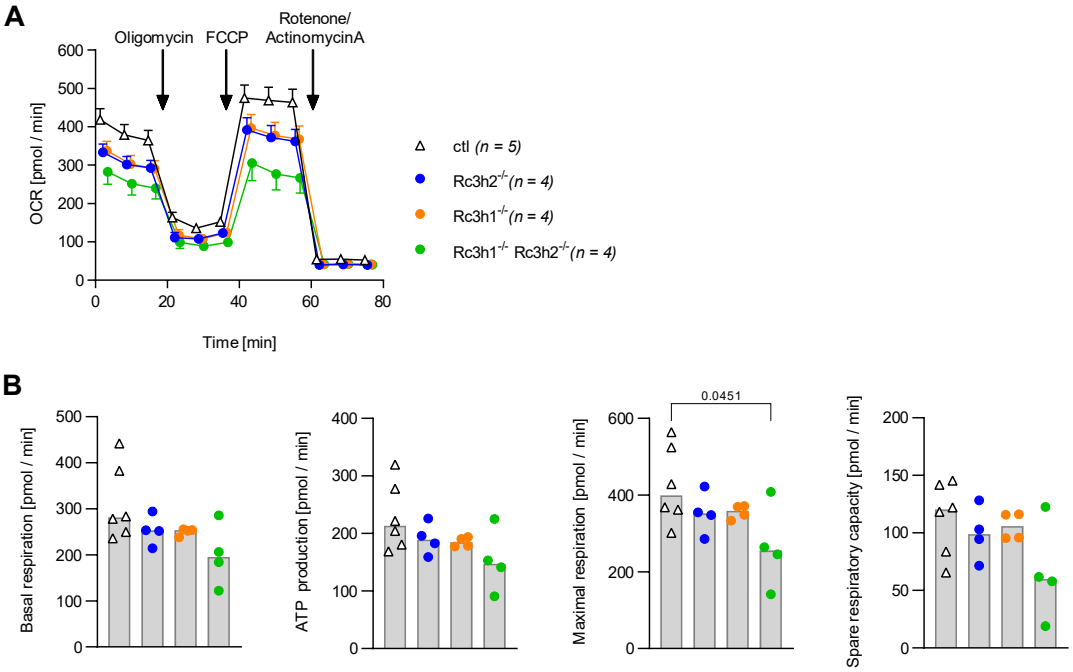

Supplemental Figure 21: Seahorse XF Cell Mito stress test in A20 Roquin KO cells.
(A) OCR measurements over time for A20 WT, A20 CDE WT and LacZ SSC 12 / 13 / 14 / 17 (ctl), Rc3h2 KO SSC 6 / 7 / 21 / 22 (Rc3h2$^{-/-}$), Rc3h1 KO SSC 9 / 10 / 23 / 25 (Rc3h1$^{-/-}$) and Rc3h 1/2 KO SSC 6B / 6C / 7B / 7C (Rc3h1$^{-/-}$ Rc3h2$^{-/-}$). Plotted are mean values + SEM. Each sample was measured in technical triplicates. (B) Assay parameters calculated by the Agilent Software. Bars show mean values. Each dot represents the average of one sample measured in technical triplicates. Statistical significance was determined by one-way ANOVA and p values are shown. Data are cumulative for 2 independent experiments.

Supplementary Tables

Table S1: Roquin targets in alphabetical order (taken from Leppek et al.)[92].
Genes written in black were also detected to be expressed in 3'-bulk RNAseq data of *ex vivo* GCBs (data not shown).

0610030E20Rik	Dpy19l4	Mlec	Rc3h1
2410042D21Rik	Epc1	Mrps33	Rc3h2
4732418C07Rik	Etaa1	Msl2	Rel
4732471D19Rik	Fam160b1	Mthfd2	Rsf1
5830415F09Rik	Fam76b	Ndst2	Rybp
Adamts1	Fam84b	Nedd1	Sacm1l
Agbl3	Fbxo11	Nfkbia	Sec24c
Aggf1	Fbxo33	Nfkbid	Slc35e3
AI597479	Gm527	Nfkbiz	Slc39a14
Ap1g1	Hcst	Nfxl1	Smek2
Ap1s3	Hinfp	Nuf2	Ss18l1
B4galt5	Hmgxb3	Papolg	Tcf7l2
B630005N14Rik	Id1	Pex1	Tfap4
Bmpr1a	Id2	Pik3ca	Tigd5
Calcrl	Id3	Pik3cb	Tm2d3
Cdc7	Ier3	Pole2	Tmem2
Cdon	Il6	Ppan	Tnf
Cenpf	Ipo11	Ppp1r10	Tnfaip3
Cgrrf1	Irf4	Pptc7	Tnfrsf4
Clk1	Kctd6	Prr3	Ube2q2
Csf3	Lfng	Ptger4	Usp53
D030056L22Rik	Lig4	Ptpre	Zbtb43
D5Ertd579e	Lysmd4	Rabl2	Zc3h12
Dcun1d1	Map3k8	Rbbp5	Zfp367
Dnajc10	Mgat5	Rbm33	Zfp408

Table S2: "TNFα-signaling via NfκB" pathway members significantly upregulated in unstimulated Roquin 1/2 double knockout SSCs as shown in Fig. 40B (www.uniprot.org and www.genecards.org)

Gene	Full name	Function
Bcl3	B cell lymphoma 3 protein homolog	Contributes to the regulation of transcriptional activation of NF-kappa-B target genes. In the cytoplasm, inhibits the nuclear translocation of the NF-kappa-B p50 subunit.In the nucleus, acts as transcriptional activator that promotes transcription of NF-kappa-B target genes. Contributes to the regulation of cell proliferation
Btg1	Btg1	Anti-proliferative protein
Btg2	Btg2	Anti-proliferative protein by association with the CCR4-NOT complex
Ccnl1	Cyclin-L1	Cell cycle regulator
CD80	CD80	Membrane receptor; costimulatory surface molecule activated by binding of CD28 and CTLA4
CD83	CD83	Cell surface protein involved in the regulation of antigen presentation
Cdkn1a	Cyclin-dependent kinase inhibitor 1	Blockage of cell cycle progression; p53-mediated inhibition of proliferation in response to DNA damage
Cebpb	CCAART enhancer binding protein beta	Transcription factor; repressor of Myc in T cells; regulation of genes involved in inflammatory and immune responses
Dusp1	Dual specificity protein phosphatase	Phosphatase negatively regulating members of the MAP kinase superfamily in particularly Mapk1 and Erk2 thereby negatively influencing cell proliferation and differentiation
Dusp2	Dual specificity protein phosphatase	Phosphatase negatively regulating members of the MAP kinase superfamily in particularly Erk1 and Erk2 thereby negatively influencing cell proliferation and differentiation
Dusp5	Dual specificity protein phosphatase	Phosphatase negatively regulating members of the MAP kinase superfamily (MAPFK/ERK/Jnk/CD38) thereby negatively influencing cell proliferation and differentiation
Egr1	Early growth response protein 1	Transcriptional regulator; activates expression of p53; regulation of cell survival, proliferation and cell death
Egr2	E3 sumo protein ligase 2	Transcription factor
Eif1a	Eucaryotic translation initiation factor 1	Involved in translation initiation
Efna1	Ephrin-A1	Cell surface ligand for Ephrin receptors on adjacent cells leading to contact dependent bidirectional signaling
Esrrg	Estrogen-related receptor gamma	Orphan receptor
Fos	c-Fos	Nuclear phosphoprotein binding to Jun
FosB	FosB	Enhances DNA binding activity of Jun family proteins; plays a role in activation-induced cell death of T cells
Gem	GTP-binding protein Gem	GTP-binding protein
Id2	DNA-binding protein inhibitor Id2	Transcriptional regulator implicated in the regulation of cel growth, senescence, differentiation and apoptosis
Ier2	Immediate early response gene 2	DNA-binding protein; involved in cell motility
Ier5	Immediate early response gene 5	Transcription factor; positive transcriptional regulation of chaperones; regulation of thermal stress
Il6st	Interleukin 6 receptor subunit beta	Receptor of Il6 among others
Irf1	Interferon regulatory factor 1	Transcriptional regulator of IFN-inducible genes, cell cycle and inflammation; induction of growth arrest and programmed cell death following DNA damage
Jun	Transcription factor Jun	Transcription factor; proto-oncogene
JunB	JunB	Transcription factor; proto-oncogene

Table S2 (continued): "TNFα-signaling via NfκB" pathway members significantly upregulated in unstimulated Roquin 1/2 double knockout SSCs as shown in Fig. 40B (www.uniprot.org and www.genecards.org)

Gene	Full name	Function
Klf2	Krueppel-like factor 2	Transcription factor recognizing GC box elements
Klf6	Krueppel-like factor 6	Transcription factor recognizing GC box elements
Klf9	Krueppel-like factor 9	Transcription factor recognizing GC box elements
Maf	Maf Bzip transcription factor	Transcription factor
Marcks	Marcks-related protein	Involved in cell migration control
Mcl1	Induced myeloid leucemia cell differentiation protein Mcl1 homolog	Belongs to the Bcl2 family; anti-apoptotic activity of the isoform 1 and pro-apoptotic activity of the isoform 2
Nr4a1	Nuclear receptor subfamily 4 group a member 1	Orphan nuclear receptor; may inhibit NfκB transactivation of IL2; participates in energy homeostasis
Phlda1	Pleckstrin homology-like domain family A member 1	Mediator of apoptosis
Plpp3	Phospholipid phosphatase 3	Phosphatase dephosphorylating glycerolipids and sphingolipid phosphate esters regulating lipid homeostasis
Ppp1r15a	Protein phosphatase 1 regulatory subunit 15A	Phosphatase preventing excessive phosphorylation of the translation initiation factor eIF-2/EIF2S1; may promote apoptosis through p53
Rela	Transcription factor p65	Rel-like domain containing protein most often in complex with Nfκb1 acting as transcriptional activator
Rhob	Rho-related GTP-binding protein RhoB	Mediates apoptosis in neoplastically transformed cells after DNA damage
Sik1	Serine/threonine-protein kinase	Involved in processes such as cell cycle, gluconeogenesis, differentiation; required for p53 phosphorylation in response to loss of adhesion; repressor of CRTC1/TORC1 and CRT2/TORC2
Sqstm1	Sequestosome-1	Autophagy receptor and regulator of NfκB1 via TNFα; adaptor that mediates the interaction between Traf6 and Cyld
Tank	TRAF family member associated NfκB activator	Adaptor protein; negatively regulates NFκB signaling and cell survival upon DNA damage
Tap1	Antigen peptide transporter 1	Translocation of peptide antigen from the cytosol to the ER
Tgif1	Homeobox protein Tgif1	Transcriptional regulator
Tnfsf9	Tumor necrosis factor ligand superfamily member 9	Cytokine binding to TNFRSF9; may play a role in cognate T-B cell interaction or activation-induced cell death
Yrdc	Threonylcarbamoyl-AMP synthase	Cytoplasmic and mitochondrial threonylcarbamoyl-AMP synthase
Zfp36	mRNA decay activator protein Zfp36	RBP facilitating cytoplasmic mRNA decay

Table S3: Significantly regulated proteins in Roquin 1 knockout A20 SSCs compared to controls as shown in Fig. 42C (www.uniprot.org and www.genecards.org)

Gene	Full name	Function
Avil	Advillin	Ca^{2+} regulated actin-binding protein
Lpin2	Phosphatidate phosphatase LPIN2	Acts as a magnesium-dependent phosphatidate phosphatase enzyme which catalyzes the conversion of phosphatidic acid to diacylglycerol during triglyceride, phosphatidylcholine and phosphatidylethanolamine biosynthesis in the reticulum endoplasmic membrane
Mier1	Mesoderm induction early response protein 1	Transcriptional repressor regulating the expression of a number of genes including SP1 target genes. Probably functions through recruitment of HDAC1 a histone deacetylase involved in chromatin silencing.
Mier3	Mesoderm induction early response protein 3	Transcriptional repressor.
Plek	Pleckstrin	Major protein kinase C substrate of platelets.
Smox	Spermine oxidase	Flavoenzyme which catalyzes the oxidation of spermine to spermidine. Plays an important role in the regulation of polyamine intracellular concentration

Table S4: Differentially downregulated transcripts both in Roquin 1/2 double knockout SSCs at steady state and in induced Roquin 1/2 double knockout SSCs 30 h and / or 54 h after electroporation as visualized in Fig. 43D (www.uniprot.org and www.genecards.org)

Gene	Full name	Function
H2-Ab1	H2-Ab1	MHCII protein complex binding
H2-Ea	H2-Ea	MHCII protein complex binding
Laptm5	Lysosomal-associated transmembrane protein 5	May have a special functional role during embryogenesis and in adult hematopoietic cells
Mybl1	Myb-related protein A	Transcription factor
Parm1	Prostate androgen-regulated mucin-like protein 1 homolog	May regulate telomerase activity
Pir	Pirin	Transcriptional coregulator of NFκB
Pou2af1	POU domain class 2-associating factor 1	Transcriptional coactivator; essential for the response of B-cells to antigens and required for the formation of germinal centers
Sh3bp5	SH3 domain-binding protein 5	Functions as guanine nucleotide exchange factor
Slamf7	SH2 domain-containing protein 1B	Cytoplasmic adapter regulating receptors of the signaling lymphocytic activation molecule (SLAM) family

Table S5: Differentially upregulated transcripts both in Roquin 1/2 double knockout SSCs at steady state and in induced Roquin 1/2 double knockout SSCs 30 h and / or 54 h after electroporation as visualized in Fig. 43D (www.uniprot.org and www.genecards.org)

Gene	Full name	Function
Bid	BH3-interacting domain death agonist	Induces caspases and apoptosis
Cd9	CD9 antigen	Integral membrane protein associated with integrins
Cog2	Conserved oligomeric Golgi complex subunit 2	Required for golgi function
Cox11	Cytochrome c oxidase assembly protein	Effect at some terminal stage of cytochrome c oxidase synthesis
Cxcr5	C-X-C chemokine receptor type 5	Cytokine receptor that binds to B-lymphocyte chemoattractant
Grn	Progranulin	Secreted protein that acts as a key regulator of lysosomal function and as a growth factor involved in inflammation and cell proliferation
Hnrnpa1	Heterogeneous nuclear ribonucleoprotein A1	Transport of poly(A) mRNA from the nucleus to the cytoplasm
Il10	Interleukin 10	Cell surface cytokine
Marcks	Marcks-related protein	Involved in cell migration control
Mpeg1	Macrophage expressed gene 1 protein	Required for antibacterial activity
Nfκbid	NF-kappa-B inhibitor delta	Regulates the expression of IL-2, IL-6, and other cytokines through regulation on NF-kappa-B activity
Pim2	Serine/threonine-protein kinase pim-2	Proto-oncogene with serine/threonine kinase activity involved in cell survival and cell proliferation
Ppan	peter pan homolog	Suppressor of mitochondrial apoptosis
Polr1c	DNA directed RNA polymerases I and III subunit RPAC1	Component of the RNA polymerases I and III
Sema3b	Semaphorin 3B	Function in growth during neuronal development
Shox2	Short stature homeobox protein 2	growth regulator
Tm2d3	TM2 domain-containing protein 3	Transmembrane protein; highest expression levels in APCs according to immgen
Tnfsf9	Tumor necrosis factor ligand superfamily member 9	Cytokine binding to TNFRSF9; may play a role in cognate T-B cell interaction or activation-induced cell death
Traf5	TNF receptor-associated factor 5	Adapter protein and signal transducer; mediates activation of NfκB
Tyw3	tRNA wybutosine-synthesizing protein 3 homologue	Methyltransferase
Ubald2	UBA-like domain-containing protein 2	Unknown
Unc119	Protein unc-119 homolog A	Involved in the signal transduction in immune cells as a Src family kinase activator

Table S6: Significantly regulated transcripts and proteins in Roquin 1 knockout A20 SSCs compared to controls after 6 h of stimulation as shown in Fig. 44F (www.uniprot.org and www.genecards.org)

Gene	Full name	Function
Atp6v0a1	V-type proton ATPase	A multisubunit enzyme composed of a peripheral complex (V1) that hydrolyzes ATP and a membrane integral complex (V0) that translocates protons
Ciita	MHC class II transactivator	Essential for transcriptional activity of the HLA class II promoter
Cd70	CD70 antigen	Cytokine which is the ligand for CD27
Cyb561a3	Lysosomal membrane ascorbate-dependent ferrireductase	Transmembrane reductase
H2-Aa	H2-Aa	MHCII protein complex binding
H2-Ab1	H2-Ab1	MHCII protein complex binding
Il4i1	L-amino-acid oxidase	Secreted L-amino-acid oxidase which regulates the development and function of B-cells
Lipg	Gastric triacylglycerol lipase	Catalyzes the hydrolysis of triacylglycerols to yield free fatty acids
Nucb2	Nucleobindin-2	Calcium-binding protein
Stap1	Signal-transducing adaptor protein 1	May function as an adapter molecule downstream of KIT in the proliferation or differentiation of hematopoietic stem cells.
Tmsb4x	Thymosin beta-4	Plays an important role in the organization of the cytoskeleton
Traf1	TNF receptor-associated factor	Adapter molecule that regulates the activation of NF-kappa-B and JNK

Table S7: Differentially regulated Roquin targets in alphabetical order and their function related to B cell biology (www.uniprot.org and www.genecards.org)

Gene	Full name	Function
Aggf1	Angiogenic factor with G patch and FHA domains 1	Upregulated in gastric cancers possibly promoting migration and EMT through Wnt signaling[234]
Ap1s3	AP-3 complex subunit sigma-1	Part of the AP-3 complex, an adaptor-related complex which is not clathrin-associated.
Calcrl	Calcitonin gene-related peptide type 1 receptor	Receptor for calcitonin-gene-related peptide (CGRP)
Cenpf	Centromere protein F	Microtubule binding protein necessary for proper kinetochore attachments and thus chromosome separation during cell division[235]; knockout fosters OXPHOS and glycolysis in prostate cancer cells[236]; not expressed in FOB or splenic PC, but PCs of the bone-marrow (www.immgen.org)
Clk1	Dual specificity protein kinase	Clk1 is a kinase localized in the nucleus and cytoplasm which modifies the activity of splice factors and spliceosome components. In addition, Clk1 is important for correct cytokinesis through phosphorylation of Aurora B at the midbody which delays abscission upon unwanted chromatin bridges and therefore inhibits chromatin breakage and DNA damage. Additionally, Clk1 is a target of the AKT-mTORC1/2 pathway in B cells[237,238]. Within the B cell lineage, Clk1 expression intensities are higher in naïve B cells than GCBs (www.immgen.org).
Etaa1	Ewing's tumor-associated antigen 1	Etaa1 ensures proper cell division in unstressed cells via correct alignment of chromosomes during metaphase, attachment of chromosomes to the spindle apparatus and activation of Aurora B through the DNA damage response kinase ATR during cytokinesis[239]. Upon replication stress due to dsDNA breaks or stalled replication forks during S-phase, Etaa1 directly binds to RPA and activates ATR to resolve the DNA errors and maintain cell survival[240]. Etaa1 deficient cells are compromised in their ability of mitotic arrest upon DNA damage and therefore suffer from genomic instability[241]. Etaa1 deficient mice fail to generate effector $CD4^+$ and $CD8^+$ T cells after TI immunization, but display otherwise normal T and B lymphocyte development. The investigators argue that particularly in fast proliferating cells, Etaa1 proteins become rate-limiting which causes accumulation of DNA damage and upregulation of p53 mediated stress response leading to diminished cell survival. This is in line with deficits in T_{FH} and GCB formation upon bone marrow transplants of Etaa1 knockout $CD45.2^+$ cells into $CD45.1^+$ congenic mice[242].
Fam160b1	FHF complex subunit HOOK interacting protein 2A	May be required for proper functioning of the nervous system.
Gm527	Gene 527	Unknown
Ipo11	Importin 11	Protein transport into the nucleus including ß-catenin and Ran[243,244]
Kctd6	Potassium channel tetramerization domain containing 6	Part of an E3 ubiquitin ligase complex; low expression associates to poor prognosis in non-small lung cancer patients[245]
Mlec	Malectin	Carbohydrate binding protein in the endoplasmatic reticulum[246]; particularly high expressed in plasmablasts
Msl2	E3 ubiquitin protein ligase Msl2	Monoubiquitination of histone H2B
Nfκbia	NF-kappa-B inhibitor alpha	Inhibits the activity of dimeric NF-kappa-B/REL complexes by trapping REL dimers in the cytoplasm through masking of their nuclear localization signals.

Table S7 (continued): Differentially regulated Roquin targets in alphabetical order and their function related to B cell biology (www.uniprot.org and www.genecards.org)

Gene	Full name	Function
Nfκbiz	Nuclear factor NF-kappa-B p105 subunit	NF-kappa-B is a pleiotropic transcription factor present in almost all cell types. Studies in $Nfκbiz^{F/F}$ $Mb1Cre^{I/-}$ mice revealed a function of IκBζ in positively regulating CSR through AID[247]. IκBζ expression is induced TLR mediated by LPS and IL4 as well as by BCR stimulation[248].
Nuf2	Kinetochore protein	Acts as a component of the essential kinetochore-associated NDC80 complex, which is required for chromosome segregation and spindle checkpoint activity.
Pole2	DNA polymerase epsilon subunit 2	Functions in DNA repair and replication
Ppan	Peter pan homolog alias suppressor of SWI4 1 homolog	The Wnt signaling target Ppan shuttles between the nucleolus where it facilitates ribosome biogenesis and mitochondria where it has been shown to avoid mitochondrial apoptosis through inhibition of BAX-mediated membrane permeabilization. Upon cellular stress induction, Ppan accumulates in mitochondria acting as a suppressor of apoptosis in HEK293T cells. Knockdown of Ppan is associated with G0/G1 cell cycle arrest, less frequent cytokinesis and elevated numbers of binucleated cells in HeLa[249,250]. According to the immgen RNAseq databrowser, GCBs are one of the highest Ppan expressing cell types.
Pptc7	Protein phosphatase PTC7 homolog	Protein phosphatase which positively regulates biosynthesis of the ubiquinone, coenzyme Q.
Rel	Proto-oncogene c-Rel	Proto-oncogene that may play a role in differentiation and lymphopoiesis. Experiments in immunized $Cγ1Cre^{I/+}$ $Rel^{F/F}$ mice could show that cRel is mandatory for GC maintenance from day 7 to day 14, but is dispensable for plamablastic differentiation. cRel ablation causes downregulation of genes involved in fatty acid metabolism and glycolysis. Hence, cRel is probably needed to maintain a metabolic program supporting the demands of highly proliferating GCBs[214]. On the contrary, gain of cRel expression causes expansion of GCBs and class-switches APCs in secondary lymphoid organs. GSEA analysis thereby revealed an enrichment in cell cycle related, metabolism related and myc related gene signatures[224].
Tfap4	BHLH domain-containing protein	unknown
Tm2d3	TM2 domain-containing protein 3	Transmembrane protein; highest expression levels in APCs (www.immgen.org).
Ube2q2	Ubiquitin-conjugating enzyme E2	Needed for cell cycle progression during mitotic prophase[251]

Table S8: Significantly upregulated (left) or downregulated (right) proteins in Roquin 1 knockout A20 SSCs compared to controls after 6 h of stimulation as visualized in Fig. 44E. Top hits with a Welch's T-test Difference > 1.0 (left) or < -1 (right) are displayed.

Genes	Welch's T-test Difference $Rc3h1^{-/-}$ vs ctl	Genes	Welch's T-test Difference $Rc3h1^{-/-}$ vs ctl
Cd70	4.49	Avil	-3.04
Hnrnpll	3.51	Il4i1	-2.47
Klhl14	3.15	Aif1l	-2.34
Cyb561a3	2.31	Ciita	-2.14
Tnfsf9	2.17	Lst1	-2.02
Ggh	1.99	Pag1	-1.68
Slc2a6	1.92	Plek	-1.54
Cemip2	1.83	H2-Ab1	-1.37
Rbm47	1.79	H2-Aa	-1.36
Bcl3	1.76	Lipg	-1.35
Histone	1.60	Clec12a	-1.34
Ugdh	1.58	Stap1	-1.14
St14	1.58	Rassf6	-1.07
Ftl1	1.55	Psen2	-1.06
Tnfrsf8	1.54	Traf4	-1.04
Itln1b	1.50		
Grn	1.48		
Gab2	1.43		
Asph	1.42		
Ssh1	1.41		
Cox6a1	1.41		
Gm2a	1.41		
Pstpip2	1.39		
Pcbp4	1.34		
Cryl1	1.33		
Lpin2	1.30		
Histone	1.29		
Tmsb4x	1.23		
Pigbos1	1.21		
Mcoln2	1.20		
Sorbs1	1.18		
Pld6	1.17		
Ahdc1	1.16		
Baiap2	1.16		
Acp3	1.10		
Mpeg1	1.10		
Nradd	1.08		
Man1a1	1.08		
Nucb2	1.08		
Grb7	1.07		
Sub1	1.07		
Cars2	1.02		

Table S9: Selection of signaling genes as well as genes involved in GCB and APC development based on literature
Genes written in italic were detected by mass-spectrometry.

BCR signaling	MHCII components	CD40 signaling	CSR	GCB state related genes	APC state related genes
Blk	*H2-Aa*	*Bcl2l1*	*Aicda*	*Bach2*	Cd27
Blnk	*H2-Ab1*	Ccl22	*Apex1*	Bcl2	Id2
Btk	H2-Bl	*Cd40*	*Apex2*	*Bcl6*	Il10
Cd19	*H2-D1*	*Cd80*	*Atm*	Cd27	*Irf4*
Cd22	*H2-DMa*	*Cd86*	*Atr*	*Cd70*	*Mcl1*
Cd72	*H2-DMb1*	*Cflar*	*Batf*	*Cd83*	Prdm1
Cd79a	*H2-DMb2*	*Ebf1*	*Chek2*	*Ciita*	*Tet2*
Cd79b	H2-Ea	*Ebi3*	*Ercc1*	*Cxcr4*	*Tet3*
Cla	H2-Eb1	*Icam1*	*Exo1*	Efnb1	*Tnfrsf13b*
Fcrl2	*H2-Eb2*	Mir155hg	*H2ax*	*Fas*	Tnfrsf17
Lyn	*H2-K1*	*Stat5a*	*Hmces*	*Foxo1*	Xbp1
Ptpn6	H2-K2	*Traf1*	*Lig1*	*Foxp1*	
	H2-Ke6		*Lig3*	Icosl	
	H2-M10.1		*Lig4*	*Id3*	
	H2-M2		*Mdc1*	Igha	
	H2-M3		*Mlh1*	Ighd	
	H2-M5		Mre11a	Ighe	
	H2-Oa		*Msh2*	*Ighg1*	
	H2-Ob		*Msh6*	Ighg2b	
	H2-Q1		*Nbn*	Ighg2c	
	H2-Q10		*Pcna*	Ighg3	
	H2-Q2		*Pms2*	*Ighm*	
	H2-Q3		*Polb*	*Il21r*	
	H2-Q4		*Pold1*	Il6	
	H2-Q5		*Pold2*	Il6r	
	H2-Q6		*Pold3*	*Irf8*	
	H2-Q7		*Pold4*	*Mef2b*	
	H2-T10		*Pole*	*Myc*	
	H2-T22		*Polh*	*Pax5*	
	H2-T23		Prkdc	*Pou2af1*	
	H2-T24		*Rad50*	Relt	
	H2-T3		Rev3l	S1pr2	
	H2-T-ps		Shld1	*Spi1*	
			Shld33	Spib	
			Tdg	*Tnfrsf13c*	
			Trp53bp1	Tnfsf11	
			Ung	Tnfsf4	
			Xrcc1		
			Xrcc4		
			Xrcc5		
			Xrcc6		

References

1. Gebauer, F., Schwarzl, T., Valcárcel, J. & Hentze, M. W. RNA-binding proteins in human genetic disease. *Nat Rev Genet* 22, 185–198 (2021).

2. Tavernier, S. J. *et al.* A human immune dysregulation syndrome characterized by severe hyperinflammation with a homozygous nonsense Roquin-1 mutation. *Nat Commun* 10, 4779 (2019).

3. Vinuesa, C. G. *et al.* A RING-type ubiquitin ligase family member required to repress follicular helper T cells and autoimmunity. *Nature* 435, 452–458 (2005).

4. Akira, S., Uematsu, S. & Takeuchi, O. Pathogen Recognition and Innate Immunity. *Cell* 124, 783–801 (2006).

5. Murphy, K. & Weaver, C. Janeway Immunologie. 3–46 (2018) doi:10.1007/978-3-662-56004-4_1.

6. Goodnow, C. C., Sprent, J., Groth, B. F. de S. & Vinuesa, C. G. Cellular and genetic mechanisms of self tolerance and autoimmunity. *Nature* 435, 590–597 (2005).

7. Goodnow, C. C. Multistep Pathogenesis of Autoimmune Disease. *Cell* 130, 25–35 (2007).

8. Goodnow, C. C., Vinuesa, C. G., Randall, K. L., Mackay, F. & Brink, R. Control systems and decision making for antibody production. *Nat Immunol* 11, 681–688 (2010).

9. Dinse, G. E. *et al.* Increasing Prevalence of Antinuclear Antibodies in the United States. *Arthritis Rheumatol* 72, 1026–1035 (2020).

10. Herzog, S., Reth, M. & Jumaa, H. Regulation of B-cell proliferation and differentiation by pre-B-cell receptor signalling. *Nat Rev Immunol* 9, 195–205 (2009).

11. Melchers, F. Checkpoints that control B cell development. *J Clin Invest* 125, 2203–2210 (2015).

12. Clark, M. R., Mandal, M., Ochiai, K. & Singh, H. Orchestrating B cell lymphopoiesis through interplay of IL-7 receptor and pre-B cell receptor signalling. *Nat Rev Immunol* 14, 69–80 (2014).

13. Luc, S., Buza-Vidas, N. & Jacobsen, S. E. W. Delineating the cellular pathways of hematopoietic lineage commitment. *Semin Immunol* 20, 213–220 (2008).

14. Martin, F. & Kearney, J. F. Marginal-zone B cells. *Nat Rev Immunol* 2, 323–335 (2002).

15. Pillai, S. & Cariappa, A. The follicular versus marginal zone B lymphocyte cell fate decision. *Nat Rev Immunol* 9, 767–777 (2009).

16. Lewis SM, Williams A, Eisenbarth SC. Structure and function of the immune system in the spleen. *Sci Immunol*. 2019;4(33):eaau6085.

17. Palm, A.-K. E. & Kleinau, S. Marginal zone B cells: From housekeeping function to autoimmunity? *J Autoimmun* 119, 102627 (2021).

18. Chaudhry, M. S. & Karadimitris, A. Role and Regulation of CD1d in Normal and Pathological B Cells. *J Immunol* 193, 4761–4768 (2014).

19. Fearon, D. T. & Carroll, M. C. Regulation of B Lymphocyte Responses to Foreign and Self-Antigens by the CD19/CD21 Complex. *Annu Rev Immunol* 18, 393–422 (2000).

20. Cariappa, A. *et al.* The Follicular versus Marginal Zone B Lymphocyte Cell Fate Decision Is Regulated by Aiolos, Btk, and CD21. *Immunity* 14, 603–615 (2001).

21. Tsay, G. J. & Zouali, M. The Interplay Between Innate-Like B Cells and Other Cell Types in Autoimmunity. *Front Immunol* 9, 1064 (2018).

22. Stebegg, M. *et al.* Regulation of the Germinal Center Response. *Front Immunol* 9, 2469 (2018).

23. Silva, N. S. D. & Klein, U. Dynamics of B cells in germinal centres. *Nat Rev Immunol* 15, 137–148 (2015).

24. Mesin, L., Ersching, J. & Victora, G. D. Germinal Center B Cell Dynamics. *Immunity* 45, 471–482 (2016).

25. Huang, C. & Melnick, A. Mechanisms of action of BCL6 during germinal center B cell development. *Sci China Life Sci* 58, 1226–1232 (2015).

26. Ye, B. H. *et al.* The BCL-6 proto-oncogene controls germinal-centre formation and Th2-type inflammation. *Nat Genet* 16, 161–170 (1997).

27. chneider C, Kon N, Amadori L, et al. FBXO11 inactivation leads to abnormal germinal-center formation and lymphoproliferative disease. *Blood*. 2016;128(5):660-666.

28. Nakagawa R, Toboso-Navasa A, Schips M, *et al.* Permissive selection followed by affinity-based proliferation of GC light zone B cells dictates cell fate and ensures clonal breadth. *Proc Natl Acad Sci U S A.* 2021;118(2):e2016425118.

29. Victora GD, Nussenzweig MC. Germinal centers. *Annu Rev Immunol.* 2012;30:429-457.

30. Silva, N. S. D. & Klein, U. Dynamics of B cells in germinal centres. *Nat Rev Immunol* 15, 137–148 (2015).

31. Pikor, N. B. *et al.* Remodeling of light and dark zone follicular dendritic cells governs germinal center responses. *Nat Immunol* 21, 649–659 (2020).

32. Garin, A. *et al.* Toll-like Receptor 4 Signaling by Follicular Dendritic Cells Is Pivotal for Germinal Center Onset and Affinity Maturation. *Immunity* 33, 84–95 (2010).

33. Zhang, Y. *et al.* Germinal center B cells govern their own fate via antibody feedback. *J Exp Medicine* 210, 457–464 (2013).

34. Tas, J. M. J. *et al.* Visualizing antibody affinity maturation in germinal centers. *Science* 351, 1048–1054 (2016).

35. Kennedy, D. E. *et al.* Novel specialized cell state and spatial compartments within the germinal center. *Nat Immunol* 21, 660–670 (2020).

36. Attaf, N., Baaklini, S., Binet, L. & Milpied, P. Heterogeneity of germinal center B cells: New insights from single-cell studies. *Eur J Immunol* 51, 2555–2567 (2021).

37. Jacob, J. & Kelsoe, G. In situ studies of the primary immune response to (4-hydroxy-3-nitrophenyl)acetyl. II. A common clonal origin for periarteriolar lymphoid sheath-associated foci and germinal centers. *J Exp Medicine* 176, 679–687 (1992).

38. Jacob, J., Kassir, R. & Kelsoe, G. In situ studies of the primary immune response to (4-hydroxy-3-nitrophenyl)acetyl. I. The architecture and dynamics of responding cell populations. *J Exp Medicine* 173, 1165–1175 (1991).

39. Jacob, J., Przylepa, J., Miller, C. & Kelsoe, G. In situ studies of the primary immune response to (4-hydroxy-3- nitrophenyl)acetyl. III. The kinetics of V region mutation and selection in germinal center B cells. *J Exp Medicine* 178, 1293–1307 (1993).

40. Toellner, K. M., Gulbranson-Judge, A., Taylor, D. R., Sze, D. M. & MacLennan, I. C. Immunoglobulin switch transcript production in vivo related to the site and time of antigen-specific B cell activation. *J Exp Medicine* 183, 2303–2312 (1996).

41. Elsner, R. A. & Shlomchik, M. J. Germinal Center and Extrafollicular B Cell Responses in Vaccination, Immunity, and Autoimmunity. *Immunity* 53, 1136–1150 (2020).

42. Maul, R. W. & Gearhart, P. J. Chapter six AID and Somatic Hypermutation. *Adv Immunol* 105, 159–191 (2010).

43. Feng, Y., Seija, N., Noia, J. M. D. & Martin, A. AID in Antibody Diversification: There and Back Again. *Trends Immunol* 41, 586–600 (2020).

44. Stavnezer, J., Guikema, J. E. J. & Schrader, C. E. Mechanism and Regulation of Class Switch Recombination. *Annu Rev Immunol* 26, 261–292 (2008).

45. Roco, J. A. *et al.* Class-Switch Recombination Occurs Infrequently in Germinal Centers. *Immunity* 51, 337-350.e7 (2019).

46. Sundling, C. *et al.* Positive selection of IgG+ over IgM+ B cells in the germinal center reaction. *Immunity* 54, 988-1001.e5 (2021).

47. sola S, Cattoretti G, Uyttersprot N, *et al.* Tracking germinal center B cells expressing germ-line immunoglobulin gamma1 transcripts by conditional gene targeting [published correction appears in Proc Natl Acad Sci U S A. 2007 Feb 6;104(6):2025. Segal, Jane [corrected to Seagal, Jane*]]. Proc Natl Acad Sci U S A.* 2006;103(19):7396-7401.

48. Kraal, G., Weissman, I. L. & Butcher, E. C. Germinal centre B cells: antigen specificity and changes in heavy chain class expression. *Nature* 298, 377–379 (1982).

49. Naito, Y. *et al.* Germinal Center Marker GL7 Probes Activation-Dependent Repression of N - Glycolylneuraminic Acid, a Sialic Acid Species Involved in the Negative Modulation of B-Cell Activation. *Mol Cell Biol* 27, 3008–3022 (2007).

50. Cervenak, L., Magyar, A., Boja, R. & László, G. Differential expression of GL7 activation antigen on bone marrow B cell subpopulations and peripheral B cells. *Immunol Lett* 78, 89–96 (2001).

51. Razzaghi, R. *et al.* Compromised counterselection by FAS creates an aggressive subtype of germinal center lymphoma. *J Exp Medicine* 218, e20201173 (2020).

52. Yoshino, T. *et al.* Inverse expression of bcl-2 protein and Fas antigen in lymphoblasts in peripheral lymph nodes and activated peripheral blood T and B lymphocytes. *Blood* 83, 1856–1861 (1994).

53. Lund, F. *et al.* Murine CD38: an immunoregulatory ectoenzyme. *Immunol Today* 16, 469–473 (1995).

54. Takahashi, Y., Dutta, P. R., Cerasoli, D. M. & Kelsoe, G. In Situ Studies of the Primary Immune Response to (4-Hydroxy-3-Nitrophenyl)Acetyl. V. Affinity Maturation Develops in Two Stages of Clonal Selection. *J Exp Medicine* 187, 885–895 (1998).

55. Nutt, S. L., Hodgkin, P. D., Tarlinton, D. M. & Corcoran, L. M. The generation of antibody-secreting plasma cells. *Nat Rev Immunol* 15, 160–171 (2015).

56. Calame, K. L. Plasma cells: finding new light at the end of B cell development. *Nat Immunol* 2, 1103–1108 (2001).

57. Chan, T. D. *et al.* Antigen Affinity Controls Rapid T-Dependent Antibody Production by Driving the Expansion Rather than the Differentiation or Extrafollicular Migration of Early Plasmablasts. *J Immunol* 183, 3139–3149 (2009).

58. Smith, K. G. C., Hewitson, T. D., Nossal, G. J. V. & Tarlinton, D. M. The phenotype and fate of the antibody-forming cells of the splenic foci. *Eur J Immunol* 26, 444–448 (1996).

59. Higgins, B. W., McHeyzer-Williams, L. J. & McHeyzer-Williams, M. G. Programming Isotype-Specific Plasma Cell Function. *Trends Immunol* 40, 345–357 (2019).

60. Phan, T. G. *et al.* High affinity germinal center B cells are actively selected into the plasma cell compartment. *J Exp Medicine* 203, 2419–2424 (2006).

61. Malkiel, S., Barlev, A. N., Atisha-Fregoso, Y., Suurmond, J. & Diamond, B. Plasma Cell Differentiation Pathways in Systemic Lupus Erythematosus. *Front Immunol* 9, 427 (2018).

62. Takahashi, Y., Dutta, P. R., Cerasoli, D. M. & Kelsoe, G. In Situ Studies of the Primary Immune Response to (4-Hydroxy-3-Nitrophenyl)Acetyl. V. Affinity Maturation Develops in Two Stages of Clonal Selection. *J Exp Medicine* 187, 885–895 (1998).

63. Manz, R. A., Thiel, A. & Radbruch, A. Lifetime of plasma cells in the bone marrow. *Nature* 388, 133–134 (1997).

64. Weisel, F. J., Zuccarino-Catania, G. V., Chikina, M. & Shlomchik, M. J. A Temporal Switch in the Germinal Center Determines Differential Output of Memory B and Plasma Cells. *Immunity* 44, 116–130 (2016).

65. Wols, H. A. M. eLS. (2013) doi:10.1038/npg.els.0004030.

66. Silva, N. S. D., Simonetti, G., Heise, N. & Klein, U. The diverse roles of IRF4 in late germinal center B-cell differentiation. *Immunol Rev* 247, 73–92 (2012).

67. Pracht, K. *et al.* A new staining protocol for detection of murine antibody-secreting plasma cell subsets by flow cytometry. *Eur J Immunol* 47, 1389–1392 (2017).

68. Diaz-Muñoz, M. D. & Osma-Garcia, I. C. The RNA regulatory programs that govern lymphocyte development and function. *Wiley Interdiscip Rev Rna* 13, e1683 (2022).

69. Akira S, Maeda K. Control of RNA Stability in Immunity. *Annu Rev Immunol*. 2021;39:481-509.

70. Behrens, G. & Heissmeyer, V. Cooperation of RNA-Binding Proteins – a Focus on Roquin Function in T Cells. *Front Immunol* 13, 839762 (2022).

71. Gerstberger, S., Hafner, M. & Tuschl, T. A census of human RNA-binding proteins. *Nat Rev Genet* 15, 829–845 (2014).

72. Toung, J. M., Morley, M., Li, M. & Cheung, V. G. RNA-sequence analysis of human B-cells. *Genome Res* 21, 991–998 (2011).

73. Schaub, A. & Glasmacher, E. Splicing in immune cells—mechanistic insights and emerging topics. *Int Immunol* 29, 173–181 (2017).

74. Kafasla, P., Skliris, A. & Kontoyiannis, D. L. Post-transcriptional coordination of immunological responses by RNA-binding proteins. *Nat Immunol* 15, 492–502 (2014).

75. Srivastava, M. *et al.* Roquin binds microRNA-146a and Argonaute2 to regulate microRNA homeostasis. *Nat Commun* 6, 6253 (2015).

76. Díaz-Muñoz, M. D. & Turner, M. Uncovering the Role of RNA-Binding Proteins in Gene Expression in the Immune System. *Front Immunol* 9, 1094 (2018).

77. Diaz-Muñoz, M. D. *et al.* The RNA-binding protein HuR (Elavl1) is essential for the B cell antibody response. *Nat Immunol* 16, 415–425 (2015).

78. Newman, R., McHugh, J. & Turner, M. RNA binding proteins as regulators of immune cell biology. *Clin Exp Immunol* 183, 37–49 (2016).

79. Monzón-Casanova, E. *et al.* The RNA binding protein PTBP1 is necessary for B cell selection in germinal centers. *Nat Immunol* 19, 267–278 (2018).

80. Schultz, C. W., Preet, R., Dhir, T., Dixon, D. A. & Brody, J. R. Understanding and targeting the disease-related RNA binding protein human antigen R (HuR). *Wiley Interdiscip Rev Rna* 11, e1581 (2020).

81. Bertossi, A. *et al.* Loss of Roquin induces early death and immune deregulation but not autoimmunity. *J Exp Medicine* 208, 1749–1756 (2011).

82. Rieß, David Karl (2017): The role of Roquin proteins in B cell physiology and pathology. Dissertation, LMU München: Fakultät für Chemie und Pharmazie

83. Vogel, K. U. *et al.* Roquin Paralogs 1 and 2 Redundantly Repress the Icos and Ox40 Costimulator mRNAs and Control Follicular Helper T Cell Differentiation. *Immunity* 38, 655–668 (2013).

84. Athanasopoulos, V. *et al.* The ROQUIN family of proteins localizes to stress granules via the ROQ domain and binds target mRNAs. *Febs J* 277, 2109–2127 (2010).

85. Pratama, A. *et al.* Roquin-2 Shares Functions with Its Paralog Roquin-1 in the Repression of mRNAs Controlling T Follicular Helper Cells and Systemic Inflammation. *Immunity* 38, 669–680 (2013).

86. Heissmeyer, V. & Vogel, K. U. Molecular control of Tfh-cell differentiation by Roquin family proteins. *Immunol Rev* 253, 273–289 (2013).

87. Tan, D., Zhou, M., Kiledjian, M. & Tong, L. The ROQ domain of Roquin recognizes mRNA constitutive decay element and double-stranded RNA. *Nat Struct Mol Biol* 21, 679–685 (2014).

88. Zhang, Q. *et al.* New Insights into the RNA-Binding and E3 Ubiquitin Ligase Activities of Roquins. *Sci Rep-uk* 5, 15660 (2015).

89. Athanasopoulos, V., Ramiscal, R. R. & Vinuesa, C. G. ROQUIN signalling pathways in innate and adaptive immunity. *Eur J Immunol* 46, 1082–1090 (2016).

90. Schlundt, A. *et al.* Structural basis for RNA recognition in roquin-mediated post-transcriptional gene regulation. *Nat Struct Mol Biol* 21, 671–678 (2014).

91. Schuetz, A., Murakawa, Y., Rosenbaum, E., Landthaler, M. & Heinemann, U. Roquin binding to target mRNAs involves a winged helix-turn-helix motif. *Nat Commun* 5, 5701 (2014).

92. Leppek, K. *et al.* Roquin Promotes Constitutive mRNA Decay via a Conserved Class of Stem-Loop Recognition Motifs. *Cell* 153, 869–881 (2013).

93. Murakawa, Y. *et al.* RC3H1 post-transcriptionally regulates A20 mRNA and modulates the activity of the IKK/NF-κB pathway. *Nat Commun* 6, 7367 (2015).

94. Maruyama T, Araki T, Kawarazaki Y, et al. Roquin-2 promotes ubiquitin-mediated degradation of ASK1 to regulate stress responses. *Sci Signal*. 2014;7(309):ra8. Published 2014 Jan 21.

95. Ivanov, P., Kedersha, N. & Anderson, P. Stress Granules and Processing Bodies in Translational Control. *Csh Perspect Biol* 11, a032813 (2018).

96. Riggs, C. L., Kedersha, N., Ivanov, P. & Anderson, P. Mammalian stress granules and P bodies at a glance. *J Cell Sci* 133, jcs242487 (2020).

97. Kedersha, N. *et al.* Stress granules and processing bodies are dynamically linked sites of mRNP remodeling. *J Cell Biology* 169, 871–884 (2005).

98. Glasmacher, E. *et al.* Roquin binds inducible costimulator mRNA and effectors of mRNA decay to induce microRNA-independent post-transcriptional repression. *Nat Immunol* 11, 725–733 (2010).

99. Heissmeyer V, Ansel KM, Rao A. A plague of autoantibodies. *Nat Immunol.* 2005;6(7):642-644.

100. Ellyard, J. I. *et al.* Heterozygosity for Roquinsan leads to angioimmunoblastic T-cell lymphoma-like tumors in mice. *Blood* 120, 812–821 (2012).

101. Linterman, M. A. *et al.* Follicular helper T cells are required for systemic autoimmunity. *J Exp Medicine* 206, 561–576 (2009).

102. Gigoux, M. *et al.* Inducible costimulator promotes helper T-cell differentiation through phosphoinositide 3-kinase. *Proc National Acad Sci* 106, 20371–20376 (2009).

103. Schubart, D. B., Rolink, A., Kosco-Vilbois, M. H., Botteri, F. & Matthias, P. B-cell-specif ic coactivator OBF-1/OCA-B/Bob1 required for immune response and germinal centre formation. *Nature* 383, 538–542 (1996).

104. Samardzic, T. *et al.* CD22 regulates early B cell development in BOB.1/OBF.1-deficient mice. *Eur J Immunol* 32, 2481–2489 (2002).

105. Chevrier, S., Kratina, T., Emslie, D., Karnowski, A. & Corcoran, L. M. Germinal center-independent, IgM-mediated autoimmunity in sanroque mice lacking Obf1. *Immunol Cell Biol* 92, 12–19 (2014).

106. Iwai, H. *et al.* Involvement of Inducible Costimulator-B7 Homologous Protein Costimulatory Pathway in Murine Lupus Nephritis. *J Immunol* 171, 2848–2854 (2003).

107. Hutloff, A. *et al.* Involvement of inducible costimulator in the exaggerated memory B cell and plasma cell generation in systemic lupus erythematosus. *Arthritis Rheumatism* 50, 3211–3220 (2004).

108. Yu, D. *et al.* Roquin represses autoimmunity by limiting inducible T-cell co-stimulator messenger RNA. *Nature* 450, 299–303 (2007).

109. Lee, S. K. *et al.* Interferon-γ Excess Leads to Pathogenic Accumulation of Follicular Helper T Cells and Germinal Centers. *Immunity* 37, 880–892 (2012).

110. Chang, P.-P. *et al.* Breakdown in Repression of IFN-γ mRNA Leads to Accumulation of Self-Reactive Effector CD8+ T Cells. *J Immunol* 189, 701–710 (2012).

111. Liblau, R. S., Wong, F. S., Mars, L. T. & Santamaria, P. Autoreactive CD8 T Cells in Organ-Specific Autoimmunity Emerging Targets for Therapeutic Intervention. *Immunity* 17, 1–6 (2002).

112. Behrens, G. *et al.* Disrupting Roquin-1 interaction with Regnase-1 induces autoimmunity and enhances antitumor responses. *Nat Immunol* 22, 1563–1576 (2021).

113. Bertino, S. A. & Craft, J. Roquin Paralogs Add a New Dimension to ICOS Regulation. *Immunity* 38, 624–626 (2013).

114. Jeltsch, K. M. *et al.* Cleavage of roquin and regnase-1 by the paracaspase MALT1 releases their cooperatively repressed targets to promote TH17 differentiation. *Nat Immunol* 15, 1079–1089 (2014).

115. Tesmer, L. A., Lundy, S. K., Sarkar, S. & Fox, D. A. Th17 cells in human disease. *Immunol Rev* 223, 87–113 (2008).

116. Wang, C., Kang, S. G., Lee, J., Sun, Z. & Kim, C. H. The roles of CCR6 in migration of Th17 cells and regulation of effector T-cell balance in the gut. *Mucosal Immunol* 2, 173–183 (2009).

117. Zhao, H. *et al.* Genome-wide fitness gene identification reveals Roquin as a potent suppressor of CD8 T cell expansion and anti-tumor immunity. *Cell Reports* 37, 110083 (2021).

118. Lu, W., Zhou, M., Wang, B., Liu, X. & Li, B. Roquin1 inhibits the proliferation of breast cancer cells by inducing G1/S cell cycle arrest via selectively destabilizing the mRNAs of cell cycle–promoting genes. *J Exp Clin Cancer Res Cr* 39, 255 (2020).

119. Rickert RC, Roes J, Rajewsky K. B lymphocyte-specific, Cre-mediated mutagenesis in mice. *Nucleic Acids Res.* 1997;25(6):1317-1318.

120. Murray, S. E. *et al.* NF-κB–inducing kinase plays an essential T cell–intrinsic role in graft-versus-host disease and lethal autoimmunity in mice. *J Clin Invest* 121, 4775–4786 (2011).

121. Song J, So T, Croft M. Activation of NF-kappaB1 by OX40 contributes to antigen-driven T cell expansion and survival. *J Immunol*. 2008;180(11):7240-7248.

122. Vallabhapurapu, S. & Karin, M. Regulation and Function of NF-κB Transcription Factors in the Immune System. *Immunology* 27, 693–733 (2009).

123. Mendel, I. & Shevach, E. M. Activated T cells express the OX40 ligand: requirements for induction and costimulatory function. *Immunology* 117, 196–204 (2006).

124. Gigoux, M. *et al.* Inducible costimulator promotes helper T-cell differentiation through phosphoinositide 3-kinase. *Proc National Acad Sci* 106, 20371–20376 (2009).

125. Jiang, S. H., Shen, N. & Vinuesa, C. G. Posttranscriptional T cell gene regulation to limit Tfh cells and autoimmunity. *Curr Opin Immunol* 37, 21–27 (2015).

126. Jacquemin, C. *et al.* OX40 Ligand Contributes to Human Lupus Pathogenesis by Promoting T Follicular Helper Response. *Immunity* 42, 1159–1170 (2015).

127. Zheng, Y. *et al.* Regulatory T-cell suppressor program co-opts transcription factor IRF4 to control TH2 responses. *Nature* 458, 351–356 (2009).

128. Hodson DJ, Screen M, Turner M. RNA-binding proteins in hematopoiesis and hematological malignancy. *Blood*. 2019;133(22):2365-2373.

129. Rickert, R. C., Roes, J. & Rajewsky, K. B Lymphocyte-Specific, Cre-mediated Mutagenesis in Mice. *Nucleic Acids Res* 25, 1317–1318 (1997).

130. Heger, K. *et al.* A novel Cre recombinase reporter mouse strain facilitates selective and efficient infection of primary immune cells with adenoviral vectors. *Eur J Immunol* 45, 1614–1620 (2015).

131. Madisen, L. *et al.* A robust and high-throughput Cre reporting and characterization system for the whole mouse brain. *Nat Neurosci* 13, 133–140 (2010).

132. Zambrowicz BP, Imamoto A, Fiering S, Herzenberg LA, Kerr WG, Soriano P. Disruption of overlapping transcripts in the ROSA beta geo 26 gene trap strain leads to widespread expression of beta-galactosidase in mouse embryos and hematopoietic cells. *Proc Natl Acad Sci U S A*. 1997

133. McAllister, E. J., Apgar, J. R., Leung, C. R., Rickert, R. C. & Jellusova, J. New Methods To Analyze B Cell Immune Responses to Thymus-Dependent Antigen Sheep Red Blood Cells. *J Immunol* 199, 2998–3003 (2017).

134. Heise, N. & Klein, U. Germinal Centers, Methods and Protocols. *Methods Mol Biology* 1623, 191–208 (2017).

135. Hartman, H., Wang, Y., Schroeder, H. W. & Cui, X. Absorbance summation: A novel approach for analyzing high-throughput ELISA data in the absence of a standard. *Plos One* 13, e0198528 (2018).

136. Weber, J. *et al.* PiggyBac transposon tools for recessive screening identify B-cell lymphoma drivers in mice. *Nat Commun* 10, 1415 (2019).

137. Feng, J., Liu, X., Ni, X. & Qi, H. External signals regulate germinal center fate-determining transcription factors in the A20 lymphoma cell line. *Mol Immunol* 93, 79–86 (2018).

138. Mandel, M. A. Establishment and characterization of BALB/c lymphoma lines with B cell properties. *Plast Reconstr Surg* 66, 812 (1980).

139. Nikolaou, C. *et al.* High-dimensional single cell mass cytometry analysis of the murine hematopoietic system reveals signatures induced by ageing and physiological pathogen challenges. *Immun Ageing* 18, 20 (2021).

140. Dietrich, F. M. & Dukor, P. The Immune Response to Heterologous Red Cells in Mice. *Pathobiology* 30, 909–917 (1967).

141. Xu MZ, Stavnezer J. Regulation of transcription of immunoglobulin germ-line gamma 1 RNA: analysis of the promoter/enhancer. *EMBO J*. 1992;11(1):145-155.

142. Álvarez-Aznar, A. *et al.* Tamoxifen-independent recombination of reporter genes limits lineage tracing and mosaic analysis using CreERT2 lines. *Transgenic Res* 29, 53–68 (2020).

143. Heise N, De Silva NS, Silva K, et al. Germinal center B cell maintenance and differentiation are controlled by distinct NF-κB transcription factor subunits. *J Exp Med*. 2014;211(10):2103-2118.

144. Cibrián, D. & Sánchez-Madrid, F. CD69: from activation marker to metabolic gatekeeper. *Eur J Immunol* 47, 946–953 (2017).

145. Vazquez, B. N., Laguna, T., Carabana, J., Krangel, M. S. & Lauzurica, P. CD69 Gene Is Differentially Regulated in T and B Cells by Evolutionarily Conserved Promoter-Distal Elements. *J Immunol* 183, 6513–6521 (2009).

146. Labiano, S. *et al.* CD69 is a direct HIF-1α target gene in hypoxia as a mechanism enhancing expression on tumor-infiltrating T lymphocytes. *Oncoimmunology* 6, 00–00 (2017).

147. Amu, S., Gjertsson, I. & Brisslert, M. Functional Characterization of Murine CD25 Expressing B Cells. *Scand J Immunol* 71, 275–282 (2010).

148. Lowenthal, J. W., Zubler, R. H., Nabholz, M. & MacDonald, H. R. Similarities between interleukin-2 receptor number and affinity on activated B and T lymphocytes. *Nature* 315, 669–672 (1985).

149. Halliday, N. *et al.* CD86 Is a Selective CD28 Ligand Supporting FoxP3+ Regulatory T Cell Homeostasis in the Presence of High Levels of CTLA-4. *Front Immunol* 11, 600000 (2020).

150. Borriello, F. *et al.* B7-1 and B7-2 Have Overlapping, Critical Roles in Immunoglobulin Class Switching and Germinal Center Formation. *Immunity* 6, 303–313 (1997).

151. Carrillo-Ballesteros, F. J. *et al.* B-cell activating factor receptor expression is associated with germinal center B-cell maintenance. *Exp Ther Med* 17, 2053–2060 (2019).

152. L. Jeffrey Medeiros *et al.* Tumors of the Lymph Nodes and Spleen. *Atlas of tumor pathology*, Series 4, chapter 1 Normal Anatomy and Function of Lymph Nodes and Spleen (2017).

153. Cremasco, V. *et al.* B cell homeostasis and follicle confines are governed by fibroblastic reticular cells. *Nat Immunol* 15, 973–981 (2014).

154. Vora, K. A. *et al.* Cutting Edge: Germinal Centers Formed in the Absence of B Cell-Activating Factor Belonging to the TNF Family Exhibit Impaired Maturation and Function. *J Immunol* 171, 547–551 (2003).

155. Yeh, C.-H., Nojima, T., Kuraoka, M. & Kelsoe, G. Germinal center entry not selection of B cells is controlled by peptide-MHCII complex density. *Nat Commun* 9, 928 (2018).

156. Descatoire, M. *et al.* Critical role of WASp in germinal center tolerance through regulation of B cell apoptosis and diversification. *Cell Reports* 38, 110474 (2022).

157. DONJERKOVIć, D. & SCOTT, D. W. Activation-induced cell death in B lymphocytes. *Cell Res* 10, 179–192 (2000).

158. Imanishi, T. & Mäukelä, O. Strain differences in the fine specificity of mouse antihapten antibodies. *Eur J Immunol* 3, 323–330 (1973).

159. Tao W, Bothwell AL. Development of B cell lineages during a primary anti-hapten immune response. *J Immunol*. 1990;145(10):3216-3222.

160. Jack, R. S., Imanishi-Kari, T. & Rajewsky, K. Idiotypic analysis of the response of C57BL/6 mice to the (4-hydroxy-3-nitrophenyl)acetyl group. *Eur J Immunol* 7, 559–565 (1977).

161. Lu, Y.-F., Singh, M. & Cerny, J. Canonical germinal center B cells may not dominate the memory response to antigenic challenge. *Int Immunol* 13, 643–655 (2001).

162. Bothwell, A. L. M. *et al.* Heavy chain variable region contribution to the NPb family of antibodies: somatic mutation evident in a γ2a variable region. *Cell* 24, 625–637 (1981).

163. Hara, Y. *et al.* High affinity IgM+ memory B cells are generated through a germinal center-dependent pathway. *Mol Immunol* 68, 617–627 (2015).

164. Cumano, A. & Rajewsky, K. Structure of primary anti-(4-hydroxy-3-nitro-phenyl)acetyl (NP) antibodies in normal and idiotypically suppressed C57BL/6 mice. *Eur J Immunol* 15, 512–520 (1985).

165. Han, S., Zheng, B., Porto, J. D. & Kelsoe, G. In situ studies of the primary immune response to (4-hydroxy-3- nitrophenyl)acetyl. IV. Affinity-dependent, antigen-driven B cell apoptosis in germinal centers as a mechanism for maintaining self- tolerance. *J Exp Medicine* 182, 1635–1644 (1995).

166. Jacob, J., Kelsoe, G., Rajewsky, K. & Weiss, U. Intraclonal generation of antibody mutants in germinal centres. *Nature* 354, 389–392 (1991).

167. Shlomchik M, Mascelli M, Shan H, et al. Anti-DNA antibodies from autoimmune mice arise by clonal expansion and somatic mutation. *J Exp Med*. 1990;171(1):265-292.

168. Weber, J. *et al.* PiggyBac transposon tools for recessive screening identify B-cell lymphoma drivers in mice. *Nat Commun* 10, 1415 (2019).

169. Zhang, Y. *et al.* Plasma cell output from germinal centers is regulated by signals from Tfh and stromal cells. *J Exp Medicine* 215, 1227–1243 (2018).

170. Bhattacharya, P. *et al.* Identification of murine B cell lines that undergo somatic hypermutation focused to A:T and G:C residues. *Eur J Immunol* 38, 227–239 (2008).

171. Redecke, V. *et al.* Generation of hematopoietic progenitor cell lines with myeloid and lymphoid potential. *Nat Methods* 10, 795–803 (2013).

172. Gewies, A. *et al.* Uncoupling Malt1 Threshold Function from Paracaspase Activity Results in Destructive Autoimmune Inflammation. *Cell Reports* 9, 1292–1305 (2014).

173. Holmes, A. B. *et al.* Single-cell analysis of germinal-center B cells informs on lymphoma cell of origin and outcome. *J Exp Medicine* 217, e20200483 (2020).

174. Schoeler, K. *et al.* TET enzymes control antibody production and shape the mutational landscape in germinal centre B cells. *Febs J* 286, 3566–3581 (2019).

175. Cox, J. & Mann, M. 1D and 2D annotation enrichment: a statistical method integrating quantitative proteomics with complementary high-throughput data. *Bmc Bioinformatics* 13, S12 (2012).

176. Ochiai, K. *et al.* Transcriptional Regulation of Germinal Center B and Plasma Cell Fates by Dynamical Control of IRF4. *Immunity* 38, 918–929 (2013).

177. Klein, U. *et al.* Transcription factor IRF4 controls plasma cell differentiation and class-switch recombination. *Nat Immunol* 7, 773–782 (2006).

178. Willis, S. N. *et al.* Transcription Factor IRF4 Regulates Germinal Center Cell Formation through a B Cell–Intrinsic Mechanism. *J Immunol* 192, 3200–3206 (2014).

179. Elenitoba-Johnson KS. FBXO11: a novel germinal center B-cell regulator?. *Blood*. 2016;128(5):611-612.

180. Jiang, C. *et al.* CRISPR/Cas9 Screens Reveal Multiple Layers of B cell CD40 Regulation. *Cell Reports* 28, 1307-1322.e8 (2019).

181. Khoenkhoen, S. *et al.* TACI expression and plasma cell differentiation are impaired in the absence of functional IκBNS. *Immunol Cell Biol* 97, 485–497 (2019).

182. Arnold, C. N. *et al.* A forward genetic screen reveals roles for Nfkbid, Zeb1, and Ruvbl2 in humoral immunity. *Proc National Acad Sci* 109, 12286–12293 (2012).

183. Strubin, M., Newell, J. W. & Matthias, P. OBF-1, a novel B cell-specific coactivator that stimulates immunoglobulin promoter activity through association with octamer-binding proteins. *Cell* 80, 497–506 (1995).

184. Song, S. & Matthias, P. D. The Transcriptional Regulation of Germinal Center Formation. *Front Immunol* 9, 2026 (2018).

185. Song, S. *et al.* OBF1 and Oct factors control the germinal center transcriptional program. *Blood* 137, 2920–2934 (2021).

186. Won, W.-J. & Kearney, J. F. CD9 Is a Unique Marker for Marginal Zone B Cells, B1 Cells, and Plasma Cells in Mice. *J Immunol* 168, 5605–5611 (2002).

187. Middendorp, S. *et al.* Mice deficient for CD137 ligand are predisposed to develop germinal center–derived B-cell lymphoma. *Blood* 114, 2280–2289 (2009).

188. Yoon, S., Zhang, X., Berner, P. & Choi, Y. S. IL-21 and IL-10 have redundant roles but differential capacities at different stages of plasma cell generation from human germinal center B cells. *J Leukocyte Biol* 86, 1311–1318 (2009).

189. Arens, R. *et al.* Signaling through CD70 Regulates B Cell Activation and IgG Production. *J Immunol* 173, 3901–3908 (2004).

190. Beishuizen, C. R. L. *et al.* Chronic CD70-Driven Costimulation Impairs IgG Responses by Instructing T Cells to Inhibit Germinal Center B Cell Formation through FasL-Fas Interactions. *J Immunol* 183, 6442–6451 (2009).

191. Bod, L. *et al.* IL-4–Induced Gene 1: A Negative Immune Checkpoint Controlling B Cell Differentiation and Activation. *J Immunol* 200, 1027–1038 (2018).

192. Bannard, O. *et al.* Ubiquitin-mediated fluctuations in MHC class II facilitate efficient germinal center B cell responses. *J Exp Med* 213, 993–1009 (2016).

193. Green, M. R., Yoon, H. & Boss, J. M. Epigenetic Regulation during B Cell Differentiation Controls CIITA Promoter Accessibility. *J Immunol* 177, 3865–3873 (2006).

194. Piskurich, J. F. *et al.* BLIMP-1 mediates extinction of major histocompatibility class II transactivator expression in plasma cells. *Nat Immunol* 1, 526–532 (2000).

195. Weisel, F. J. *et al.* Germinal center B cells selectively oxidize fatty acids for energy while conducting minimal glycolysis. *Nat Immunol* 21, 331–342 (2020).

196. Becker-Herman, S., Lantner, F. & Shachar, I. Id2 Negatively Regulates B Cell Differentiation in the Spleen. *J Immunol* 168, 5507–5513 (2002).

197. Sugai, M. *et al.* Essential role of Id2 in negative regulation of IgE class switching. *Nat Immunol* 4, 25–30 (2003).

198. Holmes, A. B. *et al.* Single-cell analysis of germinal-center B cells informs on lymphoma cell of origin and outcome. *J Exp Medicine* 217, e20200483 (2020).

199. Kang, S., Tanaka, T., Narazaki, M. & Kishimoto, T. Targeting Interleukin-6 Signaling in Clinic. *Immunity* 50, 1007–1023 (2019).

200. Karnowski, A. *et al.* B and T cells collaborate in antiviral responses via IL-6, IL-21, and transcriptional activator and coactivator, Oct2 and OBF-1. *J Exp Med* 209, 2049–2064 (2012).

201. Karnowski, A. *et al.* B and T cells collaborate in antiviral responses via IL-6, IL-21, and transcriptional activator and coactivator, Oct2 and OBF-1. *J Exp Medicine* 209, 2049–2064 (2012).

202. Suematsu S, Matsuda T, Aozasa K, et al. IgG1 plasmacytosis in interleukin 6 transgenic mice. *Proc Natl Acad Sci U S A*. 1989;86(19):7547-7551.

203. Kotani, A. *et al.* Activation-induced cytidine deaminase (AID) promotes B cell lymphomagenesis in Emu-cmyc transgenic mice. *Proc National Acad Sci* 104, 1616–1620 (2007).

204. Zhang, J., Shi, Y., Zhao, M., Hu, H. & Huang, H. Activation-induced cytidine deaminase overexpression in double-hit lymphoma: potential target for novel anticancer therapy. *Sci Rep-uk* 10, 14164 (2020).

205. Zaheen, A. & Martin, A. Activation-Induced Cytidine Deaminase and Aberrant Germinal Center Selection in the Development of Humoral Autoimmunities. *Am J Pathology* 178, 462–471 (2011).

206. Zaheen, A. *et al.* AID constrains germinal center size by rendering B cells susceptible to apoptosis. *Blood* 114, 547–554 (2009).

207. Boulianne, B. *et al.* AID and Caspase 8 Shape the Germinal Center Response through Apoptosis. *J Immunol* 191, 5840–5847 (2013).

208. Batten, M. *et al.* IL-27 supports germinal center function by enhancing IL-21 production and the function of T follicular helper cells. *J Exp Medicine* 207, 2895–2906 (2010).

209. Alfonso, C., Han, J.-O., Williams, G. S. & Karlsson, L. The Impact of H2-DM on Humoral Immune Responses. *J Immunol* 167, 6348–6355 (2001).

210. Alfonso, C. & Karlsson, L. Nonclassical MHC Class II Molecules. *Annu Rev Immunol* 18, 113–142 (2000).

211. Baygün, Seren (2017): A Novel In VivoModel to Investigate Regulators of GCB Cells and GC Derived Lymphomas. Dissertation, TU München, Fakultät für Medizin, Institut für Experimentelle Hämatologe.

212. Cyster, J. G. & Allen, C. D. C. B Cell Responses: Cell Interaction Dynamics and Decisions. *Cell* 177, 524–540 (2019).

213. Bertossi, A. *et al.* Loss of Roquin induces early death and immune deregulation but not autoimmunity. *J Exp Medicine* 208, 1749–1756 (2011).

214. Heise, N. *et al.* Germinal center B cell maintenance and differentiation are controlled by distinct NF-κB transcription factor subunits. *J Exp Medicine* 211, 2103–2118 (2014).

215. Basso, K. & Dalla-Favera, R. Germinal centres and B cell lymphomagenesis. *Nat Rev Immunol* 15, 172–184 (2015).

216. Coffey, F., Alabyev, B. & Manser, T. Initial Clonal Expansion of Germinal Center B Cells Takes Place at the Perimeter of Follicles. *Immunity* 30, 599–609 (2009).

217. Jellusova J, Rickert RC. A Brake for B Cell Proliferation: Appropriate responses to metabolic stress are crucial to maintain B cell viability and prevent malignant outgrowth. *Bioessays*. 2017;39(11):10.1002/bies.201700079.

218. Jellusova, J. *et al.* GSK3 is a metabolic checkpoint regulator in B cells. *Nat Immunol* 18, 303–312 (2017).

219. Basso, K. Biology of Germinal Center B Cells Relating to Lymphomagenesis. *Hemasphere* 5, e582 (2021).

220. Nojima, T. *et al.* In-vitro derived germinal centre B cells differentially generate memory B or plasma cells in vivo. *Nat Commun* 2, 465 (2011).

221. Nojima, T. *et al.* In-vitro derived germinal centre B cells differentially generate memory B or plasma cells in vivo. *Nat Commun* 2, 465 (2011).

222. Allen, D., Simon, T., Sablitzky, F., Rajewsky, K. & Cumano, A. Antibody engineering for the analysis of affinity maturation of an anti-hapten response. *Embo J* 7, 1995–2001 (1988).

223. Smith KG, Light A, Nossal GJ, Tarlinton DM. The extent of affinity maturation differs between the memory and antibody-forming cell compartments in the primary immune response. *EMBO J*. 1997;16(11):2996-3006.

224. Kober-Hasslacher, M. *et al.* c-Rel gain in B cells drives germinal center reactions and autoantibody production. *J Clin Invest* 130, 3270–3286 (2020).

225. Di Niro, R. *et al.* Salmonella Infection Drives Promiscuous B Cell Activation Followed by Extrafollicular Affinity Maturation. *Immunity* 43, 120–131 (2015).

226. Kuraoka, M. *et al.* Complex Antigens Drive Permissive Clonal Selection in Germinal Centers. *Immunity* 44, 542–552 (2016).

227. Di Niro, R. *et al.* Salmonella Infection Drives Promiscuous B Cell Activation Followed by Extrafollicular Affinity Maturation. *Immunity* 43, 120–131 (2015).

228. Lightman, S. M., Utley, A. & Lee, K. P. Survival of Long-Lived Plasma Cells (LLPC): Piecing Together the Puzzle. *Front Immunol* 10, 965 (2019).

229. Sze, D. M.-Y., Toellner, K.-M., Vinuesa, C. G. de, Taylor, D. R. & MacLennan, I. C. M. Intrinsic Constraint on Plasmablast Growth and Extrinsic Limits of Plasma Cell Survival. *J Exp Medicine* 192, 813–822 (2000).

230. Gitlin, A. D. *et al.* Independent Roles of Switching and Hypermutation in the Development and Persistence of B Lymphocyte Memory. *Immunity* 44, 769–781 (2016).

231. Aiba, Y. *et al.* Preferential localization of IgG memory B cells adjacent to contracted germinal centers. *Proc National Acad Sci* 107, 12192–12197 (2010).

232. Koike, T., Harada, K., Horiuchi, S. & Kitamura, D. The quantity of CD40 signaling determines the differentiation of B cells into functionally distinct memory cell subsets. *Elife* 8, e44245 (2019).

233. Zuccarino-Catania, G. V. *et al.* CD80 and PD-L2 define functionally distinct memory B cell subsets that are independent of antibody isotype. *Nat Immunol* 15, 631–637 (2014).

234. Yao, H.-H., Zhao, Y.-J., He, Y.-F., Huang, D.-B. & Wang, W. Knockdown of AGGF1 inhibits the invasion and migration of gastric cancer via epithelial–mesenchymal transition through Wnt/ß-catenin pathway. *Cancer Cell Int* 19, 41 (2019).

235. Auckland, P., Roscioli, E., Coker, H. L. E. & McAinsh, A. D. CENP-F stabilizes kinetochore-microtubule attachments and limits dynein stripping of corona cargoes. *J Cell Biology* 219, e201905018 (2020).

236. Shahid, M. *et al.* Centromere protein F (CENPF), a microtubule binding protein, modulates cancer metabolism by regulating pyruvate kinase M2 phosphorylation signaling. *Cell Cycle* 17, 2802–2818 (2018).

237. Petsalaki, E. & Zachos, G. Clks 1, 2 and 4 prevent chromatin breakage by regulating the Aurora B-dependent abscission checkpoint. *Nat Commun* 7, 11451 (2016).

238. Mohammad, D. K., Ali, R. H., Turunen, J. J., Nore, B. F. & Smith, C. I. E. B Cell Receptor Activation Predominantly Regulates AKT-mTORC1/2 Substrates Functionally Related to RNA Processing. *Plos One* 11, e0160255 (2016).

239. Bass, T. E. & Cortez, D. Quantitative phosphoproteomics reveals mitotic function of the ATR activator ETAA1. *J Cell Biology* 218, 1235–1249 (2019).

240. Lee, Y.-C., Zhou, Q., Chen, J. & Yuan, J. RPA-Binding Protein ETAA1 Is an ATR Activator Involved in DNA Replication Stress Response. *Curr Biol* 26, 3257–3268 (2016).

241. González Besteiro MA, Gottifredi V. ETAA1 ensures proper chromosome segregation: A matter of S phase or mitosis?. *J Cell Biol*. 2019;218(12):3883-3884.

242. Miosge, L. A. *et al.* Systems-guided forward genetic screen reveals a critical role of the replication stress response protein ETAA1 in T cell clonal expansion. *Proc National Acad Sci* 114, E5216–E5225 (2017).

243. Nachmias, B. *et al.* IPO11 regulates the nuclear import of BZW1/2 and is necessary for AML cells and stem cells. *Leukemia* 36, 1283–1295 (2022).

244. Mis, M. *et al.* IPO11 mediates ßcatenin nuclear import in a subset of colorectal cancers. *J Cell Biology* 219, e201903017 (2019).

245. Giannos, P., Kechagias, K. S. & Gal, A. Identification of Prognostic Gene Biomarkers in Non-Small Cell Lung Cancer Progression by Integrated Bioinformatics Analysis. *Biology* 10, 1200 (2021).

246. Schallus T, Jaeckh C, Fehér K, et al. Malectin: a novel carbohydrate-binding protein of the endoplasmic reticulum and a candidate player in the early steps of protein N-glycosylation. *Mol Biol Cell*. 2008;19(8):3404-3414.

247. Hanihara-Tatsuzawa, F. *et al.* Control of Toll-like Receptor-mediated T Cell-independent Type 1 Antibody Responses by the Inducible Nuclear Protein IκB-ζ*. *J Biological Chem* 289, 30925–30936 (2014).

248. Hijioka, K., Matsuo, S., Eto-Kimura, A., Takeshige, K. & Muta, T. Induction of the nuclear IκB protein IκB-ζ upon stimulation of B cell antigen receptor. *Biochem Bioph Res Co* 356, 476–480 (2007).

249. Keil, M. *et al.* Loss of Peter Pan protein is associated with cell cycle defects and apoptotic events. *Biochimica Et Biophysica Acta Bba - Mol Cell Res* 1866, 882–895 (2019).

250. Pfister, A. S., Keil, M. & Kühl, M. The Wnt Target Protein Peter Pan Defines a Novel p53-independent Nucleolar Stress-Response Pathway*. *J Biol Chem* 290, 10905–10918 (2015).

251. Maeda, H. *et al.* Ubiquitin-Conjugating Enzyme UBE2Q2 Suppresses Cell Proliferation and Is Down-Regulated in Recurrent Head and Neck Cancer. *Mol Cancer Res* 7, 1553–1562 (2009).

List of Tables

List of Figures

Abbreviations

"+"	wildtype	miRNA	micro RNA
AGC	automatic gain control	mLN	mesenteric lymph node
AID	activation induced deaminase	mRNP	messenger ribonucleoprotein particle
ANA	autoantibody	MZB	marginal zone B cell
APC	antibody producing cell	NcMMR	non-canoncial mismatch repair mechanism
AS	amino acid	Neu5Ac	N-acetylneuraminic acid
BCR	B cell receptor	Neu5Gc	N-glycolylneuraminic acid
BER	base excision repair	NHEJ	nonhomologous end joining
BM	bone marrow	NP-CGG	4-Hydroxy-3-nitrophenylacetyl-chicken gamma globulin
bp	base-pair	nt	nucleotide
CAG	CMV early enhancer chicken ß actin	ON	over night
CAR	coxsackie/adenovirus receptor	P body	processing body
CDE	constitutive decay element or consensus decay element	PALS	periarteriolar lymphoid sheat
CDS	coding determining sequence	PB	peripheral blood
CLP	common lymphoid progenitor	PC	plasma cell
CSR	class-switch recombination	PCA	principal component analysis
D	diversity	PCR	polymerase chain reaction
dC	deoxycytidine	PenStrep	penicillin-streptomycin
DIA	data independent acquisition	pHSC	hematopoietic stem cell
DSB	double strand break	PP	peyer's patches
dsRNA	double-stranded RNA	PTGR	post-transcritptional gene regulation
dTOM	tdTomato	qRT-PCR	quantitative real-time PCR
dU	deoxyuridine	RBP	RNA-binding protein
DZ	dark zone	rev	reverse
EJC	exon junction complex	RING	really interesting new gene
ELISA	enzyme-linked immunosorbent assay	RNAseq	RNA sequencing
FA	formic acid	RNP	ribonucleoprotein
FCS	fetal calf serum	ROS	reactive oxygen species
FDC	follicular dendritic cell	SG	stress granule
FOB	follicular B cell	SHM	somatic hypermutation
FSC-A	forward scatter-area	SLC	surrogate light chain
FSC-H	forward scatter-height	SLE	systemic lupus erythematosus
FSC-W	forward scatter-width	SLEC	short lived effector like cell
fwd	forward	SNP	single-nucleotide polymorphism
GALT	gut-associated lymphoid tissue	SP1	sphingosine-1-phosphate
GC	germinal center	SPL	spleen
GCB	germinal center B cell	SRBC	sheep-red blood cells
HEPN	higher eukaryotes and prokaryotes nucleotide-binding	SSC-A	sideward scatter-area
HLH	hemophagocytic lymphohistocytosis	SSC-H	sideward scatter-height
HRP	horseradish peroxidase	SSC-W	sideward scatter-width
HS	high-sensitivity	TCR	T cell receptor
i.p.	intra-peritoneal	TD	T cell dependent
IgH	Ig heavy chain	T_{FH}	follicular helper T cell
IKK	IκB kinase	TI	T cell independent
iNKT	invariant NKT	TLR	Toll-like receptor
J	joining	TMB	3,3',5,5'-tetramethylbenzidine
KO	knockout	TNFR	tumor necrosis factor receptor
LC-MS/MS	liquid chromatography coupled mass spectrometry	T_{reg}	regulatory T cell
LN	lymph node	UTR	untranslated region
LZ	light zone	V	variable
MACS	magnetic activated cell sorting	WT	wildtype

Acknowledgments

Most particularly, I would like to thank my advisor Prof. Marc Schmidt-Supprian for his outstanding guidance throughout the years. It was a great inspiration and honor for me to experience his way of performing science. His brilliant ideas, ample knowledge of the Roquin project and beyond and his eagerness to decode the immune system have been a constant encouragement to me. His thoughtfulness, patience and trust create a workplace that is a pleasure to go to every day.

Further thanks go to my thesis advisory committee members, Prof. Hassan Jumaa and Prof. Andreas Pichlmair, for their readiness to support my PhD project with scientific input and on-site helping hands.

I wish to express my profound appreciation to my collaboration partners Olga Baranov, Thomas Engleitner and Rupert Öllinger of the laboratory of Prof. Roland Rad and Julia Mergner without whom the insightful sequencing and proteome analysis would not have been possible. Furthermore, I am very much obliged to the coordination office of IMPRS, most importantly Hans Jörg Schaeffer, Ingrid Wolf and Marta Cipińska for greatly enriching my daily life with a comprehensive and lovingly designed Graduate School Program.

I would like to truly thank all my colleagues, past and present, for their energetic support at the bench, problem-solving skills and life-saving cake buffets at days when lunch had to be skipped.
Moreover, I would like to deeply thank Claudia Mugler, Vera Wanat, Julia Knogler, Barbara Habermehl, Madlen Oelsner and Jasmin Schröder for the significant help they provided especially at the beginning of my PhD project and during the preparation of hundreds of mouse samples for genotyping, FACS or ELISA experiments. They were always ready, no matter how big my experiments were.
Thanks to Monika Mittermeier and Christian Herrler for their assistance in the mouse house which was highly valuable to me.
Additionally, I would like to thank Nyambayar Dashtsoodol for his positive attitude and for kindly introducing me into his magic skills at the flow cytometry sorters.

Many thanks to Valeria Soberon, Carina Diehl, Laura Kraus, Lena Osswald, Ricarda Trapp, Chia-I Lien, Hyunju Oh-Strauß, Gene Swinerd, Daniel Kovacs and David Riess for warmly welcoming me in the lab, lively scientific and non-scientific discussions, experimental support and fun during conferences and coffee breaks which all truly meant a lot to me.
My deepest gratitude goes to Sabrina Bortoluzzi, Tim Ammon, Seren Bayguen and Francisco Osorio for their reliability, encouragement and friendship which I deeply hope to preserve over the years.

Beyond work, I am deeply thankful for my father who seeded the interest in natural sciences into my heart and my mother who is my most important advisor and supporter during all phases of my life. I am extremely grateful for my closest friends Simone, Maria, Lena, Doro, Ali, Lisa and Vivi who all considerably encouraged me before and after this PhD journey with their patience and positive energies. I could not have done it without them. Last but certainly not least, I would like to thank Christoph, my source of strength in life, anonymous collaborator in many analyses and IT representative without whom my mental and physical batteries would always be empty. You are my T cell to the B cell.